

This item was submitted to Loughborough University as a PhD thesis by the author and is made available in the Institutional Repository (<https://dspace.lboro.ac.uk/>) under the following Creative Commons Licence conditions.



For the full text of this licence, please go to:
<http://creativecommons.org/licenses/by-nc-nd/2.5/>

Pilkington Library

Author/Filing Title VISSEK, D

Accession/Copy No. 040129863

Vol. No.	Class Mark
---------------	------------------

LOAN COPY

0401298639



MAGNETIC ORDERING PHENOMENA IN SOME LOW-DIMENSIONAL XY-LIKE MAGNETIC MODEL SYSTEMS

by

Dirk Visser

A doctoral thesis submitted in partial fulfilment of the requirements
for the award of Doctor of Philosophy
at Loughborough University.

October 1996

© Introduction by D. Visser (1996)

This thesis comprises a collection of 17 papers and conference contributions written and/or researched while being a member of staff at the Department of Physics, Loughborough University (of Technology).


Most papers concern neutron scattering and some report on magnetisation measurements. A list of the institutes, where the research has been carried out, has been provided separately. In academic circles and especially in neutron scattering it is considered common practice and often obligatory that collaborators (local contacts) of these institutes are co-author on publications resulting from these experiments.

Therefore, all papers presented here are the final results from a series of successful collaborations with students, colleagues (and local contacts). I have tried to summarise my contribution to the papers as outlined below.

- | | | |
|----------------------|---------|----------|
| 1) Proposal written: | a) full | b) joint |
| 2) Research: | a) full | b) joint |
| 3) Data Analysis: | a) full | b) joint |
| 4) Authorship: | a) full | b) joint |

Paper:

- | | |
|-----|----------------------------------|
| 2.1 | 2a, 4a |
| 2.2 | 1a, 2b, 3b, 4b |
| 2.3 | 1a, 2b, 3b, 4b |
| 3.1 | 1a, 2b, 3b, 4b |
| 3.2 | 1a, 2b, 3a, 4a |
| 3.3 | 1a, 2b, 3b, 4b |
| 3.4 | 1a, 2b, 3a, 4a |
| 4.1 | 2b, 4a |
| 4.2 | 2b, 4a |
| 4.3 | 1a, 2b, 4a |
| 5.1 | 1a, 2b, 3a, 4a |
| 5.2 | 1a, 2b, 3a, 4a |
| 6.1 | 1b, 2b, 3b, 4b (D10 experiment). |
| 6.2 | 1b, 2b, 4b |
| 6.3 | 1a, 2b, 3b, 4a |
| 6.4 | 1a, 2b, 3b, 4b |
| 6.5 | 2a, 3b, 4b |

 Loughborough University	
Date May 97	
Class	
Acc No.	040129863

99098319

The research described in this thesis has been carried out at:

AERE- Harwell, Chilton, Didcot, UK

Institut Laue - Langevin, Grenoble, France

Institut Leon Brillouin, CEN, Saclay, France

BENSC, Hahn Meitner Institut, Berlin, Germany

Gorlaeus Laboratories, University of Leiden, Leiden, The Netherlands

Department of Physics, University of Southampton, Southampton, UK

Royal Institution of Britain, London, UK

Max Planck Institut, Stuttgart, Germany

and

has been financially supported by:

the UK EPSERC(SERC) and the European Community under their TMR programs at BENSC and LLB (Contract no. ERB CHGECT 920001).

Voor Sophie

Table of Contents

page

Abstract

1. Introduction	1
2. Magnetic ordering in induced magnetic moment systems	
2.1 Magnetic ordering in the quasi one-dimensional induced moment ferro- and anti-ferromagnets AFeX_3	23
2.2 Magnetic ordering effects in the random mixed one-dimensional ferromagnet-antiferromagnet system $\text{RbFeCl}_{3-x}\text{Br}_x$	26
2.3 Magnetic ordering effects in the mixed induced moment ferromagnetic system $\text{RbFe}_{1-x}\text{Mg}_x\text{Cl}_3$	48
3. Magnetic excitations and phase transitions in AFeBr_3 ($\text{A} = \text{Cs}, \text{Rb}$)	
3.1 Magnetic excitations and phase transition of CsFeBr_3 in an external magnetic field	63
3.2 Magnetic excitations of the singlet ground state antiferromagnet CsFeBr_3 in a magnetic field	71
3.3 A dynamic correlated effective-field treatment of the magnetic excitations in the singlet ground state antiferromagnet RbFeBr_3	76
3.4 Temperature dependence of the magnetic excitations in the modified triangular induced moment antiferromagnet RbFeBr_3 at the soft mode point	94
4. Magneto structural correlations and high pressure induced changes to the magnetic ordering phenomena in AFeX_3	
4.1 Magneto-structural correlations in the quasi one-dimensional induced moment magnets AFeX_3	103
4.2 The influence of applied pressure on the magnetic excitations and magnetic ordering in the quasi one-dimensional induced moment magnets AFeX_3	105
4.3 Magnetic excitations and magnetic ordering in the hexagonal perovskites AFeX_3 under hydrostatic pressure	114
5. Chiral ordering in the hexagonal XY-like triangular antiferromagnet	
5.1 The effect of magnetic and non-magnetic dilution on the magnetic ordering in the hexagonal antiferromagnet CsMnBr_3	121
5.2 Magnetic ordering in the stacked triangular antiferromagnet CsMnBr_3 in the presence of an electric field	123

6. Magnetic ordering phenomena in quasi two-dimensional systems with XY symmetry	
6.1 Neutron scattering investigation of the static critical properties of Rb_2CrCl_4	130
6.2 The critical line in the phase diagram of Rb_2CrCl_4	152
6.3 Magnetic structure of $\text{KMnPO}_4\cdot\text{H}_2\text{O}$	155
6.4 Dimensionality cross-overs in the magnetization of the canted antiferromagnets $\text{NH}_4\text{MnPO}_4\cdot\text{H}_2\text{O}$ and $\text{NH}_4\text{MnPO}_4\cdot\text{D}_2\text{O}$	158
6.5 Dimensionality crossovers in the magnetization of the weakly ferromagnetic two-dimensional manganese alkylphosphonate hydrates $\text{MnC}_n\text{H}_{2n+1}\text{PO}_3\cdot\text{H}_2\text{O}$, $n=2-4$	162
7. Summary and conclusions	168

Acknowledgements

Abstract

The physics of the one-dimensional (1-D) Ising, XY and Heisenberg systems as well as the two-dimensional (2-D) Heisenberg and XY systems differ from the 2-D Ising and three-dimensional (3-D) Heisenberg magnets in that they do not show magnetic order in the presence of magnetic short-range correlations for $T \rightarrow 0$ K. Small deviations from ideal behaviour induced by single-ion anisotropy, magnetic dipole interaction or intrachainar, intraplanar superexchange, can result in the introduction of long-range (3-D) magnetic ordering.

The lattice geometry in conjunction with the anisotropy of the spin system may introduce magnetic frustration effects, chirality ordering or Kosterlitz-Thouless behaviour.

In this thesis a collection of papers is presented on different aspects of the magnetic ordering behaviour in quasi 1-D and 2-D magnetic model systems with XY-like anisotropy where in the case of the quasi 1-D hexagonal ABX_3 ternary halides additional low-dimensional aspects are introduced in the magnetic ordering behaviour due to the 2-D network - a triangular lattice - of the magnetic ions perpendicular to the chain-axis. Consequently, frustration effects as well as chirality ordering can be observed for particular compounds.

The magnetic ordering phenomena in the quasi 1-D $AFeX_3$ halides will be presented. These systems show singlet groundstate or induced moment behaviour. Their magnetic ordering behaviour can be influenced by an external order parameter such as an applied magnetic field (H/c) or an applied uniaxial pressure (P/a). The ordering behaviour is strongly dependent on relatively small changes in the structural parameters. The magnetic ordering behaviour for a diluted induced-moment system is investigated for the solid solution $RbFe_{1-x}Mg_xCl_3$ and mixed ferro-antiferromagnetic induced-moment system for the solid solution $RbFeCl_{3-x}Br_x$. The magnetic phase diagrams for these systems have been determined. The effect of the magnetic ordering on the magnetic excitations was studied for the singlet groundstate system $CsFeBr_3$ in the presence of an applied field along the chain direction and perpendicular to the chain direction as well as for the induced moment system $RbFeBr_3$. The influence of a slight structural distortion of the trigonal basal plane and its influence on the magnetic ordering behaviour and excitations at the magnetic soft mode point have been investigated.

In the case of triangular antiferromagnets with XY anisotropy, geometrical frustration leads to magnetic structures of the 120° type. The magnetic moments in such a system are condensed into the basal plane where the magnetic moments form plaquettes of spins which rotate 120° either clockwise or anti-clockwise. This chirality

order introduces an extra degree of freedom which results in new universality classes for the critical exponents of such a type of system. On symmetry grounds it has been shown that the chiral ordering can be removed in the presence of an electric field along the direction of the magnetic ordering vector. Experimental evidence has been presented to underwrite this theoretical prediction.

The 2-D XY model does not sustain long-range order for $T \rightarrow 0K$. However, Berezinskii, Kosterlitz and Thouless have shown that for this model a phase transition to low temperature phase does exist. This phase has an infinite correlation length but no spontaneous order. Evidence for the existence of such a phase in the quasi 2-D ferromagnet Rb_2CrCl_4 has been presented. A similar behaviour may be present in the in the quasi 2-D weak ferromagnets $AMnPO_3 \cdot H_2O$: $A^+ = NH_4, ND_4, K, C_nH_{2n+1}$. Magnetisation data are presented in support of this hypothesis.

Chapter 1.

Introduction

During the early 1960s a number of aristotype crystal structures, in which the distinct geometrical anisotropy of the superexchange pathways indicated the possibility of realising low-dimensional magnetic systems, were identified, thus leading to a vast and still topical research area of low-dimensional magnetic model systems.^{1,2,3,4,5}

The two most basic structures with low-dimensional magnetic properties are derived from a purely three-dimensional lattice array: the aristotype structure of cubic perovskite ABX_3 ⁶ (figure 1). Firstly, two-dimensional magnetism may be observed in the aristotype structure of the tetragonal A_2BX_4 system with the K_2NiF_4 structure.⁷ The relation between the cubic perovskite structure and the K_2NiF_4 structure is straightforward (figure 2). The three-dimensional network of corner-sharing octahedra is cut along the *c*-axis to form slabs interlaced with diamagnetic ions. The interlayer distance between the magnetic ions along the *c*-axis is much larger than the intralayer distance of the magnetic ions. Therefore, the resulting magnetic superexchange interactions provide a quasi two-dimensional magnetic system.

Secondly, the aristotype structure of the hexagonal ABX_3 perovskite (figure 3) results in the formation of infinite chains of face-sharing BX_3^- octahedra.⁸ The distance of the magnetic ions in the chains is much shorter than the interchain distance. Such a system may behave as a quasi one-dimensional magnet. An additional aspect of this crystal structure is the arrangement of the magnetic B-ions in the hexagonal ab-plane. These ions form a two-dimensional simple hexagonal array. This aspect is of importance for the low-temperature magnetic behaviour and magnetic ordering as will be demonstrated in this thesis.

Examples of these structures are mostly found in the alkali first-row transition metal halides. The K_2NiF_4 structure is realised in a series of A_2BX_4 fluorides and chlorides. Recently this structure type has seen renewed interest in connection with the discovery of high T_c superconductivity in $Ln_{1-x}Ba_xCuO_4$ ⁹ and the two-dimensional $S = 1/2$ square lattice magnetic behaviour connected to the CuO_2 layer.¹⁰

The quasi one-dimensional ABX_3 halides occur most often among the alkali first-row transition metal halides. Of the ABF_3 fluorides only $CsNiF_3$ adopts the hexagonal perovskite structure.¹¹ This structure type is commonly found in $ABCl_3$ and $ABBr_3$ compounds with $A^+ = Cs, Rb, NH_4, K, Tl$, and B is a first-row transition metal. Structural phase transitions to a lower symmetry or a different structure type, like NH_4CdCl_3 ,¹² occur for a critical ratio of the radii of the A-ion and the X-ion: $r_A/r_X \sim 0.8$.¹² The large differences in the electronic structure of the B-ion in its octahedral surrounding results in a variety of different electronic level schemes, which has a direct influence on the magnetic properties and magnetic ordering behaviour of the ABX_3 halides at low temperature. Secondary effects, like single-ion anisotropy, interchain

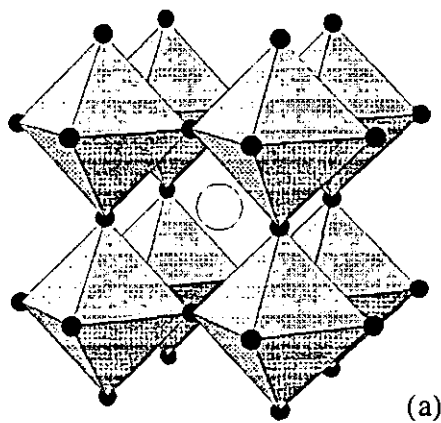


Fig.1a 3-D network of the ABX₃ cubic perovskite structure

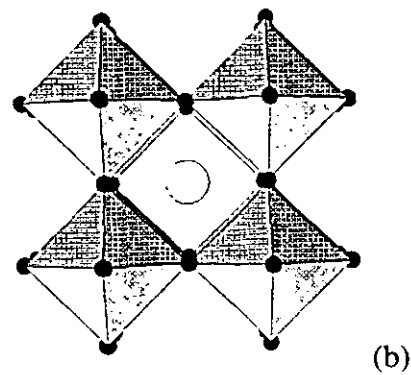


Fig.1b [001] projection of the ABX₃ cubic perovskite structure

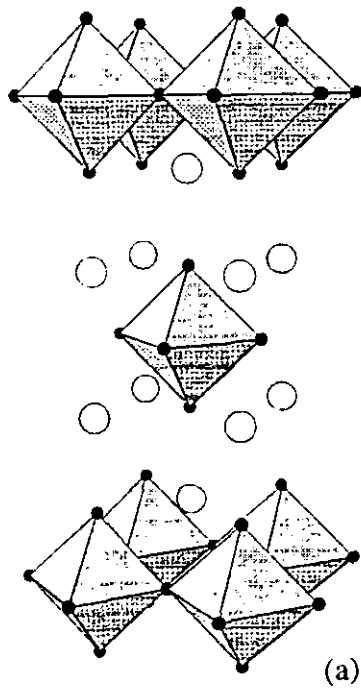


Fig.2a 2-D network of the K₂NiF₄ cubic perovskite structure

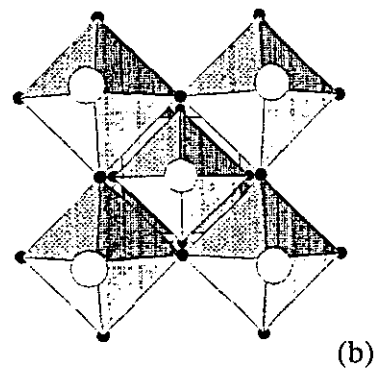


Fig.2b [001] projection of the K₂NiF₄ cubic perovskite structure

interactions, magnetic dipolar interaction, finally drive these systems to long-range magnetic ordering and determine the configuration of the magnetic moments below the magnetic ordering temperature.

In this thesis the magnetic ordering behaviour of several low-dimensional magnetic materials with XY-like anisotropy, which are related to the basic aristotype crystal structures described above, are presented:

1. The magnetic ordering behaviour in the singlet groundstate/induced moment systems AFeX_3 will be described. The magnetic structures of the induced moment AFeX_3 compounds are reported while the magnetic excitations and induced magnetic ordering due to an applied magnetic field have been studied for CsFeBr_3 . In RbFeBr_3 , an induced moment system, the influence of a slight structural distortion of the crystal structure on the magnetic excitations and magnetic structure is studied in detail. The transition between singlet groundstate and induced moment system has been studied by chemical substitution of Mg^{2+} in RbFeCl_3 and on doping Cl^- in RbFeBr_3 as well as Br^- in RbFeCl_3 . The magneto structural correlation for the AFeX_3 compounds is also reported.
2. The existence of chiral magnetic ordering in a triangular XY-like antiferromagnet has been demonstrated by means of elastic neutron scattering experiments on CsMnBr_3 and $\text{CsMn}_{1-x}\text{Mg}_x\text{Br}_3$. Definite proof of the existence of chirality ordering in CsMnBr_3 was obtained from the magnetic ordering behaviour in the presence of an electric field directed along the magnetic ordering vector.
3. The magnetic ordering behaviour of a finite quasi two-dimensional XY system has been studied in Rb_2CrCl_4 . This system shows the magnetic behaviour predicted for the Kosterlitz-Thouless transition. The response of this type of transition in the presence of an applied field along the symmetry sustaining direction is also reported.
4. The occurrence of Kosterlitz-Thouless-like behaviour in the two-dimensional weak ferromagnets $\text{AMnPO}_4\cdot\text{H}_2\text{O}$ ($\text{A}^+ = \text{K}, \text{NH}_4, \text{n-alkyl}$) has been deduced from neutron scattering data and magnetisation measurements. This behaviour is directly related to the magnetic ordering present in this type of structure.

Magnetic behaviour in insulators

On an atomic level magnetism is an effect associated with the quantum mechanics of the angular momentum of the atom. On macroscopic scale, magnetism is usually described using a statistical mechanics approach; it will be defined via the thermodynamical quantities like specific heat, magnetisation, etc. The thermodynamic state of a system

as defined by the state variables U (internal energy), S (entropy) and T (temperature) and a number of mechanical state variables.^{13,14} The behaviour of a magnetic substance is described by the mechanical state variables M (magnetisation) and H (magnetic force). At equilibrium the variable 'extensive' quantities of the system (S, M) will take on values which minimise the Gibbs free energy

$$G = U - M \cdot H - TS \quad (1)$$

where U is the internal energy of the system plus the magnetic field (H). The differential work done on the system corresponds to

$$dW = -HdM \quad (2)$$

The total derivative of the Gibbs free energy for reversible processes at constant temperature and field, and for a closed system with N particles, is given by

$$dG = -SdT - MdH - \sum_i \mu_i dN_i \quad (3)$$

where μ_i is the chemical potential of particle i . Therefore,

$$M = -(\delta G / \delta H)_{T,N} \quad (4)$$

As response of the magnetisation to changes of the field H , it is possible to define the response function

$$\chi = -(\delta M / \delta H)_{T,N} = -(\delta^2 G / \delta^2 H)_{T,N} \quad (5)$$

which is called the susceptibility.

Griffiths and Wheeler¹⁵ classify the thermodynamical variable of (1) as 'fields' (h_i) and 'densities' (ρ_i). The fields have the properties that they assume identical values in two or more phases, which are in thermodynamical equilibrium. This is not necessarily true for the conjugated densities

$$\rho = -(\delta G / \delta h_i). \quad (6)$$

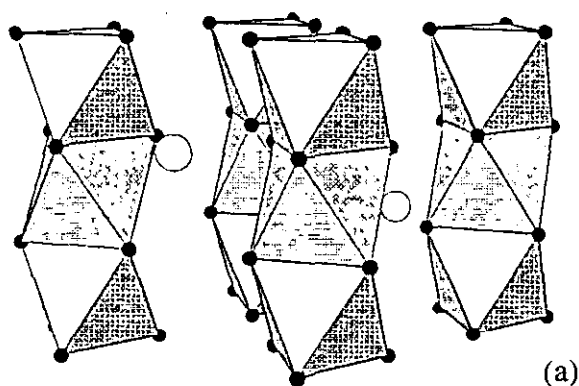


Fig.3a 1-D network of the ABX₃ hexagonal perovskite structure

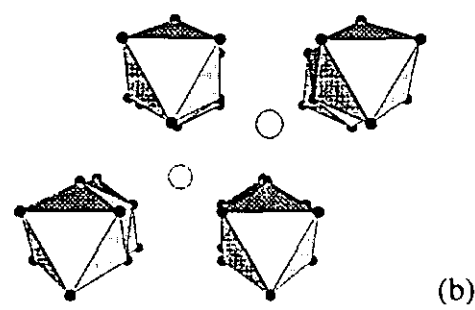


Fig.3b [001] projection of the ABX₃ hexagonal perovskite structure

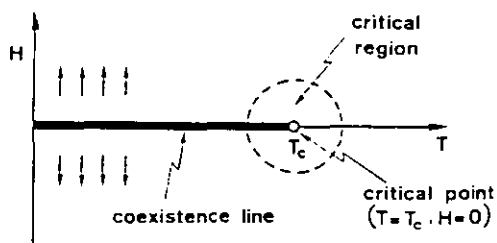


Fig.4 HT - phase diagram of a ferromagnet (after ⁵¹).

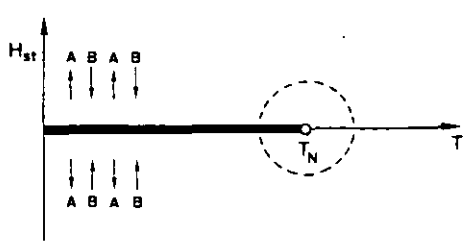


Fig.5 H_{st}T - phase diagram of an antiferromagnet (after ⁵¹).

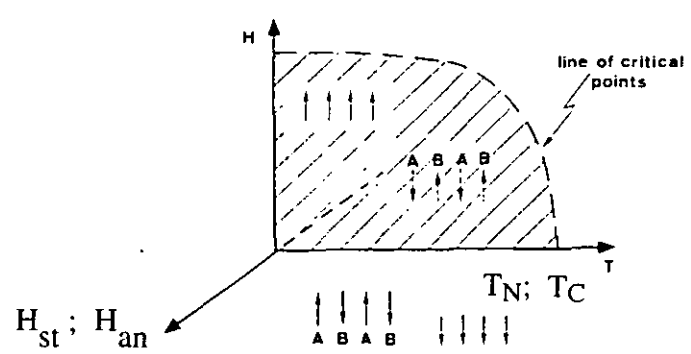


Fig.6 Possible (H_{st}, H, T) or (H_{an}, H, T) phase diagram of an antiferromagnet or anisotropic ferromagnet (after ⁵¹).

The equivalence to (3) will be obvious. H and T will be 'fields' where M and S are 'densities' according to this definition. According to (1), G may be extended with additional pairs of conjugated variables in the form of $-h_i p_i$.

In this framework, first-order transitions can be defined as a discontinuity of one (or more) of the densities p_i and its conjugated field. At the first-order transition, the state of the system is not uniquely defined. Two phases can be characterised by densities $p_i^{(1)}$ and $p_i^{(2)}$ whereas $h_i^{(1)} = h_i^{(2)}$ for all fields h_i .

In the two-dimensional field space, this first-order phase transition extends as a $(z-1)$ dimensional hypersurface, the coexistence surface (CXS) which separates phases 1 and 2. The surface may terminate in a critical boundary, a hypersurface of dimension $(z-2)$ with the property that the discontinuities in the densities vanish continuously upon approaching a point on the hypersurface or the CXS may intersect with another CXS in a triple boundary: a hypersurface of dimension $(z-2)$ where three phases are in equilibrium.

The H - T phase diagram of a ferromagnet (figure 4) provides the simplest example of a critical boundary in a magnetic system, viz. the Curie point T_C . In the two-dimensional field space spanned up by the field H , T , the first-order transition, T_C , continues in a one-dimensional CXS along the T -axis. Along this line two phases coexist, which are distinguished by the magnetisation density M : $M_2 = -M_1$. As function of T , the discontinuity of $M_1 - M_2$ vanishes continuously upon approaching T_C .

A similar phase diagram exists for an anisotropic antiferromagnet in zero magnetic field (figure 5). However, below the critical point T_N , the moments are ordered in two magnetic sublattices which are parallel and antiparallel to a particular easy-axis. The order parameter is now defined as the staggered magnetisation M_{st} and its conjugate the fictitious staggered field H_{st} . The field space can be extended in a third direction with H_{ex} perpendicular to H (anisotropic ferromagnet) or H_{st} (anisotropic antiferromagnet). The CXS in this case appears to be a coexistence surface extending to the H_{st} (H_{ani}) = 0 plane.

Therefore, an H can be seen as a non-ordering field in the antiferromagnet and anisotropic ferromagnet. The two-dimensional CXS can be limited in certain cases to a critical line. From the shape of the critical boundary, in this case, one can derive in the framework of Griffiths and Wheeler¹⁵ that H is an irrelevant field at T_N ($H = 0$, $T = T_N$) while H is relevant everywhere else. T is a relevant field along the entire critical line, except at the point $H = H_C$, $T = 0$ (figure 6).

Griffiths and Wheeler¹⁵ pointed out that the type of critical behaviour, which is observed upon approaching the critical boundary, is totally dependent on the path of

approach in field space. For the correct analysis of critical phenomena one has to choose the appropriate trajectory in field and parameter space.

Experimental evidence as well as model calculation show in many systems that a similar singular behaviour can be observed in the thermodynamic variables near a critical point. The interaction which leads to the ordering process seems to be of minor importance for the description of the ordering process itself. The critical behaviour depends only on a limited number of parameters but are specially related to spatial dimensionality (d) and the number (n) of degrees of freedom of the spin components. These common features of ordering in systems are known as *universality*.¹⁶ The origin of long-range order can be traced back to the divergence of the range of correlations in a system at the ordering temperature and is the cause of all the singularities in the system near criticality. The correlation function, which is dependent on d and n , imposes severe limitations on the functional form of the singularities, which result in close relations between the various critical quantities. This feature of the ordering of a particular system is known as *scaling*.¹⁷ The semi-phenomenological aspect of universality and scaling were integrated by Wilson¹⁸ in the Renormalisation Group approach, which provides a detailed method for the calculation of critical behaviour.

The interaction Hamiltonian

The interaction between the electron spins in the systems under discussion can be described in general with the Hamiltonian:

$$H = -2 \sum_{i,j} \{ J_x S_i^x S_j^x + J_y S_i^y S_j^y + J_z S_i^z S_j^z \} \quad (7)$$

where J is the superexchange constant and S_x , S_y and S_z are the spatial components of the spin. There are two types of interaction: $J > 0$ for ferromagnetic interaction and $J < 0$ for antiferromagnetic interaction. The exchange interaction (Heisenberg) is a result of the Pauli principle. The charge density and, therefore, the electronic energy are dependent on the spin. The total exchange coupling J is determined by two processes: the direct exchange and the kinetic superexchange, which involves the transfer of an electron between orbitals on neighbouring cations via an intermediate anion (diamagnetic). Further exchange mechanisms may also be present in the form of correlation superexchange involving a two-electron transfer and/or superexchange induced by the polarisation of ligand orbitals.¹⁹

The interaction of J also depends on how many spin components are participating. One can distinguish between three different classes for S with n degrees of freedom:

- for $n = 1$ $J_z \neq 0; J_x, J_y = 0$ the Ising system
- for $n = 2$ $J_x, J_y \neq 0; J_z = 0$ the XY system
- for $n = 3$ $J_x = J_y = J_z \neq 0$ the Heisenberg system

In practice, intermediate systems between these three classes are also realised. For a full description of the magnetic behaviour of a model system, one also has to take into account the dimensionality d . The superexchange constant is quite sensitive to the distance between the magnetic ions, the number of superexchange bridges (or intermediates) as well as the angles involved in the superexchange pathway. Consequently, there are quasi one- and quasi two-dimensional systems as well as the conventional three-dimensional system. In order to describe a real system properly, perturbation terms have to be added to the Hamiltonian (7). These are the anisotropy terms

$$\sum_{i,j} (S_i \cdot \underline{D}_{ij} \cdot S_j + \underline{d}_{ij} S_i \times S_j) \quad (8)$$

which are induced by a combined effect of kinetic superexchange and first-order spin orbit coupling: \underline{d}_{ij} and the traceless asymmetry parameter \underline{D}_{ij} introduced due to, first, second-order spin orbit coupling, respectively. The relationship between these asymmetries and the kinetic exchange are given by

$$\underline{d}_{ij} \approx J_{\text{kin}} (\Delta g/g) \quad (9)$$

and

$$\underline{D}_{ij} \approx J_{\text{kin}} (\Delta g/g)^2 \quad (10)$$

$\Delta g = g - 2$, which corresponds to the deviation of the g -factor from the free electron value $g = 2.00023\dots$

The single anisotropy term

$$\sum_{\alpha} S_{\alpha} \cdot \underline{D}_{\alpha} \cdot S_{\alpha} \quad \alpha = i \text{ or } j \quad (11)$$

relates to the second-order spin orbit coupling and the anisotropy g -tensor $g_{\mu\nu}$ via the relation

$$\underline{D}_\alpha = -\lambda^2 \Lambda_{\alpha\alpha} \quad (12)$$

$$g_{\mu\nu} \approx 2(\delta_{\mu\nu} - \lambda \Lambda_{\mu\nu}) \quad (13)$$

where λ is the spin orbit coupling parameter and $\Lambda_{\mu\nu}$ are the coefficients arising from second-order perturbation theory.

The magnetic dipolar interaction H_{dip} between magnetic spins in a lattice depends upon a term equivalent to $\sum 1/r^3$. It manifests itself through domain formation and demagnetisation effects.¹ Such effects are not negligible for compounds with ferromagnetic interactions as will be demonstrated in chapter 2.

Additional anisotropy may be induced due to externally applied perturbations like the magnetic field

$$\mu_B \sum_{\mu\nu} \mathbf{B}_\mu \cdot g_{\mu\nu} \mathbf{S}_\nu \quad (14)$$

(Zeeman effect) or electric field (Stark effect) and pressure (hydrostatic, uniaxial - symmetry breaking). Finally, the effect of small spin values (quantum effects) has to be considered, too.²⁰

Critical behaviour

Phase transitions of the order-disorder type are characterised by an order parameter which decreases towards zero. At a first-order phase transition the order parameter changes discontinuously whereas at a second-order phase transition the change in order parameter is continuous upon approaching the phase transition from the disordered phase. The magnetic susceptibility $\delta M / \delta H$ becomes infinite while the correlation length ξ diverges.²¹

In a real system the singular behaviour of a particular thermodynamic quantity is limited to a particular region of the phase diagram known as *critical region*. Within the critical region²² the various thermodynamic quantities often depend on each other in a rather simple way, viz.

$$\begin{aligned} M_S &\propto (T/T_C - 1)^\beta \\ C_p &\propto (T/T_C - 1)^{-\alpha} \\ \chi &\propto (T/T_C - 1)^{-\gamma} \end{aligned} \quad \alpha, \beta, \gamma \text{ are critical exponents.}$$

Equivalent exponents can be found in many dissimilar systems and are often found experimentally to have universal values, viz. $\beta = 1/8$, $\gamma = 1\ 3/4$ (2-D Ising), while mean field theory²³ predicts $\beta = 1/2$, $\gamma = 1$. In general, mean field theory is not valid to describe a phase transition because of the neglect of very short wavelength fluctuations. It was shown by Ginzberg that it was generally inadmissible to neglect fluctuations with wavelengths $< \xi$. The importance of the short wavelength fluctuations becomes more acute for reduced lattice dimensionality, since the energy content of the fluctuations will be confined to fewer degrees of freedom. For $d < 4$ the mean field approach breaks down in the region where 'critical' fluctuations are present. The extent of the critical region can be estimated from the Ginzberg criterion²⁴ and is larger for lower lattice dimensionality.

The modern RG theory description of critical phenomena take the fluctuations of smaller wavelengths $< \xi$ into account. This theory allows one to identify those parameters in the Hamiltonian which are dominant in determining the critical properties. For Hamiltonians with short-range interactions the relevant parameters are d and n . The critical properties depend in general not on microscopic detail but on symmetry and dimensionality. Therefore, the concept of universality is justified and one may define universality classes according to the broad division in behaviour. In studying the critical behaviour of magnetic systems one usually divides them into nine universality classes ($1 \leq d, n \leq 3$: see table 1) characterised by their specific critical constants. It has been shown for one-dimensional systems that no long-range magnetic order occurs.^{25,26} Only recently has it been shown that the two-dimensional XY system displays a quasi ordering behaviour.²⁷ However, it has also been demonstrated by simulation and experimental data that, depending on the symmetry present within a magnetic ordered phase, the actual symmetry can be lowered (chiral ordering) and new universality classes may be identified (see table 2 and chapter 4).

In practice, low-dimensional magnets do not exist but are true three-dimensional systems at T_c . This may manifest itself through cross-over in the critical region from low-dimensional to three-dimensional behaviour. In order to describe the real behaviour of the magnetic systems, perturbation terms have to be added to the model Hamiltonian to account for increasing cooperative interactions. A criterion for the observation of lattice dimensionality cross-over has been given by De Jongh and Stanley²⁸. When cross-over occurs in the critical region, a gradual or abrupt change in the critical exponent will be observed. In the latter case, the perturbation will switch the system to a different universality class. In real systems multiple cross-over phenomena may take place (see chapters 5 and 6).

The thermodynamic function $f(\varepsilon)$ near the critical point often depends on the reduced temperature $\varepsilon = (T - T_c)/T_c$ as $f(\varepsilon) = A\varepsilon^x (1 + B\varepsilon^y + \dots)$ where A and B are constants, x is the critical exponent. Near T_c , $f(\varepsilon)$ can be described by a power law $\sim A\varepsilon^x$ and x can be obtained from a log-log plot. The critical exponents are dependent on d and n , S . The critical exponents referred to in this thesis are:

correlation length	$\xi = \xi_0 t^{-\nu}$
magnetic susceptibility	$\chi = \chi_0 t^{-\gamma}$
specific heat	$C = (A/\alpha) (t^{-\alpha} - 1) + B$
spontaneous magnetisation	$M_s = B t^\beta$
magnetisation at $T = T_c$	$M = D H^{1/\delta}$

$\varepsilon = t = (T - T_c) / T$ for $T > T_c$ or $\varepsilon = (T_c - T) / T_c$ for $T < T_c$. Each critical component can be expressed as a linear function of two other exponents through scaling.^{29,30}

$$\begin{aligned}\alpha + 2\beta + \gamma &= 2 \quad \text{and} \quad \chi = \xi^{2-\eta} \\ \gamma &= (2 - \eta)\nu \\ \gamma &= \beta(\delta - 1) \\ d\nu &= 2 - \alpha\end{aligned}$$

Neutron scattering

A large part of the research in this thesis is based on neutron scattering experiments. The theoretical background can be found in many good textbooks;³¹ therefore, no explicit resumé will be given. However, some specific features will be pointed out in relation to measurements of critical phenomena.

A system near the critical point is characterised by large fluctuations in the order parameter, which slows down and will extend over an increasingly large spacial range. In a magnetic system these fluctuations are introduced through the space-time spin correlation function:

$$G^{\alpha\beta}(\mathbf{R}, t) = \langle S_0^\alpha(0) S_{\mathbf{R}}^\beta(t) \rangle \quad (15)$$

The bracket indicates the thermal average value at a particular temperature T .

In an (anti)ferromagnet the order parameter is proportional to $\langle S_{\mathbf{R}} \rangle$. Approaching the critical point, the area of \mathbf{R} for which $G^{\alpha\alpha}(\mathbf{R}, t)$ has a functional value which will

increase, although $\langle \mathbf{S_R}(t) \rangle$ still zero. Therefore, short-range order increases and the correlations between the spins increase until $\langle \mathbf{S_R}(t) \rangle$ starts to deviate from zero. In that case, the system will show long-range magnetic ordering. In the ordered phase, fluctuations still exist due to regions with non-aligned spin moments. The fluctuations around the equilibrium value of $\mathbf{S_R}$ expressed by the net correlation function

$$G_n^{\alpha\beta}(\mathbf{R},t) = \langle S_0^\alpha(0) \mathbf{S_R}^\beta(t) \rangle - \langle S_0^\alpha(0) \rangle \langle \mathbf{S_R}^\beta(t) \rangle \quad (16)$$

This correlation function is zero far away from the critical point in both ordered and disordered phase. The study of the temperature, field behaviour of this type of spin fluctuation is accessible by means of neutron scattering.

Being interested in the scattering of neutrons (spin = 1/2) by magnetic media and using unpolarised neutrons, the double-differential magnetic scattering cross-section per unit solid angle Ω and per unit energy E is given:³¹

$$d^2\sigma/d\Omega dE \propto k/k_0 |f(Q)|^2 \sum_{\alpha\beta} (\delta_{\alpha\beta} - Q_\alpha Q_\beta) G^{\alpha\beta}(\mathbf{Q},\omega) \quad (17)$$

and

$$G^{\alpha\beta}(\mathbf{Q},\omega) = 1/2\pi \int_{-\infty}^{\infty} dt \sum_{\mathbf{R}} \exp \{i(\mathbf{Q} \cdot \mathbf{R} - \omega t)\} G^{\alpha\beta}(\mathbf{R},t) \quad (18)$$

The scattering vector \mathbf{Q} is defined as

$$\mathbf{Q} = \mathbf{k} - \mathbf{k}_0 \quad (19)$$

where \mathbf{k} and \mathbf{k}_0 are the scattered and incoming wave vectors of the neutron. The corresponding energy loss in a scattering process is

$$E_0 - E = \hbar\omega = \hbar^2/2m (k_0^2 - k^2) \quad (20)$$

\hbar = Planck's constant and m = the neutron mass while $f(Q)$ is the magnetic form factor. Q_α, Q_β are the α or β component of the unit vector \mathbf{Q}/Q . This factor allows one to distinguish between the different directions of the fluctuations Q_x, Q_y or Q_z .

Expression (18) shows that the differential cross section is proportional to the space-time Fourier transform of the correlation function (15). The fluctuations in the order parameter close to the critical point are quasi-static in their behaviour towards neutrons.^{32,33} This means that $G^{\alpha\beta}(\mathbf{Q},\omega)$ will be nearly elastic and its profile will be narrow and centred at $\omega = 0$. Upon approaching the critical point T_C (T_N) the width

(4 ω) decreases (critical slowing down). For determining the static correlation function $G^{\alpha\beta}(\mathbf{R}) \equiv G^{\alpha\beta}(\mathbf{R}, t = 0)$ one can omit the energy analysis in (17) resulting in the determination of

$$G^{\alpha\beta}(\mathbf{Q}) \equiv \sum_{\mathbf{R}} \exp(i\mathbf{Q} \cdot \mathbf{R}) G^{\alpha\beta}(\mathbf{R}) = \int_{-\infty}^{\infty} d\omega G^{\alpha\beta}(\mathbf{Q}, \omega) \quad (21)$$

$G^{\alpha\beta}(\mathbf{Q})$ is the wave-vector representation of the spin fluctuations and has the periodicity of the reciprocal lattice. $\mathbf{Q}_0 = 2\pi\mathbf{e}$ can be defined in an ordered system and corresponds to the magnetic unit cell.

$$G^{\alpha\beta}(\mathbf{Q}) \equiv G^{\alpha\beta}(\mathbf{q}), \quad (22)$$

where $\mathbf{q} = \mathbf{Q} - 2\pi\mathbf{e}$ can be seen as the *deviation vector*. The Fourier transform of $S_{\mathbf{R}}^{\alpha}$ is given by

$$S_{\mathbf{q}}^{\alpha} = \sum_{\mathbf{R}} \exp(i\mathbf{q} \cdot \mathbf{R}) S_{\mathbf{R}}^{\alpha} \quad (23)$$

substituting in (21) one obtains the usual form for

$$G^{\alpha\beta}(\mathbf{Q}) \equiv G^{\alpha\beta}(\mathbf{q}) = \sum_{\mathbf{R}} \exp(i\mathbf{q} \cdot \mathbf{R}) \langle S_0^{\alpha} S_{\mathbf{R}}^{\beta} \rangle = \langle S_{\mathbf{q}}^{\alpha} S_{-\mathbf{q}}^{\beta} \rangle \quad (24)$$

The similarity of (24) with (16) allows one to define the net correlation function

$$G_n^{\alpha\beta}(\mathbf{q}) = G^{\alpha\beta}(\mathbf{q}) - \langle S_{\mathbf{q}}^{\alpha} \rangle \langle S_{\mathbf{q}}^{\beta} \rangle \quad (25)$$

This function is bell-shaped with a maximum at $\mathbf{q} = 0$ and width $\kappa_{a,b}$ or c along the three principal crystallographic axes. $G_n^{\alpha\beta}(\mathbf{q})$ can be determined by measuring the differential cross-section ($d\sigma/d\Omega$), assuming that the quasi-static approximation

$$\Delta k = -(m\omega/\hbar k) \quad (26)$$

holds. In that case,

$$d\sigma/d\Omega(\mathbf{Q}) \propto |f(\mathbf{Q})|^2 \sum_{\alpha\beta} (\delta_{\alpha\beta} - Q_{\alpha}Q_{\beta}) G^{\alpha\beta}(\mathbf{Q}). \quad (27)$$

The differential cross-section can be split into two terms:

$$d\sigma/d\Omega(\mathbf{Q}) \propto |f(\mathbf{Q})|^2 \sum_{\alpha\beta} (\delta_{\alpha\beta} - Q_\alpha Q_\beta) G^{\alpha\beta}(\mathbf{Q}) \cdot \\ \cdot [G_n^{\alpha\beta}(\mathbf{Q}) + \sum_{\mathbf{R}} \exp(i\mathbf{Q} \cdot \mathbf{R}) \langle S_0^\alpha \rangle \langle S_{\mathbf{R}}^\beta \rangle]. \quad (28)$$

The first term concerns the short-range fluctuations while the second term represents Bragg scattering in an ordered magnetic system and has normally a Gaussian form. The shape of $G_n^{\alpha\beta}(\mathbf{q})$ is dependent on the crystal system.³⁴ For a cubic system

$$G_n^\alpha(\mathbf{q}) = [A^\alpha / \{(k^\alpha)^2 + q^2\}]^{1-\eta/2} \quad (29)$$

The correspondence net static correlation function

$$G_n^\alpha(\mathbf{R}) \propto \exp(-\kappa^\alpha R) / R^{d-2+\eta}, \quad R \rightarrow \infty \quad (30)$$

The exponent η represents the deviation of shape of G_n from the Ornstein-Zernike theory.³¹ $1/\kappa^\alpha \equiv \xi^\alpha$ corresponds clearly to the role of correlation length, being a measure of the range of

$$G_n^\alpha(\mathbf{R}) = \langle S_0^\alpha \rangle \langle S_{\mathbf{R}}^\alpha \rangle \quad (31)$$

In general different amplitudes A^α and κ^α are found for each spin component. The fluctuation-dissipation theory provides the connection between the thermodynamic quantities, viz. $\chi^{\alpha\beta}(\mathbf{Q})$ the generalized susceptibility and the static correlation function $G_n^{\alpha\beta}(\mathbf{Q})$. For a static spatially modulated magnetic field

$$H^\alpha(\mathbf{R}) = H^\alpha(\mathbf{Q}) \exp(i\mathbf{Q} \cdot \mathbf{R}) \quad (32)$$

and the response function of the magnetic system

$$\chi^{\alpha\beta}(\mathbf{Q}) = \delta M^\beta(\mathbf{Q}) / \delta M^\alpha(\mathbf{Q}) \quad (33)$$

For $\mathbf{Q}_0 = 2\pi\mathbf{e}$, (33) corresponds to the normal susceptibility $\chi^{\alpha\beta} = \delta M^\beta / \delta M^\alpha$ of the ferromagnet and its staggered equivalent in the case of the antiferromagnet. In reference 31 it is shown that

$$(34) \quad k_B T / g^2 \mu_B^2 \chi^{\alpha\beta}(\mathbf{Q}) = \int_{-\infty}^{\infty} d\omega [(1 - \exp(-\hbar\omega/k_B T)) / (\hbar\omega/k_B T)] G_n^{\alpha\beta}(\mathbf{Q}, \omega)$$

where k_B is the Boltzmann factor and g the effective g -value of a magnetic ion and μ_B is the Bohr magneton. Under the quasi-elastic approximation

$$\hbar\omega \ll k_B T \quad (35)$$

reduces to

$$(k_B T / g^2 \mu_B^2) \chi^{\alpha\beta}(\mathbf{Q}) = G_n^{\alpha\beta}(\mathbf{Q}) \quad (36)$$

when $\hbar\omega \ll k_B$ (quasi-elastic approximation).

Singlet groundstate and the induced-moment state systems in the hexagonal AFeX₃ perovskites

Among the many different electronic systems of the ABX₃ halides, the AFeX₃ compounds crystallising with the hexagonal perovskite structure have special significance as a testing ground for the theoretical predictions concerning singlet groundstate and induced-moment behaviour. This behaviour is directly related to the 3d⁶ configuration of the Fe²⁺ ion in the BX₆²⁻ octahedron in the hexagonal perovskite structure. The cubic exponent of the crystal field splits the free ion D⁵ term in an upper-orbital doublet (⁵E) and a lower triplet (⁵T₂). The lower term splits by spin-orbit coupling into the states ⁵T_{2a,b} and c spaced according to the Landé interval rule by 2λ and 3λ, λ being the spin-orbit coupling parameter. The trigonal distortion of the octahedron splits the term further into a singlet groundstate and a doublet (energy difference between the states equals D): see figure 7. The Zeeman effect splits the doublet further in the presence of an 'ordering' magnetic field (H // c). Such a magnetic system in an isolated surrounding should have no magnetic long-range order and the corresponding magnetic excitations are non-dispersive (E = D). In the case of an extended network of superexchange between such Fe²⁺ sites, as present in the hexagonal perovskite, the superexchange mechanism will induce dispersion into the magnetic excitation spectrum and may cause these systems to order.³⁵ At low temperatures (T < 100K) only the singlet groundstate and the first low-lying doublet state determine the magnetic behaviour. These systems can be described by an effective S = 1 formalism instead of the full spin moment (S = 2). This fact may induce

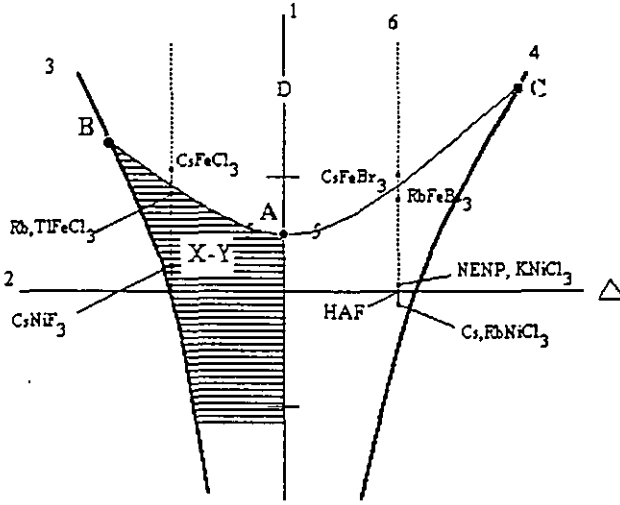


Fig.8 Phase diagram for the Ising-Heisenberg chain (after ⁵²).

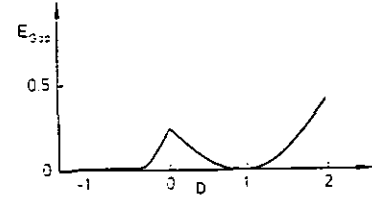


Fig.9 Energy of the Haldane gap versus single-ion anisotropy (line 6 in fig.7, after ⁵²).

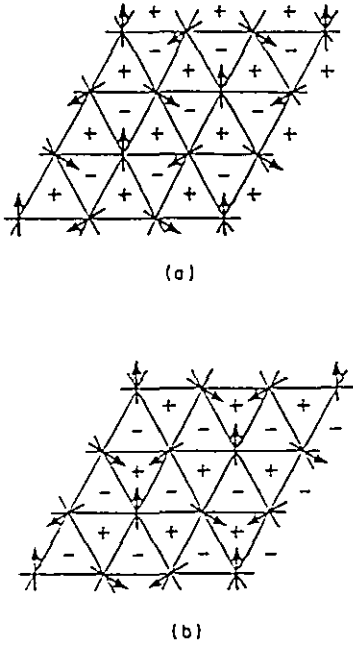


Fig. 10 Typical groundstate patterns for the triangular lattice. The + and - signs indicate the helicity of each triangle. The pattern shown in (a) and (b) cannot be obtained from (a) by a global spin rotation (after ⁴⁹).

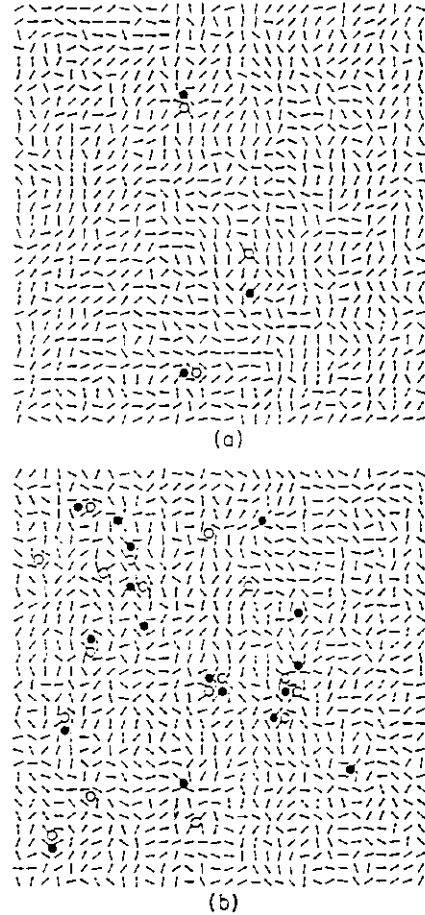


Fig. 11 Monte Carlo 'snapshots' showing the spin and vortex configuration for the XY model at T^* and T_C . Solid (open) circles represent positive (negative) vortices centered on plaquettes with a circulation of $+\pi$ ($-\pi$) (after ²⁷).

quantum effects in these in principle quasi one-dimensional ($S = 1$) systems.²⁰ The phase diagram for the Ising-Heisenberg $S = 1$ chain is given in figure 8. This rich phase diagram shows the expected position of the AFeX_3 compounds. On the antiferromagnetic exchange side novel groundstates are found, which include an ordinary singlet groundstate as well as a system with a Haldane gap for the values of D around 0: see figure 9.

The magnetic ordering behaviour in the AFeX_3 systems are described in detail in chapters 2, 3 and 4 as well as the different approaches necessary to describe the magnetic excitations in the different regimes. The theoretical predictions on which the phase diagram of figure 8 is based, predicts a special behaviour at the phase transition line from singlet groundstate to the induced-moment state, viz. a Kosterlitz-Thouless type behaviour.³⁶ The magnetic ordering process at this point of the phase diagram should show a specific critical behaviour. Attempts to chemically realise such a system have been made for the mixed solution $\text{Rb}_{1-x}\text{Cs}_x\text{FeCl}_3$ ³⁷ and $\text{RbFeCl}_{3-x}\text{Br}_x$ and $\text{RbFeBr}_{3-x}\text{Cl}_x$ (see Chapter 2.2). The experimental results of the 'short-range' magnetic ordering could be described by a semi-spinnglass behaviour.³⁸

Magnetic ordering in XY-like triangular antiferromagnets

Not so long ago it was realised that the magnetic-ordering process in several types of magnetic structures, on particular magnetic lattices, possess an additional degeneracy of the symmetry in the form of chiral ordering. Kawamura³⁹ predicted that the 120° -type triangular antiferromagnets may belong to a new universality class due to the presence of a staggered chirality ordering: see figure 10. This helicity degree of freedom gives rise to an Ising-like (Z_2) discrete degeneracy in addition to the XY (S_1) continuous degeneracy. In this case, the order parameter is defined by the symmetry $V = \text{Z}_2 \times \text{S}_1$. It has to be noted that Azarai *et al.*⁴⁰ suggest that such systems are either tricritical with $\beta = 0.25$ or exhibit a weak first-order transition.

Experimental evidence for the new chirality universality classes has been obtained for several triangular antiferromagnets.^{41,42} Especially the critical exponent of the sublattice magnetisation and the specific heat are excellent probes to establish the validity of these predictions. In this thesis, two experimental studies are described (Chapter 4) which support the predictions of Kawamura. CsMnBr_3 has been doped with diamagnetic impurities (Mg^{2+}) and a non-magnetic but superexchange sustaining impurity (Fe^{2+}). In both cases, the critical exponents β and α change gradually from the chiral universal values to those of the 3D universality class.

Plumer *et al.*⁴³ predicted that an applied electric field in the direction of the ordering vector, [110] direction, could remove the chiral ordering of the triangular system. In Chapter 5.2 experimental data are presented in support of this magneto-electric effect. Later experimental work⁴⁴ reconfirmed these results and the final value of β in the presence of an applied 'saturating' E-field has been established as $\beta = 0.170(5)$. Subsequently it has been shown that the application of an electric and magnetic field has the same renormalising effect on β as an applied magnetic field in the absence of an electric field.^{45, 46} The value of β increases slowly towards the 3D universal Ising values.

Kosterlitz-Thouless behaviour in quasi 2-D XY systems

According to the theoretical predictions of Mermin and Wagner,⁴⁷ spin systems with continuous symmetry and short-range order cannot sustain long-range magnetic order for $d < 3$. This statement still holds for 1d systems. However, recent evidence from computational simulation and RG analysis suggests that a staggered magnetisation and long-range magnetic order exist in a 2D antiferromagnetic Heisenberg model.⁴⁸ For nearly twenty-five years there has been a similar debate on whether the Kosterlitz-Thouless (K-T) theory provides an adequate and correct description of the 2-D XY system. Kosterlitz and Thouless described the phase transition in the 2-D XY model using an alternative but equivalent Hamiltonian

$$H = -J \sum_{\langle i,j \rangle} \cos(\theta_{ij}) \quad (37)$$

θ_{ij} has been defined as the angle between the spins S_i and S_j . The phase transition in this type of system can be seen as the unbinding of vortex-antivortex pairs (see figure 11). The singularities associated with this transition do not follow the usual power law behaviour. The susceptibility varies as an exponential $\chi = \chi_0 \xi^{2+\eta}$ and the corresponding correlation length as $\xi = \xi_0 \exp(at^{-\nu})$. The XY model shows distinct size effects. Several different predictions for the critical exponents have been obtained from computer simulations.⁴⁹ Bramwell and Holdworth²⁷ recently showed using the RG approach that for finite sized samples the 2D XY model has a power law behaviour over a restricted temperature range. The magnetisation can be characterised by a power law exponent $\beta = 0.23$. A survey of a large number of quasi 2-D systems shows that these systems are classified between the extremes of the 2-D Ising ($\beta = 0.125$) and the finite size 2-D XY system ($\beta = 0.23$). These systems show in reality often cross-over behaviour between the 3-D universality class and 2-D universality class behaviour.

In this thesis the statistical critical properties of Rb_2CrCl_4 are reported. The critical behaviour in this compound can be fully described by the predictions of the K-T model. The effect of an applied magnetic field in the symmetry sustaining direction is also reported. The observed behaviour in the magnetisation as function of an applied magnetic field, obtained from bulk magnetisation measurements, can also be modelled by Monte Carlo simulations using (37) extended with the usual magnetic field term.

A second example of K-T behaviour has been found in a layered phosphate: $\text{KMnPO}_4 \cdot \text{H}_2\text{O}$. The sublattice magnetisation data as well as the dc-magnetisation data show that the critical behaviour and spin symmetry in this layered weak-ferromagnetic system must be 2-D XY. As will be shown in chapter 6.3, a symmetry analysis predicts two possible magnetic structures which allow a weak-ferromagnetic moment. In the critical region magnetic fluctuations will occur between these two possible states giving rise to the XY-like behaviour. Slight distortions in the crystal structure in comparison to $\text{KMnPO}_4 \cdot \text{H}_2\text{O}$ change the critical behaviour towards Ising-like behaviour and β decreases following the trend as outlined by Bramwell and Holdworth 50.

References

1. L.J. de Jongh and A.R. Miedema, *Adv. Phys.* **23**, 1-260 (1974).
2. R.L. Carlin, *Magnetochemistry*, Springer Verlag, Berlin (1986).
3. R.D. Willett, D. Gatteschi and O. Kahn, *Magneto-Structural Correlations in Exchange Coupled Systems*. NATO ASI C140, Riedel Dordrecht (1983).
4. P. Delheas and M. Drillon, *Organic and Inorganic Low-dimensional Crystalline Materials*. NATO ASI B168, Plenum Press New York (1986).
5. R.L. Carlin and A.J. van Duyneveld, *Magnetic Properties of Transition Metal Compounds*. Springer Verlag Berlin (1977).
6. H. Megaw, *Crystal Structures, A working Approach*. W.B. Saunders Philadelphia (1973).
7. E. Legrand and R. Plumier, *Phys. Stat. Sol.* **2**, 317 (1962); *J. Phys.* **23**, 474 (1962).
8. G.L. McPherson, T.J. Kistenmacher and G.D. Stucky, *J. Chem. Phys.* **52**, 815 (1970).
9. J.G. Bednorz and K.A. Muller, *Z. Phys.* **B64**, 189 (1986).
10. S. Chakraborty, B.I. Halperin and D.R. Nelson, *Phys. Rev. Lett.* **60**, 1057 (1988) and *Phys. Rev.* **B39**, 2344 (1989). S.J. Clarke, A. Harrison, T.E. Mason, G.J. McIntyre and D. Visser, *J. Phys: Cond. Matter* **4**, L71 (1992).

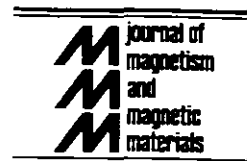
11. D. Babel, Z. Anorg. Allgem. Chem. **369**, 117 (1969).
12. D. Visser. Doctoraal Thesis, Rijks Universiteit Leiden (1979).
13. F.W. Sears and G.L. Salinger, *Thermodynamics, Kinetic Theory and Statistical Thermodynamics*. Addison and Wesley (1975).
14. L.E. Reidel, *A Modern Course in Statistical Physics*. Edward Arnold Publishers (1980).
15. R.B. Griffiths and J.C. Wheeler, Phys. Rev. A **2**, 1074 (1970).
16. H.E. Stanley, *Introduction to Phasetransitions and Critical Ordering*. Oxford University Press (1971); L.P. Kadanoff, *Phasetransitions and Critical Phenomena*, Vol.5, ed. C. Domb and M.S. Green, Academic Press (1972-77).
17. S.K. Ma. Rev. Mod. Phys. **46**, 597 (1974); S.K. Ma, *Modern Theory of Critical Phenomena*. W.A. Benjamin Inc. Massachusetts (1976).
18. K.G. Wilson and J.B. Kogut, Phys. Reports **12C**, 75 (1974).
19. K.P. Sinha And N. Kumer, *Interactions in Magnetically Ordered Solids*. Oxford University Press (1980).
20. M. Steiner, see reference 4, p 63 (1987).
21. P.-A. Lindgard, *Topics in Current Physics 6: Neutron Diffraction*, p 197. ed. H. Dachs. Springer Verlag Berlin (1978).
22. M. Fisher, Rept. Prog. Phys. **XXX** (part II), 615 (1967).
23. C. Kittel, *Introduction to Solid State Physics*. 5th edition, John Wiley (1976).
24. P. Pfeuty and G. Toulouse, *Introduction to the Renormalisation Group and Critical Phenomena*. John Wiley (1978).
25. H.E. Stanley, *Phasetransitions and Critical Phenomena*. Vol.2 & 3, ed. C. Domb and M.S. Green, Academic Press (1972-77).
26. J.P. Renard, see reference 4, p 125 (1987).
27. S.T. Bramwell and P.C.W. Holdsworth, J. Phys.: Condens. Matter **5**, L53 (1993); Phys. Rev. **B49**, 8811 (1994).
28. L.J. de Jongh and H.E. Stanley, Phys. Rev. Lett. **36**, 817 (1976).
29. B.I. Halperin and P.C. Hohenberg, Phys. Rev. **177**, 952 (1969).
30. K.G. Wilson, Phys. Rev. **B4**, 3197 (1971).
31. S.W. Lovesey, *Theory of Neutron diffraction from Condensed Matter*, Vol. 1 & 2, Oxford University Press (1986).
32. M.P. Schulhof, P. Heller, R. Nathans and A. Linz, Phys. Rev. **B1**, 2304 (1970).
33. A. Tucciarone, H.Y. Lau, L.M. Corliss, A. Delapalme and J. Hastings, Phys. Rev. , 3206 (1971).
34. J. Als-Nielsen, *Phasetransitions and Critical Phenomena*. Vol.5a, ed. C. Domb and M.S. Green, Academic Press (1972-77).

-
35. P.-A. Lindgard, J. Phys. **C8**, L178 (1975); Physica **120B**, 190 (1983). J. Villain, J. de Phys. **35**, 27 (1974).
 36. J.M. Kosterlitz and D.J. Thouless, J. Phys. **C6**, 1181 (1973).
 38. J. Villain, Z. Phys. **B33**, 31 (1979).
 37. A. Harrison, D. Visser, P. Day, W. Knop and M. Steiner, J. Phys. **C19**, 6811 (1986).
 39. H. Kawamura, J. Appl. Phys. **63**, 3086 (1988); J. Phys. Soc. Japan **58**, 584 (1989); **59**, 2305 (1990).
 40. P. Azaria, B. Delamotte and T. Jolicoeur, Phys. Rev. Lett. **64**, 3175 (1990).
 41. H. von Lohneysen, D. Beckmann, J. Wosnitza and D. Visser, J. Magn. Magn. Mat. **140-144**, 1469 (1990); B. D. Gaulin. Experimental Studies of Geometrically-Frustrated Magnetic systems in *Magnetic Systems with Competeting Interactions*, ed. H. Diep. World Scientific Publishing Co. (1994)
 42. H. Weber, D. Beckmann, J. Wosnitza, H. von Lohneysen and D. Visser, Int. J. Mod. Phys. **B9**, 1387 (1995).
 43. M.L. Plumer, H. Kawamura and A. Caillé, Phys. Rev. **B43**, 13786 (1991).
 44. D. Visser, Th. Zeiske and L. Weiss, *BENSC Experimental Report 1994*, HMI - B525, p 64 (1994).
 45. B.D. Gaulin. T.E. Mason, M.F. Collins and J.F. Larese, Phys. Rev. Lett. **62**, 1380. (1992).
 46. D. Visser, A.R. Monteith, A.Y. Bargawi and Th. Zeiske, *BENSC Experimental Report 1994*, HMI - B525, p 68. (1994).
 47. N.D. Mermin and H. Wagner, Phys. Rev. Lett. **17**, 1133 (1966).
 48. H.Q. Lin, D.K. Campbell and C.Y. Pan, J. Appl. Phys. **73**, 6102 (1993).
 49. D.P. Landau, J. Appl. Phys. **73**, 6091 (1993).
 50. S.T. Bramwell and P.C.W. Holdsworth, J. Appl. Phys. **73**, 6093 (1993).
 51. J.A.J. Basten, *Multicritical Points in Weakly Anisotropic Magnetic Systems*. Doctoral thesis, T.U. Eindhoven (1975).
 52. A.R. Monteith, *Magnetic Excitations in the Quasi One-Dimensional Singlet Groundstate Systems CsFeBr₃ and CsFeCl₃ under Hydrostatic Pressure*. MPhil. thesis, Loughborough University (1996).

Chapter 2.

Magnetic ordering in induced magnetic moment systems

Journal of Magnetism and Magnetic Materials 116 (1992) 80–82
North-Holland



Magnetic ordering in the quasi-one-dimensional induced moment ferro- and antiferromagnets AFeX₃ *

D. Visser ^a and A. Harrison ^b

^a Department of Physics, Loughborough University of Technology, Loughborough LE11 3TU, UK

^b Inorganic Chemistry Laboratory, University of Oxford, South Parks Road, Oxford OX1 3QR, UK

The ternary halide hexagonal perovskites AFeX₃ shows a local singlet ground state behaviour. Depending on the strength of the exchange constants and the single-ion anisotropy, these systems will show an induced magnetic moment. In this paper we discuss the magnetic ordering behaviour in this series of compounds and the effect on the magnetic ordering due to an applied magnetic field.

1. Introduction

The hexagonal perovskites AFeX₃ (A = Cs, Rb, Tl, NH₄ and X = Cl, Br (and I)) show a magnetic ordering behaviour which is strongly dependent on the chemical composition and the subsequent small changes in their crystal structure [1,2]. The quasi one-dimensional structure of the hexagonal perovskite (space group P6/3mmc) induces a trigonal distortion in the face-sharing FeX₆⁴⁻ octahedra situated along the *c*-axis. The combination of the cubic component of the ligand field and the spin-orbit coupling λ on the ⁵D term of the Fe²⁺ ion gives a $J = 1$ ground state which is further split by the trigonal component, Δ , of the ligand field into a low-lying doublet state and a singlet ground state.

These systems can be described with the following effective Hamiltonian with $S = 1$:

$$H = -2J \sum_i S_i \cdot S_{i+1} - J' \sum_{i \neq j} S_i \cdot S_j + A \sum_i (S_i^z)^2 - g\mu_B m H_{\text{ex}}^z \sum_i S_i^z. \quad (1)$$

J and J' are the intrachain and interchain superexchange parameters, respectively. A , whose value is positive, denotes the energy gap between the singlet ground state $m = 0$ and the degenerate doublet states $m = \pm 1$, while H_{ex}^z represents an externally applied magnetic field.

The Hamiltonian (1) provides in the absence of a magnetic field two different domains:

(a) For $T \rightarrow 0$ and $A < 8|J| + 12|J'|$ the system has an *XY* character and is magnetically ordered, e.g. the AFeX₃ compounds with A = Rb, Tl, NH₄.

(b) For $T \rightarrow 0$ and $A > 8|J| + 12|J'|$ the system has a singlet ground state and consequently does not order magnetically. The application of an external field along the *c*-axis (*z*-direction) induces Zeeman splitting of the $m = \pm 1$ states and introduces a long-range magnetic ordering at sufficiently high magnetic fields, e.g. the CsFeX₃ salts.

2. Magnetic ordering in AFeCl₃

The intrachain superexchange interaction in the AFeCl₃ compounds is ferromagnetic. This results in strong magnetic dipolar interactions at low temperatures and has a large influence on the magnetic ordering behaviour [3,4]. Normally the antiferromagnetic intrachain superexchange

Correspondence to: Dr. D. Visser, Department of Physics, Loughborough University of Technology, Loughborough LE11 3TU, UK.

* Paper presented at the International Conference on Magnetism (ICM '91), Edinburgh, Scotland, 2–6 September 1991.

D. Visser, A. Harrison / Ordering in ferro- and antiferromagnets AFeX_3

interaction within the triangular lattice of the B ions in the *ab* plane of the hexagonal perovskite gives rise to a frustrated 120° type spin structure. A magnetic Bragg reflection appears at the K point, $Q(\frac{1}{3}\frac{1}{3}0)$, of the Brillouin zone. The magnetic dipolar ordering tends towards M-point ordering at $Q(\frac{1}{2}00)$. In RbFeCl_3 one finds a delicate interplay between dipolar and superexchange forces resulting in a magnetic ordering behaviour which takes place first by adopting a helical spin structure; the IC_1 phase with the satellites positioned on the K–M line of the Brillouin zone, changing over into a sinusoidal one; the IC_2 phase with the satellites on the K– Γ line and finally locking into the 120° type triangular spin array; the C phase at the K point [5]. TiFeCl_3 undergoes structural phase transitions which finally results in a magnetic lattice in which the Fe^{2+} ions are arranged similar to those of the low-temperature phase of RbFeBr_3 (space group $\text{P6}_3\text{cm}$) [6]. The inequivalence in the interchain superexchange interactions causes the magnetic structure to stabilise in the helical IC_1 phase with a temperature-independent k vector. The value for $k = (0.3200.3200)$ shows that this magnetic structure is nearly commensurate with the C phase. The details of the nuclear structure of ND_4FeCl_3 are strongly influenced by the rotation/librational behaviour of the NH_4^+ group. Thermodiffraction data and DSC measurements showed that a structural phase transition occurs from hindered rotational to free rotor behaviour at about 400 K. At about 35 K a further structural phase transition takes place related to the ordering of the NH_4^+ groups. Both phases are strongly related to the hexagonal perovskite structure at $T > 400$ K. At low temperatures magnetic scattering is detected around positions related to $Q(\frac{1}{3}\frac{1}{3}0)$ of the simple hexagonal lattice. This relates to a K point type ordering.

Long-range magnetic ordering can be induced in CsFeCl_3 by applying a magnetic field along the *c*-axis [7]. At $T = 0.7$ K and $H = 3.7$ T a similar behaviour has been observed as in CsFeBr_3 . However, the magnetic field changes the magnetic domain distribution while the helical magnetic (IC_1) phase represents only a short-range magnetic order. A similar short-range ordered

phase has been observed in TiFeCl_3 at $2.0 \text{ K} < T < 2.5 \text{ K}$.

3. Magnetic ordering in AFeBr_3 and CsFeI_3

The AFeBr_3 compounds have an antiferromagnet intrachain superexchange interaction, thus the magnetic dipolar exchange interactions are less important and one expects the 120° type magnetic ordering. RbFeBr_3 undergoes a structural phase transition at $T_{\text{ph}} = 108$ K which causes one of the linear chains to move slightly along the *c*-axis [6]. This causes an inequivalence of superexchange pathways in the basal plane which results in a release of the frustration. The magnetic ordering in this case involves first a partially ordered phase in which one out of the three chains in the magnetic unit cell is disordered. Finally at $T = 2.0$ K the full magnetic ordering is built up in the form of a modified triangular spin structure [8]. ND_4FeBr_3 undergoes a similar magnetic ordering process; however, the magnetic ordering does not take place at the H point, $Q(\frac{1}{3}\frac{1}{3}1)$ but at the A point, $Q(\frac{1}{2}01)$ of the BZ. This has been related to a larger distortion of the low-temperature crystal structure of ND_4FeBr_3 [9].

Polymorphic behaviour has been reported for TiFeBr_3 [10]. The orthorhombic NH_4CdCl_3 type structure as well as the hexagonal perovskite structure can be obtained. The hexagonal phase shows a structural phase transition at 657 K. The low-temperature phase has the same crystal structure as the low-temperature phase of RbFeBr_3 . No information is available on the magnetic ordering, but a similar behaviour to that of RbFeBr_3 is expected.

A powder neutron diffraction study of CsFeI_3 at 4.2 K [11] shows that this compound is magnetically ordered in a 120° type triangular magnetic structure. From magnetic susceptibility studies a $T_N = 10(1)$ K was deduced. CsFeI_3 is the only AFeI_3 hexagonal perovskite which crystal structure is stable. For smaller A^+ ions a A_2FeI_4 phase will be formed.

CsFeBr_3 is a singlet ground state system and does not show magnetic order for $T \rightarrow 0$. How-

Table 1
Magnetic phases and phase transition temperatures of the hexagonal AFeX_3 ternary halides

Compound	T_N	Comment	Reference
CsFeCl_3	0.7	H induced IC_1 at $H = 3.8$ T IC_2 at $H = 3.94$ T C, K point at $H = 4.55$ T	[7]
RbFeCl_3	2.50 (5) 2.35 (5) 1.95 (5)	IC_1 IC_2 C, K point	[5]
TiFeCl_3	2.05 (3)	IC_1	this work
ND_4FeCl_3	1.7 (2)	M point	this work
CsFeBr_3	H induced 1.65 (5)	C, H point at $H = 3.9$ T	this work
RbFeBr_3	5.5 (5) 2.0 (1)	partially ordered modified C, H point	[6] this work
TiFeBr_3		like RbFeBr_3	
ND_4FeBr_3	4.8 (2) 2.8 (2)	partially ordered A point	[9]
CsFeI_3	10 (1)	C, H point	[11]

ever, magnetic ordering can be induced as in CsFeCl_3 by applying a magnetic field along the c -axis. In comparison to CsFeCl_3 , CsFeBr_3 orders at higher temperatures and at lower magnetic fields than CsFeCl_3 . This is directly related to slightly different anisotropy and exchange values. Only the long-range magnetic order in this case involves the 120° type magnetic structure. A summary of the magnetic phases and ordering temperatures is given in table 1.

4. The effect of a magnetic field, $H \parallel c$, on the ordered magnetic phases of the AFeX_3 compounds

The magnetic ordering in RbFeCl_3 in the presence of a magnetic field applied along the c -axis was studied by Wada et al. [5]. In this case the magnetic field enhances the exchange field. Consequently the factors which induce the incommensurate ordering become less important which results finally in the formation of the commensurate 120° type C phase. This effect is well demonstrated in the random singlet magnetic ground state system $\text{Rb}_{1-x}\text{Cs}_x\text{FeCl}_3$ [12].

For the antiferromagnetic linear chain RbFeBr_3 , the application of a magnetic field up to 5 T

has little effect on T_N . However, the transition temperature from the partially ordered phase to the modified triangular structure is strongly influenced and increases rapidly. This indicates that the applied magnetic field couples with the non-magnetically ordered sites in the partially ordered phase and induces a magnetic moment, likewise magnetic ordering is induced in the singlet ground state compounds.

A general picture of the magnetic phase diagrams of the AFeX_3 compounds in an applied magnetic field has been obtained by specific-heat studies [13].

The new information provided in this paper has been obtained from powder and single-crystal neutron diffraction experiments carried out at the Institut Laue-Langevin, Grenoble and the Hahn Meitner Institut, Berlin. The full details of these experiments will be published elsewhere.

Acknowledgements

The authors wish to thank the UK SERC for financial support and the Institut Laue-Langevin for providing the neutron beam facilities.

References

- [1] D. Visser and A. Harrison, *J. de Phys.* 49 (1988) C8-1467.
- [2] H. Yoshizawa, W. Kozukue and H. Hirakawa, *J. Phys. Soc. Jpn.* 49 (1980) 144.
- [3] H. Shiba, *Solid State Commun.* 41 (1982) 511.
- [4] N. Suzuki, *J. Phys. Soc. Jpn.* 52 (1983) 1383.
- [5] N. Wada, K. Ubukoshi and H. Hirakawa, *J. Phys. Soc. Jpn.* 51 (1982) 283.
- [6] M. Eibschutz, G.R. Davidson and D.E. Cox, *AIP Conf. Proc.* 18 (1973) 386.
- [7] W. Knop, M. Steiner and P. Day, *J. Magn. Magn. Mater.* 31-34 (1983) 1033.
W. Knop, Thesis, TU Berlin (1985) unpublished.
- [8] N. Suzuki and M. Shirai, *Physica B* 136 (1986) 346.
D. Visser, B. Dorner and A. Harrison, *J. Appl. Phys.* 69 (1991) 6232.
- [9] A. Harrison, C.V. Stager and D. Visser, *J. Appl. Phys.* 69 (1991) 5998.
- [10] N. Jouini, L. Guen and M. Tournoux, *Mater. Res. Bull.* 17 (1982) 1421.
- [11] H.W. Zandbergen, Thesis, University of Leiden (1981) unpublished.
- [12] A. Harrison, D. Visser, P. Day, W. Knop and M. Steiner, *J. Phys. C* 19 (1986) 6811.
- [13] T. Haseda, N. Wada, M. Hata and K. Amaya, *Physica B* 108 (1981) 841.

J. Phys.: Condens. Matter 1 (1989) 733–754. Printed in the UK

Magnetic ordering effects in the random mixed one-dimensional ferromagnet–antiferromagnet system $\text{RbFeCl}_3-x\text{Br}_x$

A Harrison and D Visser

Oxford University, Inorganic Chemistry Laboratory, South Parks Road, Oxford
OX1 3QR, UK

Received 28 April 1988, in final form 3 August 1988

Abstract. Elastic neutron scattering experiments were performed on single crystals of the solid solution $\text{RbFeCl}_{3-x}\text{Br}_x$ ($x = 0.03, 0.06, 0.15, 1.0, 2.56, 2.76, 2.85$ and 2.94) to study the magnetic ordering behaviour and the magnetic phase diagram of this mixed pseudo-one-dimensional ferromagnetic–antiferromagnetic system. Small amounts of dopant destroy the magnetic long-range order of the pure parent compounds, RbFeCl_3 and RbFeBr_3 . On the RbFeCl_3 side of the phase diagram the magnetic correlations appear finite for x as small as 0.03 . The periodicities of these correlations are similar to those of the incommensurate and commensurate magnetic phases of pure RbFeCl_3 . On the RbFeBr_3 side of the phase diagram the ordering vector remains at the H point ($Q = (\frac{1}{2} \frac{1}{2} 1)_N$). At an intermediate composition ($x = 1.0$) there are no detectable one-dimensional ferro- or antiferromagnetic correlations down to a temperature of 1.3 K.

1. Introduction

1.1. Engineering insulating spin glasses

Early experimental studies of spin-glass behaviour concentrated on metallic alloys. The combination of quenched spatial disorder and frustration required to impart spin-glass properties to a material (Toulouse 1977, Sherrington 1983) was produced by diluting magnetic atoms in a non-magnetic matrix and exploiting the dependence of the sign of the RKKY exchange constant on the inter-atomic separation. More recently, attention has turned to insulators as bases for spin-glass properties. The short-range nature of the superexchange mechanism allows one to predict the most favourable conditions for spin-glass behaviour using a knowledge of the topology of the important exchange pathways and of the signs of the NN (nearest-neighbour) (and sometimes also the NNN (next-nearest-neighbour)) magnetic exchange constants (Villain 1979).

The following categories emerge:

(i) A solid solution of a NN ferromagnet with a NN antiferromagnet, e.g. $\text{Rb}_2\text{Cr}_{1-x}\text{Mn}_x\text{Cl}_4$ (Katsumata *et al* 1982, Katsumata 1986, Munninghof *et al* 1984), $\text{K}_2\text{Cu}_x\text{Mn}_{1-x}\text{F}_4$ (Kimishima *et al* 1986) and $\text{Co}_{1-x}\text{Mn}_x\text{Cl}_2 \cdot 2\text{H}_2\text{O}$ (Defotis and Mantis 1986).

(ii) Diamagnetically diluted frustrated magnets where the host material has (a) NN

A Harrison and D Visser

antiferromagnetic exchange with an odd number of bonds in some of the loops of exchange pathways, e.g. spinels (Hubsch *et al* 1978) and the pyrochlores CsMnFeF_6 (Bevaart *et al* 1983) or CsNiFeF_6 (Pappa *et al* 1984); (b) NN and NNN antiferromagnetic exchange, e.g. the pseudo-one-dimensional (1D) antiferromagnet FeMgBO_4 (Wiedenmann *et al* 1981, 1983); and (c) NN ferromagnetic and NNN antiferromagnetic exchange, e.g. $\text{Eu}_{1-x}\text{Sr}_x\text{S}$ (Maletta 1982).

In some materials it is believed that spin-glass properties co-exist with long-range or medium-range magnetic order to form a 'semi spin glass'. The predictions of Villain concerning the sort of magnets in which properties may be found have been realised in a number of materials (Brand *et al* 1985, Wong *et al* 1985; but see also Maletta and Felsch 1980, Maletta *et al* 1982, Aeppli *et al* 1982).

Finally, it should be noted that magnetic properties characteristic of a spin glass may be seen in materials that do not have competing magnetic exchange interactions but have random magnetic anisotropy, e.g. $\text{Dy}(\text{VO}_4)_{1-x}(\text{PO}_4)_x$ (Kettler *et al* 1981) and the metallic alloys a-DyFeB (Sellmyer and Nafis 1986).

In this paper we present a single-crystal neutron diffraction study of the mixed ferromagnet-antiferromagnet system $\text{RbFeCl}_3-x\text{Br}_x$. Previous workers (Bontemps *et al* 1982, Visser and Harrison 1982) studied these materials as potential insulating spin glasses, using a combination of magnon side-band and magnetic circular dichroism measurements and powder neutron diffraction. No conclusive evidence was found for spin-glass behaviour. The present study gives a classification of the magnetic structure of $\text{RbFeCl}_3-x\text{Br}_x$ over the full compositional range and at temperatures down to 1.3 K. In order to present clearly the reasons behind the experimental procedure it is necessary to consider the particular magnetic properties of the parent compounds, RbFeCl_3 and RbFeBr_3 .

1.2. Properties of AFEX_3 magnets

Both RbFeCl_3 and RbFeBr_3 adopt the hexagonal perovskite structure in which chains of face-sharing FeX_6^{4-} octahedra lie parallel to the crystal c axis. The chains are separated by Rb ions in twinned cuboctahedra (12-fold coordination) which are also stacked in a linear fashion along the c axis. The space group is $\text{P6}_3/\text{mmc}$. At 108 K (Visser 1988b) RbFeBr_3 undergoes a phase transition in which two-thirds of the Fe chains (A sites) move by approximately 0.5 Å out of the basal plane, forming a honeycomb lattice (Eibschutz *et al* 1973, Adachi *et al* 1983). The remaining one-third (B sites) lie in a triangular array. The new crystal structure is that of KNiCl_3 at room temperature (Visser *et al* 1980) with space group $\text{P6}_3\text{cm}$ and the cell parameters a and b enlarged by a factor of $\sqrt{3}$. ABX_3 crystals undergoing phase transitions of this sort have been shown to possess structural disorder in the $\text{P6}_3\text{cm}$ phase (Visser and Prodan 1980). The structural parameters of RbFeCl_3 and RbFeBr_3 are given in table 1. In the case of RbFeBr_3 at 20 K and 1.5 K the averaged value of the positional parameter, x_{Br} , is given to aid a direct comparison with RbFeCl_3 .

By virtue of the chain structure the intra-chain exchange constant J_1 is an order of magnitude greater than the inter-chain exchange constant J_2 , giving rise to pseudo-one-dimensional magnetic behaviour. In both cases J_2 is antiferromagnetic and induces three-dimensional magnetic long-range order at low temperatures. However, J_1 is very sensitive to the angle α of the intra-chain exchange constant bridge Fe-X-Fe. The bromide has antiferromagnetic J_1 whereas the less covalent chloride, with a larger value

Magnetic ordering in $\text{RbFeCl}_3-x\text{Br}_x$

Table 1. Structural parameters for RbFeCl_3 and RbFeBr_3 as determined by powder neutron diffraction.

Compound	T (K)	a (Å)	c (Å)	$x(\text{Cl}, \text{Br})$	α (deg)	Space group	Source
RbFeCl_3	293.0	7.100	6.048	0.1610	75.01	$\text{P6}_3/\text{mmc}$	^a
	4.2	6.933	5.954	0.1628	74.09	$\text{P6}_3/\text{mmc}$	^b
	1.5	6.933	5.954	0.1628	74.09	$\text{P6}_3/\text{mmc}$	^a
RbFeBr_3	300.0	7.422	6.304	0.1600	74.28	$\text{P6}_3/\text{mmc}$	^a
	150.0	7.380	6.28	0.1643	—	$\text{P6}_3/\text{mmc}$	^c
	20.0	12.78	6.28	0.1700 ^d	—	$\text{P6}_3\text{cm}$	^c
	1.5	12.72	6.263	0.1683 ^d	72.45	$\text{P6}_3\text{cm}$	^a

^a Visser and Harrison (1982).
^b Visser *et al* (1985).
^c Eibschutz *et al* (1973).
^d This value is the average of the x parameter for the different halide positions in the $\text{P6}_3\text{cm}$ space group.

of α , has ferromagnetic J_1 . The change in the sign of J_1 has been attributed (Lines and Eibschutz 1975, Eibschutz *et al* 1975) to an increase in the antiferromagnetic 'kinetic' component of superexchange relative to the ferromagnetic 'potential' component.

There are two other important forms of balance between competing magnetic effects in these AFexX_3 magnets.

(i) The cubic component of the ligand field acts on the ^5D free-ion term of Fe^{2+} to give a ground singlet ($m_J = 0$) and an excited doublet ($m_J = \pm 1$). For an isolated ion the doublet lies at an energy D above the singlet state, but as a magnetic field is applied parallel to the c axis, or through the influence of the inter-ion perturbation provided by superexchange, the excited doublet is mixed into the singlet ground state. In the absence of an applied magnetic field the size of the induced moment depends on the ratio D/J_Q , where J_Q is the magnetic exchange field experienced at a single ion when the configuration of moments has the ordering vector Q . For low values of D/J_Q the induced moment may be sufficiently large for magnetic long-range order to occur at low temperatures. Thus, RbFeBr_3 and RbFeCl_3 show magnetic long-range order at 5.5 and 2.5 K respectively. The caesium salts, with larger unit cells and smaller exchange constants, show no magnetic long-range order down to 80 mK for CsFeCl_3 (work reported by D P E Dixon in 1981 and cited by Baines 1983) and 69 mK for CsFeBr_3 (Visser 1988a). When a magnetic field is applied along the crystal c axis of CsFeCl_3 three-dimensional magnetic long-range order is observed (Knop *et al* 1983) which is similar to that seen in RbFeCl_3 (Wada *et al* 1982).

The magnetic exchange parameters for RbFeCl_3 and RbFeBr_3 are presented in table 2. A survey of the values available in the literature shows them to be very dependent on the type of measurement made and the model used to interpret the data. Thus, we have only used values which have been determined in the most reliable fashion for both compounds. The magnetic susceptibility measurements of Lines and Eibschutz (1975) and of Eibschutz *et al* (1975), interpreted by Lines' correlated effective field (CEF) approximation (Lines 1974), and inelastic neutron scattering measurements, interpreted using the CEF model and Suzuki's dynamical CEF approximation (DCEFA) (Suzuki 1983, Harrison and Visser 1988a), are suitable for this purpose.

A Harrison and D Visser

Table 2. Magnetic exchange parameters and single-ion anisotropies calculated by previous workers for RbFeCl₃ and RbFeBr₃. The exchange parameters all refer to an effective spin $S' = 1$ Hamiltonian and all energies are given in meV. The source of the data is given as a superscript letter which tallies with the references below the table. The work of Lines and Eibschutz (1975) and of Eibschutz *et al* (1975) involved the application of the Lines (1974) CEF model to magnetic susceptibility data. The other values were derived from inelastic neutron scattering data using the Suzuki (1983) DCEFA model.

Parameter	RbFeBr ₃	RbFeCl ₃
J_1^\perp	-0.525 ^a	0.325 ^c
	-0.394 ^b	0.405 ^d
J_1^\parallel	-0.35 ^a	0.216 ^c
	-0.411 ^b	0.527 ^d
J_2	-0.008 ^a	-0.008 ^c
J_2^\perp	-0.046 ^b	-0.034 ^d
J_2^\parallel	-0.079 ^b	-0.045 ^d
D	1.0-1.1 ^a	1.0-1.1 ^c
	1.96 ^b	1.92 ^d

^a Eibschutz *et al* (1975). ^c Lines and Eibschutz (1975).
^b Harrison and Visser (1988a). ^d Suzuki (1983).

(ii) The one-dimensional ferromagnetic intra-chain correlations in RbFeCl₃ give rise to an inter-chain magnetic dipole-dipole interaction γ of significant magnitude relative to the intra-chain superexchange constant J_2 . The former alone would give rise to a free-energy minimum at the M point of the reciprocal lattice ($Q = (\frac{1}{2} 0 0)_N$) and the latter at the K point ($Q = (\frac{1}{3} \frac{1}{3} 0)_N$) (Shiba 1982, Shiba and Suzuki 1983). Competition between these forces leads to the formation of two incommensurate magnetic phases, IC₁ and IC₂, on cooling from the paramagnetic phase to 2.5 and 2.35 K respectively. At 1.95 K a transition to the commensurate 120° configuration occurs (Wada *et al* 1982). The IC phases are characterised in neutron scattering by satellite Bragg peaks centred around the K point, on the KM lines (IC₁ and IC₂ phases) and on the KT lines (IC₂ phase only). Similar phases have been observed in CsFeCl₃ when a magnetic field is applied along the crystal *c* axis (Knop *et al* 1983) and in TlFeCl₃ below 2.02 K (Visser and Knop 1988).

1.3. Structural and magnetic properties of RbFeCl_{3-x}Br_x

The search for spin-glass behaviour in the mixed ferromagnet-antiferromagnet RbFeCl_{3-x}Br_x followed the theoretical work of Medvedev and Rumyantsev (1978), Chen and Lubensky (1977) and Fishman and Aharony (1979). These theorists proposed two schematic phase diagrams to describe the magnetic structure of alloys formed by mixing a nearest-neighbour ferromagnet with a nearest-neighbour antiferromagnet. At intermediate compositions and low temperatures the formation of either a paramagnetic phase (figure 1(a)) or a spin-glass phase (figure 1(b)) is envisaged.

Previous x-ray and neutron powder diffraction measurements (Visser and Harrison 1982) showed that the components of RbFeCl_{3-x}Br_x form a single solid solution. The cell parameters of the mixed compounds at room temperature are those of a hexagonal perovskite with space group P6₃/mmc. The neutron diffraction data taken at 1.3 K show that compounds of composition $x > 2.0$ undergo a phase transition similar to that of pure RbFeBr₃: the unit-cell parameters *a* and *b* enlarge by a factor of $\sqrt{3}$, and the space

Magnetic ordering in $\text{RbFeCl}_{3-x}\text{Br}_x$

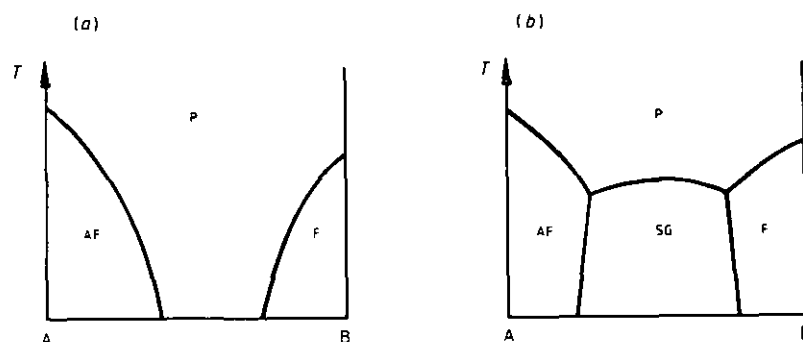


Figure 1. Schematic phase diagram for an alloy of an antiferromagnet (A) with a ferromagnet (B), depicting the possibility of the formation of (a) a paramagnetic phase (P) or (b) a spin-glass phase (SG) at intermediate compositions. The calculations assume single nearest-neighbour exchange linkages (Fishman and Aharony 1979).

group changes to $\text{P6}_3\text{cm}$. There was no observable magnetic long-range order down to 1.3 K for compositions with x as low as 0.3 or as high as 2.7.

Bontemps *et al* (1982) performed magneto-optical measurements on $\text{RbFeCl}_{3-x}\text{Br}_x$ and concluded that for $x = 0.04, 0.2$ and 1.0 the intra-chain exchange constant was not substantially modified relative to that found in the pure chloride. The sample with $x = 2$, however, behaved in a manner which could not be described simply as a mole-fraction-weighted average of the parent compounds' behaviour. This was attributed to extensive magnetic disorder in RbFeClBr_2 . The position and intensity of the optical absorption bands of $\text{RbFeCl}_{3-x}\text{Br}_x$ changed gradually with composition between the values measured for the pure compounds. This also indicates that $\text{RbFeCl}_{3-x}\text{Br}_x$ behaves as a solid solution.

The compounds RbFeCl_3 and RbFeBr_3 differ in two respects from the end-members of the phase diagrams drawn up by Fishman and Aharony (1979). First, the induced-moment nature of the compounds introduces another possible phase to the diagram—namely a singlet ground-state phase. Secondly, the nature of the superexchange between two Fe^{2+} ions connected by a mixture of halide ions is unknown at the microscopic level. The average macroscopic exchange is known and is described below. It is likely that for a wide range of compositions there will be a distribution of intra-chain exchange constants ranging from positive to negative values. Some spin-glass character is expected so long as the impurities do not disrupt the exchange field to such an extent that the induced moments are destroyed. Consequently, spin-glass behaviour is more likely on the RbFeBr_3 side of the phase diagram, closer to the parent compound with larger induced moment.

The bulk magnetic behaviour of the compounds $\text{RbFeCl}_{3-x}\text{Br}_x$ ($x = 1.0, 1.5, 2.0$ and 3.0) has been studied at the Gorlaeus Laboratories, University of Leiden, using single-crystal DC magnetic susceptibility measurements over the temperature range 2–120 K and by magnetisation measurements at 2 K in fields of up to 5.6 T (Visser 1988a).

The magnetic susceptibility behaviour is similar to that measured in the pure compounds RbFeCl_3 (Eibschutz *et al* 1975) and RbFeBr_3 (Lines and Eibschutz 1975). The susceptibility perpendicular to the c axis, χ^\perp , was found to vary linearly with composition over the range $1.0 < x < 3.0$. For all the mixed compounds no evidence has been found for magnetic long-range order. The magnetic susceptibility along the c axis, χ^\parallel , showed a maximum at T_{max} for all compositions; the position of this maximum increased from

A Harrison and D Visser

11 to 13.5 K for $x = 0$ to $x = 3.0$. For compositions $1.5 < x < 3.0$ the overall magnetic exchange was found to be antiferromagnetic as indicated by the plots of $1/\chi^1$ against T . The sign of the exchange for $x = 1.0$ could not be determined with much confidence, so this compound appears to lie near the crossover from ferro- to antiferromagnetic intra-chain exchange.

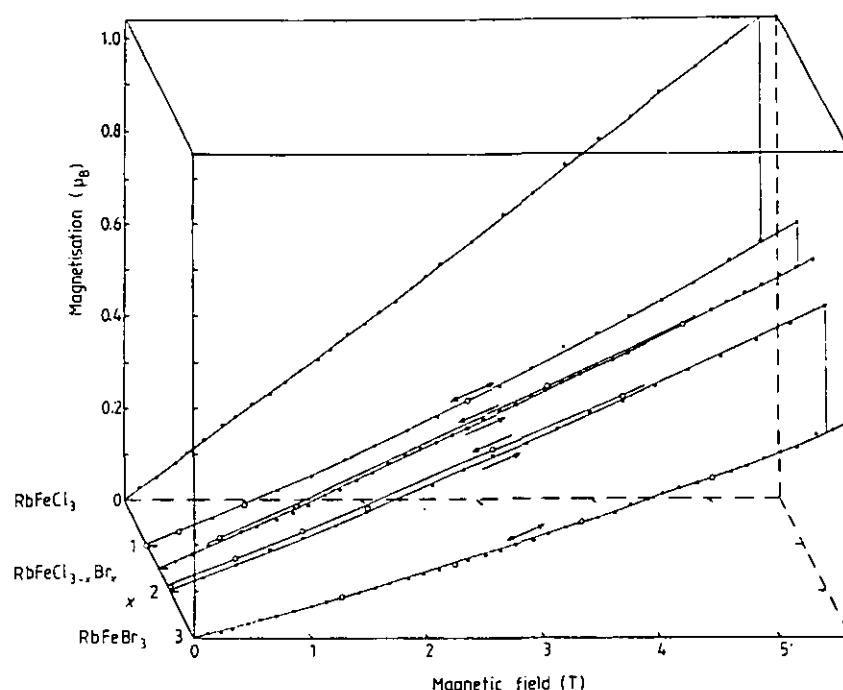


Figure 2. Magnetisation curves for the mixed system $\text{RbFeCl}_{3-x}\text{Br}_x$ with the field applied parallel to the crystal c axis at 2.0 K for various compositions ($x = 0, 1, 2$ and 3). The full circles denote measurements taken as the field was increased and the open circles those taken on reducing the field. The lines drawn through the points merely provide a guide to the eye.

The magnetisation data at 2.0 K with a magnetic field of 5.6 T show that the components of the induced moment parallel and perpendicular to the crystal c axis vary smoothly with composition over the range $1.0 < x < 3.0$. The magnetisation curves show remanent magnetic behaviour for the compound RbFeClBr_2 and to a lesser degree for the compound $\text{RbFeCl}_{1.5}\text{Br}_{1.5}$ (figure 2). No remanent effects could be detected at lower values of x or for pure RbFeBr_3 or RbFeCl_3 . Similar remanent behaviour has been observed in a wide range of spin-glass or semi-spin-glass compounds (Hubsch and Gavaille 1982, Grest and Soukoulis 1983).

Thus, we have performed single-crystal neutron diffraction on samples with *higher* ($x > 2.7$) or *lower* ($x < 0.3$) values of x than used previously to study the effect of small amounts of dopant on the magnetic structure of the pure compounds. In addition, we have measured the diffuse scattering from samples of intermediate compositions to try to deduce the nature of any short-range magnetic correlations.

Magnetic ordering in $\text{RbFeCl}_{3-x}\text{Br}_x$

2. Experimental details

Stoichiometric amount of 'ultrapure'-grade (purity >99.99%) RbCl and RbBr, obtained from Alfa Inorganics, Ventron Ltd, were melted with sublimed FeCl_2 and FeBr_2 in sealed silica ampoules. The FeCl_2 had been prepared from the Analar-grade hydrate, $\text{FeCl}_2 \cdot 4\text{H}_2\text{O}$, by heating to 700 °C in a stream of dried nitrogen and HCl gas; FeBr_2 was prepared at 700 °C by passing HBr and nitrogen gas over iron powder, purchased from Goodfellow Metals Ltd, at 99.99% purity. Single crystals of these mixtures were grown by the Bridgman method by pulling the ampoules at 1.2–1.5 mm h⁻¹ in a Crystallox twin-zone Bridgman furnace.

To determine the compositions of the $\text{RbFeCl}_{3-x}\text{Br}_x$ samples used in the neutron diffraction experiments we analysed pieces taken from different regions of the same boule by argentimetric titration and x-ray microprobe analysis (Cheetham and Skarnulis 1981). Both methods indicated that the samples used in the diffraction measurements were homogeneous to within 1% of the total halide content, i.e. in the case of boules with nominal chloride contents of 14% and 2% the analysis revealed $14 \pm 1\%$ and $2 \pm 1\%$ chloride respectively.

Samples, typically measuring $3 \times 3 \times 5 \text{ mm}^3$, were cleft from the boules. Crystals rich in RbFeBr_3 were mounted with the $(002)_\text{N}$ and $(220)_\text{N}$ reflections in the horizontal scattering plane, while those rich in RbFeCl_3 or intermediate in composition were mounted with the $(100)_\text{N}$ and $(220)_\text{N}$ reflections in the scattering plane. Neutron diffraction experiments were performed on single crystals of $\text{RbFeCl}_{3-x}\text{Br}_x$ (where $x = 0.03, 0.06, 0.15, 2.58, 2.76$ and 2.94) using the two-axis diffractometer D15 at the Institut Laue-Langevin (ILL), Grenoble. The neutron wavelength was 1.174 Å and collimation before and after the sample was provided by two sets of apertures measuring 12 mm square and set at 10 cm from the sample. The divergence of the neutron beam was 1° at the sample. A tilting counter allowed the scattered neutron intensity to be mapped in the $l = 0$ plane as well as parts of the $l = 1$ plane while the sample remained fixed with the c axis vertical. Temperatures down to 1.3 K were provided by an ILL 'Orange' cryostat. The scattered neutron intensity was mapped as a function of temperature in the regions of the K point and the M point of the hexagonal reciprocal lattice. These maps consisted of a series of parallel scans centred on and perpendicular to the $[110]_\text{N}$ direction. Further scans were made along the high-symmetry directions KM and KΓ in the Brillouin zone. For crystals in which no scattering maxima were found in the $l = 0$ or $l = 1$ planes, scans were made parallel to the c axis, cutting the $l = 0$ or $l = 1$ planes at $Q = (0.30.3l)_\text{N}$. Such measurements probed the form of any one-dimensional magnetic short-range order.

3. Results

3.1. Data analysis procedure

The elastic neutron scattering lineshapes in reciprocal space are proportional to the Fourier transform of the static spin pair-correlation function. In solids which have magnetic long-range order this results in δ -functions in reciprocal space, and scattering profiles that are equal to the instrumental resolution function, generally taken to be a Gaussian curve. For inhomogeneous magnets there are two common forms that the

A Harrison and D Visser

resolution-corrected lineshape may take. Dilute magnets in the absence of a magnetic field usually show a Lorentzian lineshape that arises from an exponential decay of the spin correlation function in real space. In the presence of random magnetic fields—which may be produced either by applying a magnetic field to a dilute Ising antiferromagnet or in a body of ferromagnetically correlated moments containing frozen moments of random orientation—a distinct Lorentzian-plus-Lorentzian-squared lineshape is seen (Birgeneau *et al* 1984). Thus, a plot of $\log I$ against $\log(|q|)$ (where I is the neutron scattering intensity at a wavevector q from the scattering maximum) should be a straight line with a gradient between 2 and 4. Finally, it should be noted that a different form of lineshape has been seen in the quadrupolar glass $(\text{KBr})_{1-x}(\text{KCN})_x$ (Loidl *et al* 1985). There, the dependence of I on $|q|$ may be divided into a term proportional to q^{-2} and a term proportional to q^{-1} . Contours of equal intensity drawn in reciprocal space were also found to be very anisotropic. The origin of this effect is uncertain and has been proposed to arise from randomly distributed mechanical strains caused by the chemical disorder. Similar behaviour has been seen in the randomly mixed ferroelectric-antiferroelectric compounds $\text{Rb}_{1-x}(\text{NH}_4)_x\text{H}_2\text{PO}_4$ (Hayase *et al* 1985).

The data were corrected for background scattering measured for each sample at 6 or 20 K. The remaining intensity was then least-squares-fitted to the lineshape functions described in the previous paragraph, i.e. to the pure Gaussian resolution function or to Lorentzian or Lorentzian-plus-Lorentzian-squared lineshapes convoluted with the instrumental resolution function. In all the cases where $x < 0.15$ an ω (tangential) scan through the nuclear Bragg peaks revealed a symmetric lineshape whose form was very close to that of a Gaussian curve. The resolution function of the instrument was derived from the width of the magnetic Bragg peak at the K point of a sample of RbFeCl_3 which had nuclear peak widths within 10% of the compounds with low x . It was found that the scattering from samples with $x = 0.06$ and 0.15 was much better described by a Lorentzian curve convoluted with the instrumental resolution function compared with a Gaussian curve: χ^2 for the fits generally lay between 1 and 2, improving by only 0.05 on the inclusion of an additional Lorentzian-squared component.

It was not possible to assign a lineshape unambiguously to the scattering from samples rich in RbFeBr_3 ($x > 2.58$) since they possessed broad, asymmetric nuclear and magnetic Bragg reflections (typically 0.7° at $|Q| = 1.2 \text{ \AA}^{-1}$, where $|Q| = 4\pi(\sin\theta)/\lambda$) compared with the narrower, symmetric reflections from samples rich in RbFeCl_3 (typically 0.3° at the same value of $|Q|$).

In addition to the distinct peaks at the K point or at the incommensurate satellite positions a broad, diffuse peak was seen that was centred at the K point. An example is given in figure 3. The background scans along the KM direction for the $x = 0.03$ and $x = 0.06$ samples were taken at a maximum temperature of 6 K. Careful peak fitting revealed a broad maximum centred at the K point at this temperature. A similar, though more distinct, maximum was observed at the same temperature in a sample of RbFeCl_3 doped with 2% of the diamagnet RbMgCl_3 (Harrison and Visser 1988b), but was found to have disappeared at 20 K. We conclude that the 6 K scans are invalid for the purpose of background correction. The scan depicted in figure 3 was taken at 1.6 K through $(\frac{1}{2}\frac{1}{2}0)_N$ in a direction perpendicular to $[110]_N$. It was corrected for background scattering measured at 20 K and clearly reveals scattering intensity in addition to a strong Gaussian or Lorentzian central component. Similar values of χ^2 were obtained for fits to a Lorentzian curve convoluted with the instrumental resolution function, describing the diffuse component, and either a pure Gaussian curve or a Lorentzian curve convoluted with the instrumental resolution function describing the sharper peak. The latter was

Magnetic ordering in $\text{RbFeCl}_{3-x}\text{Br}_x$

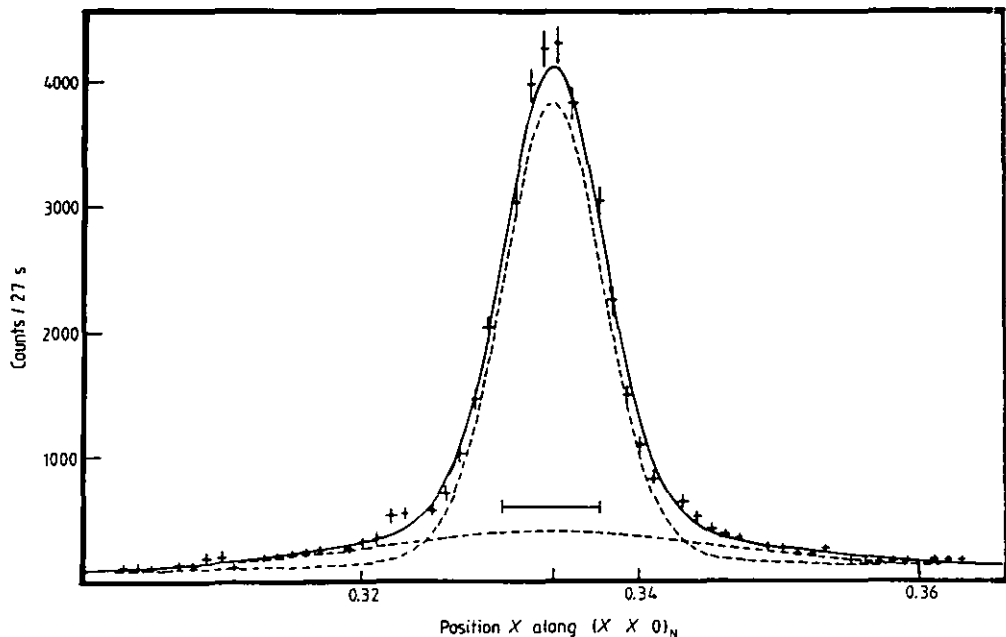


Figure 3. Neutron scattering profile at $(\frac{1}{2}\frac{1}{2}0)_N$ for the $x = 0.03$ sample at 1.6 K. The scan was taken in a direction perpendicular to $[110]_N$ and corrected for background scattering taken at 20 K. The full curve through the points is the least-squares-fitted sum of a sharp and a broad Lorentzian curve convoluted with the instrumental resolution function. The resolution width at this point is denoted by a horizontal bar at the centre of the peak.

preferred to the former on the grounds that the reflection is slightly wider than the resolution width. This apparent broadening could arise from errors in the estimate of the resolution width. Consequently, the resolution-corrected peak widths for the scattering maxima in $\text{RbFeCl}_{3-x}\text{Br}_x$ could be significantly smaller than those displayed later in figure 8 and should be treated with caution.

The intensities of the magnetic scattering from each sample, scanned perpendicular to the $[110]_N$ direction, were normalised to the intensities of their respective $(110)_N$ reflections. These in turn had to be corrected for the change in structure factor, $F_{110}(x)$,

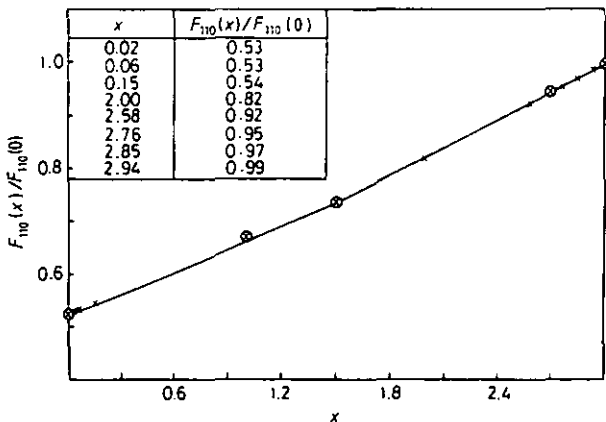


Figure 4. The dependence of the structure factor of the $(110)_N$ reflection in $\text{RbFeCl}_{3-x}\text{Br}_x$ on composition x at 1.3 K. Experimental values were calculated from the powder neutron diffraction data of Visser and Harrison (1982), and are denoted by crosses in circles. An arbitrary curve has been drawn through these points to obtain values of $F_{110}(x)$ for the values of x possessed by the samples used in the single-crystal work. These are denoted by crosses alone.

A Harrison and D Visser

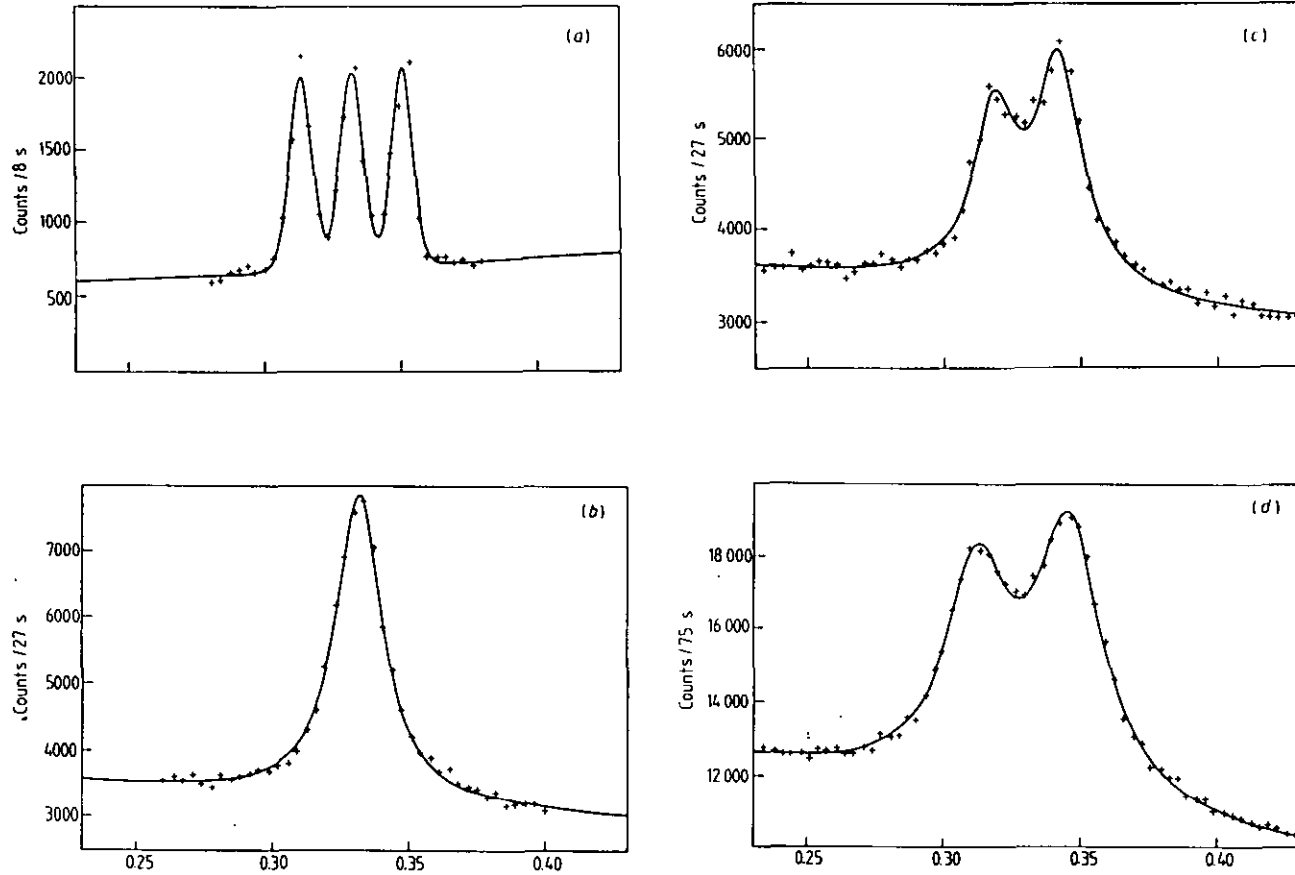


Figure 5. Examples of single-crystal neutron scattering data for: (a) pure RbFeCl_3 at 2.07 K; (b) and (c) the $x = 0.03$ sample at 1.65 and 1.83 K respectively; (d) the $x = 0.06$ sample at 1.38 K. These data have not been scaled against the relative intensities of the $(110)_N$ reflections, nor have they been corrected for background scattering. All scans were taken along the KM direction, through the K point. The axis label X is thus the position along KM: $(X\frac{1}{2} - \frac{1}{2}X0)_N$.

Magnetic ordering in $\text{RbFeCl}_{3-x}\text{Br}_x$

which depends on the composition x on account of the difference in the scattering lengths of Br and Cl, and the change with composition of the average position of the halide ion within the unit cell. A value for the latter was taken from the powder diffraction measurements of Visser and Harrison (1982) on a wide range of $\text{RbFeCl}_{3-x}\text{Br}_x$ compounds at 1.3 K. The results are displayed in figure 4, which was used to scale the intensities of the $(110)_N$ reflections of the present set of samples.

3.2. Neutron scattering from samples with small concentrations of impurities ($x \leq 0.15$ and $x \geq 2.76$)

On the RbFeCl_3 side of the phase diagram we observed narrow neutron scattering intensity maxima at the positions of the magnetic Bragg peaks of pure RbFeCl_3 (figure 5). The magnetisation curves for crystals of composition $x = 0.03, 0.06$ and 0.15 , measured at $(\frac{1}{2}\frac{1}{2}0)_N$, are displayed in figure 6(a). The curve for pure RbFeCl_3 , measured on the same instrument at the same wavelength, is included for comparison. These data have all been normalised to the relative intensities of their $(110)_N$ reflections as described in the previous section.

Correlations corresponding to the c phase of pure RbFeCl_3 were only observed at the lowest experimental temperature for the $x = 0.03$ sample. At higher T or larger values of x the scattering intensity was much lower and one only saw the satellite peaks arising from the IC_1 and IC_2 type magnetic correlations. The displacement of the satellite peaks from the K point, δR , increased with temperature and dopant concentration as depicted in figure 7. The value of the maximum displacement is independent of dopant concentration as is the temperature at which the magnetic scattering near the K point

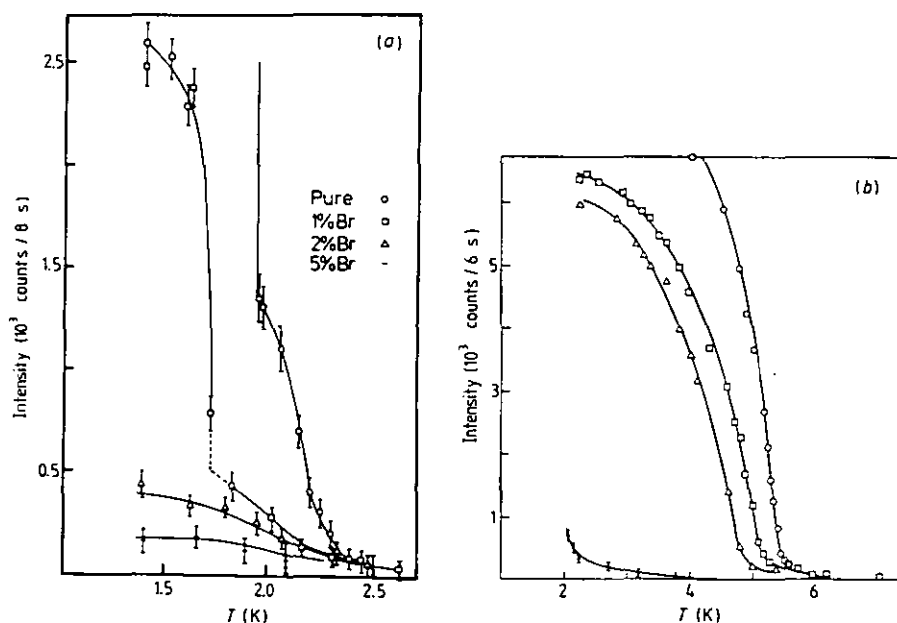


Figure 6. The temperature dependence of the integrated scattering intensity for (a) small values of x , measured at the K point, and (b) large values of x , measured at the H point. All data have been scaled against the relative intensities of the nuclear (110) and (220) reflections.

A Harrison and D Visser

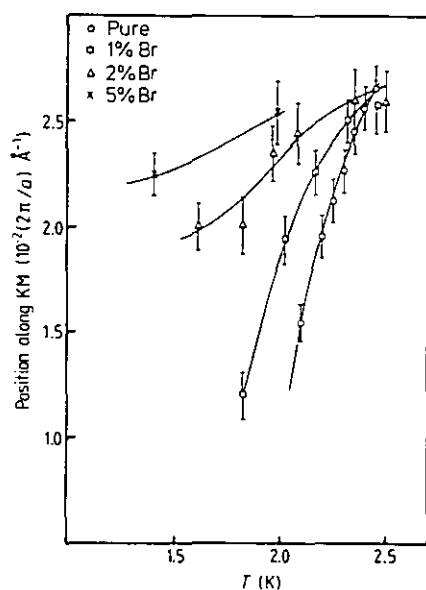


Figure 7. The displacement δR from the K point of the magnetically scattered neutron intensity maxima for samples of composition $x = 0.03, 0.06$ and 0.15 . Values for pure RbFeCl_3 measured on the same instrument have been added for comparison.

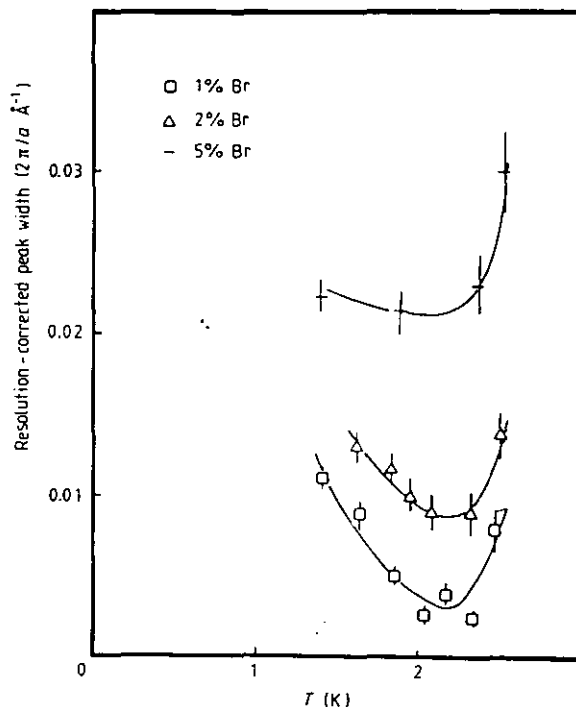


Figure 8. The dependence of the resolution-corrected peak width on temperature and composition for samples of composition $x = 0.03, 0.06$ and 0.15 . The peak in question is the distinct peak at the K point. Note that the data for $x = 0.03$ depend very much on our estimate of the resolution width, the uncertainty in which is not accounted for in the error bars on the data points.

tended to zero, remaining at 2.5 ± 0.1 K. A similar result was found for $\text{Rb}_{1-x}\text{Cs}_x\text{FeCl}_3$ (Harrison *et al* 1986a) and $\text{RbFe}_{1-y}\text{Mg}_y\text{Cl}_3$ (Harrison and Visser 1988b).

The Lorentzian peak width *always* increased with dopant concentration. The widths of the magnetic Bragg peaks of RbFeCl_3 remained strictly resolution-limited throughout the IC_1 , IC_2 and C phases, but those for crystals of composition $x = 0.03, 0.06$ and 0.15 appeared to pass through a minimum at about 2.1 K (figure 8).

In addition to the relatively distinct features noted above, all the doped samples on the RbFeCl_3 side of the phase diagram showed a diffuse peak centred at the K point (figure 3). We cannot be very explicit about the nature of this peak for two reasons. First, for the $x = 0.15$ crystal, and to a lesser extent for the $x = 0.06$ crystal, the diffuse character of the principal peaks made them very difficult to resolve from this secondary feature. Secondly, the background scans along the KM direction for the $x = 0.03$ and $x = 0.06$ crystals were not at a sufficiently high temperature for them to be valid (see § 3.1). The scan of figure 5, which was adequately corrected for background scattering, is the only one taken in the $[1\bar{1}0]_N$ direction, through the K point. However, it is possible to deduce from the data that for crystals of composition $x = 0.03$ and 0.06 the diffuse component became broader and more intense as the temperature was raised and it persisted to at least 6 K. The magnetic correlation length in the ab plane of the $x = 0.03$

Magnetic ordering in $\text{RbFeCl}_3-x\text{Br}_x$

sample appeared to be approximately $16a$ at 2.02 K and about $5a$ at 2.9 K , where a is a unit-cell parameter.

Turning now to samples on the RbFeBr_3 side of the phase diagram, we also observed narrow neutron scattering intensity maxima at the positions of the magnetic Bragg peaks of pure RbFeBr_3 . The magnetisation curves for crystals of composition $x = 2.94, 2.85$ and 2.76 are shown in figure 6(b). The measurements were made at the H point ($Q = (\frac{1}{2}\frac{1}{2}1)_N$) and the intensities were normalised to the relative intensities of the $(110)_N$ reflections. Poor crystal quality invalidated attempts to assign a lineshape to the peaks; both the nuclear and the magnetic reflections increase in width with the proportion of RbFeCl_3 present.

A possible explanation for the large mosaic spread and poor crystal quality at high values of x may be found in the structural phase transition of RbFeBr_3 . The electron diffraction measurements of Visser and Prodan (1980) showed that this type of structural phase transition in ABX_3 compounds from $\text{P6}_3/\text{mmc}$ to $\text{P6}_3\text{cm}$ symmetry is accompanied by a large increase in structural disorder. The introduction of small amounts of Cl^- to RbFeBr_3 may help to trigger such disorder by acting as nucleating points for structural domains. The $\text{P6}_3/\text{mmc}$ lattice of RbFeCl_3 does not appear to be so susceptible towards distortion.

The crystals with $x = 0.06$ and 0.15 showed distinct maxima in the neutron scattering intensity at the H point ($Q = (\frac{1}{2}\frac{1}{2}1)_N$) but the $x = 0.24$ sample only showed a broad weak maximum at this position at temperatures down to 2.07 K . However, the temperature dependence of the integrated intensity shows a sharp increase near 2.1 K , implying

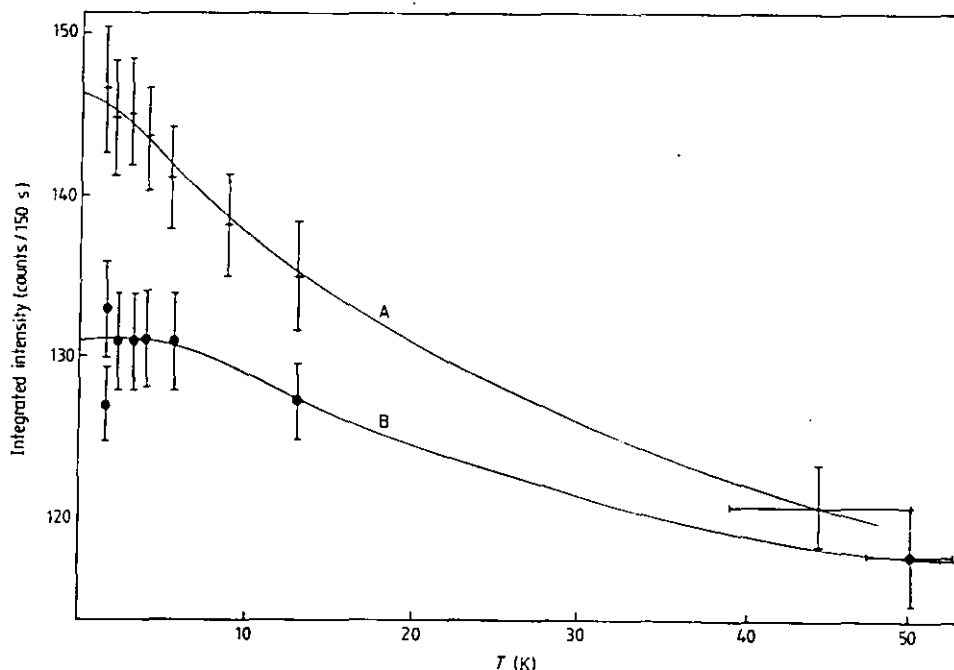


Figure 9. The dependence on temperature of the magnetically scattered neutron intensity in the $l = 1$ plane centred at $Q = (0.60, 0.61)_N$ (curve A) and $Q = (\frac{1}{2}\frac{1}{2}1)_N$ (curve B). The data were collected by making scans parallel to the crystal c axis from $l = 0.7$ to $l = 1.3$. No background correction has been made to these data.

A Harrison and D Visser

either a rapid increase in the magnetic correlation length or an increase in the magnitude of the magnetic moment (figure 6(b)).

3.3. Neutron scattering from samples with high concentrations of impurities ($0.15 < x < 2.76$)

The $x = 2.76$ crystal represents a borderline case, showing some evidence for the onset of long-range order at about 2.1 K. The $x = 2.58$ crystal, however, showed no maximum when scanned within the $l = 1$ plane near the H point. A scan perpendicular to the $l = 1$ plane, cutting it at $Q = (\frac{1}{2}\frac{1}{2}1)_N$ or $Q = (0.60.61)_N$, displays a broad maximum in the scattering intensity at $l = 1$. The dependence on temperature of this intensity is shown in figure 9.

The crystal of RbFeCl_2Br ($x = 1.0$) showed no maximum at all in the scattered neutron intensity when scanned parallel to the crystal c axis through the $l = 0$ or $l = 1$ planes and cutting them at $(0.10.1l)_N$, using a counting time as long as 5 min/point at temperatures down to 1.6 K.

4. Discussion

4.1. The magnetic structure of $\text{RbFeCl}_{3-x}\text{Br}_x$ for small concentrations of dopant ($x \leq 0.15$ and $x \geq 2.76$)

4.1.1. The effect of dopant on the magnetic ordering temperatures. Very low concentrations of either type of dopant destroys the magnetic long-range order of the majority component. RbFeBr_3 is more resilient towards this effect than RbFeCl_3 as would be expected of the compound with the larger induced moment and the higher value of T_N .

The mixing of RbFeCl_3 and RbFeBr_3 in any proportion introduces randomness in J_1, J_2 and D as a result of the delicate balance between the local crystal structure and the magnetic parameters of these materials. There are many examples in the literature of models that treat disorder in any one of these magnetic parameters but there does not seem to be a model that embraces all of these sources of disorder to produce a net result. The effect of diamagnetic impurities of randomness in intra-chain exchange on the magnetic ordering in classical Heisenberg or Ising chains weakly coupled by a molecular field was modelled by Hone *et al* (1975). This model has enjoyed considerable success in describing the effect of diamagnetic impurities on the Néel temperature of the ferromagnetic linear-chain compound CsNiF_3 (Steiner and Axmann 1976) as well as antiferromagnetic linear-chain compounds such as TMMC (Takeda and Schouten 1981 and references therein). In these cases the ratio J_2/J_1 is small (10^{-2} – 10^{-4}).

In figure 10 we plot the predictions of the Hone model for the dependence of the ordering temperature of RbFeCl_3 and RbFeBr_3 on diamagnetic impurity concentration. It has been assumed that both magnets have Heisenberg symmetry and spin $S = 1$. The different values for J_1 and J_2 are taken from table 2 and result in two different predicted dependences of T_N on dopant concentration. It is clear that the measured fall-off of T_N with dopant concentration is much faster than that calculated here. It is also clear that there are several difficulties in implementing the Hone model in the present case.

First, it is not obvious how one should relate the concentration of Br^- ions to the concentration of either site or bond impurities in the Hone model. This would require a microscopic understanding of the exchange in the intra-chain bridges containing mix-

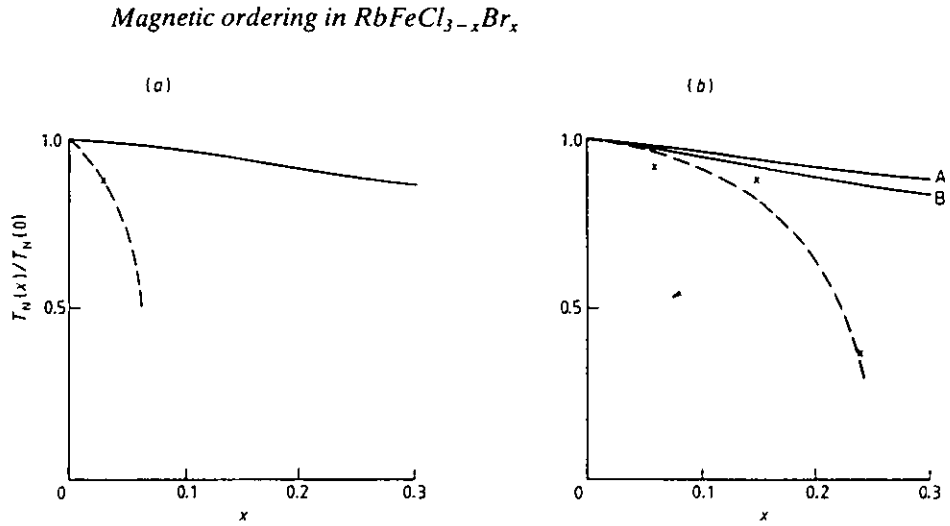


Figure 10. The dependence of the ordering temperature of (a) RbFeCl_3 and (b) RbFeBr_3 on concentration of impurity. The points plotted as crosses are experimental values for T_N taken from the present work and the full curves represent the predictions of the Hone model for diamagnetic impurities in a Heisenberg magnet. The broken curves drawn through the experimental points are merely a guide to the eye. In case (a) the ordering temperature is taken as the $C\text{-IC}_1$ transition temperature. The values for exchange constants are taken from table 2. In case (b) there are two ratios of J_1/J_2 that could be chosen: values taken from the data of Lines and Eibschutz (1975) are used for curve A and those from Harrison and Visser (1988a) for curve B.

tures of halide ions. Secondly, the $\text{RbFeCl}_{3-x}\text{Br}_x$ system cannot be treated as an assembly of classical moments. Molecular-field calculations are not suitable for the treatment of induced-moment magnets that are close to the magnetic singlet ground-state threshold. Thirdly, it is not certain what value we should take for $T_N(x)$ or even for $T_N(0)$: the added influence of the large magnetic dipole-dipole interaction on the ordering process obscures the value of T_N that would arise from just the superexchange interactions, as modelled by Hone *et al* (1975). It should be noted that the Hone model is best applied to magnets for which $J_2/J_1 \ll 1$. This ratio appears to range from 10^{-1} to 10^{-2} for RbFeCl_3 and RbFeBr_3 according to the values given in table 2 and this may limit the accuracy of the model. It should also be noted that the single-ion anisotropy D , which is neglected in the Hone model, may also be important. It has been shown that the inclusion of D in the calculation of T_N of undiluted one-dimensional magnets has a significant effect (Boersma *et al* 1981).

Existing theories that treat randomness in D are also not appropriate in the present case, being concerned either with mixtures of magnets with Ising and XY anisotropies (Bevaart *et al* 1978, Wong *et al* 1980, Katsumata *et al* 1982), or with cases in which D is uniaxial and constant in magnitude but in which the direction of the anisotropy axis varies with site (Rhyne *et al* 1972, Kettler *et al* 1981). In the case of $\text{RbFeCl}_{3-x}\text{Br}_x$ the sign of D remains the same; it is XY in character throughout and has a magnitude that we expect to vary only weakly with composition (compare the values of D for the two pure compounds in table 2).

A quantitative interpretation of our results may only be obtained from a very specific model, designed to meet all the peculiarities of the present system. Thus we shall only attempt a qualitative explanation by considering the effect of dopant on the ratio D/J_Q .

It is likely that J_1 is reduced or made negative by the replacement of one or two

A Harrison and D Visser

chloride ions by bromide ions in the intra-chain exchange bridges. It is also probable that J_2 is increased in magnitude on replacing Cl^- by Br^- in the inter-chain exchange bridges. This is expected to be a less important effect than that concerning J_1 because the values of J_2 for the chloride and bromide are close in value (Harrison and Visser 1988a), and J_2 is smaller than J_1 by a factor of 5–10. Thus, in the vicinity of Br^- ions in RbFeCl_3 , J_Q (where $Q = (\frac{1}{2}\frac{1}{2}0)_N$) will also be reduced, and a lowering in size of the neighbouring magnetic moments will occur. The proximity of the magnetic-singlet ground-state threshold will sensitise the reduction of the magnetisation by impurities, making it more severe than would be predicted from molecular-field arguments. On this basis the ordering temperature of RbFeBr_3 is expected to be less sensitive towards dopant than that of RbFeCl_3 . This is consistent with our results (Figure 10).

Finally, it should be noted that the magnetic inhomogeneities not only reduce T_N but also destroy the long-range character of the magnetism in the 'ordered' magnetic phases for $x < 0.15$. No clear explanation of this phenomenon can be found in the literature. It has been stated that small concentrations of impurities in a frustrated two- or three-dimensional lattice of moments with spin dimensionality $n \geq 1$ at $T = 0$ give rise to random magnetic fields that destroy the magnetic long-range order (Matsubara 1985).

4.1.2. The effect of dopant on the balance between magnetic dipolar and superexchange ordering. Let us now consider the effect of doping RbFeCl_3 with RbFeBr_3 on the balance between the magnetic dipole-dipole interaction γ and J_2 . Several effects must be considered. First, the reduction or elimination of magnetic moments at the iron sites will reduce the magnitude of both γ and J_2 . Intuitively one might expect that the longer-range dipolar interaction would be disrupted less by reduction of moments at random sites. Secondly, the replacement of Cl^- by the more covalent Br^- is likely to increase J_2 (compare the values of J_2 for the pure compounds in table 2). Finally, the substitution of Br^- ions into the chains reduces the intra-chain ferromagnetic interactions, which in turn reduce γ .

There is no ready way in which the net result of these competing effects may be assessed theoretically. Experimentally, the ratio γ/J_2 appears to increase on doping RbFeCl_3 with RbFeBr_3 : doping has little effect on the P-IC_1 transition temperature and the C-IC_2 transition temperature falls with dopant concentration (figure 11); the displacement from the K point, δR , of the satellite peaks in the IC phases at a particular temperature increases with dopant concentration.

On comparing figure 7 with figure 4 of Harrison *et al* (1986a) we see that the displacement of the satellite peaks from the K point is smaller at a given temperature and impurity concentration for the bromide- than for the caesium-doped materials. This indicates that doping with Cs^+ favours γ/J_2 more than doping with Br^- . In some respects the effect of Cs^+ on the ratio γ/J_2 should be similar to that of Br^- . The reduction or elimination of magnetic moments close to Cs^+ impurities throughout the crystal reduces both γ and J_2 . However, Cs^+ is expected to have a different effect on J_2 than Br^- . The larger Cs^+ ion ($r_{\text{Cs}} = 2.00 \text{ \AA}$) pushes the iron chains further apart than those in pure RbFeCl_3 ($r_{\text{Rb}} = 1.85 \text{ \AA}$). The value of γ depends on inter-chain separation r as r^{-3} whereas the dependence of J_2 on r is of the order of r^{-10} (Bloch 1966). Bromine ions will also cause the iron chains to be displaced further than in pure RbFeCl_3 but this is offset by the increase in the covalency of the inter-chain exchange bridges, leading to an increase in J_2 from the chloride to the bromide (table 2). Furthermore, the bromide ion is more polarisable than the Cs^+ ion and should be more easily accommodated in the RbFeCl_3 lattice causing less local structural distortion.

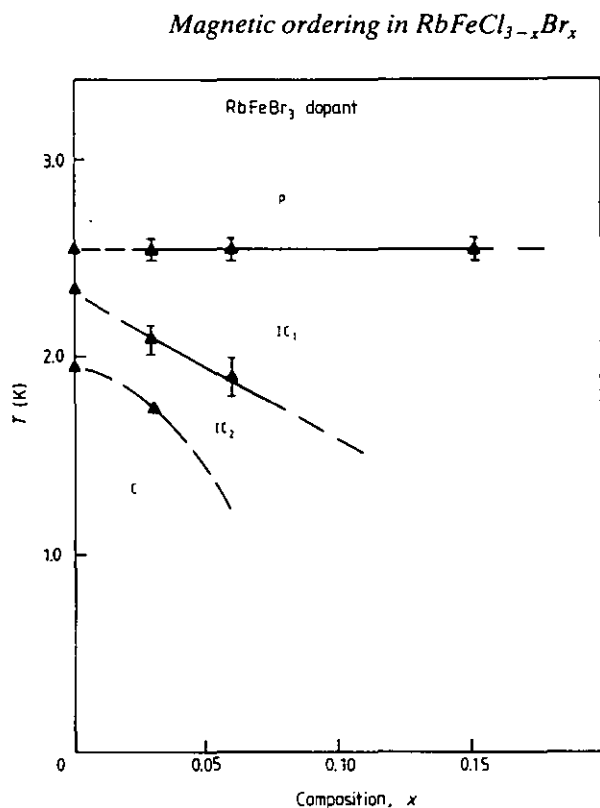


Figure 11. The dependence on temperature and concentration of Br^- of the periodicity of the magnetic correlations in RbFeCl_3 . The magnetic correlations are finite in extent so that these phases differ from those found in the pure chloride—hence the broken curves extrapolated to zero impurity level. Symbols $1C_1$, $1C_2$ and C refer to the incommensurate and commensurate periodicities predicted by Shiba (1982). The two lower phase boundaries were not seen down to the base temperature of 1.3 K for the $x = 0.15$ sample, so again the phase boundary is drawn as a broken line.

4.2. Diffuse magnetic scattering from $\text{RbFeCl}_3-x\text{Br}_x$ ($0 < x \leq 0.15$ and $2.76 \leq x < 3.0$)

A diffuse neutron scattering component is seen in samples rich in RbFeCl_3 ($x < 0.15$), in addition to the relatively narrow intensity maxima seen near the K point below 2.5 K. Only one scan ($x = 0.03$ at 1.6 K) containing information about this feature could be corrected for background scattering. The diffuse scattering profile could be fitted to a Lorentzian curve of width $(\pi/25a) \text{ \AA}^{-1}$, where a is the nuclear unit-cell parameter. There are several interpretations that may be given to this feature.

(i) Scattering arises from small ($\approx 50 \text{ \AA}$ diameter) magnetically ordered clusters with a 120° antiferromagnetic configuration in the ab plane.

(ii) The magnetically ordered regions are large but the orientation of the moments adopts a distribution of canting angles which is centred on the 120° antiferromagnetic array. When inhomogeneities are introduced to a triangular antiferromagnetic array of moments the balance of force producing the 120° Néel ground state is broken and the formation of 'canted local states' is expected (Villain 1979, Harrison 1987). Significant canting about a single impurity may extend over several neighbouring shells of moments, setting up a medium-range magnetic disordering potential. Interactions between such centres occurs through polarisation of the intervening medium, and may lead to semi-spin-glass formation (Villain 1979). In that case a longitudinal lattice or sublattice magnetisation co-exists with a random transverse lattice or sublattice magnetisation. The one-dimensional antiferromagnet CsMnBr_3 undergoes three-dimensional magnetic long-range order to produce a 120° antiferromagnetic array in the ab plane and this material also shows diffuse neutron scattering about the H point ($Q = (\frac{1}{2}, \frac{1}{2}, 1)$) when doped with diamagnetic (Mg^{2+}) or magnetic (Fe^{2+}) impurities (Visser and McIntyre

A Harrison and D Visser

1988, Visser *et al* 1988). Another reason that the moments may deviate from the ordered 120° antiferromagnetic array is that they may lie at the boundary between two magnetic domains.

An additional source of diffuse magnetic scattering may be present in RbFeBr_3 . A recent specific-heat study of this material (Adachi *et al* 1983) showed that it orders in two steps: there is a sharp specific-heat anomaly at 5.5 K and a broad, weak one at 2.0–2.5 K. The phase that exists between these two anomalies has been postulated to be a partially ordered one in which one of the three magnetic chains in the $a\sqrt{3} \times c$ unit cell is disordered. Similar partially disordered magnetic phases have been observed in the 1D Ising system CsCoCl_3 (Mekata *et al* 1986). They have also been proposed as an explanation for the diffuse neutron scattering observed in the powder diffraction patterns of undoped samples of the two-dimensional triangular Heisenberg antiferromagnets VCl_2 and VBr_2 below T_N (Hirakawa *et al* 1983). At 2.5 K the third chain in RbFeBr_3 orders to give a slightly modified 120° degree structure (Adachi *et al* 1983). However, the scattering from the disordered chain should merely contribute to the magnetic diffuse scattering background in an isotropic fashion within $l = 2n - 1$ planes in reciprocal space. As the temperature falls below that of the second ordering transition this diffuse intensity should condense at the magnetic Bragg positions, increasing their intensity by 50%. It should be noted that our measurements do not provide any evidence for such an ordering sequence.

A modification of this ordering process is expected in pure RbFeBr_3 and samples of $\text{RbFeCl}_{3-x}\text{Br}_x$ of composition $x > 2.76$. The structural phase transition that creates two nuclear sublattices, A and B, as described in § 1.2, gives rise to different inter-chain exchange constants, J_{A-B} and J_{B-B} (where the subscript describes the sublattice to which each moment belongs). This will upset the balance of forces that leads to the 120° antiferromagnetic array when J_2 is uniform in the ab plane and pin the mobile character of the triangular antiferromagnetic array.

4.3. Magnetic ordering behaviour of RbFeCl_3 at intermediate compositions ($0.15 > x > 2.76$)

The neutron scattering measurements clearly demonstrate that the $x = 2.56$ crystal has significant one-dimensional antiferromagnetic correlations at 1.6 K and that the RbFeCl_2Br crystal ($x = 1.0$) has no detectable long-range ferro- or antiferromagnetic intra-chain correlations at the lowest experimental temperature for this sample of 1.6 K.

The magnetisation and susceptibility measurements (see § 2.2) shed more light on these observations.

(i) The magnitude of the induced magnetisation and of the maximum magnetic susceptibility parallel to the crystal c axis dropped from RbFeCl_3 to RbFeBr_3 , reflecting the transition from ferro- to antiferromagnetic J_1 . The drop in the susceptibility was most marked between $x = 0.0$ and $x = 1.0$. This crossover is illustrated schematically in figure 12(a). At a microscopic level we expect there to be a distribution of compositions of magnetic exchange bridges and consequently a distribution of values of the individual intra-chain exchange constant, J_{ii} . For individual bridges for a particular impurity concentration x . This is illustrated schematically in figure 12(b). Note that J_{ii} appears to have a continuous range of values for a given x despite there being only four different types of $\text{Fe-X}_3\text{-Fe}$ bridge. This is because J_{ii} is very sensitive to structural distortions and therefore also depends on the distribution of other neighbouring halide ions. Note

Magnetic ordering in $\text{RbFeCl}_{3-x}\text{Br}_x$

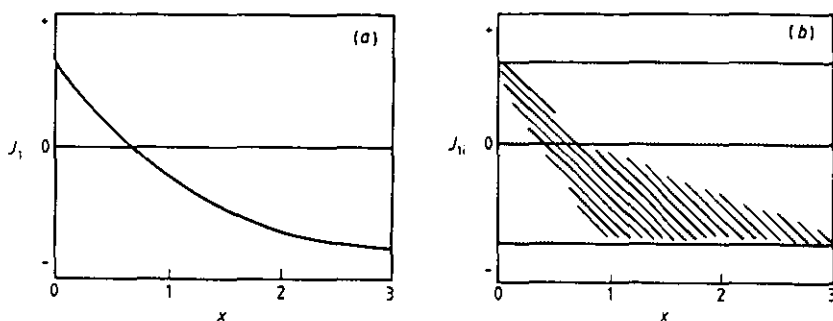


Figure 12. (a) Schematic representation of the dependence of the macroscopic intra-chain exchange constant J_1 on composition x as measured by static susceptibility methods (Visser 1988a). Samples with $x = 0, 1, 1.5, 2.0$ and 3.0 were used. (b) Schematic illustration of the distribution of individual Fe-Fe intra-chain exchange interactions, J_{ij} , as the composition x of $\text{RbFeCl}_{3-x}\text{Br}_x$ is varied. We have arbitrarily defined the upper and lower limits of J_{ij} as the bulk values, J_1 , of the pure materials as discussed in the text. The more heavily shaded area denotes the most probable value of J_{ij} at a particular composition and this is based on the knowledge that the macroscopic exchange constant J_1 shown in figure 12(a) arises from the average of J_{ij} at a particular composition.

too that we have arbitrarily defined the upper and lower limits of J_{ij} as the values found in the pure compounds. It is possible that at intermediate compositions these boundaries are quite different. For instance, we do not expect a Fe-Cl₃-Fe bridge in an $x = 1.5$ sample necessarily to have the same value of J_{ij} as in an $x = 0$ sample.

(ii) There is a distinct remanence in the magnetisation measured parallel to the crystal c axis for $x = 2.0$ after the applied magnetic field had been raised to 5.6 T then returned to zero at a constant temperature of 2.0 K. This effect was much weaker for the $x = 1.5$ sample and could not be detected for the $x = 1.0$ sample. This indicates that at low temperature the $x = 2.0$ and to a lesser extent the $x = 1.5$ sample possess frozen magnetic disorder (Grest and Soukoulis 1983).

4.4. The magnetic phase diagram of $\text{RbFeCl}_{3-x}\text{Br}_x$

The interpretation of the neutron scattering and magnetisation measurements taken together is presented in the schematic magnetic phase diagram of figure 13. At intermediate compositions the exchange field is disrupted to such an extent that the system appears to have true singlet ground-state character. On the RbFeBr_3 side of the magnetic phase diagram the addition of approximately 10% of RbFeCl_3 ($x = 2.7$) destroys the magnetic long-range order and at 33% of RbFeCl_3 ($x = 2.0$) one observes a phase in which there is no detectable magnetic long-range order but in which there is remanent magnetic behaviour at 2.0 K. We shall tentatively call this a 'spin glass'. We have no estimate of the boundaries, either in temperature or composition, of this 'phase' other than a knowledge that it does not appear to exist for RbFeCl_2Br ($x = 1.0$) at 2.0 K and that it does appear to exist for RbFeClBr_2 ($x = 2.0$) at the same temperature. Furthermore, we have no measure of the spatial magnetic homogeneity of this 'phase'. It is possible that RbFeClBr_2 at low temperatures is composed of regions behaving as singlet ground-state material and regions in which the induced moments are sufficiently large to support spin-glass 'ordering'.

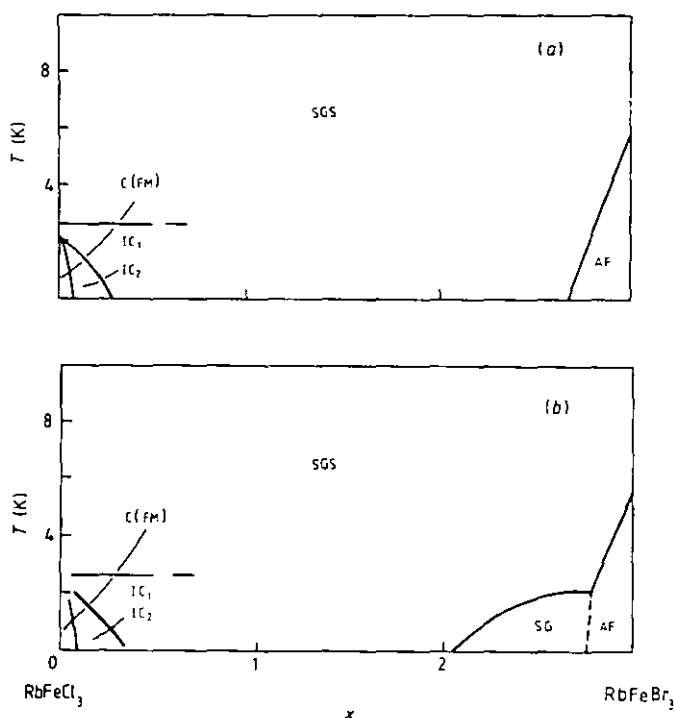


Figure 13. Schematic magnetic phase diagram for $\text{RbFeCl}_{3-x}\text{Br}_x$ showing two possibilities for the magnetic structure at intermediate compositions. (a) Only singlet ground-state (SGS) behaviour at intermediate composition is shown. (b) The case where there is a spin glass (SG) phase on the bromide side of the phase diagram. The remainder of the symbols have been explained in figure 11.

On the RbFeCl_3 side of the magnetic phase diagram there is the additional complication of IC phase formation. Boundaries between IC_1 , IC_2 and c magnetic phases were deduced from a study of the satellite structures and this portion of the phase diagram is shown enlarged in figure 11. It must be stressed that these 'phases' contain magnetic correlations that are certainly spatially finite for the $x = 0.06$ and $x = 0.15$ samples and which may or may not be finite for the $x = 0.03$ sample.

The magnetic phase diagram of $\text{RbFeCl}_{3-x}\text{Br}_x$ may be extended and elucidated by the application of an external magnetic field parallel to the crystal c axis ($H \parallel c$). In the mixed singlet ground-state system $\text{Rb}_{1-x}\text{Cs}_x\text{FeCl}_3$ the application of $H \parallel c$ was found greatly to increase the magnetic correlation length (Harrison *et al* 1986a). By mixing the excited doublet into the ground singlet $H \parallel c$ compensates for the reduction of moments on iron atoms in the vicinity of Cs^+ impurities. Similarly, the application of a magnetic field parallel to the c axis of RbFeCl_3 should counteract the disruptive effect of either dopant with regard to the size of the induced moments; the combination of magnetic frustration and larger induced moments might then produce a spin glass at intermediate compositions. The character of such a glassy phase could be tuned by altering the magnitude of this applied magnetic field. We shall report a neutron scattering study of such effects in a forthcoming paper.

Magnetic ordering in $\text{RbFeCl}_3-x\text{Br}_x$

5. Conclusions

The mixed ferromagnet-antiferromagnet linear-chain compound $\text{RbFeCl}_3\text{Br}_x$ shows a complex array of magnetic ordering processes that depend on the composition x and temperature T . These phenomena may be rationalised qualitatively by considering the distribution of D/J_0 and γ/J_2 as a function of x .

The value of D/J_0 for the induced-moment magnets RbFeCl_3 and RbFeBr_3 is very close to the value at which a crossover from magnetic to singlet ground-state properties is expected. This sensitises the magnetic ordering processes to any impurities that disrupt the local magnetic exchange field J_0 . Magnetic correlations in the $x = 0.03$ sample at low temperatures were found to be finite, in contrast to the predictions of molecular-field-based models such as that of Hone *et al* (1975). Consequently, the magnetic phase diagrams are different from those predicted by Fishman and Aharony (1979) for a mixed ferromagnet-antiferromagnet. At intermediate compositions one observes a singlet ground-state phase rather than a spin-glass phase. It is possible that when a magnetic field is applied parallel to the crystal c axis of these materials there will be the necessary combination of quenched spatial disorder and magnetic frustration necessary for spin-glass formation to occur.

Acknowledgments

We thank the UK Science and Engineering Research Council for financial support. AH is grateful to St John's College, Oxford, for further financial support. We also wish to thank Professor K R A Ziebeck of ILL (now at Loughborough University of Technology) for assistance with the neutron scattering experiments and Dr P Day (Oxford) for encouragement throughout the project and for interesting discussions. Our thanks are also due to Dr T E Wood for bringing our attention to this system initially.

References

- Adachi K, Takeda K, Matsubara F, Mekata M and Haseda T 1983 *J. Phys. Soc. Japan* **52** 2202
- Aeppli G, Shapiro S M, Birgeneau R J and Chen H S 1982 *Phys. Rev. B* **25** 4882
- Baines J A, Johnson C A and Thomas M F 1983 *J. Phys. C: Solid State Phys.* **16** 3579
- Bevaart L, Frikee E, Lebesque J V and de Jongh L J 1978 *Phys. Rev. B* **18** 3376
- Bevaart L, Tegelaar P M L H, van Duynveldt A J and Steiner M 1983 *J. Magn. Magn. Mater.* **31-34** 1447
- Birgeneau R J, Cowley R A, Shirane G and Yoshizawa H 1984 *J. Stat. Phys.* **34** 817
- Bloch D 1966 *J. Phys. Chem. Solids* **27** 881
- Boersma F, de Jonge W J M and Kopinga K 1981 *Phys. Rev. B* **23** 186
- Bontemps N, Grisolia C, Nerozzi M and Briat B 1982 *J. Appl. Phys.* **53** 2710
- Brand R A, Georges-Gibert H, Hubsch J and Heller J A 1985 *J. Phys. F: Met. Phys.* **15** 1987
- Cheetham A K and Skarnulis A J 1981 *Anal. Chem.* **53** 1060
- Chen J H and Lubensky T C 1977 *Phys. Rev. B* **16** 2106
- Defotis G C and Mantis D S 1986 *J. Magn. Magn. Mater.* **54-57** 79
- Eibschutz M, Davidson G R and Cox D E 1973 *AIP Conf. Proc.* **18** 386
- Eibschutz M, Lines M E and Sherwood R C 1975 *Phys. Rev. B* **11** 4595
- Fishman S and Aharony A 1979 *Phys. Rev. B* **19** 3776
- Grest G S and Soukoulis C M 1983 *Springer Series in Solid State Sciences* vol 48, ed. M Ausloos and R J Elliott (Berlin: Springer) p 223

A Harrison and D Visser

- Harrison A 1987 *J. Phys. C: Solid State Phys.* **20** 6287
- Harrison A and Visser D 1988a *J. Phys. C: Solid State Phys.* submitted
- 1988b *J. Phys. C: Solid State Phys.* submitted
- Harrison A, Visser D, Day P, Knop W and Steiner M 1986a *J. Phys. C: Solid State Phys.* **19** 6811
- Harrison A, Visser D, Day P and Ziebeck K R A 1986b *J. Magn. Magn. Mater.* **54–57** 1273
- Hayase S, Futamura R, Sakushita H and Terauchi H 1985 *J. Phys. Soc. Japan* **54** 812
- Hirakawa K, Kadowaki H and Ubukoshi K 1983 *J. Phys. Soc. Japan* **52** 1814
- Hone D, Montano P A, Tonegawa T and Imry Y 1975 *Phys. Rev. B* **12** 5141
- Hubsch J and Gavaille G 1982 *Phys. Rev. B* **26** 3815
- Hubsch J, Gavaille G and Bolfa J 1978 *J. Appl. Phys.* **49** 1363
- Katsumata K 1986 *J. Magn. Magn. Mater.* **54–57** 75
- Katsumata K, Nire T, Tanimoto M and Yoshizawa H 1982 *Phys. Rev. B* **25** 428
- Kettler P, Steiner M, Dachs H, Germer R and Wanklyn B 1981 *Phys. Rev. Lett.* **47** 1329
- Kimishima Y, Ikeda H, Furukawa A and Nagoro H 1986 *J. Phys. Soc. Japan* **55** 3574
- Knop W, Steiner M and Day P 1983 *J. Magn. Magn. Mater.* **31–34** 1033
- Loidl A, Mullner M, McIntyre G J, Knorr K and Jex H 1985 *Solid State Commun.* **54** 367
- Lines M E 1974 *Phys. Rev. B* **9** 3827
- Lines M E and Eibschutz M 1975 *Phys. Rev. B* **11** 4583
- Maletta H 1982 *J. Appl. Phys.* **53** 2185
- Maletta H, Aeppli G and Shapiro S M 1982 *Phys. Rev. Lett.* **48** 1490
- Maletta H and Felsch W 1980 *Z. Phys. B* **37** 55
- Matsubara F 1985 *J. Phys. Soc. Japan* **54** 1677
- Medvedev M V and Rumyantsev E L 1978 *Phys. Status Solidi b* **85** 427
- Mekata M, Ajiro Y and Adachi K 1986 *J. Magn. Magn. Mater.* **54–57** 1265
- Munninghof G, Hellner E, Treutmann W, Lehner N and Heger G 1984 *J. Phys. C: Solid State Phys.* **17** 1281
- Pappa C, Hammann J and Jacoboni C 1984 *J. Phys. C: Solid State Phys.* **17** 1303
- Rhyne J J, Pickart S J and Alperin H A 1972 *Phys. Rev. Lett.* **29** 1562
- Sellmyer D J and Nafis S 1986 *J. Magn. Magn. Mater.* **54–57** 113
- Sherrington D 1983 *Springer Lecture Notes in Physics* vol 192, ed. J L van Hemmen and I Morgenstern (Berlin: Springer) p 348
- Shiba H 1982 *Solid State Commun.* **41** 511
- Shiba H and Suzuki N 1983 *J. Phys. Soc. Japan* **52** 1383
- Steiner M and Axmann A 1976 *Solid State Commun.* **19** 115
- Suzuki N 1983 *J. Phys. Soc. Japan* **52** 3907
- Takeda K and Schouten J C 1981 *J. Phys. Soc. Japan* **50** 2554
- Toulouse G 1977 *Commun. Phys.* **2** 115
- Villain J 1979 *Z. Phys. B* **33** 31
- Visser D 1988a *J. Phys. C: Solid State Phys.* submitted
- Visser D 1988b unpublished work
- Visser D, Brown P J and Ziebeck K R A 1985 *Annex to the ILL Annual Report* p 93
- Visser D and Harrison A 1982 unpublished results
- Visser D, Harrison A and McIntyre G J 1988 *Proc. Int. Conf. Magnetism: J. Physique Coll.* at press
- Visser D and Knop W 1988 unpublished observations
- Visser D and McIntyre G J 1988 *Proc. Int. Conf. Neutron Scattering (Paris) 1988*
- Visser D and Prodan A 1980 *Phys. Status Solidi a* **58** 481
- Visser D, Verschoor G C and IJdo D W J 1980 *Acta Crystallogr. B* **36** 28
- Wada M, Ubukoshi K and Hirakawa K 1982 *J. Phys. Soc. Japan* **51** 283
- Wiedenmann A, Burllet P, Scheuer H and Convert P 1981 *Solid State Commun.* **38** 129
- Wiedenmann A, Gunsser W, Burllet P and Mezei F 1983 *J. Magn. Magn. Mater.* **31–34** 1395
- Wong P Z, Horn P M, Birgeneau R J, Safinya C R and Shirane G 1980 *Phys. Rev. Lett.* **45** 1974
- Wong P Z, von Molnar S, Palstra T T M, Mydosh J A, Yoshizawa H, Shapiro S M and Ito A 1985 *Phys. Rev. Lett.* **55** 2043

J. Phys.: Condens. Matter **2** (1990) 10487–10500. Printed in the UK

Magnetic ordering effects in the mixed induced-moment ferromagnetic diamagnetic system $\text{RbFe}_{(1-x)}\text{Mg}_x\text{Cl}_3$

A Harrison and D Visser†

Oxford University, Inorganic Chemistry Laboratory, South Parks Road, Oxford, OX1 3QR, UK

Received 25 June 1990

Abstract. Elastic neutron scattering experiments were performed on single crystals of the solid solution $\text{RbFe}_{(1-x)}\text{Mg}_x\text{Cl}_3$ ($x = 0.02, 0.03$ and 0.05) to study the influence of diamagnetic dilution on the magnetic ordering processes of the induced-moment, pseudo-one-dimensional ferromagnet RbFeCl_3 . All the samples appeared to have finite-range magnetic correlations with ordering vectors similar to those of the commensurate, C, and the two incommensurate magnetic phases, IC_1 and IC_2 , of pure RbFeCl_3 . The $x = 0.02$ and 0.03 samples showed transitions from the paramagnetic to the IC_1 phase at the same temperature of 2.55 K, then transitions to the IC_2 and C phases at temperatures that decreased sharply with x . The $x = 0.05$ sample also showed a transition to the IC_1 phase at 2.55 K, but no further transitions down to the lowest experimental temperature of 1.38 K. All samples showed an additional elastic diffuse magnetic scattering component centred at the commensurate magnetic ordering vector $(\frac{1}{3}, \frac{1}{3}, 0)_N$. This diffuse component became broader and weaker as x increased from 0.02 to 0.05 and as the sample was warmed, but persisted until about 10 K.

1. Introduction

This paper follows recent work on the inhomogeneous magnetic materials $\text{Rb}_{(1-x)}\text{Cs}_x\text{FeCl}_3$ (Harrison *et al* 1986), which is a mixed magnetic-singlet ground state material, and $\text{RbFeCl}_{(3-x)}\text{Br}_x$ (Harrison and Visser 1989), which is a mixed induced-moment ferromagnetic-antiferromagnetic material. We will henceforth refer to these two works as I and II respectively. In order to demonstrate the motivation for the present work it is necessary to consider briefly the delicate balance of competing influences that govern the magnetic behaviour of the pure compounds AFeX_3 ($A = \text{Rb}, \text{Cs}$; $X = \text{Cl}, \text{Br}$). Fuller reviews are given in Lines and Eibschutz (1975), Eibschutz *et al* (1975) and II.

All of these materials have a hexagonal perovskite structure (space group $P6_3/mmc$) in which chains of face-sharing FeX_6^{4-} octahedra lie parallel to the crystal c axis. The chain structure leads to pseudo-one-dimensional magnetic behaviour: the intrachain magnetic exchange constant J_1 is an order of magnitude greater than the interchain magnetic exchange constant J_2 . J_2 is antiferromagnetic for all the AFeX_3 compounds, but the sign of J_1 depends on the Fe–X–Fe intrachain superexchange bridge angle α : the bromides are found to have antiferromagnetic J_1 , whereas the chlorides, with larger α , have ferromagnetic J_1 .

The single-ion electronic ground state of isolated Fe^{2+} ions in the trigonally-distorted

† Present address: Department of Physics, Loughborough University of Technology, Loughborough, LE11 3TU, UK.

A Harrison and D Visser

octahedral ligand field environment in these materials would be a singlet, $|m_J = 0\rangle$, with a low-lying excited doublet, $|m_J = \pm 1\rangle$, at an energy D . Perturbation of this three-level system through magnetic superexchange or a magnetic field applied parallel to the crystal c axis can induce a magnetic ground state. In zero applied magnetic field the rubidium salts show magnetic long-range ordering at low temperatures, whereas the caesium salts, with larger unit cells, and smaller magnetic exchange interactions, show true singlet ground state character.

A third form of competition between different types of magnetic behaviour exists in the chlorides, in which the ferromagnetic intrachain correlations lead to an appreciable interchain magnetic dipole-dipole interaction, γ (Shiba 1982, Shiba and Suzuki 1983). The exchange field provided by J_2 favours a free-energy minimum at the K point of the hexagonal reciprocal lattice ($Q = (\frac{1}{3} \frac{1}{3} 0)_N$), whereas γ favours a minimum at the M point ($Q = (\frac{1}{2} 0 0)_N$ and equivalent positions). Competition between J_2 and γ in pure RbFeCl_3 leads to the formation of two incommensurate magnetic phases, IC_1 and IC_2 , as it is cooled from the paramagnetic phase to 2.55 and 2.35 K respectively. The commensurate magnetic phase, C, which has 120° antiferromagnetic order in the triangular basal plane, forms at 1.95 K (Wada *et al* 1982).

The mixed singlet-magnetic ground state compounds $\text{Rb}_{(1-x)}\text{Cs}_x\text{FeCl}_3$ were studied by single-crystal neutron diffraction and their magnetic structures found to be very dependent on the composition x , temperature and magnetic field applied parallel to the c axis (I). In particular, the magnetic ordering observed in the pure rubidium salt was found to be destroyed on the addition of small concentrations of CsFeCl_3 , and the degree of magnetic inhomogeneity found to decrease strongly as a magnetic field was applied parallel to the c axis. Distinct differences were found between the zero-field-cooled, and the field-cooled sublattice magnetization.

The mixed ferromagnet-antiferromagnet $\text{RbFeCl}_{(3-x)}\text{Br}_x$ was also studied by single-crystal neutron diffraction (II) in order to investigate the possibility of forming a spin-glass phase at intermediate composition (Fishman and Aharony 1979, Bontemps *et al* 1982, Katsumata *et al* 1982, and Munninghof *et al* 1984). However, the induced-moment character of these materials sensitizes them towards impurities: 1 or 2% of the dopant RbFeBr_3 was sufficient to destroy the magnetic long-range order in RbFeCl_3 . At intermediate composition the magnetic phase was best described as a singlet ground state material with random intrachain magnetic exchange.

In both mixed systems the neutron scattering maxima near the magnetic Bragg positions of the pure compounds were greater than the instrumental resolution width, corresponding to magnetic correlations of *finite* range. It was not possible to explain this satisfactorily using existing models. In addition to the relatively sharp scattering maxima in the mixed compounds, a diffuse scattering component was observed at the same positions, but persisting to higher temperatures. The origin of this effect was also uncertain.

It is difficult to treat either of these systems at a microscopic level because of the complexity of the structural or magnetic disturbances produced by the impurities. It is *likely* that Cs^+ produces a shell of structural distortions, accompanied by a reduction in the magnitude of the induced moments on some of the neighbouring iron atoms. Doping RbFeCl_3 with Br^- gives rise to superexchange bridges of various compositions, with indeterminate exchange constants J_{ij} . By doping RbMgCl_3 into RbFeCl_3 we exchange Fe^{2+} ions for the diamagnetic Mg^{2+} , and produce an inhomogeneous magnet in which the microscopic picture might be clearer. In addition, the substitution of Fe^{2+} by Mg^{2+} is expected to have a less disruptive influence on the crystal structure, and consequently on the superexchange pathways, than the substitution of Rb^+ by Cs^+ or Cl^- by Br^- . In the present paper we report a single-crystal neutron diffraction study of the magnetic ordering of $\text{RbFe}_{(1-x)}\text{Mg}_x\text{Cl}_3$ for small values of x ($0 < x < 0.05$) with the aim of clarifying some of the disordering effects in the Rb-Cs and Cl-Br mixed compounds.

Magnetic ordering in $\text{RbFe}_{(1-x)}\text{Mg}_x\text{Cl}_3$

2. Experimental method

All the samples used in these experiments were prepared in precisely the same manner as the $\text{RbFeCl}_{(3-x)}\text{Br}_x$ compounds, as described in II. MgCl_2 was prepared from the Analar grade hydrate, $\text{MgCl}_2 \cdot 6\text{H}_2\text{O}$. Analysis of the magnesium and iron contents of the boules by flame photometry revealed them to be homogeneous down their entire lengths to within 5% of the nominal concentration of Mg^{2+} .

Small parts of the boules of the mixed compounds were checked with x-ray powder diffraction to establish their homogeneity and crystal structure. RbMgCl_3 crystallizes in a slightly different structure (Seifert and Fink 1975) to RbFeCl_3 with a hexagonal-cubic (HC) anion stacking sequence, space group $P6_3/mmc$ and unit cell dimensions $a = 7.090 \text{ \AA}$ and $c = 11.844 \text{ \AA}$. It was thought possible that the Mg^{2+} impurities could induce stacking faults. The diffraction patterns of the mixed compounds could be fully indexed on the simple hexagonal unit cell of RbFeCl_3 , for which the space group is $P6_3/mmc$ and the unit cell dimensions are $a = 7.100 \text{ \AA}$ and $c = 6.048 \text{ \AA}$ (II). A careful investigation of the background scattering in the powder diffraction patterns showed no indications of a HC-type crystal structure, nor were there any indications of line-broadening effects due to HC stacking faults as observed in TiFeCl_3 (Zodkevitz *et al* 1970). We may conclude that small concentrations of RbMgCl_3 form a solid solution with RbFeCl_3 .

Samples, typically measuring $3 \times 3 \times 5 \text{ mm}^3$, were cleft from the boules and mounted with the $(100)_N$ and $(220)_N$ reflections in the horizontal scattering plane. Neutron diffraction was performed on samples of $\text{RbFe}_{(1-x)}\text{Mg}_x\text{Cl}_3$ of composition $x = 0.02$ and $x = 0.05$ on the two-axis diffractometer D15 at the ILL (Institut Laue-Langevin), at a neutron wavelength of 1.174 \AA . Temperatures down to 1.3 K were provided by an ILL 'Orange' cryostat. Collimation before and after the sample was provided by two sets of apertures measuring 12 mm square. The divergence of the neutron beam was 1° at the sample. The instrumental resolution function at the K point of the mixed samples was determined by measuring the width of the same magnetic Bragg peak in a sample of pure RbFeCl_3 . The widths of the nuclear Bragg peaks in the sample of pure RbFeCl_3 lay within 10% of those of the same nuclear Bragg peaks in the $\text{RbFe}_{(1-x)}\text{Mg}_x\text{Cl}_3$ samples used in the present measurements when those peaks were scanned in both a tangential (ω scan) and a radial fashion ($(\omega - 2\theta)$ scan).

The scattered neutron intensity was then mapped in the regions of the K point and the M point of the hexagonal reciprocal lattice as a function of temperature. These measurements revealed satellite peaks centred on the K point at low temperatures, plus an additional diffuse scattering component centred at that point, which persisted to higher temperatures. These results prompted a second study using an instrument of higher spatial resolution, with energy resolution and a lower background count. The neutron scattering study of the sample of composition $x = 0.03$ was carried out on the triple-axis diffractometer D10 at the ILL at a wavelength of 2.363 \AA . The spectrometer was set up to detect elastically scattered neutrons. The full width at half maximum of the Bragg peak at $Q = (\frac{1}{3} \frac{1}{3} 0)$ equalled 0.7° in ω .

3. Results

The scattered neutron intensity from all samples revealed maxima at or around the K point, corresponding to magnetic correlations similar to those found in pure RbFeCl_3 (figure 1). Scans were made through the K point along the KM direction and also perpendicular to the $[110]_N$ direction. These maxima were fitted to a variety of lineshape functions, as described in II. In all cases the best least-squares fit was found for Lorentzian curves convoluted with the

A Harrison and D Visser

Gaussian resolution function. As with the $\text{RbFeCl}_{(3-x)}\text{Br}_x$ compounds the analysis was complicated by the appearance of a broad, weak maximum centred at the K point which persisted to 6–10 K. There was the additional complication of uncertainty in the instrumental resolution width near the K point.

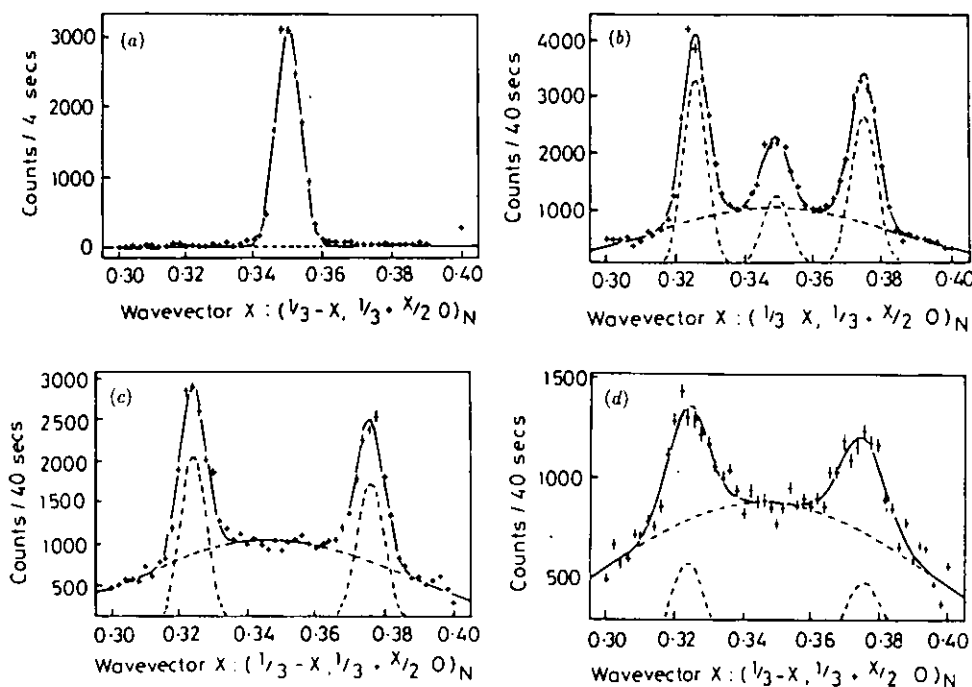


Figure 1. Examples of the diffuse scattering component in the $x = 0.02$ sample at (a) 1.32 K, (b) 2.15 K, (c) 2.24 K and (d) 2.34 K. The full curves in figures 1(b)–(d) represent the best fits to the background-corrected data of Lorentzian curves convoluted with the Gaussian resolution function, and the broken curves give the separate contributions, clearly showing the diffuse part. In figure 1(a) the full curve does *not* include the diffuse component, demonstrating how the it was first detected.

Magnetization curves for all the doped samples, measured at $Q = (\frac{1}{3} \frac{1}{3} 0)_N$, are presented in figures 2(a) and (b). The magnetization curve for pure RbFeCl_3 , taken on instrument D15 at the same wavelength as the measurements made on the $x = 0.02$ and $x = 0.05$ samples, is presented for comparison. Data for the $x = 0.02$ and 0.05 samples have been scaled against the intensities of the respective $(110)_N$ reflections. The scaling of intensities for different samples should also take into account the different structure factors of the nuclear peaks used for normalization. However, over the composition range considered here this change is expected to be very small (I, II).

These curves clearly demonstrate the successive paramagnetic–IC–C phase transitions in the pure and $x = 0.02$ and 0.03 samples, and this is confirmed by the form of the satellite and central Bragg peaks in and around the K point. However, the $x = 0.05$ sample only exhibited the satellite structure indicative of magnetic correlations with an IC_1 -type periodicity below 2.55 K and down to the lowest experimental temperature of 1.38 K.

The displacement of the satellite peaks in the IC_2 - and IC_1 -like phases increased with temperature and concentration of dopant as illustrated in figure 3. This result is very similar to those for $\text{Rb}_{(1-x)}\text{Cs}_x\text{FeCl}_3$ and $\text{RbFeCl}_{(3-x)}\text{Br}_x$, with the satellite displacement at higher

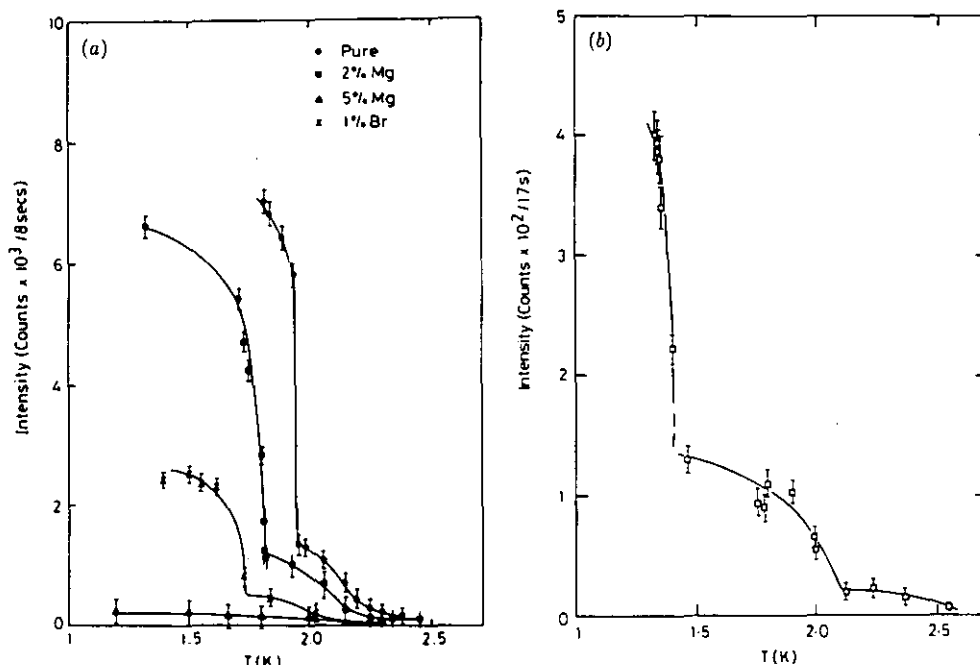
Magnetic ordering in $\text{RbFe}_{(1-x)}\text{Mg}_x\text{Cl}_3$ 

Figure 2. The temperature dependence of the magnetization measured at the K point for samples of $\text{RbFe}_{(1-x)}\text{Mg}_x\text{Cl}_3$ of (a) composition $x = 0.02$ and 0.05 and (b) composition $x = 0.03$. The data for the $x = 0.02$ and 0.05 samples have been scaled against each other using the intensities of the nuclear (110) and (220) reflections. The result of a similar measurement (I) on $\text{RbFeCl}_{(3-x)}\text{Br}_x$ ($x = 0.03$) is included for comparison. The data for the $x = 0.03$ sample were scaled in a similar manner, and a further correction was also made for the change in neutron wavelength.

temperatures (≈ 2.5 K) tending to a similar asymptotic value ($\delta R \approx 2.5 \times 10^{-2} 2\pi/a \text{ \AA}^{-1}$).

The widths of the neutron scattering maxima for all the samples increased as the concentration of dopant was increased (figure 4). The pure and $x = 0.02$ samples had peak widths which were independent of temperature through all the ordered magnetic phases: the peak widths of the $x = 0.02$ sample lay within the experimental uncertainty in the resolution width so it is quite possible that they are also resolution limited, as has been established for pure RbFeCl_3 (II). The $x = 0.05$ sample, and to a lesser degree the $x = 0.03$ sample, showed a monotonic increase in peak width with temperature.

The diffuse scattering component centred at the K point, seen in addition to the relatively sharp scattering maxima described above, clearly persisted above 2.5 K in the $x = 0.02$ and $x = 0.05$ samples; it was less distinct above 2.55 K in the measurements made on the $x = 0.03$ sample on the triple-axis spectrometer D10. This was probably due to the different experimental set-up for this sample. However, the measurements made with D10 *did* show that the diffuse component is primarily elastic in origin and has little, if any, contribution from low-energy magnetic fluctuations. Furthermore, the intensity of the scattering continued to rise as the temperature was lowered from T_N , which is contrary to what would be expected for quasi-elastic scattering.

More detailed information about the additional diffuse component below T_N could only be obtained for the $x = 0.02$ sample in which the diffuse component is most intense. The data were fitted to Lorentzian curves convoluted with the Gaussian resolution function describing

A Harrison and D Visser

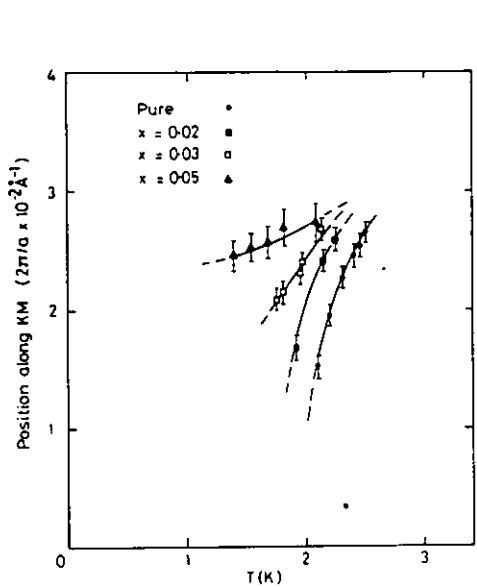


Figure 3. The displacement δR from the K point of the magnetically scattered neutron intensity maxima for $\text{RbFe}_{(1-x)}\text{Mg}_x\text{Cl}_3$ ($x = 0.02, 0.03$ and 0.05) as a function of temperature. Data for pure RbFeCl_3 are included for comparison, and were taken from the paper of Wada *et al* (1982).

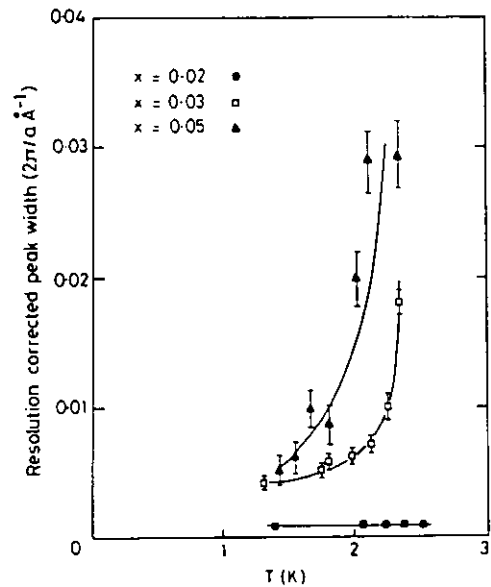


Figure 4. The dependence of the resolution-corrected peak width on temperature and composition for samples of $\text{RbFe}_{(1-x)}\text{Mg}_x\text{Cl}_3$ ($x = 0.02, 0.03$ and 0.05). Note that the data for the $x = 0.02$ sample depend very much on our estimate of the resolution width, the uncertainty in which is not accounted for in the energy bars on the data points.

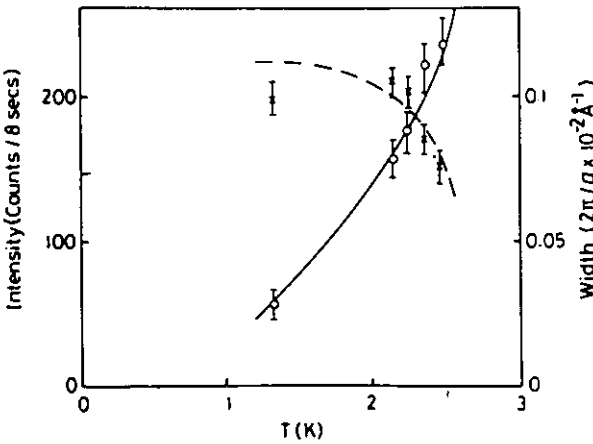


Figure 5. The dependence of the height (x) and width (O) of the diffuse scattering intensity observed near the K point of $\text{RbFe}_{(1-x)}\text{Mg}_x\text{Cl}_3$ ($x = 0.02$). Intensities have been scaled as for figure 2, and all the parameters were derived by least-squares-fitting Lorentzian curves convoluted with the Gaussian resolution function. The curves drawn through the experimental points are merely a guide to the eye, the full curve tracing the width, and the broken curve the intensity.

both the distinct and the diffuse scattering intensity. The heights and widths of the curves describing the diffuse component are presented in figure 5. The diffuse component could not

Magnetic ordering in $\text{RbFe}_{(1-x)}\text{Mg}_x\text{Cl}_3$

be fitted to a Gaussian peak and we did not attempt to fit it to more sophisticated lineshapes such as Lorentzian plus Lorentzian-squared functions (Birgeneau *et al* 1984) because of the large number of independent variables already used to describe the scattering profiles. We return to the spatial distribution of this component of the scattered neutron intensity in the next section.

4. Discussion

The change in the magnetic ordering of RbFeCl_3 when it is doped with RbMgCl_3 is quantitatively very similar to the effect of doping with CsFeCl_3 or RbFeBr_3 : small amounts of dopant destroy the magnetic long-range order found in the pure compound, and the periodicity of the finite magnetic correlations that remain is similar to that of the C, IC_2 and IC_1 phases of RbFeCl_3 , depending on the temperature and composition. The balance between incommensurate and commensurate magnetic correlations at low temperatures was displaced towards the former, as shown by the lowering of the temperature of the IC_2 -C phase transition, whilst the paramagnetic- IC_1 phase transition temperature remained constant (figure 6).

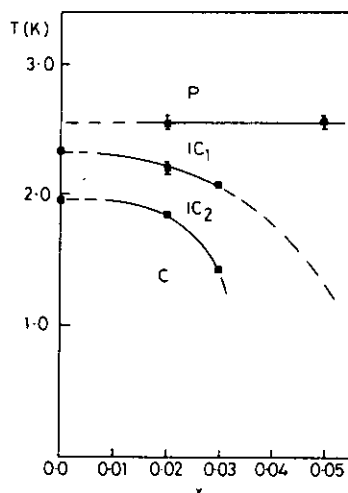


Figure 6. The dependence of the periodicity of the magnetic correlations in $\text{RbFe}_{(1-x)}\text{Mg}_x\text{Cl}_3$ ($x = 0.02, 0.03$ and 0.05) as a function of composition and temperature. It must be stressed that the correlations at higher impurity levels are finite in extent, so that these phases differ from those found in the pure chloride—hence the broken curves extrapolated to zero impurity level. Symbols IC_1 , IC_2 and C refer to the incommensurate and commensurate periodicities predicted by Shiba (1982). The two lower phase boundaries were not seen down to the base temperature of 1.3 K for the $x = 0.05$ sample, so again the broken curves extrapolate to the phase boundary.

The effect of impurities on the magnetic ordering temperature and the IC-C phase equilibria in RbFeCl_3 has been discussed in I and II. It was concluded that existing models cannot adequately describe the reduction of the magnetic ordering temperature of RbFeCl_3 in a quantitative manner because they neglect the induced-moment character of the host. In particular, the model of Hone *et al* (1975), which deals with the influence of diamagnetic impurities on the Néel temperature of chains of Heisenberg or Ising moments, weakly coupled by a molecular field, underestimates the fall-off in $T_N(x)/T_N(0)$ with diamagnetic impurity concentration x .

A Harrison and D Visser

More recently (Harrison 1989), a simple molecular field model has been used to study the effects of diamagnetic dilution on an induced-moment magnet (DIMM). The DIMM model involves setting up a randomly-diluted collection of singlet-doublet sites, with a singlet-doublet splitting D , on one- two- or three-dimensional lattices of various connectivities and joined to other active sites with magnetic exchange constants J . All active sites are given a uniform initial moment then each moment in the lattice is taken in turn and a new value calculated in the exchange field supplied by the neighbouring moments. This process is repeated until the moments attain self-consistent values. Here we use this model to calculate the mean magnetic moment per Fe^{2+} ion in $\text{RbFe}_{(1-x)}\text{Mg}_x\text{Cl}_3$ at $T = 0$ as a function of x using values of J_1 , J_2 and D derived from inelastic neutron scattering measurements of the dispersion of magnetic excitations in RbFeCl_3 (Yoshizawa *et al* 1983). We chose an interpretation of the data that was based on a molecular field excitonic model rather than a more realistic model that took account of short-range magnetic correlations (Suzuki 1983) because the DIMM model also uses the molecular field approximation. It is clear that the fall-off in mean magnetic moment at $T = 0$ with x is very rapid (figure 7). This is probably more informative than deriving the dependence of $T_N(x)/T_N(0)$ because there are several magnetic ordering temperatures for RbFeCl_3 and the magnetically 'ordered' phase appears to lack long-range magnetic order in the case of the $x = 0.03$ and 0.05 samples, and perhaps also the 0.02 sample. The extension of this model to finite temperatures requires a proper treatment to be made of the influence of magnetic fluctuations and excitations on the ordering processes. Furthermore, we assume that the diamagnetic impurities are distributed homogeneously throughout the crystal and do not show any chemical clustering. The validity of such an assumption could be checked by Mössbauer spectrometry, as performed on $\text{CsFe}_{(1-x)}\text{Mg}_x\text{Cl}_3$ (Lai and Ward 1988).

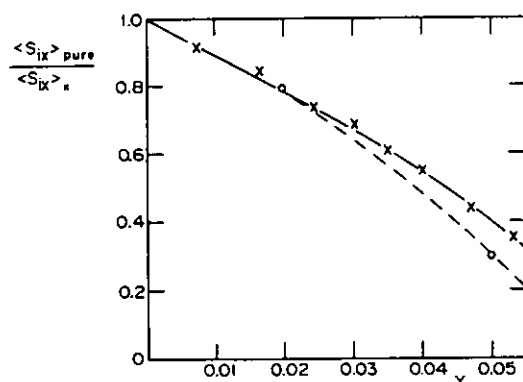


Figure 7. The dependence on composition x of the mean magnetic moment at $T = 0$, expressed as a proportion of the pure moment and calculated using the DIMM model. The exchange parameters and single-ion anisotropy are those derived by Yoshizawa *et al* (1983) for RbFeCl_3 and the calculation was performed for a hexagonal lattice of 1000 sites, averaged over several starting configurations. A comparison is made with experimental data derived from figures 2(a) and 4 at 1.38 K, depicted as circles. The broken curve through these circles merely provides a guide to the eye.

Despite its simplicity, the DIMM model provides some insight into the behaviour of $\text{RbFe}_{(1-x)}\text{Mg}_x\text{Cl}_3$. It demonstrates that on dilution with diamagnetic impurities, not only is the number of active sites reduced, but also the magnitude of the moments on those sites is greatly diminished. It also gives a picture of the spatial distribution of the magnetic moments in the dilute materials. Figure 8 shows the effect of doping a square lattice of singlet-doublet

Magnetic ordering in $\text{RbFe}_{(1-x)}\text{Mg}_x\text{Cl}_3$

sites with 1, 2 and 4% of diamagnetic impurities. In the 4% sample we see that statistical fluctuations in the distribution of diamagnetic impurities give rise to relatively large regions where there are no diamagnetic impurities and where the moments are almost as large as in the pure material. These 'islands' of large moments are surrounded by a distribution of much smaller moments. As the temperature is raised from zero the smaller moments melt first, leaving frozen moments on the islands in the form of superparamagnetic clusters. Thus, we expect that as the concentration of the diamagnetic impurity is increased, the intensity of the magnetic scattering of neutrons in the region of the K point at $T = 0$ will rapidly fall, and that some elastic magnetic scattering will remain at temperatures up to the Néel temperature of the pure compound.

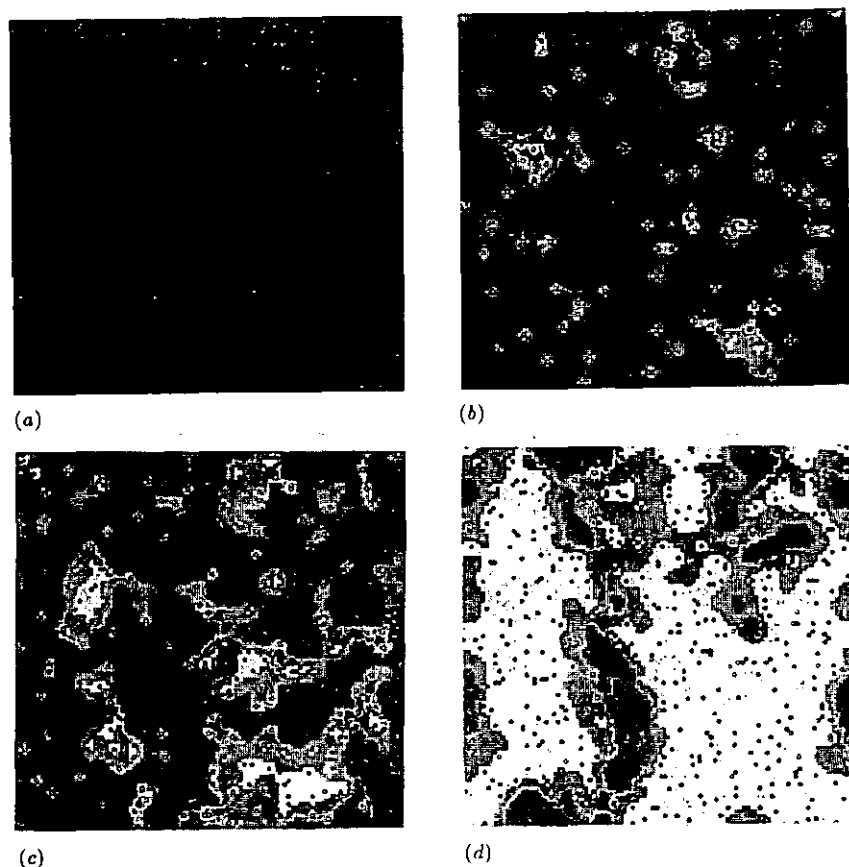


Figure 8. The distribution of induced moments on a square lattice of side 100 containing active sites in which the ratio of single-ion anisotropy to exchange field is just 2% above the critical value below which the pure magnet shows no induced moment. (a) depicts the pure lattice and (b)–(d) lattices with 1, 2 and 4% diamagnetic impurity. The magnitude of the moments at each sites is depicted in quartiles as a fraction of the moment in the pure magnet. For example, the darkest shade corresponds to moments that are (0.75–1.00) times those in the pure material.

Figure 7 illustrates clearly the large reduction in the observed ordered moment at low temperatures as x is increased. Note that the experimental points included in this figure differ from those in figure 2(a) in that they have been modified to take account of the increase in the widths of the scattering maxima and therefore they give a more direct measure of the average

A Harrison and D Visser

ordered moment. The reduction in the size of the regions of large moments is implied in figure 4: for the finite region displayed for the $x = 0.02$ sample, relatively large ordered moments percolate; for the $x = 0.03$ sample such moments are confined to small isolated clusters. Uncertainties remain: the contribution of the smaller moments to the neutron scattering is not given explicitly, nor are we able to be precise about the change in the character of the magnetic phase transitions on doping. Figure 2(a) shows that the first-order C- IC_2 phase transition seen in pure RbFeCl_3 rapidly broadens on dilution but, until a full Monte Carlo simulation is performed, we have no means of quantifying such effects.

The application of a magnetic field H_z parallel to the crystal c axis is expected to compensate to some extent for the disruptive influence of the dopant. Experimental work (I) and computer simulations (Harrison 1989) have shown that such a field raises the mean of the magnetic moments and reduces the variance. In figure 9(a) we display a schematic magnetic H_z - T phase diagram for a pure induced-moment magnet governed by the molecular field approximation. As H_z is increased, the induced moment is increased until the field pulls the moment out of the x - y plane. In 9(b) we illustrate the influence of small amounts of diamagnetic impurities, producing the continuous range of moments denoted by the shaded area whose upper boundary is close to that of the pure material. As the concentration of diamagnetic impurities is increased, the shaded region increases in width and both boundaries are lowered until (figure 9(c)) almost all of the magnet is like a pure singlet ground state material such as CsFeCl_3 (figure 9(d)).

Suppose a sample of $\text{RbFe}_{(1-x)}\text{Mg}_x\text{Cl}_3$ of composition $x = 0.05$ – 0.10 was cooled to low temperatures and then a significant magnetic field H_z was applied parallel to the c axis. The 'zero-field-cooled' state that existed before the field was applied is one in which the larger moments are frozen in superparamagnetic clusters. These clusters grow when H_z is applied until they are separated only by narrow domain walls. The merging of domains may require much reorganization and at low temperatures may occur on a timescale that is long enough for it to be observable in a neutron scattering experiment. The growth could be followed by scanning through the elastic scattering intensity in the region of the K point.

A comparison between the different influences of the dopants Cs^+ , Mg^{2+} and Br^- on the magnetic ordering processes of RbFeCl_3 sheds some light on the influence of each dopant at a microscopic level. In figure 10 we present a plot of the maximum inverse peak width for the magnetically scattered neutron intensity near the K point, as a function of temperature and the concentration of the dopant. This implies that a hierarchy of disruptive power of the various dopants may be set up as follows:

$$\text{Br}^- > \text{Cs}^+ > \text{Mg}^{2+}.$$

The relative influences of Br^- and Mg^{2+} are also implied in figure 2(a).

The Mg^{2+} ion replaces the Fe^{2+} ion on a one-to-one basis, severing the intrachain superexchange link. However, RbFeCl_3 is not particularly one-dimensional ($J_2/J_1 \simeq 10^{-1}$) so the effect of this substitution is much less severe than in most other pseudo-one-dimensional magnets (Takeda and Schouten 1981). Cs^+ ions appear to remove or reduce moments on Fe^{2+} on a much greater than one-to-one basis as quantified either in figure 10 in terms of the diffraction peak widths or in terms of the reduction in scattering intensity at the magnetic Bragg positions with dopant concentration is increased. When a Rb^+ ion is replaced by a larger Cs^+ ion a local structural distortion will probably occur and there will also probably be a local reduction in J_2 and consequently in the ratio J_Q/D . A comparison between the values of J_1 , J_2 and D for RbFeCl_3 and CsFeCl_3 (Visser and Harrison 1988) reveals that D and J_1 do not change very much with composition but J_2 does, being greater for RbFeCl_3 by a factor of about 1.8.

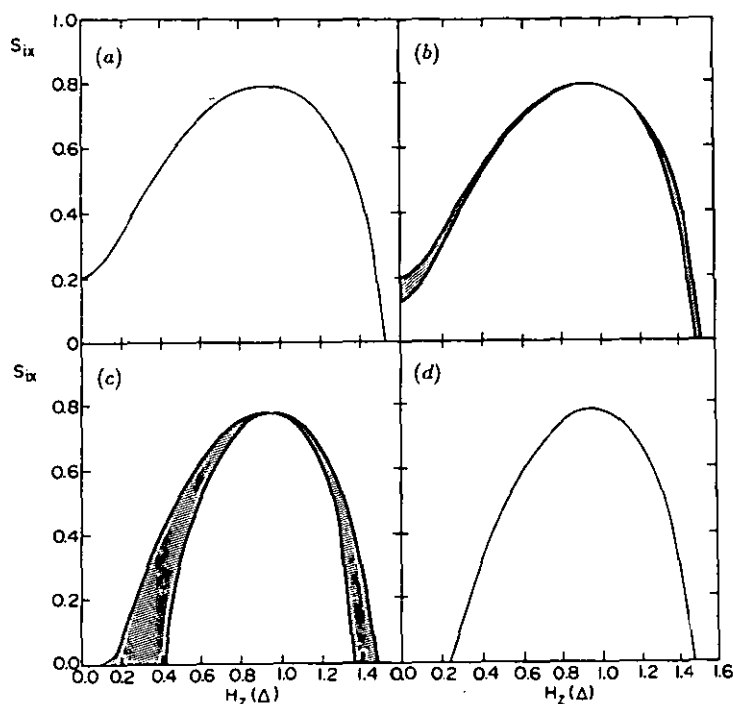
Magnetic ordering in $\text{RbFe}_{(1-x)}\text{Mg}_x\text{Cl}_3$ 

Figure 9. The dependence of the size of the induced moments S_{ix} in a selection of induced-moment magnets similar to $\text{RbFe}_{(1-x)}\text{Mg}_x\text{Cl}_3$ as a function of the magnetic field H_z applied parallel to the z direction. (a) depicts the change in the homogeneous moment with H_z in a magnet such as RbFeCl_3 which possesses a moment in zero applied magnetic field, and (b) and (c) depict the effect of increasing amounts of diamagnetic dopant on the distribution of moments in such a material, producing a range of values of increasing variance and decreasing mean as the concentration of dopant increases. (d) shows the dependence of mean moment on H_z for a magnet such as CsFeCl_3 which has zero induced moment when H_z is zero.

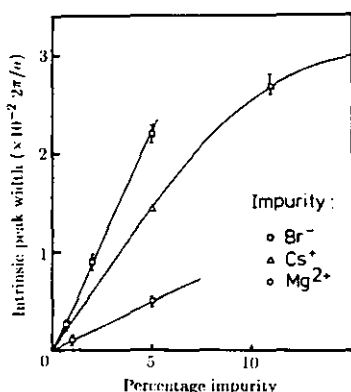


Figure 10. The dependence on the sample composition of the maximum magnetic correlation length (expressed here as its reciprocal value) in all of the doped compounds based on RbFeCl_3 . These values were measured at 2–2.2 K, depending on the temperature at which the minimum resolution-corrected peak widths lay. The full curves merely provide a guide to the eye, and values at low dopant levels should be treated with caution: their error bars are underestimated, since they include no measure of the uncertainty in the instrumental resolution width.

A Harrison and D Visser

The replacement of Cl^- ions in the interchain superexchange bridges by Br^- ions will probably increase J_2 slightly. It is also likely that the substitution of Cl^- ions by Br^- ions in the intrachain exchange bridges changes it from a positive value to a smaller positive value or a negative value, reducing J_Q locally and consequently reducing the size of the induced moments on neighbouring ions. A very small proportion of intrachain bridges may have *antiferromagnetic* exchange so may cause greater disruption of the ordered spin structures of RbFeCl_3 . If we compare figure 4 with the plot of the dependence of the scattering maxima peak widths for $\text{RbFeCl}_{(3-x)}\text{Br}_3$ in II, we see a marked difference. The widths of the peaks in $\text{RbFeCl}_{(3-x)}\text{Br}_3$ pass through a minimum as the temperature is reduced, implying a *reduction* in the length of the C or IC_1 magnetic correlations when the samples are cooled below about 1.8 K. The samples of $\text{RbFe}_{(1-x)}\text{Mg}_x\text{Cl}_3$ all show a monotonic change in width with temperature down to the lowest experimental value. One interpretation of this result is that the freezing of the smaller moments in $\text{RbFeCl}_{(3-x)}\text{Br}_3$ at lower temperatures—that is, the moments which are connected to neighbouring moments through bridges with one or more bromine atoms—introduces disorder (Aeppli *et al* 1982). No such source of disorder is expected in $\text{RbFe}_{(1-x)}\text{Mg}_x\text{Cl}_3$.

The influence of impurities on the balance between J_2 and γ in RbFeCl_3 doped with RbFeBr_3 was discussed in II, as was the nature of the diffuse scattering observed near the K point of those materials. The following two reasons for the form of the diffuse scattering in mixed compounds based on RbFeCl_3 were postulated there.

(i) Impurities break the spin structure up into smaller domains with the 120° antiferromagnetic spin structure of the pure magnet at low temperatures. The diameter of these domains may be estimated from the neutron diffraction peak widths to be of the order of 50 Å.

(ii) The frustration inherent in the 120° spin structure may be released near impurities, causing local canting of moments and producing a distribution of canting angles centred on the angle of the pure magnet (Villain 1979, Harrison 1987). Canting will also occur near domain walls.

The anisotropic nature of the scattering intensity in the $l=1$ plane would appear to rule out interpretation (i) as the sole origin of the diffuse scattering. Furthermore, local canting of moments may be the reason why the diffuse scattering component appears to persist to temperatures above T_N . First, let us consider the moments to be classical and not have an induced-moment character. Local canting of moments in the nearest-neighbour shell about a diamagnetic impurity causes them to adopt orientations relative to moments in the next-nearest shells that are closer to the 180° angle that maximizes the pairwise exchange energy. Thus, the exchange field experienced by next-nearest-neighbour moments increases and consequently the temperature at which the correlation between such moments is destroyed is higher. Of course in the induced-moment case the size of the moments in nearest-neighbour shells will also be reduced in size as their exchange field is decreased and the net influence on the exchange field acting on next-nearest neighbours will depend on J_1 , J_2 and D and would have to be calculated explicitly.

A similar type of diffuse neutron scattering has recently been seen in other pure and dilute frustrated magnets. The pure hexagonal XY antiferromagnet CsMnBr_3 , as well as samples doped with the diamagnet CsMgBr_3 , show a significant elastic, diffuse neutron scattering component centred at $(\frac{1}{3}, \frac{1}{3}, 1)_N$ at temperatures between T_N and $3T_N$ (Visser and McIntyre 1987, Visser *et al* 1988). The spatial distribution of this scattering adopts the same form in the $l=1$ plane as that seen in the $l=0$ plane of $\text{RbFe}_{(1-x)}\text{Mg}_x\text{Cl}_3$. Similar observations have been made in TlFeCl_3 (Visser and Knop 1984), a pseudo-one-dimensional ferromagnet whose magnetic properties resemble those of pure RbFeCl_3 . In all these compounds the single-ion

Magnetic ordering in $\text{RbFe}_{(1-x)}\text{Mg}_x\text{Cl}_3$

anisotropy confines the magnetic moment to the a - b plane and the interchain magnetic exchange directs the magnetic scattering of neutrons towards $(\frac{1}{3} \frac{1}{3} l)_N$. For the pure and doped CsMnBr_3 samples it was also found that a small amount of diffuse elastic scattering persisted below T_N . In a magnetization study of RbFeCl_3 (Kato *et al* 1985), remanent magnetic behaviour was found in the C phase. One interpretation given to this observation was that it arose from moments trapped between domains in the magnetically frustrated ground state. No indication of this effect was seen in the neutron scattering measurements of Wada *et al* (1982), though Kato *et al* (1985) thought it unlikely that such a type of experiment would detect it.

5. Conclusions

The induced-moment character of RbFeCl_3 sensitises it towards doping with diamagnetic impurities, causing the reduction of T_N with impurity concentration to be greater than that predicted by models in which classical moments are coupled by a molecular field. A qualitative explanation of the neutron scattering measurements is given by a simple molecular field calculation that takes account of the induced-moment character of the Fe^{2+} sites. It also provides a picture of the spatial distribution of the moments: at all but the lowest values of x the majority of moments are very small, but islands of moments whose magnitudes are comparable with those in the pure RbFeCl_3 remain. This is consistent with the experimental observation that the doped materials contain finite regions of moments with orientations similar to those in the pure material which remain frozen at temperatures comparable with the ordering temperature of the pure material. The model is unable to predict what contribution the smaller moments make to the neutron scattering, nor does it elucidate the strong elastic diffuse scattering component centred at the K point that persists to temperatures well above T_N . The treatment of such effects would require a full Monte Carlo simulation to be made.

A possible explanation for the diffuse scattering is the canting of moments near impurities, driven by the release of magnetic frustration. This could be studied further by Mössbauer spectrometry, which provides a measure of $\langle \sin^2 \theta \rangle$ (where θ is the angle between nearest-neighbour moments). At temperatures below T_N the induced-moment character of the host material is expected to greatly complicate canting models, as it produces a wide distribution of moment sizes. Such complications could be greatly reduced by repeating the measurements in doped materials subjected to a magnetic field H_z parallel to the crystal c axis, making the variance in the distribution of moment magnitudes much smaller. The application of H_z might also be used to study the relaxation of frozen magnetic disorder (I).

Thus, $\text{RbFe}_{(1-x)}\text{Mg}_x\text{Cl}_3$ may not only be used to rationalize the complicated disordering phenomena observed in $\text{Rb}_{(1-x)}\text{Cs}_x\text{FeCl}_3$ and $\text{RbFeCl}_{(3-x)}\text{Br}_x$, but it might also be used to model a number of problems concerning ordering in inhomogeneous materials. Along with similar materials derived from the induced-moment magnets RbFeBr_3 and TlFeCl_3 it appears to be the only insulating magnet suitable for a study of bootstrap percolation (Branco *et al* 1988, Harrison 1989).

Acknowledgments

The authors are grateful to the Institut Laue-Langevin for technical support and assistance during the experiments and in particular to G J McIntyre and K R A Ziebeck (now at the Department of Physics at Loughborough University of Technology). They would also like to thank the UK Science and Engineering Research Council for financial support and AH wishes to thank St John's College, Oxford for further financial aid.

A Harrison and D Visser

References

- Aeppli G, Shapiro S M, Birgeneau R J and Chen H S 1982 *Phys. Rev. B* **25** 4882
Birgeneau R J, Cowley R A, Shirane G and Yoshizawa H 1984 *J. Stat. Phys.* **34** 817
Bontemps N, Grisolia C, Nerozzi M and Briat B 1982 *J. Appl. Phys.* **53** 2710
Branco N S, de Queiroz S L A and dos Santos R R 1988 *J. Phys. C: Solid State Phys.* **19** 1909
Eibschutz M, Lines M E and Sherwood R C 1975 *Phys. Rev. B* **11** 4595
Fishman S and Aharony A 1979 *Phys. Rev. B* **19** 3776
Harrison A 1987 *J. Phys. C: Solid State Phys.* **20** 6281
— 1989 *J. Phys.: Condens. Matter* **1** 6695
Harrison A and Visser D 1989 *J. Phys.: Condens. Matter* **1** 733
Harrison A, Visser D, Day P, Knop W and Steiner M 1986a *J. Phys. C: Solid State Phys.* **19** 6811
Harrison A, Visser D, Day P and Ziebeck K R A 1986b *J. Magn. Magn. Mater.* **54–7** 1273
Hone D, Montano P A, Tonegawa T and Imry Y 1975 *Phys. Rev. B* **12** 5141
Kato H, Tomikawa T, Amaya K and Wada N 1985 *J. Phys. Soc. Japan* **54** 3942
Katsumata K, Nire T, Tanimoto M and Yoshizawa H 1982 *Phys. Rev. B* **25** 428
Knop W, Steiner M and Day P 1983 *J. Magn. Magn. Mater.* **31–4** 1033
Lai K K and Ward J B 1988 *J. Phys. C: Solid State Phys.* **21** 2279
Lines M E and Eibschutz M 1975 *Phys. Rev. B* **11** 4583
Munringhof G, Hellner E, Treutmann W, Lehner N and Heger G 1984 *J. Phys. C: Solid State Phys.* **17** 1281
Seifert H-J and Fink H 1975 *Rev. Chim. Miner.* **12** 466
Shiba H 1982 *Solid State Commun.* **41** 511
Shiba H and Suzuki N 1983 *J. Phys. Soc. Japan* **52** 1383
Suzuki N 1983 *J. Phys. Soc. Japan* **52** 3907
Takeda K and Schouten J C 1981 *J. Phys. Soc. Japan* **50** 2554
Villain J 1979 *Z. Phys.* **B 33** 31
Visser D and Harrison A 1988 *J. Physique C* **8** 1467
Visser D, Harrison A and McIntyre G J 1988 *J. Physique Coll. C* **8** 1255
Visser D and Knop W 1984 unpublished results
Visser D and McIntyre G J 1987 *Annual Report of the Institut Laue-Langevin*
Wada M, Ubukoshi K and Hirakawa K 1982 *J. Phys. Soc. Japan* **51** 283
Yoshizawa H, Kozukue W and Hirakawa K 1983 *J. Phys. Soc. Japan* **52** 1814
Zodkevitz A, Makovsky J and Kalman Z H 1970 *Israel. J. Chem.* **8** 755

Chapter 3.

Magnetic excitations and phase transitions in AFeBr_3 ($\text{A} = \text{Cs}, \text{Rb}$)

Magnetic excitations and phase transition of CsFeBr₃ in an external magnetic field

B. Dorner¹, D. Visser², and M. Steiner³

¹ Institut Laue-Langevin, F-38042 Grenoble Cedex, France

² University of Technology, Department of Physics, Loughborough, Leicestershire LE11 3TU, Great Britain

³ Johannes Gutenberg Universität, Institut für Physik, D-6500 Mainz, Federal Republic of Germany

Received March 9, 1990; revised version April 30, 1990

In CsFeBr₃ the Fe²⁺ ion with effective spin one has locally a singlet ground state ($m=0$). The antiferromagnetic interactions between neighbouring Fe-ions are too weak as compared with the anisotropy constant to introduce long range order in the absence of an external field. By inelastic neutron scattering we studied the magnetic excitations in an external magnetic field up to 5 Tesla applied along the c -axis. A linear Zeeman splitting was observed with a Landé factor $g=2.4$. The field renormalizes the dispersion curves in such a way that the exchange interaction has decreasing influence with increasing field. Theoretical calculations according to the excitonic model of Lindgård describe the experimental results very well. At 4.1 Tesla a phase transition appears to a commensurate long range order with a 120° arrangement of the spins in the hexagonal plane. Within the limits of experimental observation this phase transition has no influence on the dynamical behaviour. No critical phenomena could be observed. The dynamical structure factor $|G_j(Q)|^2$ of the lower Zeeman split modes decreases with increasing field.

1. Introduction

At room temperature the members of the AFeX₃ family (with A=Rb and Cs; X=Cl and Br) have the same hexagonal structure with space group P6₃/mmc and at low temperature they exhibit quasi one dimensional (1- D) magnetic behaviour. Chains of face sharing FeX₆ octahedra along the c -axis are separated by Rb or Cs ions. Thus the magnetic interaction along the chains is stronger than that between the chains. In all cases the Fe²⁺ ion has an effective spin $S=1$ and locally a singlet ground state (SGS) with $m=0$ due to the single ion anisotropy. If the exchange interaction is small compared to this anisotropy the whole system has an SGS at $T \rightarrow 0$. This is the case for CsFeCl₃ [1] and CsFeBr₃ [2], while in RbFeCl₃ [3, 4] and RbFeBr₃ [5–7] the total exchange

energy is large enough to produce magnetic long range order at low temperatures. Some characteristics of these four compounds are summarized in [8].

In all Cl compounds the 1- D exchange interaction is positive and creates ferromagnetic behaviour along the chains while in the Br compounds this interaction is negative and thus antiferromagnetic behaviour occurs.

A characteristic feature of these SGS systems is the softening of a magnetic mode at the magnetic zone centre with decreasing T due to correlations induced by the exchange interaction. Such a soft mode has been observed in all four compounds. In the Rb systems it condenses out and leads to long range static order. In the Cs compounds the soft mode approaches a finite value for $T \rightarrow 0$ as expected for SGS systems.

The application of an external magnetic field along the c -direction (chain direction) on the SGS materials leads to a phase transition to an ordered state. In CsFeCl₃, with ferromagnetic exchange interaction along the chains, three consecutive phase transitions have been observed [9] at 0.7 K. The first two at 3.8 and 4.1 Tesla lead to incommensurate structures and at 4.5 Tesla a commensurate 120° order appears. The modulated structures are explained by the influence of a dipole-dipole interaction [9]. In CsFeBr₃, with antiferromagnetic coupling along the chains, the phase transition leads immediately to the commensurate order at 1.6 K in a field of 4.1 Tesla [10]. The magnetic moments lie in the hexagonal plane with a 120° orientation relative to each other. In chain direction they are ordered antiferromagnetically.

In this paper we report on the study of magnetic excitations in CsFeBr₃ by inelastic neutron scattering in an applied magnetic field up to 5 Tesla.

The next chapter, concerning theoretical aspects, provides dispersion relations to be fitted to the data. Then we give the experimental conditions followed by a presentation of the experimental results. In the last chapter we compare experiment and theory and discuss the observations.

II. Theoretical aspects

The different materials mentioned above can be described by the following Hamiltonian

$$\mathcal{H} = -2J \sum_i S_i S_{i+1} - J' \sum_{i,j} S_i S_j + A \sum_i (S_i^z)^2 + g \mu_B m H_{ex}^z \sum_i S_i^z. \quad (1)$$

Here J is the exchange parameter between nearest neighbours along the chain and J' is that between the chains. The quasi 1-D character is related to the fact that $J \gg J'$. g is the Landé factor and μ_B the Bohr-magneton. For all four compounds presented in the introduction, the anisotropy parameter A is positive. A is then the energy gap between $m=0$ and $m=\pm 1$ states. This means that the Fe^{2+} ion has locally (without magnetic interaction) a SGS.

Including the exchange interaction into the consideration, but still without an external magnetic field H_{ex}^z , there are two regimes which are separated by a phase transformation. For $T \rightarrow 0$ and

$$A < 8|J| + 12|J'|, \quad (2)$$

the arrangement is called an easy plane or $x-y$ system which has a magnetic ground state [11–14]. The SGS for the whole crystal appears then for

$$A > 8|J| + 12|J'|. \quad (3)$$

In absence of an external magnetic field, the states $m=\pm 1$ are degenerate. In other words the dispersion curves measured earlier in CsFeBr₃ [2] are doubly degenerate. The application of a magnetic field along z gives rise to a Zeeman splitting of the modes. The dispersion of these split modes has been derived from the Hamiltonian, (1) [15, 16].

$$v^\pm(\mathbf{q}) = \{A[A - 2J(\mathbf{q}) \cdot R(T, H)] + J^2(\mathbf{q})(g \mu_B m M_z)^2\}^{1/2} + g \mu_B m \{H_{ex}^z + [2J_0 - J(\mathbf{q})] M_z\} \quad (4)$$

with

$$J(\mathbf{q}) = 4[J \cos(\pi q_c) + J' \gamma(2\pi q_\perp)]. \quad (5)$$

Within the excitonic model (5) holds for positive as well as for negative values of J [2, 14]. Here q_c is the wave vector in chain direction taken in reciprocal lattice units $[2\pi/c]$ starting from the origin of reciprocal space. The dispersion function for negative J' and a triangular arrangement within the hexagonal plane reads

$$\gamma(2\pi q_\perp) = 2 \cos(2\pi q_y) [\cos(2\pi q_x) + \cos(2\pi q_y)] - 1 \quad (6)$$

where q_x relates to units of (100) $\left[\frac{4\pi}{\sqrt{3}a}\right]$ and q_y to units

of (110) $\left[\frac{4\pi}{a}\right]$. $M_z = (H_{eff} - H_{ex}^z)/2J_0$ is the induced moment $\langle S^z \rangle$. In CsFeCl₃ it was found [12] that up to an external field of 5 Tesla the internal effective field

H_{eff} increased due to M_z only by 4%. M_z is zero for $H_{ex}^z=0$ and can be calculated self-consistently at each H_{ex}^z , but we do not go into details here, because the experiment presented later showed that M_z was negligibly small for CsFeBr₃.

$R(T, H_{ex}^z)$ is a renormalization factor first introduced by Lindgård [11] for the temperature dependence and then calculated by Knop and Lindgård [15, 16] for the field dependence. If one neglects the dispersion of the magnetic excitations in a SGS system, R is given by

$$R = R'/R'_0 = \left(n_1 - \frac{n_2 + n_3}{2}\right) / R'_0 \quad (7)$$

n_1 is the occupation factor for the ground state $m=0$ and n_2, n_3 for the Zeeman split states $m=-1, m=+1$, respectively. Without dispersion, R' is the difference of the occupation of the groundstate minus the occupation of the excited states and for $T \rightarrow 0$ and $H=0$ its value would become 1. R' is the negative of the quadrupole moment of the Fe^{2+} ion. For the states $m=0, +1, -1$ the corresponding values of the quadrupole moment are $-1, +1/2, +1/2$ respectively. For CsFeBr₃ R' has been determined from the experimental data for $T \rightarrow 0$ to be $R' = R'_0 = 0.64$ [2], the same value as found by Lindgård [11] for CsFeCl₃. For convenience in the definition of J and J' in Eq. (4) we use R normalised to one for $T \rightarrow 0$ and $H_{ex}^z=0$, see Eq. (7).

Knop [15] also gives a complicated formula for a self-consistent calculation of R including the complete dispersion curves. Lacking sufficient experimental data on the dispersion throughout the Brillouin zone, we will not go into detail here. Nevertheless we can derive here already the qualitative conclusion that R will decrease with increasing external field. Due to the increasing Zeeman splitting the occupation n_2 will increase faster than n_3 decreases.

The intensities I of the excitations v_j are assumed, as described in [2], to be given by

$$I(\mathbf{Q}, v_j) \approx |G_j(\mathbf{Q})|^2 \frac{\langle n_j \rangle + 1}{v_j}. \quad (8)$$

Here $\hbar\mathbf{Q}$ is the momentum transfer of the neutron. G_j and $\langle n_j \rangle$ are the dynamical structure factor and the Bose occupation factor for the mode j with frequency v_j .

III. Experiment

The single crystal of CsFeBr₃ was the same as the one used in the foregoing experiment [2]. It was grown by the Bridgeman method at the ICL, Oxford, being 8 mm in diameter and 15 mm in length. The mosaic width was about 1 degree and showed some structure, but the momentum transfers in the experiment were sufficiently small to allow neglect of its influence. We used the hexagonal lattice parameters $a=7.497 \text{ \AA}$ and $c=6.281 \text{ \AA}$, as adjusted to the instrument. They are in close agreement with the values from the structure determination $a=7.507 \text{ \AA}$ and $c=6.291 \text{ \AA}$ [8, 10].

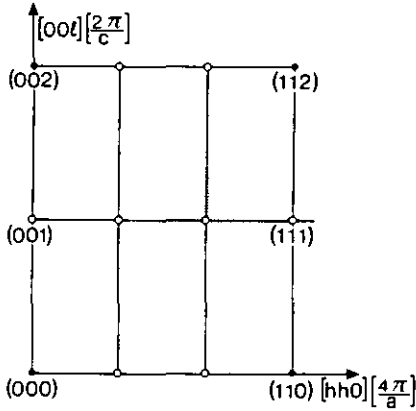


Fig. 1. Experimental plane in reciprocal space. Full dots indicate nuclear Bragg reflections, while the open ones indicate the centres of the magnetic Brillouin zones in the ordered phase

Inelastic neutron scattering was performed on the cold neutron three-axis spectrometer IN 12 with collimations $50' - 60' - 60' - 60'$. The wave vector of the monochromatic neutrons k_i was fixed to 1.3 or 1.5 or 1.8 \AA^{-1} . For $k_i = 1.3$ and 1.5 \AA^{-1} a cooled Be filter in front of the sample reduced the higher order contamination. For $k_i = 1.8 \text{ \AA}^{-1}$ the S-type curvature of the neutron guide eliminates the higher order contaminations.

It was necessary to use a horizontal field magnet, because on the one hand the field has to be applied along the c -axis, while on the other hand the magnetic superstructure position $(1/3 \ 1/3 \ 1)$ or $(2/3 \ 2/3 \ 1)$ had to be in the experimental plane. As the magnetic structure is hexagonal [10], the contributions from different domains coincide in these points. The different values of k_i have been chosen mainly to fulfil geometrical requirements of the magnet configuration and partly to improve resolution.

Constant Q -scans at 1.6 K were performed at points along the hatched paths in Fig. 1. The accessible area in reciprocal space was severely limited by the beam channels in the magnet. The highest possible field in the magnet was 5 Tesla. We took very great care in aligning the crystal c -axis parallel to the field direction to within 1 degree.

IV. Results

At 7 different values of the external field, H_{ex}^z between 0 and 5 Tesla, we measured the dispersion curves in the accessible range of Q -space, see Fig. 2. The constant Q -scans were fitted by a least squares routine to Gaussians, when the width corresponded to the calculated resolution, and to the damped harmonic oscillator formula, if the signal was broader. As the scans were performed with fixed incoming energy, the variation of the analyser transmission proportional to $k_f^3 \cot \theta_A$ [17] was included into the fitting procedure. For typical scans see Fig. 3. At 1.5 Tesla the Zeeman splitting produces two well separated excitations. The higher frequency mode was fitted to a gaussian and the lower one to a damped harmonic oscillator. This formula provides an asymmet-

ric line shape with more intensity on the low frequency side of the peak and accounts for the intensity on the energy gain side. At 2.5 Tesla the upper mode is out of the region of the scan and the lower one could only be separated from the incoherent elastic part by the improved resolution going from $k_i = 1.5 \text{ \AA}^{-1}$ to $k_i = 1.3 \text{ \AA}^{-1}$. The damped harmonic oscillator formula fitted simultaneously both, energy loss and gain, signals very well.

Some of the modes at high fields and low frequencies are overdamped, indicated by open circles in Fig. 2. Overdamped means that the signal has a maximum at zero energy transfer. This appears for

$$\Gamma \geq \sqrt{2} v_{\text{harm}} \quad (9)$$

where Γ is the frequency proportional damping parameter. The harmonic frequency v_{harm} has a finite value, even if the oscillator is overdamped. An overdamped mode is not any more of oscillatory character but of a relaxation one. Nevertheless v_{harm} is the frequency to be compared to those calculated later.

To extract the frequency v_{harm} from an overdamped signal is not an easy task, because the three fitting parameters: signal height, Γ and v_{harm} are strongly correlated. A further complication came from the fact that there was considerable incoherent elastic scattering on a relatively small general background. This incoherent intensity and the background was determined as an average from scans at low fields, see Fig. 3, as well as from scans sufficiently far away from $(2/3 \ 2/3 \ 1)$ at high fields.

At positions away from $(2/3 \ 2/3 \ 1)$ we were able to extract reasonable values for v_{harm} at all fields. But on the magnetic superstructure position itself no reliable values for v_{harm} could be obtained for fields $H_{ex}^z \geq 4.2$ Tesla, because the growing Bragg intensity did not anymore allow a fit of the damped harmonic oscillator function. In Fig. 4 we present the constant Q scans at $(2/3 \ 2/3 \ 1)$ for three different fields.

It can be seen very clearly in Fig. 2 that at each field the Zeeman splitting is independent of q .

The accessible Q range, see Fig. 1, contains the superlattice position $(2/3 \ 2/3 \ 1)$ of expected magnetic order. A Bragg peak appears there for $H_{ex}^z \geq 4.1$ Tesla, see Figs. 4 and 5. The intensity rises rapidly with further increasing field without a sign of saturation at 5 Tesla. By constant Q - and constant E -scans through the Bragg peak we verified that the widths corresponded to the instrumental resolution for all full circles given in Fig. 5. Within the resolution we concluded to observe long range magnetic order at the commensurate position. In Fig. 5 we also give the intensity contribution from field independent incoherent scattering. In addition, we present the integrated intensity of the lowest magnetic excitation. This integrated intensity was determined in two ways: *i*) from the fit of the damped harmonic oscillator by means of height times Γ (still valid in the weakly overdamped case) and *ii*) from fitting a Lorentzian to the magnetic quasielastic signal. The Bose occupation factor was always included in the fits. The Lorentzian intensity (height times full width at half maximum) came

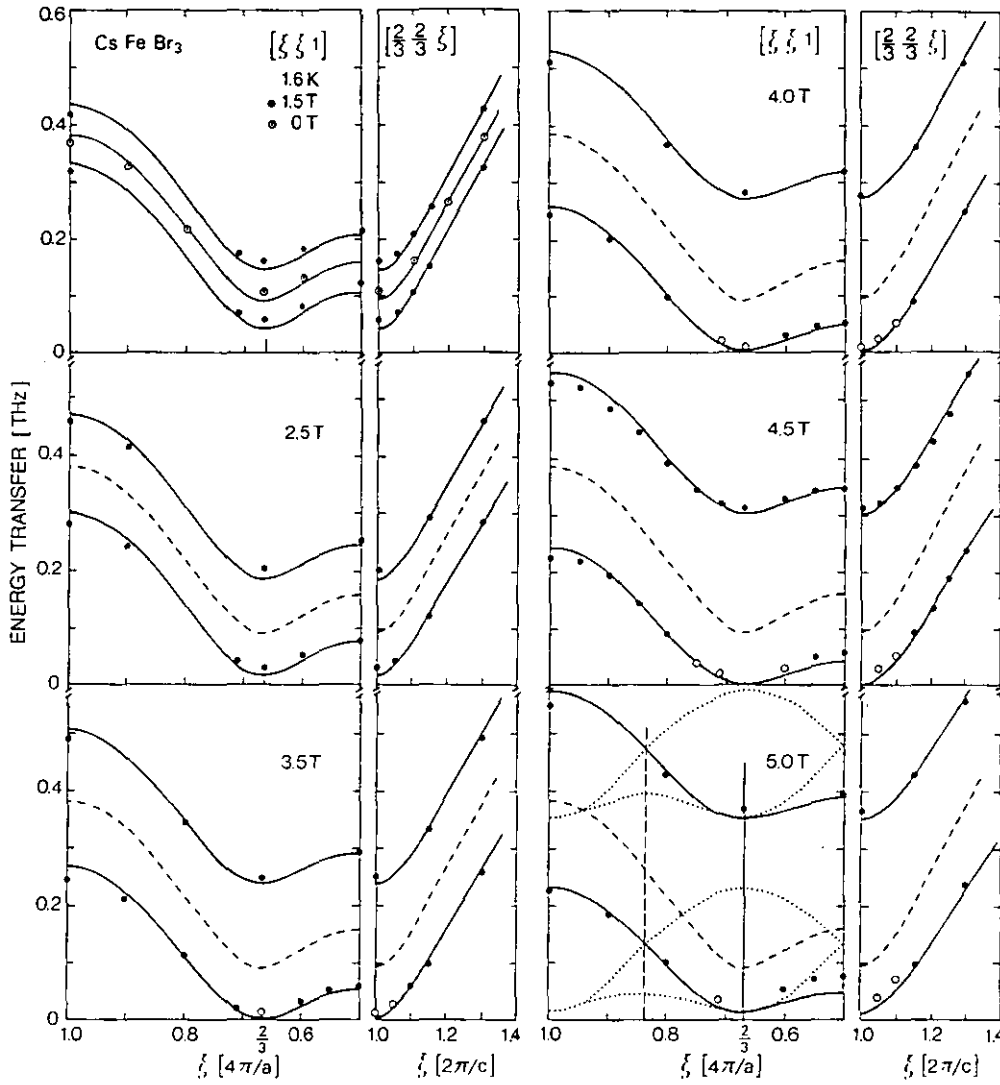


Fig. 2. Magnetic excitations under external magnetic fields from 0 to 5 Tesla as observed by constant Q scans. The errors on the frequencies are not bigger than the size of the symbols. The curves are calculated with the help of (4). The dispersion at zero field is repeated at each field by the dashed curves. The open symbols indicate overdamped modes. At 5 Tesla the Brillouin zones are indicated together with the six dispersion curves (dotted lines) in this energy range. 6 other dispersion curves must exist at higher frequencies around 0.9 THz

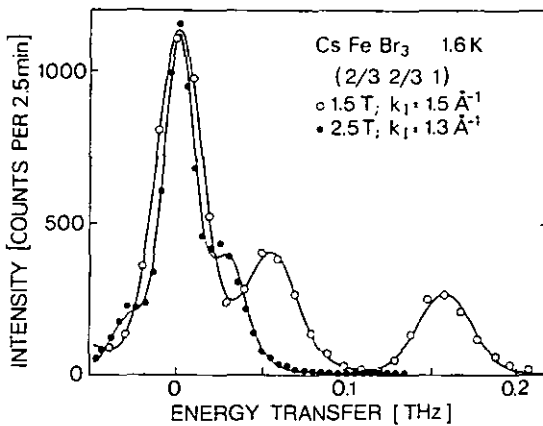


Fig. 3. Constant Q scans at $(2/3\ 2/3\ 1)$ at two different fields with different resolution, depending on k_1 . The intensity at zero energy transfer comes from incoherent elastic scattering and was fitted to a Gaussian. At 1.5 Tesla the high frequency mode was fitted to a Gaussian, while the low frequency mode was fitted to a damped harmonic oscillator at both fields

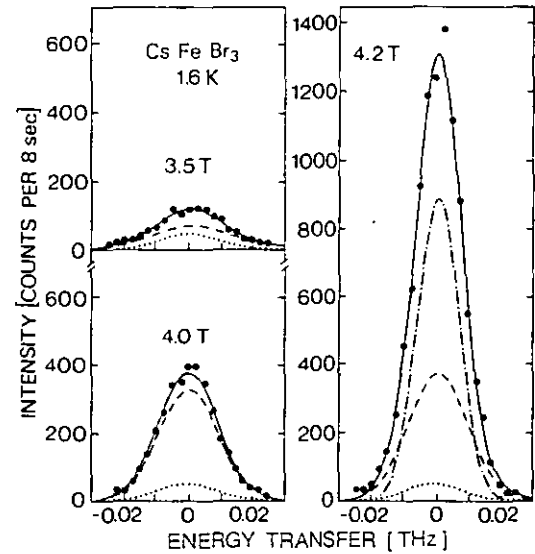


Fig. 4. Constant Q scans at $(2/3\ 2/3\ 1)$ at different fields with the good resolution of $k_1 = 1.3\ \text{\AA}^{-1}$... gives the contribution from incoherent elastic scattering described by a Gaussian with fixed parameters, --- the signal from inelastic scattering, ----- Bragg intensity fitted to a Gaussian with fixed width of 0.015 THz. The overall background was kept fixed during the fitting procedure and is too small to be seen

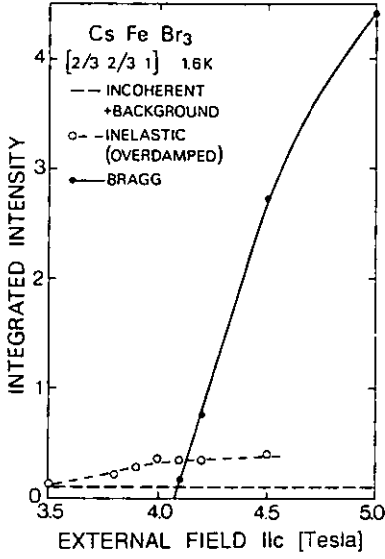


Fig. 5. Different intensities around zero energy transfer in the neighbourhood of the phase transition at 4.1 Tesla

out to be two times ($\pm 10\%$) the one from the harmonic oscillator fit. This was expected, because the Lorentzian fit covers energy gain and loss signals simultaneously. This intensity increases monotonously towards higher fields and does not show any sign of critical increase near the phase transformation at $H_{ex}^z \approx 4.1$ Tesla.

We searched carefully at several fields below, but close to the phase transformations for signs of precursors at incommensurate positions along $[\xi \xi 1]$ and $[2/3 \ 2/3 \ \xi]$. No indication could be seen. The $[\xi 0 1]$ could not be investigated, because it was perpendicular to the experimental plane.

In the SGS system for fields $H_{ex}^z < 4.1$ Tesla we expect two excitonic transitions per Fe^{2+} ion: $m=0$ to $m=-1$ and $m=0$ to $m=+1$. Within the excitonic description [2] all Fe^{2+} ions are identical as far as their magnetic properties are concerned. Therefore translational symmetry requires only one Fe^{2+} ion per unit cell in real space. This unit cell has the same dimensions as the chemical one in the hexagonal plane and half the dimension in z -direction. Correspondingly only two modes (and not more) should be observable at any given position in reciprocal space. In contrast to this postulation, additional modes, the "mirror modes" have been seen earlier [2]. In the present case the limited scattering geometry in the magnet prohibited a search for such additional modes.

In the ordered phase, $H_{ex}^z > 4.1$ Tesla, on the other hand, we have magnetic moments on the 6 Fe^{2+} ions in the magnetic unit cell, which has in z -direction the same dimension as the chemical one and is three times bigger within the hexagonal plane. The positions $(0 0 1)$, $(1/3 \ 1/3 \ 1)$, $(2/3 \ 2/3 \ 1)$, $(1 \ 1 \ 1)$ etc. are centers of the corresponding magnetic Brillouin zones. The magnetic Bragg intensities are extinct at $(0 0 1)$ and $(1 \ 1 \ 1)$ due to the interference in the triangular arrangement of the spins. The positions $(1/2 \ 1/2 \ 1)$ and $(5/6 \ 5/6 \ 1)$ are Brillouin zone boundaries.

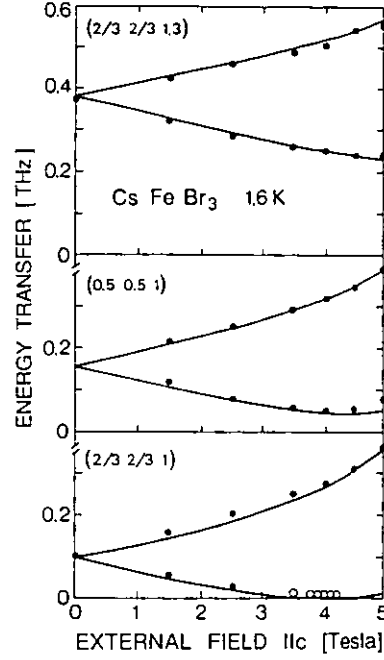


Fig. 6. Splitting of modes versus the applied external field

Now, with six magnetic ions per unit cell and with two excitations per ion, we expect 12 branches of spin wave dispersion per Brillouin zone. Within the investigated energy range and in the ordered phase we observe 6 different dispersion branches along the $[\xi \xi 1]$ direction. For visualisation they are sketched in Fig. 2 for $H_{ex}^z = 5$ Tesla. There must be 6 other modes at higher frequencies (around 0.9 THz) visible along $[\xi \xi 2]$. Generally speaking, up to 12 excitations could be visible at any given position in reciprocal space. We searched carefully at 4.5 Tesla but only two excitations could be identified at any examined position.

In Fig. 6 we present the Zeeman splitting at different positions in reciprocal space. Here it can be seen again that the observed splitting is independent of \mathbf{q} , but it is asymmetric and all curves show an upward curvature with increasing field. This curvature is stronger for the frequencies which are lower at zero field. The variations of the low frequencies have a shallow minimum around the phase transition field. At $(2/3 \ 2/3 \ 1)$ the minimum experimental frequencies are (0.01 ± 0.002) THz without a significant variation between 3.8–4.2 Tesla.

At $Q = (2/3 \ 2/3 \ 1)$ and at 5 Tesla the inelastic low energy signal was still overdamped. But in the presence of the strong Bragg intensity at this field no reliable parameters could be extracted.

In each field we determined the Zeeman splitting by taking the average over the available data, see Figs. 2 and 6. The variation between different \mathbf{q} positions stayed within the statistical errors of the frequency determination. The field dependence is linear within experimental errors. From the slope in Fig. 7 we obtain the Zeeman splitting to be

$$\nu_+ - \nu_- = \Delta \nu_{\text{Zeeman}} = 0.068 \pm 0.001 \left[\frac{\text{THz}}{\text{Tesla}} \right] \cdot H_{ex}^z. \quad (10)$$

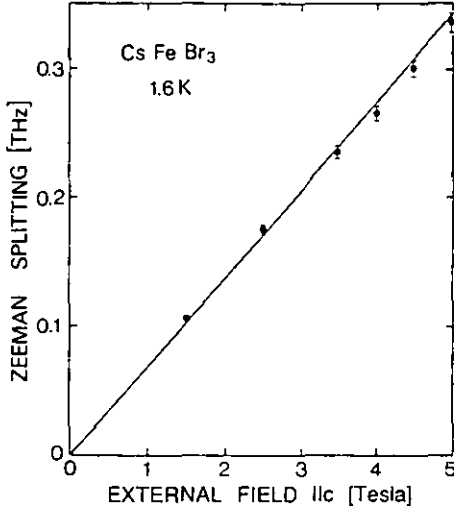


Fig. 7. Slope of Zeeman splitting

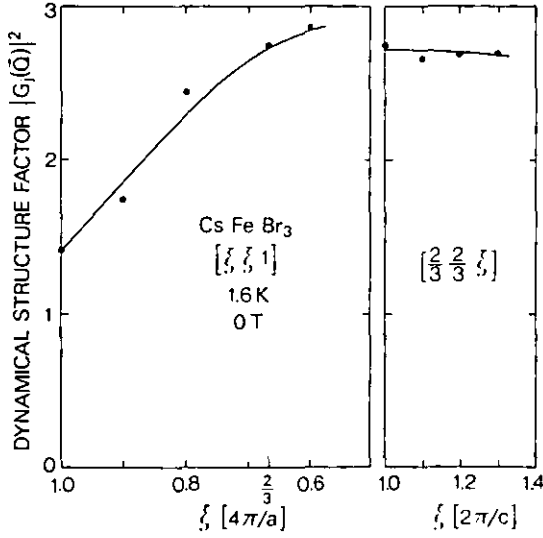


Fig. 8. Dynamical structure factor at zero field in arbitrary units. The curves are guidelines to the eye

From this slope we can calculate the Landé factor g of the excited state by

$$\frac{1}{2} \Delta \nu_{\text{Zeeman}} = g \cdot \mu_B m \cdot H_{\text{ex}}^z. \quad (11)$$

We obtain

$$g = 2.4, \quad (12)$$

a very similar value as compared to that obtained for CsFeCl₃ [1] with $g = 2.5$. For RbFeCl₃ Suzuki [13] calculated $g = 2.35$.

Besides extracting frequencies from the experimental data, we also derived intensities. As the varying analyser transmission was corrected for, the integrated intensity of an excitation could be taken as the product of height times width, as coming out of the fitting procedure [17]. The intensity, see Eq. (8), will depend on the applied field, because the frequencies ν_j depend on the field. We considered this frequency dependence as trivial and deter-

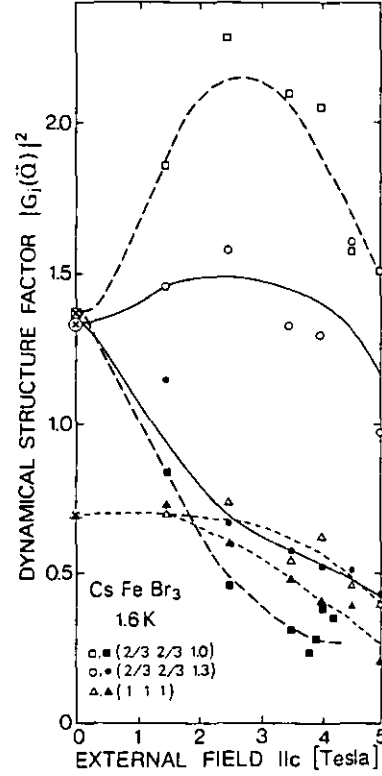


Fig. 9. Dynamical structure factor versus external field. The units are the same as in Fig. 8. The open symbols correspond to the higher and the closed ones to the lower frequencies. The curves are guidelines to the eye

mined the dynamical structure factor by multiplying the integrated intensity by

$$|G_j(Q)|^2 \approx I(Q, \nu_j) \times \nu_j \times [1 - \exp(-h \nu_j / k T)]. \quad (13)$$

In this way we determined first the dynamical structure factor in the available Q range for zero field, see Fig. 8. The field dependence of $|G_j(Q)|^2$ for the Zeeman split modes is presented in Fig. 9 for three different Q -positions. In Fig. 9 the values at zero field marked by an additional cross in the symbol, are taken as half of the corresponding values in Fig. 8 because at zero field both modes $m = +1$ and $m = -1$ contribute to the same peak. The scatter of the data corresponds to statistical and systematic uncertainties in the data. It is estimated to be $\pm 15\%$.

The curves in Fig. 9 are guidelines to the eye. Apparently the dynamical structure factor of the lower frequency mode of the Zeeman doublet decreases with increasing field in all cases. The upper modes behave differently – within experimental errors – but at high fields their dynamical structure factors decrease as well. We took the sum of the $|G_j(Q)|^2$ for each doublet and found that in average this sum is at 5 Tesla (0.53 ± 0.1) times the value at zero field.

V. Discussion

At first sight the observed Zeeman splitting, see Fig. 6, has an astonishing field dependence. At small fields the

slopes are asymmetric – faster increasing than decreasing frequencies and at larger fields the variation of frequencies shows an upwards curvature. Some initially decreasing frequencies go through a minimum and then increase with higher fields. At the same time the Zeeman splitting, Fig. 7, is, within experimental errors, linear with the field and independent of q . To understand this and the frequency dependence as seen in Fig. 6 we have to assume that the underlying frequencies (the non split ones) are field dependent. Indeed Eq. (4) contains the temperature and field dependent renormalization factor R . Its temperature dependence has been observed [2] to be in good agreement with theory [11, 12]. Its field dependence has been calculated for CsFeCl₃ [15, 16].

In the present case we defined a frequency ν_{Disp} for the underlying dispersion as the middle between the split frequencies

$$\nu_{\text{Disp}} = \frac{1}{2}(\nu_+ + \nu_-). \quad (14)$$

Then we used the values for A , J , J' as obtained earlier [2] together with ν_{Disp} to determine R as a function of field with Eq. (4) setting $H_{\text{ex}}^z = M_z = 0$.

In this procedure we encountered a small problem. The parameter values obtained by a least square fitting procedure to the whole set of measured frequencies [2] gave dispersion curves in the $[\xi \xi \Gamma]$ direction with less dispersion than experimentally observed for the high frequencies and stronger than the experimental dispersion for the low frequencies which we investigated here. To reduce the discrepancy for the present interpretation we used $J' = -0.0062$ THz (instead of $J' = -0.0067 \pm 0.0005$ [THz]), $A = 0.62$ THz and $J = -0.066$ THz as determined in [2].

The R values obtained in this way, see Fig. 10, decrease with increasing field, a behaviour which was expected as explained in the chapter on theoretical aspects. Our derived R decreases slightly less with field than the one calculated for CsFeCl₃ [15, 16]. As pointed out by Lindgard [11, 12], R' , see Eq. (7), is the negative of the local quadrupole moment. It controls the contribution of the exchange interaction and leads to different dispersion curves at different temperatures (to be calculated in a self-consistent way). The dispersion curves around $Q = (2/3, 2/3, 1)$ lead to correlations building up with decreasing temperature. Obviously an increasing magnetic field reduces the quadrupole moment and in turn the contribution of the exchange interaction to the dispersion curves, see Eq. (4).

With R taken from Fig. 10, with $g = 2.4$ as derived above and the parameters A , J , J' as given above we used (4) (still $M_z = 0$) to calculate the dispersion curves drawn in Fig. 2 as well as the frequencies in Fig. 6.

We decided to set $M_z = 0$ in the calculation, because the Zeeman splitting was q independent within experimental error. Inspecting Eq. (4) M_z would create a q dependent splitting. As predicted for CsFeCl₃ [15], M_z is negligibly small at low field and should come up to a 4% effect on the effective field at 5 Tesla.

Apparently the agreement of calculated and measured frequencies is very good. Most strikingly, there

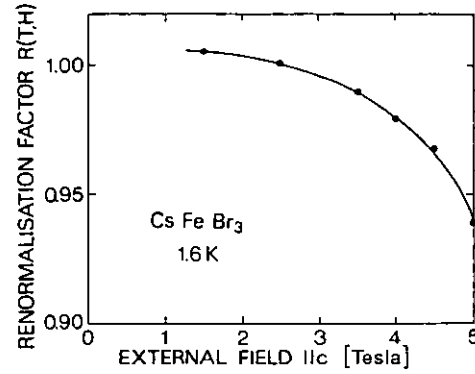


Fig. 10. The renormalisation factor $R(T, H_{\text{ex}}^z)$ versus field

is no visible influence from the phase transformation appearing at 4.1 Tesla. There is a mode becoming soft at $(2/3, 2/3, 1)$ and showing a broad minimum versus field around 4.1 Tesla, but experimentally no critical behaviour was observed. The calculated frequencies are very small for this mode. They can even come out negative, for example using the parameter $J' = -0.0067$. We think that the absence of critical behaviour is not a question of the value of the frequency. It is the consequence of the fact that the derivative of the frequency versus field near the phase transition has a value of about zero in the calculation as well as in the experimental results. In the soft mode picture the divergence of the critical scattering intensity is created by the soft mode frequency going towards zero.

Unfortunately the experimental data could only be obtained for a limited area in Q -space. We do not have reliable information on the overall dispersion relations at applied magnetic fields. Therefore we did not make the attempt to derive R and M_z from the measured excitation frequencies in an independent way [11].

As far as the dynamical structure factors $|G_j(Q)|^2$ are concerned, a heuristic model has been presented [2] for zero field but restricted to the q_c dependence along the chains. The overlap of the new data and the earlier ones exists only for two points $q_c = 1.2$ and 1.3 . The results agree because the intensities determined earlier [2] for these q 's close to $q_c = 1$ decrease proportional to ν^{-1} . This dependence, $|G_j(Q)|^2 = \text{constant}$, was predicted by Papanicolaou and Spathis [14] in an approximate semiclassical theory based on a $1/n$ expansion. The index n characterizes a general symmetric representation of $U(3)$. An independent calculation, same reference, was performed based on an expansion in powers of $1/a$, where $a = A/2J$. Then the resulting $|G_j(Q)|^2$ increases slowly with increasing q_c in contrast to our observations [2], where $|G_j(Q)|^2$ was slowly decreasing from 1 at $q_c = 1$ to 0.5 at $q_c = 2$.

It was observed already, that for q_\perp (perpendicular to the chains) the dynamical structure factor has a maximum at the superlattice positions $(1/3, 1/3, 1)$ and $(2/3, 2/3, 1)$. Here we have now more data on the $[\xi \xi \Gamma]$ direction, see Fig. 8. But the interpretation stays qualitative in postulating interference between neighbouring chains in the excited state.

Figure 9 shows that $|G_j(Q)|^2$, in particular for the low frequency modes on the Zeeman split doublets, depends strongly on the applied magnetic field. We see two possible explanations for this effect. First the interference between neighbouring Fe²⁺ ions may vary with the field. However, it would be unlikely that modes at different Q positions behave so similarly. Therefore we favour the second explanation, that the amplitudes of the dynamical spin components depend on the field. Within the heuristic model in [2] it was concluded that all the modes observed in the present experiment are visible exclusively due to their IP (in plane, perpendicular to the chains) dynamical components. Following this line of interpretation we postulate that the amplitudes of the IP components decrease with increasing field. Then in turn the OP (out of plane) components should increase.

Unfortunately, as mentioned above, we were not able to look for the "mirror modes" which are predicted to be exclusively visible due to OP amplitudes. But we plan another experiment with different geometry to study the "mirror modes" under an applied field.

VI. Conclusion

We investigated the SGS system CsFeBr₃ under an external magnetic field applied along the c -axis at 1.6 K. In a field of 4.1 Tesla a well defined Bragg peak appears at $(2/3\ 2/3\ 1)$ indicating long range commensurate order with a triangular 120° arrangement in the basal plane. Within the experimental accuracy there is a second order phase transition at 4.1 Tesla from a SGS system to one with static magnetic moments. This type of long range order was already presumed, when we wrote the dispersion relation (4). The lowest frequency appears then at $(2/3\ 2/3\ 1)$. We expected a soft mode with increasing field at this position condensing out into long range order. But this is not observed. Instead the lowest frequency mode, which behaves like a soft mode for small fields, levels off near the phase transformation, and so does the integrated inelastic intensity. The derivative of frequency versus field becomes zero experimentally and in the calculation; i.e. the frequency of this (overdamped) mode stays finite. The Bragg intensity appears without precursors near the phase transformation.

The excitations in this ordered phase may be called spin waves in contrast to excitons. The dynamical struc-

ture factor $|G_j(Q)|^2$ in particular for the low frequency modes decreases with increasing field. At 5 Tesla the sum of the dynamical structure factors over the Zeeman split doublets amounts to $53 \pm 10\%$ of the value at zero field.

The excitonic picture and the corresponding equations as derived by Lindgård [11, 12, 16] and Knop [15] have been applied in the whole range of fields up to 5 Tesla. This description reproduces the experimental results on the dynamics of the system very well and in a continuous way. Within the experimental errors we are unable to detect any influence of the long range order on the dynamical behaviour of the system.

We like to thank D. Puschner and P. Suttling for technical assistance during the experiment and R. Utermann, who participated in the experiments, for his valuable help in the data analysis.

References

- Steiner, M., Kakurai, K., Knop, W., Dorner, B., Pynn, R., Happek, U., Day, P., McLeen, G.: *Solid State Commun.* **38**, 1179 (1981)
- Dorner, B., Visser, D., Steigenberger, U., Kakurai, K., Steiner, M.: *Z. Phys. B - Condensed Matter* **72**, 487 (1988)
- Yoshizawa, H., Axe, J.D., Shirane, G.: *Solid State Commun.* **38**, 241 (1981)
- Petitgrand, D., Hennion, B., Radhakrishna, P., Escribe, C., Legrand, S.: *Recent developments in condensed matter physics*. Devreese, J.T., et al. (eds.), Vol. 4, p. 205. New York: Plenum Press 1981
- Adachi, K., Takeda, K., Matsubara, F., Mekata, M., Haseda, T.: *J. Phys. Soc. Jpn.* **52**, 2202 (1983)
- Harrison, A., Visser, D.: *Phys. Lett. A* **137**, 79 (1989); *J. Phys. Condensed Matter* (to be published)
- Visser, D., Dorner, B.: (to be published)
- Visser, D., Harrison, A.: *J. Phys. (Paris)* **49**, C8-1467 (1988)
- Knop, W., Steiner, M., Day, P.: *J. Magn. Magn. Mater.* **31-34**, 1033 (1983)
- Visser, D., Harrison, A., Vrtis, M., Brown, P.J.: (to be published)
- Lindgård, P.A.: *J. Phys. C* **8**, L178 (1975)
- Lindgård, P.A.: *Physica* **120B**, 190 (1983)
- Suzuki, N.: *J. Phys. Soc. Jpn.* **50**, 2931 (1981)
- Papanicolaou, N., Spathis, P.: *J. Phys.: Condens. Matter* **1**, 5555 (1989)
- Knop, W.: Thesis, Technische Universität, Berlin (1985)
- Lindgård, P.A.: *J. Magn. Magn. Mater.* **54-57**, 1227 (1986)
- Dorner, B.: *Acta Crystallogr. A* **28**, 319 (1972)

Physica B 174 (1991) 25–29
North-Holland

Magnetic excitations of the singlet ground state antiferromagnet CsFeBr₃ in a magnetic field

D. Visser^a, B. Dörner^b and M. Steiner^c

^aLoughborough University of Technology, Department of Physics, Loughborough, LE11 3TU, UK

^bInstitut Laue–Langevin, BP 156X, Centre de Tri, F-38042 Grenoble Cedex, France

^cJohannes Gutenberg Universität, Institut für Physik, W-6500 Mainz, Germany

The magnetic excitations in the quasi-one-dimensional singlet ground state antiferromagnet CsFeBr₃ have been studied by inelastic neutron scattering in the presence of an applied magnetic field, $H\parallel c$ and $H\perp c$. With $H\parallel c$, the dispersion curves renormalise so that the exchange interaction has a decreasing influence with increasing field. $H\perp c$ has little or no effect on the dispersion of the magnetic excitations.

1. Introduction

The ternary halide CsFeBr₃ adopts the hexagonal perovskite structure with space group P6₃/mmc [1]. The Fe²⁺ ions in this structure type are located in bromide octahedra which form infinite linear chains along the c direction due to the face sharing of the octahedra. The interchain separation is much larger than the intrachain separation which results in quasi-one-dimensional magnetic behaviour at low temperatures.

The effect of the cubic component of the ligand field and spin–orbit coupling on the D term of the Fe²⁺ ion gives rise to a $J = 1$ ground state which is further split by the trigonal component Δ into a singlet ground state (SGS) and a low-lying excited doublet [2]. At low temperatures only these two states are sufficiently populated. Therefore, one can describe the magnetic behaviour at low temperatures with an effective Hamiltonian with $S = 1$:

$$H = -2J \sum_i \mathbf{S}_i \cdot \mathbf{S}_{i+1} - J' \sum_{i \neq j} \mathbf{S}_i \cdot \mathbf{S}_j + A \sum_i (S_i^z)^2 - g\mu_B m H_{ex}^z \sum_i S_i^z. \quad (1)$$

Here J and J' are the intrachain and the interchain superexchange parameters, respectively,

and A , the value of which is positive, equals the energy gap between the $m = 0$ and $m = \pm 1$ states; g is the Landé factor, μ_B the Bohr magneton and H_{ex}^z an externally applied magnetic field.

In case the exchange interactions are weak in comparison to the anisotropy, the whole system has a SGS at $T \rightarrow 0$. The application of an external magnetic field along the chain direction (c axis) in such a type of hexagonal AFeX₃ compound leads to a magnetic phase transition [3, 4]. A further characteristic feature of this type of SGS system is the softening of a magnetic mode at the magnetic zone centre with decreasing temperature [5]. A similar effect will be observed at low temperatures when an increasing magnetic field ($H\parallel c$) is applied.

In the absence of an external magnetic field, eq. (1) represents two different regimes:

– For $T \rightarrow 0$ and $A < 8|J| + 12|J'|$ the system has an easy plane xy -character and has a magnetic ground state [6].

– For $T \rightarrow 0$ and $A > 8|J| + 12|J'|$ the system has a singlet ground state and consequently does not order magnetically.

In the absence of an external magnetic field H_{ex}^z , the states $m = \pm 1$ are degenerate. The application of a magnetic field along the z axis gives rise to a Zeeman splitting of these modes.

The dispersion of the split modes have been derived from eq. (1) [7, 8],

$$\begin{aligned} \nu^{\pm}(q) = & \{ A[A - 2J(q)R(T, H_z^{\text{ex}})] + J^2(q) \\ & \times (g\mu_B m M_z)^2 \}^{1/2} \\ & - g\mu_B m \{ H_z^{\text{ex}} + \{ 2J_0 - J(q) \} M_z \}, \end{aligned} \quad (2)$$

with

$$J(q) = 4[J \cos(\pi q_c) + J' \gamma(2\pi q_{ab})] \quad (3)$$

and

$$\begin{aligned} \gamma(2\pi q_{ab}) = & 2 \cos(2\pi q_y) [\cos(2\pi q_x) \\ & + \cos(2\pi q_z)] - 1. \end{aligned} \quad (4)$$

Within the excitonic model eq. (3) can be used for positive as well as negative values of J [9]. Here q_c is the wavevector in the c direction expressed in reciprocal lattice units ($2\pi/c$). $R(T, H_z^{\text{ex}})$ is a renormalisation factor introduced by Lindgård [7] in order to account for the temperature renormalisation. M_z is the induced magnetic moment, which is negligible in the present case.

CsFeBr₃ has been characterised by elastic and inelastic neutron-scattering techniques. Powder neutron diffraction indicated that no magnetic scattering can be observed at temperatures down to 67 mK [10]. Single-crystal neutron diffraction in an applied magnetic field ($H \parallel c$) showed that magnetic ordering is induced at $H = 3.9$ T, $T = 1.35$ K gradually changing to $H = 4.5$ T at 2.3 K [11]. The magnetic Bragg intensity appeared at $Q = (\frac{1}{3} \frac{1}{3} 1)$; $Q = (\frac{2}{3} \frac{2}{3} 1)$ and equivalent positions indicating a 120°-type antiferromagnetic ordering in the ab plane in the induced magnetic phase. The magnetic excitations were measured at $T = 1.4$ K [12]. The magnetic dispersion surface shows a strong soft-mode behaviour and a minimum in energy at $Q = (\frac{1}{3} \frac{1}{3} 1)$ and the equivalent position $Q = (\frac{2}{3} \frac{2}{3} 1)$. The observed dispersion surface at $T = 1.4$ K can be described by eq. (2) with the parameters $J = -0.066$ THz; $J' = -0.006$ THz and $A = 0.62$ THz ($R = 1$ at $T = 1.4$ K) [12]. The splitting of the magnetic

excitations and the induced soft-mode behaviour in an external magnetic field ($H \parallel c$) at $T = 1.6$ K have also been studied [13]. The observed behaviour is equally well described by eq. (2) and a magnetic phase transition was observed at $H = 4.1$ T. Due to geometrical restrictions of the horizontal-field cryomagnet, only a small section of reciprocal space around the magnetic zone centre at $Q = (\frac{2}{3} \frac{2}{3} 1)$ has been studied so far. In this paper we present further data on the magnetic excitations in CsFeBr₃ in an external magnetic field ($H \parallel c$) at the zone boundary. The behaviour of the magnetic excitation of CsFeBr₃ in an external magnetic field applied in the non-ordering direction, ($H \perp c$), is also presented.

2. Experimental

A single-crystal boule of CsFeBr₃ being 15 mm in diameter and 25 mm in length was grown by the Bridgman method. The mosaic width was about 0.8°. This crystal was mounted in an Oxford Instruments Cryomagnet with a vertical magnetic field of 6 T and aligned with its hexagonal a - b directions in the scattering plane. The final alignment of the crystal was within 1° of the vertical field direction (c axis). The optimised lattice parameters from the experiment were $a = 7.534$ Å and $c = 6.310$ Å. These values are in good agreement with those obtained from the structure determination, $a = 7.509$ Å and $c = 6.291$ Å [1].

Inelastic neutron scattering was performed on the thermal source neutron three-axis spectrometer IN20 at the Institut Laue-Langevin. The collimation used was 35'–40'–60'–60'. The experiment was carried out with constant $k_f = 2.662$ Å^{−1}. Pyrolytic graphite was used as a monochromator and a Heusler crystal as an analyser. A PG filter was used to reduce the second-order contamination of the neutron beam.

With this orientation we are only able to study the splitting of the magnetic excitations in the plane perpendicular to the chain direction.

A second crystal, the one used for previous experiment [12, 13] was mounted with the [001]/[110] directions in the scattering plane. With this

D. Visser et al. / Magnetic excitations of CsFeBr₃ in a magnetic field

orientation we can probe the influence of an external magnetic field on the magnetic excitations in the non-ordering direction. The magnetic excitations at a number of positions along $[00\zeta]$ and $[\frac{1}{3}\frac{1}{3}\zeta]$, $[\frac{2}{3}\frac{2}{3}\zeta]$ directions were measured as a function of field. All the experiments were carried out at $T = 2.5$ K.

3. Results and discussion

3.1. $H \parallel c$

At $H = 5$ T, we measured the magnetic excitations along the $[\xi\xi0]$ and $[\xi00]$ directions, fig. 1. The $m = \pm 1$ magnetic excitations, which are degenerate in zero field, are split by the external magnetic field and are well resolved for high magnetic fields, fig. 2. The magnetic excitations were fitted by at least-squares routine to Gaussians. Their widths were comparable to the resolution width of the instrument. It can be seen that the Zeeman splitting is independent of q . The limited data taken at different magnetic fields show that this is also the case for each field, fig. 3.

The Zeeman splitting was determined from the data taken at $Q(0.5, 0.5, 0)$. The field depen-

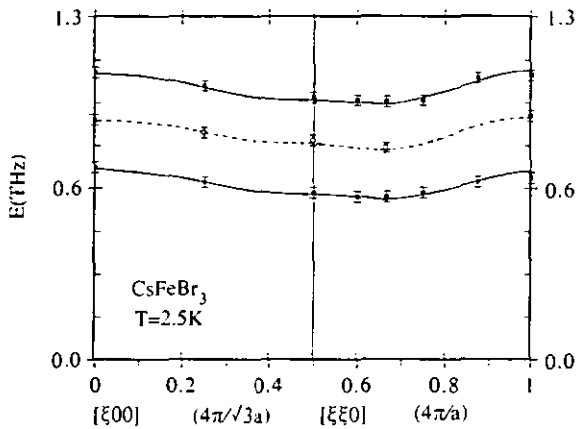


Fig. 1. The magnetic excitations in zero field, (O), and in an external magnetic field of 5 T (●). The dashed curve represents the best fit at zero field calculated according to eq. (1): $J = -0.064(2)$ THz, $J' = -0.008(3)$ THz and $A = 0.64(2)$ THz. The solid curves at $H = 5$ T were calculated according to eq. (4) using $R(T, H_{ex}^2) = 0.94$.

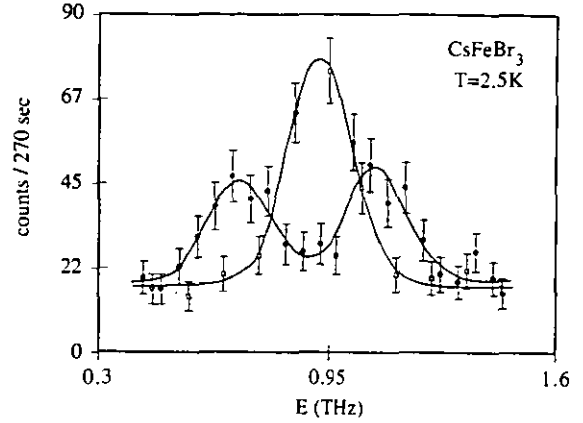


Fig. 2. Constant- Q scans at $Q(110)$ at 0 T (O) and at 5 T (●).

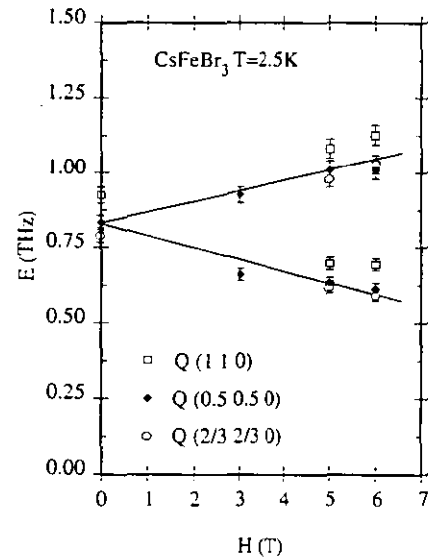


Fig. 3. Splitting of the modes versus the applied field.

dence is linear within the experimental errors. The slope in fig. 4 was fitted to the relation

$$\begin{aligned} \nu_+ - \nu_- &= \Delta\nu_{\text{zeeman}} \\ &= 0.074(4)[\text{THz/T}] \cdot H_{\text{ex}}^2. \end{aligned} \quad (5)$$

From this slope we can calculate the Landé factor g of the excited state by

$$\frac{1}{2} \Delta\nu_{\text{zeeman}} = g\mu_B m H_{\text{ex}}^2. \quad (6)$$

D. Visser et al. / Magnetic excitations of CsFeBr₃ in a magnetic field

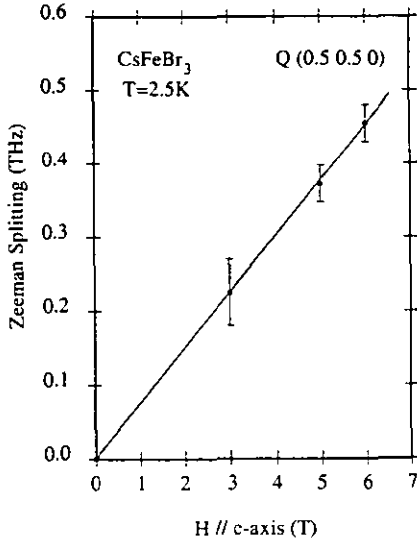


Fig. 4. Slope of the Zeeman splitting.

We derive for $g = 2.6(2)$. This value is, within the error, comparable with the previously obtained value of $g = 2.4$ at $T = 1.6$ K [13]. This value is also very similar to the one obtained for CsFeCl₃ [4].

The field dependence of the magnetic excitations at the zone boundary shows a similar behaviour as observed for the magnetic excitations near the zone centre [13]. The high frequencies ν_+ increase slower than the low frequencies ν_- decrease and the resulting slopes are asymmetric. We do not have sufficient data to show the field dependence in detail. However, the indication of non-linear behaviour at high magnetic field has been clearly established for magnetic excitations around the magnetic zone centre. As eq. (2) shows, the underlying magnetic excitations of fig. 3 are field and temperature dependent. In a previous paper [13] we defined a frequency for the underlying dispersion as the middle between the split frequencies: $\nu_{\text{disp}} = \frac{1}{2}(\nu_+ - \nu_-)$. Then we used the values of J , J' and A [12] as constants and fitted the expression (2) to the values ν_{disp} in order to obtain a value for $R(T, H_{\text{ex}}^z)$ setting $R = 1$ at $H_{\text{ex}}^z = 0$. For the data at $H = 5$ T we obtain a renormalisation constant $R(T, H_{\text{ex}}^z) = 0.94(2)$. This value of R is in agreement with the R value determined from the

low-frequency excitations in the previous study [13]. The factor $R(T, H_{\text{ex}}^z)$ decreases with increasing field and temperature. The factor R is the negative of the local quadrupole moment [7, 8, 13] and controls the contribution of the exchange interaction and consequently, as eq. (2) shows, the dispersion behaviour of the magnetic excitations. So an increasing magnetic field reduces the quadrupole moment and thus the contribution of the exchange interactions to the dispersion curve, which is in accordance with the observations. Using the assumed parameters of J , J' , A , M_z , R and the above derived value of g and $R(T, H_{\text{ex}}^z)$, we calculated the dispersion curves in an applied magnetic field of 5 T. The results are displayed in fig. 1 and show a good agreement with the observed data.

3.2. $H \perp c$

The magnetic excitations in CsFeBr₃ were also measured with the magnetic field applied in the non-ordering direction ($H \perp c$). The magnetic-field dependence of the magnetic excitations at selected points along the $[00\zeta]$ direction are displayed in fig. 5a. A similar set of data for selected points along the $[\frac{1}{3}\frac{1}{3}\zeta]$ direction is

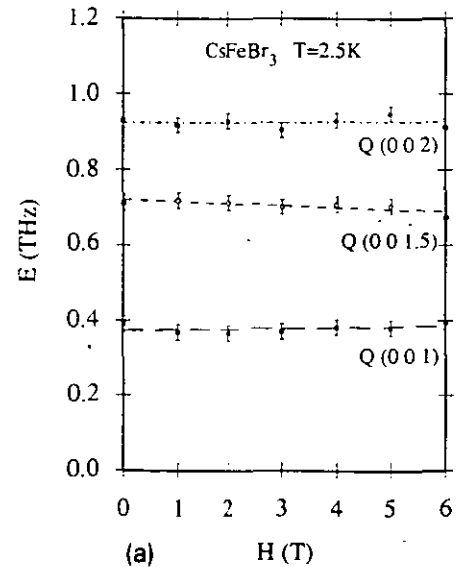


Fig. 5a. Field dependence of the magnetic excitations along $[00\zeta]$ with $H \perp c$.

D. Visser et al. / Magnetic excitations of CsFeBr₃ in a magnetic field

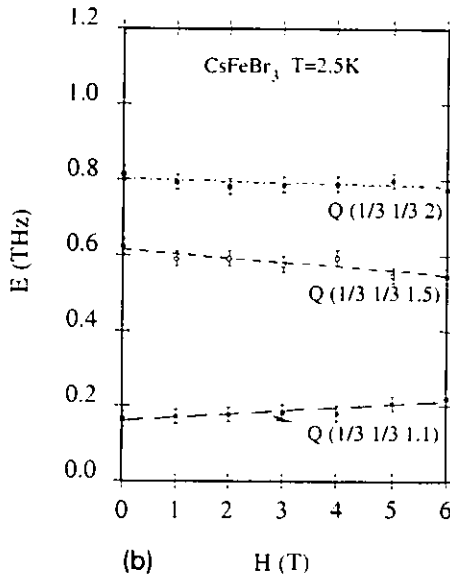


Fig. 5b. Field dependence of the magnetic excitations along $\left\{\frac{1}{3} \frac{1}{3} \zeta\right\}$ with $H \perp c$.

given in fig. 5b. Along the $[00 \zeta]$ direction the applied magnetic field does not seem, within the error bars, to have any effect. Along the $\left\{\frac{1}{3} \frac{1}{3} \zeta\right\}$ direction one may see an indication of a slight continuous renormalisation behaviour. The fits to the data show that at $Q\left(\frac{1}{3} \frac{1}{3} 2\right)$ the renormalisation is -3.1% (-0.025 THz) by increasing the field from 0–6 T. This value lies well within the error bar. At $Q\left(\frac{1}{3} \frac{1}{3} 1.5\right)$ the difference is -11.3% (-0.065 THz), while at $Q\left(\frac{1}{3} \frac{1}{3} 1.1\right)$ the renormalisation is 24% (0.04 THz). All these values are very small compared to the energy of the magnetic excitations. The experimental resolution in the present case is also not high enough for the observed differences to be considered significant. Least-squares fits to the data taken at each different magnetic field using eq. (2) and ignoring the magnetic-field contribution showed that exchange and anisotropy parameters obtained from these fits are within the limit of the error equal to the values obtained from the zero data.

Renormalisation effects due to an applied

magnetic field perpendicular to the c axis are predicted for AFeX₃-type materials with a magnetic ground state and positive J [14]. That such effects should also happen for the pure SGS systems is not yet clear. Although this study provided more information on the magnetic excitations in CsFeBr₃ in an applied field, one can conclude that very precise and complete magnetic dispersion curves in an applied magnetic field are necessary in order to test the present theoretical description [7, 8, 15] properly.

Acknowledgements

D.V. would like to thank the UK SERC and The Royal Society, Britain, for financial support. We would like to thank B. Smid for helpful discussions and P. Sutling, A. Dorn, for technical assistance during the measurements.

References

- [1] D. Visser and A. Harrison, *J. Phys. (Paris)* 49 (1988) C8–1467.
- [2] H. Yoshizawa, W. Kozukue and K. Hirakawa, *J. Phys. Soc. Jpn.* 49 (1980) 144.
- [3] W. Knop, M. Steiner and P. Day, *J. Magn. Magn. Mater* 31–34 (1981) 1033.
- [4] M. Steiner, K. Kakurai, W. Knop, B. Borner, U. Happek, P. Day and G. McLeen, *Solid State Commun.* 38 (1981) 1179.
- [5] M.E. Lines, *Phys. Rev. Lett.* 42 (1979) 533.
- [6] N. Suzuki, *J. Phys. Soc. Jpn.* 50 (1981) 2931.
- [7] P.A. Lindgård, *J. Phys. C* 8 (1975) L178.
- [8] P.A. Lindgård, *Physica B* 120 (1983) 190.
- [9] N. Pappanicolaou and P. Spathis, *J. Phys. Condens. Matter* 1 (1988) 1227.
- [10] D. Visser, *Z. Phys. B*, submitted.
- [11] D. Visser, A. Harrison, M. Vrtis and P.J. Brown, *Z. Phys. B*, submitted.
- [12] B. Dörner, D. Visser, U. Steigenberger, K. Kakurai and M. Steiner, *Z. Phys. B* 72 (1988) 487.
- [13] B. Dörner, D. Visser and M. Steiner, *Z. Phys. B* 81 (1990) 75.
- [14] N. Suzuki, *J. Magn. Mater.* 90 & 91 (1990) 69.
- [15] W. Knop, Thesis, Technische Universität Berlin (1985).

J. Phys.: Condens. Matter 4 (1992) 6977-6992. Printed in the UK

A dynamical correlated effective-field treatment of the magnetic excitations in the singlet ground state antiferromagnet RbFeBr_3

A Harrison and D Visser†

Oxford University, Inorganic Chemistry Laboratory, South Parks Road, Oxford OX1 3QR, UK

Received 6 March 1992, in final form 22 May 1992

Abstract. The dispersion of magnetic excitations in the pseudo-one-dimensional induced-moment antiferromagnet RbFeBr_3 has been measured at 4.5 K using inelastic neutron scattering. Below $T_N = 5.5$ K a distinct dispersion of magnetic excitations was observed along and between the magnetic chains. The energies and scattering intensities of these excitations was described well using Suzuki's DCEFA model. The components of intrachain superexchange perpendicular and parallel to the crystal c -axis were found to be $J_1^\perp = -0.40(1)$ and $J_1^\parallel = -0.43(4)$ meV respectively. The corresponding interchain exchange constants were found to be $J_2^\perp = -0.044(3)$ and $J_2^\parallel = -0.065(13)$ meV. Above T_N the magnetic excitations at $(001)_N$ dropped in intensity and their small renormalization in energy was described well by the DCEFA model.

1. Introduction

RbFeBr_3 is one of a series of isomorphous AFeX_3 compounds ($A = \text{Rb, Cs, Tl}$ or NH_4 and $X = \text{Cl}$ or Br) that have been used as model magnets (Achiwa 1969, Yoshizawa *et al* 1980, Steiner *et al* 1981, Wada *et al* 1982, Shiba and Suzuki 1982, Lindgård 1983, Knop *et al* 1983, Suzuki 1983a, c, Visser and Steigenberger 1984, Harrison 1986, Visser and Harrison 1988, Dorner *et al* 1988, Harrison and Visser 1989a, b, Harrison *et al* 1991, Plumer and Caillé 1991). The magnetic behaviour of these materials is the result of a delicate balance between several competing interactions. All the salts listed above crystallize in the hexagonal perovskite structure, but have the following differences in magnetic properties.

(i) The chlorides behave as pseudo one-dimensional ferromagnets, whereas the bromides that have been characterized so far ($A = \text{Rb, Cs, NH}_4$) (Visser and Harrison 1988, Harrison *et al* 1991) are pseudo one-dimensional antiferromagnets.

(ii) The caesium salts behave as singlet ground state materials, but the rubidium, ammonium and thallium salts that have been studied have magnetic ground states with long-range magnetic order at low temperatures.

† Present address: Loughborough University of Technology, Department of Physics, Loughborough LE11 3TU, UK.

A Harrison and D Visser

The task of explaining the relationship between magnetic character and the chemical composition or changes in the superexchange bridging angles depends on reliable values of exchange parameters and ligand field parameters. Previous measurements on AFeX_3 magnets have yielded a wide distribution of values for these quantities and it is clear from table 1 that they depend very much on the experimental method and the model used to interpret the data. In this paper we seek to provide a reliable set of magnetic parameters for RbFeBr_3 using a technique that probes the magnetic susceptibility over both energy and wavevector, namely inelastic neutron scattering. We interpret the data using a model appropriate to this class of material and compare our results with those for other AFeX_3 magnets.

1.1. Properties of RbFeBr_3 and related materials

1.1.1. The crystal structure of RbFeBr_3 . At room temperature the space group of RbFeBr_3 is $P6_3/mmc$. Chains of face-sharing FeBr_6^{4-} octahedra lie parallel to the c -axis, separated by Rb^+ ions. At 108 K a structural phase transition occurs (Harrison and Visser 1989a) in which two-thirds of the Fe chains (A sites) move out of the basal plane by about 0.5 Å to form a honeycomb lattice, leaving the remaining chains (B sites) arranged on a triangular lattice. The unit cell expands in volume by a factor of 3 ($a' = \sqrt{3}a, c' = c$) and the new space group is $P6_3cm$, the structure being the same as that of KNiCl_3 at room temperature (Visser and Prodan 1980). The distortion does not alter the environment of the iron atoms sufficiently to allow the A and B sites to be distinguished by Mössbauer spectroscopy.

1.1.2. Electronic and magnetic properties. In the weak-field coupling scheme the cubic component of the ligand field acts on the free-ion ground term 5D of Fe^{2+} to produce a lower orbital triplet (5T_2) and an orbital doublet (5E) at an energy of $6,500 \text{ cm}^{-1}$ (Putnik *et al* 1976). The 5T_2 term is split further by spin-orbit coupling, λ' , and by the trigonal component of the ligand field, Δ' . The Hamiltonian representing these perturbations may be written as

$$H_i = \Delta' (L_{iz}^2 - 2/3) + \lambda' L'_i \cdot S'_i \quad (1)$$

where $S' = 2$ and, using the isomorphism of the symmetry groups representing T_2 and P terms, $L = 1$. $\lambda' = -k\lambda$, where k is the orbital reduction factor. Among the 15 eigenstates we find a singlet ground state, $|m_j = 0\rangle$, and an excited doublet, $|m_j = \pm 1\rangle$, at an energy of about 10 cm^{-1} . The next-nearest excited state lies at about 150 cm^{-1} . Consequently, at low temperatures we may describe the electronic and magnetic properties of RbFeBr_3 well using the effective spin Hamiltonian

$$H_i = DS_{iz}^2 - \sum_j 2[J_1^\perp (S_{ix}S_{jx} + S_{iy}S_{jy}) + J_1^\parallel S_{iz}S_{jz}] \\ - \sum_{j'} 2[J_2^\perp (S_{ix}S_{j'x} + S_{iy}S_{j'y}) + J_2^\parallel S_{iz}S_{j'z}] \quad (2)$$

where the sums are over the nearest neighbours j in the chains and j' between chains. J_1^γ and J_2^γ are the intra- and interchain exchange constants ($\gamma = \perp, \parallel$) and D is the single-ion anisotropy. Clearly, D , J_1^γ and J_2^γ all depend on Δ'/λ' . If D/J_K (where J_K is the optimum exchange energy and corresponds to a magnetic ordering

Magnetic excitations in RbFeBr₃

Table 1. Electronic and magnetic parameters for AFeX₃ compounds. All energies are in meV, and the numbers in brackets give the source of the data, listed below the table. Dq is the cubic component of the ligand field, B and C are the Racah parameters, λ is the spin-orbit coupling constant, Δ the trigonal component of the ligand field and D the single-ion anisotropy that results from Δ in the $S = 1$ single-ion Hamiltonian. k is the orbital reduction factor and J_1^{\parallel} and J_2^{\parallel} denote the components of the intra- and interchain superexchange constants ($\gamma = \perp, \parallel$, defined relative to the crystal c -axis).

Parameter	Compound			
	RbFeCl ₃	RbFeBr ₃	CsFeCl ₃	CsFeBr ₃
Dq	90.62[3]	81.25[3]	90.62[3]	81.25[3]
B	109.4	112.5[3]	109.4[3]	112.5[3]
C	475[3]	450[3]	475[3]	450[3]
λ	9.185[1] 12.88(8)	10[4]	9.82[2]	
Δ	7.59(1)	13[4]	8.64[2]	
D	1.525[3] 1.0[5] 0.7[6C] 2.45[6E] 1.71[6S] 2.08[8] 1.92[12]	1-1.1[4]	1.625[2] 1.23[6C] 2.18[6E] 1.01[10] 2.1[11] 2.03[13]	1.85 [14] 2.48 [15]
k	0.85[4]	0.78[4]		
J_1^{\parallel}	0.625[1] 0.25[5] 0.375[6C] 0.075[6E] 0.4625[6S] 0.125[8] 0.52[12]	-0.883[4]	0.313[2] 0.0002[6E] 0.616[7] 0.4[10] 0.262[11] 0.25[13]	-0.42 [14] -0.264 [15]
J_1^{\perp}	1.375[1] 0.338[5] 0.525[6C] 0.275[6E] 0.488[6S] 0.275[8] 0.405[12]	-0.525[4]	0.625[2] 0.325[6C] 0.227[6E]	-0.38 [14]
J_2	-0.048[6C] -0.025[6E] -0.068[6S] -0.034[12]	-0.025[4] -0.0833[9]	-0.012[6C] -0.012[6E] -0.009[7] -0.017[11] -0.017[13]	-0.039 [14] -0.0248 [15]

- [1] Montano *et al* (1973). Mössbauer + pair model. [2] Montano *et al* (1974). Mössbauer + pair model. [3] Putnik *et al* (1976). Optical absorption. [4] Lines and Eibschutz (1975). Magnetic susceptibility and correlated effective-field (CEF) model. [5] Eibschutz *et al* (1975). Magnetic susceptibility and CEF model. [6] Yoshizawa *et al* (1980). Inelastic neutron scattering with CEF (C), exciton (E) and spin-wave (S) models for magnon dispersion. [7] Steiner *et al* (1981). Inelastic neutron scattering with heuristic expression. [8] Suzuki (1981). Magnetic susceptibility, inelastic neutron scattering and far-infrared data with DCEFA model. [9] Adachi *et al* (1983). Heat capacity data with molecular-field approximation (MFA). [10] Baines *et al* (1983). Mössbauer data with MFA. [11] Lindgård (1983). Inelastic neutron scattering with correlation model. [12] Suzuki (1983c). Inelastic neutron scattering with DCEFA model. [13] Knop and Steiner (1984). Inelastic neutron scattering with correlation model. [14] Visser and Harrison (1988). Inelastic neutron scattering with DCEFA model. [15] Schmid *et al* (1992b) Inelastic neutron scattering with correlation model.

A Harrison and D Visser

vector K) lies above a critical value, the ground state acquires a finite magnetic moment: three-dimensional magnetic long-range order occurs in the rubidium and thallium salts at low temperatures, but the caesium salts, in which the cell constants are larger and the exchange constants smaller, behave as 'true' singlet ground state materials. Néel temperatures, where applicable, are given in table 1. However, if a magnetic field is applied parallel to the crystal c -axis, the excited doublet is Zeeman-split and mixed into the ground state. In this way magnetic long-range order may be induced in CsFeCl_3 (Haseda *et al* 1981, Steiner *et al* 1981, Dickson 1981, Dörner *et al* 1990, Knop *et al* 1983, Chiba *et al* 1988) and CsFeBr_3 (Visser and Steigenberger 1984, Visser *et al* 1991a, Schmid *et al* 1992a, b).

The interchain exchange J_2 propagates through two bromine atoms in the bridge $\text{Fe}-\text{Br}-\text{Br}-\text{Fe}$. Direct $\text{Fe}-\text{Fe}$ orbital overlap is negligible here, so magnetic exchange is almost entirely due to superexchange involving valence p orbitals on bromine and the orbitally non-degenerate orbitals of e symmetry on the iron atoms. Consequently, J_2 should have a Heisenberg symmetry and should be negative in sign, since the $\text{Fe}-\text{Br}-\text{Br}$ angle of 134° lies well above the value beyond which the antiferromagnetic 'kinetic' component of exchange dominates the ferromagnetic 'potential' component.

There is much less certainty about the sign of J_1 . The $\text{Fe}-\text{Br}-\text{Fe}$ bridging angle lies in the transition region where ferromagnetic 'potential' terms give way to antiferromagnetic 'kinetic' terms as the angle is lowered (for empirical illustrations of this see Hatfield *et al* 1983). Indeed, the chloride has ferromagnetic J_1 and the bromide, with a smaller value of bridging angle θ and a more covalent superexchange bridge, has antiferromagnetic J_1 .

In addition to the path involving orbital overlap between the e symmetry d orbitals on iron and the p orbitals on bromine, there may be a significant direct component of exchange across the shared face of the FeBr_6^{4-} trigonally distorted octahedra (Goodenough 1960). This would involve the orbitally degenerate t_2 -symmetry d orbitals and give a non-Heisenberg component to the exchange parameters. Lines and Eibschutz (1975) and Eibschutz *et al* (1975) considered this to be significant and antiferromagnetic for the chloride, but insignificant for the bromide in which the $\text{Fe}-\text{Fe}$ separation is much larger. Goodenough (1960) considered such exchange to be ferromagnetic and weak for the case of an interaction between two cations with greater than half-filled d subshells.

Finally, the inequivalence of the A and B iron sites in the low-temperature structural phase of RbFeBr_3 may lead to an inequivalence in the magnetic exchange between these sites. The shorter A-A distance is expected to lead to an increased intersite magnetic exchange constant J_2 (A-A) relative to the A-B site exchange J_2 (A-B). The heat capacity measurements of Adachi *et al* (1983) revealed two transitions at low temperatures: there was a sharp anomaly at 5.61 ± 0.02 K, and a broad weak one at 2.00 ± 0.04 K. The first transition was interpreted as being from a paramagnetic to a 'disordered' phase in which the moments on the A sites freeze in a bipartite antiferromagnetic array, leaving the B sites disordered. At lower temperatures the B-site moments contribute to the magnetic long-range order, forming a 120° array with the A sites. Suzuki and Shirai (1986) calculated magnon dispersion curves for RbFeBr_3 using the molecular field approximation. As the ratio of $J_2(\text{A-A})/J_2(\text{A-B})$ was changed from unity, the degeneracies of the magnon energies at the Brillouin zone centre was removed. However, for reasonable values of $J_2(\text{A-A})/J_2(\text{A-B})$ the splitting of the dispersion curves is expected to be very small. Even when this ratio took the unrealistically high value of 1.25 the splittings were about $0.3 D$, which is

Magnetic excitations in RbFeBr₃

0.3–0.5 meV if we substitute previous estimates of D . More recently (Visser 1990) the sublattice magnetization of RbFeBr₃ has been measured by neutron scattering down to 1.3 K. The curve has an anomaly at 2.0 K which is consistent with a transition from the partially disordered to the six-sublattice magnetic phase.

1.2. INS characterization of RbFeBr₃

In a previous communication (Harrison and Visser 1989a) we reported an inelastic neutron scattering study of the dispersion of magnetic excitations in RbFeBr₃ at 4.5 K. We found that the form of the dispersion parallel to the crystal c -axis is unique among insulating ordered antiferromagnets: the periodicity of the dispersion in this direction was *half* that expected for a one-dimensional antiferromagnet. The energy of these excitations rose continuously from $l = 1$ to $l = 2$ rather than passing through a maximum at $l = 1.5$ and falling to another minimum at $l = 2$ (where l is defined relative to the magnetic unit cell).

Loveluck and Lovesey (1975) considered the effect of increasing the ratio D/J_1 on the magnon dispersion in an easy-plane one-dimensional magnet with Heisenberg exchange. The gap at $l = 2.0$ for the branch corresponding to in-plane (xy) fluctuations was shown to increase, and the maximum in the dispersion moved from $l = 1.5$ to $l = 2.0$, remaining at that value for $D/J_1 > 2$. This model was found to describe the form of the dispersion well, but strictly speaking it is invalid for an induced-moment system, and the values of D and J_1 derived using it are physically unreasonable. We also obtained a good fit to the data using an excitonic model with the molecular field approximation (MFA). Again, the values of D and J_1 derived with this model are suspect because the MFA neglects local fluctuations in the magnetic exchange field, which are important for induced-moment low-dimensional magnets.

In this paper we present a description of the magnetic excitations in RbFeBr₃ in the intermediate magnetically ordered phase as well as new data taken in the paramagnetic phase at temperatures up to 30 K. We interpret our data with the aid of a model that *does* describe local fluctuations in the exchange field—the dynamical correlated effective-field approximation (DCEFA) (Suzuki 1983b).

2. Theories of magnetic excitations in singlet ground state magnets

The use of spin-wave theory in describing the dispersion of magnetic excitations in induced-moment magnets such as AFeX₃ violates one of the conditions of spin-wave theory, namely that the excitations are not small deviations from a known ordered ground state. The failings of spin-wave models in describing the magnetic excitations in RbFeBr₃ have been discussed by Harrison and Visser (1989a). For such a material, excitonic models are to be preferred. In order to derive an expression for the generalized susceptibility, $\chi^{\alpha\beta}(q, \omega)$, it is necessary to decouple products of operators such as $S_i S_j$, converting them to sums of expressions in just one spin operator. This is most easily done using the MFA, which involves the substitution

$$S_{i\gamma} S_{j\gamma} \rightarrow S_{i\gamma} \langle S_{j\gamma} \rangle + S_{j\gamma} \langle S_{i\gamma} \rangle \quad (3)$$

where $\gamma = x, y, z$. $\langle S_{i\gamma} \rangle$ is the expectation value of the operator $S_{i\gamma}$, and may be calculated self-consistently from the thermal average of $S_{i\gamma}$ over the single-ion

A Harrison and D Visser

crystal field levels, or from $\chi^{\alpha\beta}(q, \omega)$ with the aid of the random phase approximation (RPA). The RPA method may be modified by introducing the effect of nearest-neighbour spin correlations (Callen 1963), which may cause the local exchange field to deviate substantially from the ensemble average. This 'correlated effective-field approximation' (Lines 1974) involves the substitution

$$S_{i\gamma} S_{j\gamma} \rightarrow S_{i\gamma} [\langle S_{j\gamma} \rangle + \alpha(S_{i\gamma} - \langle S_{i\gamma} \rangle)] + S_{j\gamma} [\langle S_{i\gamma} \rangle + \alpha(S_{j\gamma} - \langle S_{j\gamma} \rangle)] \quad (4)$$

where α is a parameter that describes the nearest-neighbour magnetic correlations. Suzuki *et al* (1977) showed that Lines' model had certain non-physical consequences which could be corrected by taking an isotropic correlation parameter α which was derived self-consistently using a fluctuation-dissipation expression involving the dynamic susceptibility $\chi^{+-}(q, \omega)$. This approach was called the dynamical CEF approximation (DCEFA).

Lindgård (1984a) pointed out that both the RPA and the CEF approaches ignore magnon-magnon interactions. By including coupling between excitations their lifetimes become finite and their energies may be significantly altered. The effects of magnon-magnon coupling are seen most strongly for magnets at temperatures above T_N or for magnets with pronounced induced-moment character. However, Suzuki's model is presented in the literature in a very general form applicable to any singlet-doublet system. An explicit expression is given for $\chi^{\alpha\beta}(q, \omega)$ which may be readily solved by numerical methods such as that described by Buyers *et al* (1975). Furthermore, Suzuki has performed a thorough study of the magnetic properties of RbFeCl_3 above and below T_N and derived a consistent set of exchange parameters to explain the behaviour in both temperature regimes (Suzuki 1983a, c). Thus we shall use Suzuki's model to obtain a consistent set of magnetic parameters RbFeBr_3 and RbFeCl_3 . The extension of Suzuki's model to the paramagnetic phase for this specific case is described in the appendix.

3. Experiment

The sample of RbFeBr_3 used in all the experiments was grown by Dr P J Walker of the Clarendon Laboratory, Oxford, by the Bridgman method. It was cylindrical in shape, measuring 15 mm long by 10 mm in diameter and mounted with the $(0\ 0\ 1)_N$ and $(1\ 1\ 0)_N$ reflections in the horizontal scattering plane.

Inelastic neutron scattering experiments were performed on this sample using the Pluto Triple Axis Spectrometer (TAS), AERE, Harwell. Two experimental set-ups were used, according to the type of measurement. First, a relatively high flux at a wavelength of 2.3512 Å was provided using the $(0\ 0\ 2)$ reflection of pyrolytic graphite. The dispersion of the magnetic excitations was then measured by the constant- Q method along $[00l]_N$ and $[\frac{1}{3}\frac{1}{3}l]_N$ ($l = 1 - 2$) and along $[hk1]_N$ and $[hk2]_N$ ($h = k = 0 \rightarrow 1$) at 4.5 K. The temperature dependence of these excitations was also studied up to 30 K. The low scattering intensity of the excitations at high values of $|Q|$ and high temperatures limited such measurements to points near $(\frac{1}{3}\frac{1}{3}1)_N$ and $(0\ 0\ 1)_N$. The positions of the experimental measurements in reciprocal space are indicated in figure 1.

The second set of measurements used the $(1\ 1\ 1)$ reflection from an aluminium monochromator to provide higher resolution at a wavelength of $\lambda = 2.391$ Å. In

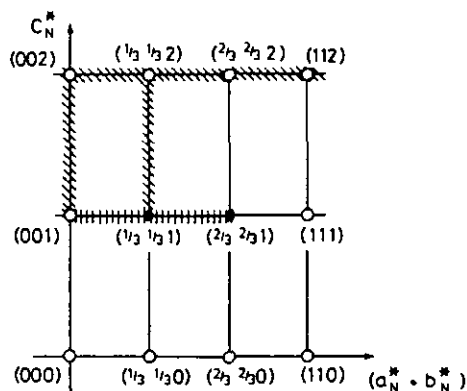
Magnetic excitations in RbFeBr_3 

Figure 1. A reciprocal space diagram for RbFeBr_3 showing the scattering plane in the present experiment. The axes lie along c_N and $(a_N + b_N)$. Magnetic Bragg points are denoted by \bullet and nuclear Bragg peaks by \circ . The regions scanned with the spectrometer are hatched diagonally for measurements with the pyrolytic graphite monochromator and vertically for measurements with the aluminium monochromator.

both cases the pyrolytic graphite $(0\ 0\ 2)$ reflection was used as the analyser and the collimation was provided by soller slits of $20'$ (M-S), $30'$ (S-A) and $40'$ (A-D) (where M, S, A and D are monochromator, sample, analyser and detector). The incoherent elastic neutron scattering at the magnetic reflection $(\frac{1}{3}\frac{1}{3}1)_N$ had widths in energy of 0.6 meV and 0.3 meV with the pyrolytic graphite and aluminium monochromators respectively. Thus, a more careful study of the dispersion along $[hk1]_N$ ($h = k = 0 \rightarrow 1$) was performed with the second experimental arrangement. Study of the dispersion of the magnetic excitations at higher Q was limited by the lower neutron flux provided by the aluminium monochromator. In both experimental arrangements contamination of the incident beam by neutrons of wavelength $\lambda/2$ was reduced using a pyrolytic graphite plate as a filter.

4. Results

The inelastic neutron scattering measurements at 4.5 K showed distinct dispersion of magnetic excitations along and between the magnetic chains. The scattering intensity fell off rapidly as the temperature was raised, but dispersion along the chain axis persisted well above T_N , showing a small degree of renormalization.

The inelastic neutron scattering peaks were least-squares-fitted to Lorentzian curves convoluted with the Gaussian instrumental resolution function. Examples of fits to the data are presented in figure 2. The width of the Gaussian peak was calculated with the program RESCAL at AERE, Harwell for which the input data were provided by a set of careful measurements in energy and reciprocal space of several Bragg peaks. The results of the peak fitting are summarized in figures 3 and 4: figure 3 shows the magnetic excitation energies and figure 4 the relative scattering intensities.

It is clear (figure 2(a)) that magnetic excitations of low energy are difficult to resolve from the central coherent peak with the present set-up. In addition, at lower energies there may be several overlapping peaks contributing to the scattering cross section. In order to treat the data in such cases it was necessary to make assumptions about the relative widths of the contributing peaks: the widths were taken to be equal to each other, and to have the same value as that of the peak which was closest in Q but still fully resolved. Nevertheless, the remaining independent parameters in the fit were highly correlated such that low values of χ^2 ($1 \rightarrow 1.3$) could be obtained for a wide range of combinations of parameters.

A Harrison and D Visser

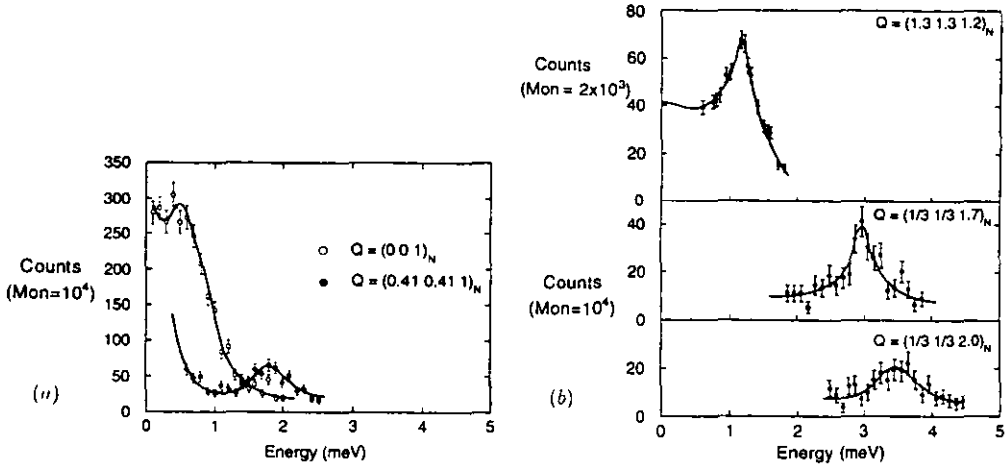


Figure 2. Examples of constant- Q scans on RbFeBr_3 at 4.5 K. The value of Q is indicated on the figure, as is the monitor count of the instrument. The full line is the least-squares fit to the data of a scattering background plus a Lorentzian peak convoluted with the instrumental resolution function. (a) shows the excitations at $(0\ 0\ 1)_N$ and $(0.41\ 0.41\ 1)_N$, and (b) the excitations at $(\frac{1}{3}\ \frac{1}{3}\ 1.2)_N$, $(\frac{1}{3}\ \frac{1}{3}\ 1.7)_N$ and $(\frac{1}{3}\ \frac{1}{3}\ 2.0)_N$ as indicated on the figure.

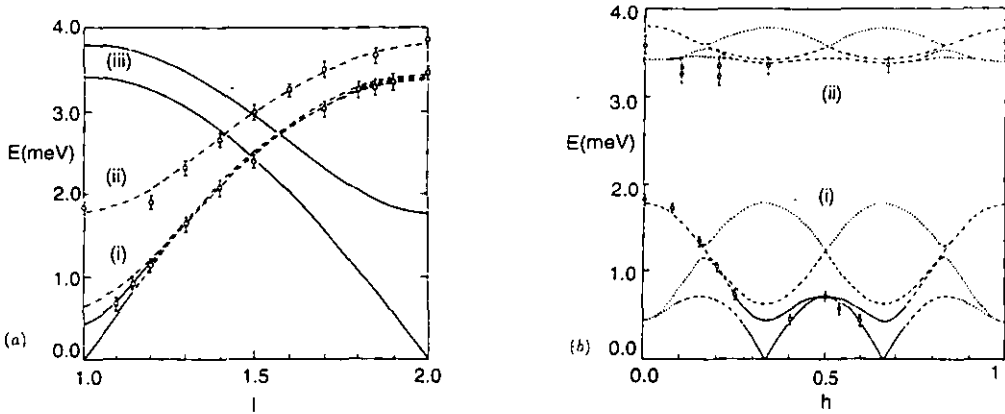


Figure 3. The best fits of the appropriate DCEFA magnon dispersion curves to the data. (a) shows the magnon dispersion along (i) $[00l]_N$ and (ii) $[\frac{1}{3}\ \frac{1}{3}\ l]_N$ ($l = 1 - 2$) and (b) shows the dispersion within the a - b plane in (i) the $[hk1]_N$ direction and (ii) the $[hk2]_N$ direction ($h = k = 0 - 1.0$). In both cases the density of the lines represents the relative magnitude of the calculated scattering cross section. In (a) the continuous lines (iii) depict the so-called 'mirror modes' discussed in the text; their scattering intensity is very small.

At higher temperatures the scattering intensities fell off rapidly and limited measurements to low values of Q . The dependence on temperature of energy and scattering intensity of the magnetic excitation peaks at $(0\ 0\ 1)_N$ and $(\frac{1}{3}\ \frac{1}{3}\ 1)_N$ is displayed in figure 5. The magnetic excitation at $(001)_N$ was a weak scatterer but easily distinguished from the rest of the neutron scattering at this position; the peak at $(\frac{1}{3}\ \frac{1}{3}\ 1)_N$ appeared as a broad, weak shoulder on the strong central incoherent contribution.

Magnetic excitations in RbFeBr_3

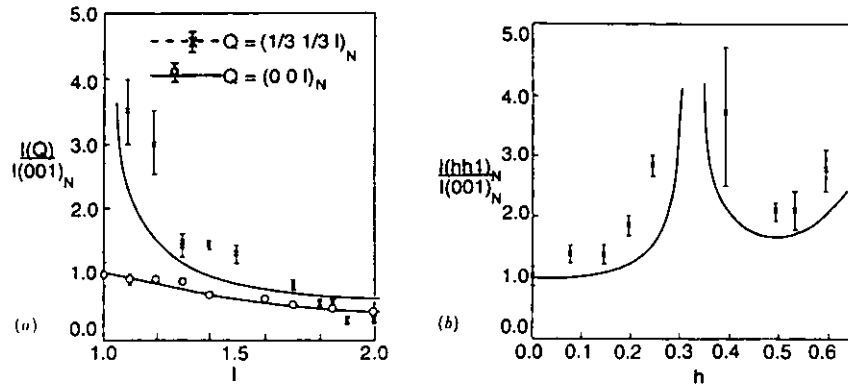


Figure 4. The dependence on wavevector of the inelastic magnetic neutron scattering cross section for the strongest branches observed in our experiments at (a) $(\frac{1}{3} \frac{1}{3} l)_N$ and $(00l)_N$ ($l = 1 \rightarrow 2$) and (b) $(hh1)_N$ ($h = 0.0 \rightarrow 0.6$). The full lines are the results of calculations using the DCEFA model, corrected for the magnetic form factor and the scattering geometry; the crosses are the experimental values. Both the calculated and the experimental values have been normalized to the magnon scattering intensity at $Q = (001)_N$.

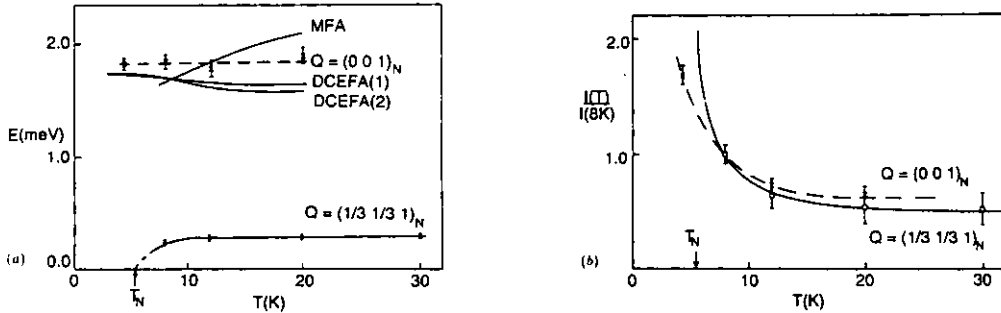


Figure 5. The dependence on temperature of (a) the energy and (b) the scattering intensity associated with the magnetic excitations at $(001)_N$ and $(\frac{1}{3} \frac{1}{3} 1)_N$. In (a) the data taken at $Q = (001)_N$ are compared with the results of calculations using the MFA and DCEFA models. In (b) the two positions are denoted by dotted and full lines respectively, and the intensities have been normalized to the value at 8 K. The lines are merely a guide to the eye.

5. Analysis and discussion

Initially, estimates were made for the starting values of J_1^γ , J_2^γ and D and the magnetic excitation energies and scattering intensities calculated for all branches. The data points were assigned to particular branches or combinations of branches. The values of J_1^γ , J_2^γ and D were then refined by least-squares fitting these branches to the data.

Dispersion curves have previously been calculated at $T = 0$ and at finite temperatures using an excitonic model with the MFA (Harrison and Visser 1989a): α was set to zero and the self-consistency equation for the ordered moment, $\langle S_i \rangle$, solved numerically. The results of all these fits are presented in table 2. An estimate for T_N was derived from equation (A13) with α and $\omega_i(q)$ set to zero and q set to the magnetic ordering vector $K = (\frac{1}{3} \frac{1}{3} 1)_N$.

A Harrison and D Visser

Table 2. Magnetic exchange parameters (J_i^{γ}), single-ion anisotropies (D) and correlation parameters (α) for RbFeCl_3 and RbFeBr_3 derived from inelastic neutron scattering data. The parameters for RbFeCl_3 were calculated by Suzuki (1983c) from the data of Petitgrand *et al* (1981). The parameters for RbFeBr_3 have been calculated using the DCEFA model and the molecular field approximation (MFA). The three types of DCEFA calculations used were: (1) all parameters taken to be independent; (2) $J_1^{\perp}/J_1^{\parallel} = J_2^{\perp}/J_2^{\parallel} = \delta$; (3) $J_1^{\perp}/J_1^{\parallel} = J_2^{\perp}/J_2^{\parallel} = 0.67$ as suggested by Lines and Eibschutz (1975). The effective anisotropy E is defined in equation (A2) of the appendix and J_K is the exchange field in meV experienced by a moment in the magnetically ordered ground state. T_N is the magnetic ordering temperature in K calculated with each model.

Model	Compound				
	RbFeCl_3 DCEFA	RbFeBr_3 DCEFA(1)	RbFeBr_3 DCEFA(2)	RbFeBr_3 DCEFA(3)	RbFeBr_3 MFA
J_1^{\perp}	0.405	-0.398(10)	-0.400(40)	-0.400(59)	-0.288(4)
J_2^{\perp}	-0.0344	-0.044(3)	-0.044(5)	-0.044(3)	-0.031(5)
J_1^{\parallel}	0.527	-0.431(44)	-0.555(17)	-0.600(88)	—
J_2^{\parallel}	-0.045	-0.065(13)	-0.061(28)	-0.066(46)	—
D	1.92	1.94(2)	2.02(10)	2.07(15)	2.55(4)
E	1.79	1.86	1.85	1.85	
δ	0.77	0.92 0.67	0.72	0.67	
α	0.78	-0.414	-0.418		
J_K	0.91	0.928(30)	0.933	0.932	
T_N		2.1	2.15	2.2	6.7

Suzuki (1981, 1983a) asserted that the parameters J_1^{\perp} , J_2^{\perp} , J_1^{\parallel} , J_2^{\parallel} and D are not independent of each other. He argued that the ratios $J_1^{\perp}/J_1^{\parallel}$ and $J_2^{\perp}/J_2^{\parallel}$ should be equal and determined by the ratio Δ'/λ' . This is because in the fictitious $S = 1$ Hamiltonian the exchange constants incorporate the orbital contribution to the angular momentum. This assertion is valid if the superexchange pathways along and between the chains make the same use of the σ -bonding 3d orbitals on the iron atoms. It is not valid if there is an appreciable direct component of intrachain exchange arising from overlap of the t_2 orbitals, or any other reason for differing contributions being made by the t_2 and e orbitals to inter- and intrachain exchange.

In our fits of the DCEFA model to the data we first assumed all the parameters in the single-ion Hamiltonian to be independent. We call this procedure DCEFA(1). As a starting point for the fits we assumed the direct contribution to J_1^{γ} to be negligible. Lines and Eibschutz (1975) used the same assumption to calculate the ratio $J_1^{\perp}/J_1^{\parallel}$ to be 1.5. The value of this ratio for RbFeCl_3 was calculated by Eibschutz *et al* (1975) to be 1.3, which does not agree well with the value of 0.77 derived by Suzuki (1983c) from inelastic neutron scattering measurements of the magnetic excitations. We have also derived values for J_1^{γ} and J_2^{γ} and D subject to the restriction that $J_1^{\perp}/J_1^{\parallel} = J_2^{\perp}/J_2^{\parallel} = \delta$. This ratio may be allowed to vary or it may be fixed at the value of 1.5 calculated by Lines and Eibschutz (1975). These procedures are called DCEFA(2) and DCEFA(3) respectively. The results of all fits have been listed in table 2. The DCEFA(1) model, with more independent variables, provides a better least-squares fit to the data than the other DCEFA models, but only by about 1%. δ for DCEFA(2) settles at 0.72, which is quite different from the value

Magnetic excitations in RbFeBr₃

provided by Lines and Eibschutz (1975) which was used in DCEFA(3). However, δ and D are highly correlated in the fitting process and consequently the uncertainty in both is high. Thus, without a reliable, independent way of fixing relations between some of the parameters fitted it would be meaningless to try to interpret small differences in the calculated exchange parameters in terms of the magnetostructural trends in these compounds. However, there do seem to be some significant differences in the parameters calculated for RbFeBr₃ and RbFeCl₃.

(i) The value of J_2^γ is greater for the bromide than for the chloride. The bridging angle for the two compounds is very similar and the halogen-halogen bond length is also similar, but the larger valence orbitals on the bromine atom are expected to have a larger degree of overlap with the iron atoms. A similar relation is found for the caesium salts (Visser and Harrison 1988).

(ii) The value of D appears to be similar in the two compounds. On the grounds of the structural trigonal distortion away from perfect octahedral symmetry ($\theta = 70.53^\circ$), the bromide with bridging angle $\theta = 72.45^\circ$ should have a smaller value of D than the chloride with $\theta = 73.43^\circ$. This would be reinforced by the greater orbital reduction factor of the bromide (Lines and Eibschutz 1975), which reduces the value of D in the effective $S = 1$ Hamiltonian.

Lindgård (1983) pointed out that the dispersion of magnetic excitations in CsFeCl₃ was best described with an expression that included next-nearest-neighbour antiferromagnetic intrachain exchange. He calculated this to be significant relative to J_1 (-0.044 meV compared with 0.262 meV). The effect of this extra term on the predicted magnon dispersion curves is to lower the energy of the lowest branch at $l = 0.5$ relative to that at $l = 1$. An inspection of the appearance of Suzuki's fits of the DCEFA model to inelastic neutron scattering data (Suzuki 1983c) suggests that his model could also be improved in this manner. However, it is less easy to determine the importance of this term in a one-dimensional antiferromagnet because the relative energy of magnons at $(hk0.5)_N$ and $(hk1)_N$ also depends on the balance between D and J_1 .

A further test of the ability of the DCEFA model to explain the experimental observations was provided by comparing the calculated and measured scattering intensities. The calculated scattering intensity at a wavevector Q is proportional to the imaginary part of the susceptibility for each branch, as described by Suzuki (1983c). The constant of proportionality contains two Q -dependent factors: one is the geometric factor, $(1 \pm (Q_z/Q)^2)$, and the other is the magnetic form factor for Fe²⁺ (Watson and Freeman 1961). Figure 4 shows the agreement between calculated and measured intensity to be good, though not significantly different from the results of the MFA fits reported by Harrison and Visser (1989a).

The DCEFA model is less successful at predicting the behaviour of RbFeBr₃ at or near T_N . Using the optimized values of the exchange parameters obtained from the fits to the magnon dispersion curves, a value of 2.1 ± 0.1 K was deduced for T_N using equation (A13) from the appendix with the value of α calculated self-consistently with expression (A17). The temperature dependence of the energy of the magnetic excitation at $(001)_N$ was successfully predicted (figure 5), but not that at the H point ($Q = (\frac{1}{3}\frac{1}{3}1)_N$) (figure 6). The failure to predict T_N correctly may be largely due to the way in which the DCEFA model has been implemented. We used an expression appropriate for $T = 0$ to obtain exchange parameters from data taken at about $T = 0.8T_N$. At this temperature the effective exchange parameters may

A Harrison and D Visser

be significantly smaller than those at $T = 0$ and the predicted value of T_N would consequently be lower. The MFA method is more successful at predicting T_N , giving a value of $T_N \simeq 6.7$ K. However, when the temperature dependence of the energy of the magnetic excitation at the A point ($Q = (001)_N$) is calculated using the DCEFA models and the MFA models; the DCEFA(1) model is found to give the best treatment of the data (figure 5(a)). Furthermore, the DCEFA models (1) and (2), in which the ratio $J_1^\perp / J_1^\parallel$ is appreciably smaller than that calculated by Lines and Eibschutz (1975), are also significantly better at treating the temperature dependence of the energy of the same magnetic excitation. This suggests that J^\parallel is anomalously high relative to J^\perp . One explanation for this is that there is a significant direct component of magnetic exchange in RbFeBr₃ and RbFeCl₃. However, this implies that the direct exchange is ferromagnetic for RbFeCl₃ and antiferromagnetic for RbFeBr₃, which is unlikely because the orbitals that would be involved in such coupling should be of the same symmetry in both compounds. Consequently the direct exchange should have the same sign in both cases.

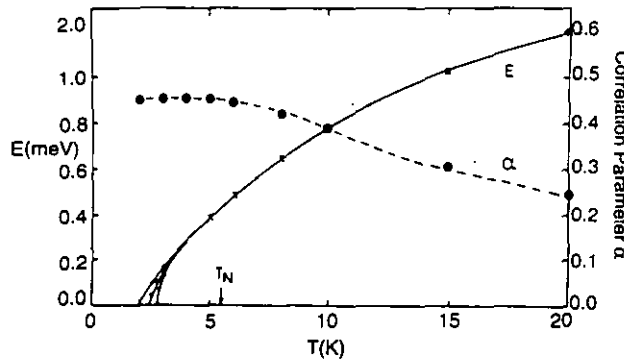


Figure 6. The dependence on temperature of the energy of the magnon at $(\frac{1}{3}\frac{1}{3}1)_N$ as calculated by the DCEFA model. This is represented by the full lines through the crosses. The calculated value of T_N is seen to increase as the fineness of the grid used in the numerical integration in equation (A17) increases. The full circles represent the values of the correlation parameter α . The values of J_1^\perp , J_2^\perp and D used in the calculations are the ones given in table 2.

The reason for the discrepancy between the theoretical and experimental value of the energy of the magnetic excitation at the H point probably lies in the experimental data. On comparison with the renormalization of the energy of the magnetic excitation at the K point in RbFeCl₃ and CsFeCl₃ (Yoshizawa *et al* 1980), our data appear anomalous. The strength of the coherent scattering intensity at the H point obscures the inelastic excitations with low cross section. A fuller experimental study using an instrument of higher resolution is needed to settle this issue.

The present set of data do not provide firm evidence for a magnetically ordered phase below T_N other than the regular triangular structure. Even if such a phase did exist at 4.5 K it is very unlikely that the difference between $J_2(A-B)$ and $J_2(B-B)$ would be sufficient to produce a splitting in the energy of the magnetic excitations at $(0\ 0\ 1)_N$ and $(\frac{1}{2}\frac{1}{2}1)_N$ that could be resolved with Pluto TAS. However, a set of measurements of the magnetic excitations at these points over a range of temperatures might reveal a change in the width in energy of the excitations. Certainly the

Magnetic excitations in RbFeBr_3

excitation at $(0\ 0\ 1)_N$ was broader than those at $(0.08\ 0.08\ 1)_N$ and at $(0.15\ 0.15\ 1)_N$, with resolution-corrected energy widths of 0.60(13), 0.39(10) and 0.40(10) meV respectively. Further measurements are needed to show that these values are reliable.

In the present study the magnetic excitations in RbFeBr_3 have been presented in the extended zone scheme. In addition to the distinct excitations observed at $[\frac{1}{3}\frac{1}{3}l]_N$ and $[00l]_N$ for $l = 1 \rightarrow 2$, which correspond to in-plane (xy) fluctuations, we expect a second set of excitations corresponding to the out-of-plane (zz) fluctuations. The latter set are obtained from the former by folding the dispersion curves about $l = 1.5$. The scattering cross sections of the second set of excitations are, however, very weak. An example of the scattering strengths of these 'mirror modes' relative to the modes that we observed is given in figure 7. In the case of the excitations along $[00l]_N$ the scattering cross section is reduced to zero by the geometric factor $(1 \pm (Q_z/Q)^2)$. In our measurements no such branches were seen. It was claimed that such branches could be seen in the isomorphous singlet ground state antiferromagnet CsFeBr_3 (Visser and Steigenberger 1984, Dorner *et al* 1988) but more recent measurements using neutron polarization analysis and the temperature dependence of the inelastic neutron scattering demonstrated that the 'mirror modes' observed to date are artefacts (Visser *et al* 1991b, Schmid *et al* 1992a).

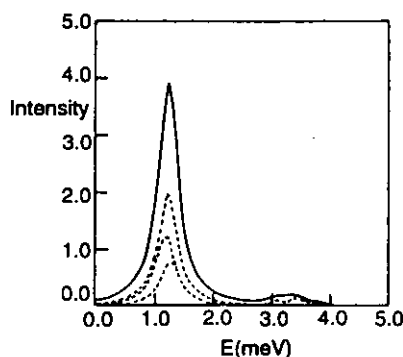


Figure 7. A simulation of an inelastic neutron scattering constant- Q scan at $Q = (\frac{1}{3}\frac{1}{3}1.2)_N$. The energy and scattering cross section of each magnon at this wavevector was calculated using the DCEFA model, corrected for the magnetic form factor and the geometric term $1 \pm (Q_z/Q)^2$ and convoluted with the instrumental resolution function. The units of intensity are arbitrary. This demonstrates the weakness of the scattering from the 'mirror modes'.

6. Conclusions

Suzuki's DCEFA model is successful in explaining the form of the inelastic magnetic neutron scattering from RbFeBr_3 below the magnetic ordering temperature: the energies and scattering intensities of the magnetic excitations are treated well, and the optimized values of J_1 , J_2 and D relate in a sensible way to the values derived for RbFeCl_3 in the same manner. There is less success in predicting the value of T_N from the values of these parameters. Further experiments are needed to test the predictions of Suzuki and Shirai (1986), measuring the magnetic excitation dispersion within the a - b plane with greater resolution, over a range of temperatures.

A Harrison and D Visser

A comparison between the DCEFA and MFA models is inconclusive, and suggests that further measurements are needed, using a variety of experimental probes over a wider range of temperatures. However, discrepancies in both models might arise through the neglect of magnon-magnon interactions. An adequate treatment of this effect requires a fuller correlation theory such as that of Lindgård (1984b).

Acknowledgments

The authors wish to express their thanks to Dr N Suzuki of Osaka University for his invaluable help with the DCEFA calculations, for stimulating discussions and the loan of his computer programs. Thanks are also due to Dr P J Walker of the Clarendon Laboratory, Oxford for growing the sample of RbFeBr₃. We thank Mr N Clarke and Mr P Bowen at AERE, Harwell for their technical assistance with the experiment. We are grateful to SERC for financial support and to Dr P Day of this laboratory for his encouragement and provision of research facilities. AH is grateful to St John's College, Oxford and to the Royal Society for financial support.

Appendix

We derive an expression for the determination of α in the paramagnetic phase. First we establish Suzuki's DCEFA model. The coordinate system used involves the rotating coordinates (ξ, η, ζ) in which η is parallel to the crystal c -axis, ζ parallel to the equilibrium spin direction at each site and ξ perpendicular to both these axes. The effective single-ion Hamiltonian is then

$$H_i^{\text{eff}} = ES_{i\eta}^2 - BS_{i\zeta} \quad (\text{A1})$$

where

$$E = D + \alpha(J_0^\perp - J_0^\parallel) \quad (\text{A2})$$

and

$$B = 2(J_K^\perp - \alpha J_0^\perp)\langle S_\zeta \rangle. \quad (\text{A3})$$

J_q is the Fourier transform of the exchange integral:

$$J_q = 2J_1 \cos(2\pi q_c) + 2J_2 \{ \cos(2\pi q_a) + \cos(2\pi q_b) + \cos(2\pi(q_a + q_b)) \} \quad (\text{A4})$$

where J_K is the value of J_q when q equals the helical magnetic ordering vector K . $\langle S_\zeta \rangle$ is determined self-consistently from

$$\langle S_\zeta \rangle = \sum_i \langle i | S_\zeta | i \rangle \rho_i \quad (\text{A5})$$

$$= 2B(\rho_0 - \rho_2)/W \quad (\text{A6})$$

Magnetic excitations in $RbFeBr_3$

where ρ_i is the Boltzmann population of the S_i levels $i=0, 1, 2$ and the correlation parameter α is calculated in the fashion described by Suzuki (1983b, c) using the expression:

$$\langle\{S_{i\xi}, S_{j\xi}\}\rangle = (1/N) \sum_{\mathbf{q}} (1/\pi) \int d\omega \coth((\beta\omega)/2) \text{Im} \chi^{\xi\xi}(\mathbf{q}, \omega). \quad (\text{A7})$$

The left-hand side of this equation simplifies:

$$\langle\{S_{i\xi}, S_{j\xi}\}\rangle = \langle S_i^+ S_j^- + S_i^- S_j^+ \rangle \quad (\text{A8})$$

$$= 1 + \rho_1 + E(\rho_0 - \rho_2)/W. \quad (\text{A9})$$

In the paramagnetic state $\langle S_i \rangle$ is set to zero and $\chi^{\xi\xi}(\mathbf{q}, \omega)$ then becomes $\chi^\perp(\mathbf{q}, \omega)$, given by

$$\chi^\perp(\mathbf{q}, \omega) = \phi^\perp(\omega) / [1 - (J_q^\perp - \alpha J_0^\perp) \phi^\perp(\omega)] \quad (\text{A10})$$

where

$$\phi^\perp(\omega) = -4E\rho/(\omega^2 - E^2) \quad (\text{A11})$$

and

$$\rho = (e^{\beta E} - 1)/(e^{\beta E} + 2). \quad (\text{A12})$$

$\chi^\perp(\mathbf{q}, \omega)$ has poles at energies $\omega_i(\mathbf{q})$ given by

$$\omega_i^2(\mathbf{q}) = E^2 - 4E\rho(J^\perp \mathbf{q} - \alpha J_0^\perp). \quad (\text{A13})$$

Therefore

$$\chi^\perp(\mathbf{q}, \omega) = -4E\rho/(\omega^2 - (\omega_i^2(\mathbf{q}))) \quad (\text{A14})$$

$$= \frac{-2E\rho}{\omega_i(\mathbf{q})} \left(\frac{1}{\omega - \omega_i(\mathbf{q})} - \frac{1}{\omega + \omega_i(\mathbf{q})} \right). \quad (\text{A15})$$

Using the identity

$$\lim_{\epsilon \rightarrow 0} \text{Im} \left(\frac{1}{(\omega - \omega_i(\mathbf{q}) - i\epsilon)} - \frac{1}{(\omega - \omega_i(\mathbf{q}) + i\epsilon)} \right) = 2\pi\delta(\omega - \omega_i(\mathbf{q})). \quad (\text{A16})$$

We find that (A9) becomes

$$1 + \rho_0 = 4E\rho \sum_{\mathbf{q}} \coth((\beta\omega)/2) + (1/\omega_i(\mathbf{q})). \quad (\text{A17})$$

References

- Achiwa N 1969 *J. Phys. Soc. Japan* **27** 561
 Adachi K, Takeda K, Matsubara F, Mekata M and Haseda T 1983 *J. Phys. Soc. Japan* **52** 2202

A Harrison and D Visser

- Baines J A, Johnson C A and Thomas M F 1983 *J. Phys. C: Solid State Phys.* **16** 3579
 Buyers W J L, Holden T M and Perreault A 1975 *Phys. Rev. B* **11** 266
 Callen H B 1963 *Phys. Rev.* **130** 890
 Chiba M, Ajiro Y, Adachi K and Morimoto T 1988 *J. Phys. Soc. Japan* **57** 3178
 Dickson D P E 1981 cited in Baines *et al* (1983)
 Dörner B, Visser D, Steigenberger U, Kakurai K and Steiner M 1988 *Z. Phys.* **72** 487
 Dörner B, Visser D and Steiner M 1990 *Z. Phys. B* **81** 75
 Eibschutz M, Lines M E and Sherwood R C 1975 *Phys. Rev. B* **11** 4595
 Goodenough J B 1960 *Phys. Rev.* **100** 564
 Harrison A 1986 *D Phil Thesis* Oxford University
 Harrison A, Stager C V and Visser D 1991 *J. Appl. Phys.* **69** 5998
 Harrison A and Visser D 1989a *Phys. Lett.* **137A** 79
 — 1989b *J. Phys.: Condens. Matter* **1** 733
 Haseda T, Wada N, Hata M and Amaya K 1981 *Physica B* **108** 841
 Hatfield W E, Estes W E, Marsh W E, Pickens M W, ter Haar L W and Weller R R 1983 *Extended Linear Chain Compounds* vol 3, ed J S Miller (New York: Plenum)
 Knop W and Steiner 1984 private communication
 Knop W, Steiner M and Day P 1983 *J. Magn. Magn. Mater.* **31–4** 1033
 Lindgård P A 1983 *Physica B* **120** 190
 — 1984a *Condensed Matter Research Using Neutrons (NATO ASI Series B 112)* ed S W Lovesey and R Scherm (New York: Plenum) p 163
 — 1984b *Phys. Rev. B* **30** 2729
 Lines M E 1974 *Phys. Rev. B* **9** 3927
 Lines M E and Eibschutz M 1975 *Phys. Rev. B* **11** 4583
 Loveluck J M and Lovesey S W 1975 *J. Phys. C: Solid State Phys.* **8** 3857
 Montano P A, Cohen E, Shechter H and Makovsky J 1973 *Phys. Rev. B* **7** 1180
 Montano P A, Shechter H, Cohen E and Makovsky J 1974 *Phys. Rev. B* **9** 1066
 Plumer M L and Caillé A 1991 *J. Appl. Phys.* **70** 5961
 Putnik C F, Cole G M, Garrett B B and Holt S L 1976 *Inorg. Chem.* **15** 189
 Schmid B, Dörner B, Visser D and Steiner M 1992a *Z. Phys. B* **86** 257
 — 1992b *J. Magn. Magn. Mater., Proc. 1991 Int. Conf. on Magnetism* **104–107** 771
 Shiba H and Suzuki N 1982 *J. Phys. Soc. Japan* **51** 3488
 Steiner M, Kakurai K, Knop W, Dörner B, Pynn R, Happek Y, Day P and McLeen G 1981 *Solid State Commun.* **38** 1179
 Suzuki N 1981 *J. Phys. Soc. Japan* **50** 2931
 — 1983a *J. Phys. Soc. Japan* **52** 1002
 — 1983b *J. Phys. Soc. Japan* **52** 1009
 — 1983c *J. Phys. Soc. Japan* **52** 3907
 Suzuki N, Isu T and Motizuki K 1977 *Solid State Commun.* **23** 319
 Suzuki N and Shirai M 1986 *Physica B* **136** 346
 Visser D 1990 Private communication
 Visser D, Dörner B and Steiner M 1991a *Physica B* **174** 25
 — 1991b *Z. Phys. B* submitted
 Visser D and Harrison A 1988 *J. Physique Coll.* **C8** 1467
 Visser D and Prodan A 1980 *Phys. Status Solidi A* **58** 481
 Visser D and Steigenberger U 1984 *Annex to the Annual Report of the Institut Laue-Langevin* p 92
 Wada M, Ubokoshi K and Hirakawa K 1982 *J. Phys. Soc. Japan* **51** 283
 Watson R E and Freeman A J 1961 *Acta Crystallogr.* **14** 27
 Yoshizawa H, Kozukue W and Hirakawa K 1980 *J. Phys. Soc. Japan* **49** 144

Temperature dependence of the magnetic excitations in the modified triangular induced moment antiferromagnet RbFeBr_3 at the soft mode point (abstract)

D. Visser

*Department of Physics, Loughborough University of Technology, Loughborough LE11 3TU,
United Kingdom*

B. Dorner

Institut Laue Langevin, BP 156X, Centre de tri, 38042 Grenoble, France

A. Harrison

*Inorganic Chemistry Laboratory, University of Oxford, South Parks Road, Oxford OX1 3QR,
United Kingdom*

The singlet ground state antiferromagnet RbFeBr_3 shows an induced moment behavior at low temperatures and orders antiferromagnetically at $T_N = 5.5$ K. A second magnetic phase transition takes place at 2.0 K. The magnetic phase between $2 \text{ K} < T < 5.5 \text{ K}$ may be partially ordered while at $T < 2.0 \text{ K}$ a modified triangular magnetic structure will be adopted. The temperature dependence of the magnetic excitations at the soft mode point $Q(1/3, 1/3, 1)$ show a switching of intensity at 2 K. Above 4 K the magnetic excitations start to broaden. Above T_N the magnetic excitations show a renormalization behavior. The temperature dependence of renormalization is well described by the theoretical predictions of the DCEFA model.

Introduction

Among the class of ABX_3 halides which adopt the hexagonal perovskite structure, the $AFeX_3$ compounds form a unique series with respect to their magnetic properties,¹ viz. these $AFeX_3$ compounds are singlet ground state systems. This is a direct consequence of the trigonal distortion of the FeX_3^- infinite chain of face-sharing octahedra in this structure type. The cubic component of the ligand field and the spin-orbit coupling working on the 5D term of the Fe^{2+} will result in a $J = 1$ ground state, which is further split by the trigonal component, Δ , of the ligand field. This will result in a ground state singlet and an excited low-lying doublet. At low temperatures only these two states are sufficiently populated and account for the observed magnetic properties. Within this subset we can describe the system with an effective-spin Hamiltonian and $S = 1$:

$$H = -2J_1 \sum_i S_i S_{i+1} - 2J_2 \sum_{i,j} S_i S_j + D \sum_i (S_i^z)^2$$

where J_1 and J_2 denote the intrachain and interchain superexchange constants, respectively, and D the single-ion anisotropy being related to the trigonal component Δ .

Recently the quasi one-dimensional antiferromagnetic ABX_3 compounds with integer spin values, like $CsNiCl_3$; $S = 1$,² which can be described by (1) have attracted much attention. Theoretical calculations predict non-classical and a fundamentally different behaviour for their static and dynamic magnetic properties, compared with magnets with half integer spin values. In this case the values of $D/|J|$ are small.

For the $AFeX_3$ compounds where the values of $D/|J|$ are large and positive, these systems will have singlet ground state properties. Therefore, one can no longer describe the magnetic behaviour with a spinwave-like approach but one has to take the induced moment character explicitly into account.³ Depending on whether the value of D/J_Q is less or equal to 4, where J_Q is the maximum exchange field, these compounds order magnetically or are true singlet ground state systems. $CsFeBr_3$ is a pure singlet ground state system and does not show magnetic ordering for $T \rightarrow 0K$ ⁴ while $RbFeBr_3$ orders magnetically at $T_N = 5.6K$.⁵ Normally these compounds order magnetically with the magnetic moments in a 120° type triangular antiferromagnetic array in the basal plane and antiferromagnetic stacking along the chain direction. However, $RbFeBr_3$ undergoes a structural phase transition at $108K$,⁶ which results in a modified triangular nuclear structure.⁷ In this phase one out of the three magnetic chains of the new unit cell is shifted along the c -direction and so causes inequivalence

in the interchain superexchange interactions. This may result in a magnetic ordering process with a sequence of magnetic phases. Specific heat measurements⁵ indicate a magnetic transition at $T = 5.61(5)\text{K}$, and an anomaly has also been observed between 2.8K and 1.3K. Single crystal elastic neutron scattering data confirm the presence of two magnetic transitions at $T_{N1} = 5.6(3)\text{K}$ and $T_{N2} = 2.0(1)\text{K}$.⁸ The magnetic phase between 5.6K - 2.0K is assumed to be partially ordered, which means that one out of the three magnetic chains is not magnetically ordered. Below T_{N2} the third chain becomes ordered. The resulting magnetic ordering will have a modified triangular magnetic structure.^{5,6}

We have studied the magnetic excitations in RbFeBr_3 with inelastic neutron scattering experiments at 4.5K¹⁰ and with high resolution at 1.6K¹¹ ($\Delta E = 0.02\text{ THz}$). The overall features of the 4.5K data were described well with Suzuki's dynamical correlated effective field approach using a 120° triangular magnetic structure. The high resolution data in the second magnetic phase show that the degeneracy of a number of the magnetic excitation branches is lifted and a second interchain exchange J_2' has to be taken into account in order to describe these observations.

A second characteristic of this type of singlet ground state system is the strong renormalisation of the magnetic excitations upon raising the temperature while the magnetic Bragg positions function as soft mode points.

In this paper the temperature dependence of the magnetic excitations at the magnetic Bragg point Q ($1/3\ 1/3\ 1$) is described and their relevance to the magnetic ordering processes in RbFeBr_3 is discussed.

Experimental

The sample of RbFeBr_3 used in this experiment was grown by the Bridgman technique and had a volume of about 4 mm^3 . The crystal was mounted with the $(002)_N$ and $(110)_N$ reflections in the horizontal scattering plane. Inelastic neutron scattering experiments were performed at temperatures between 1.6K and 20K using the IN12 triple axis spectrometer at the Institut Laue Langevin, Grenoble, France. The wavelength used was $k_I = 1.55 - 1.3\text{\AA}^{-1}$.

The dispersion along the $[h\ h\ l]$ direction with $l = 1$ was measured at 1.6K. The magnetic excitations at the soft mode point $Q = (1/3\ 1/3\ 1)$ were also studied as function of temperature.

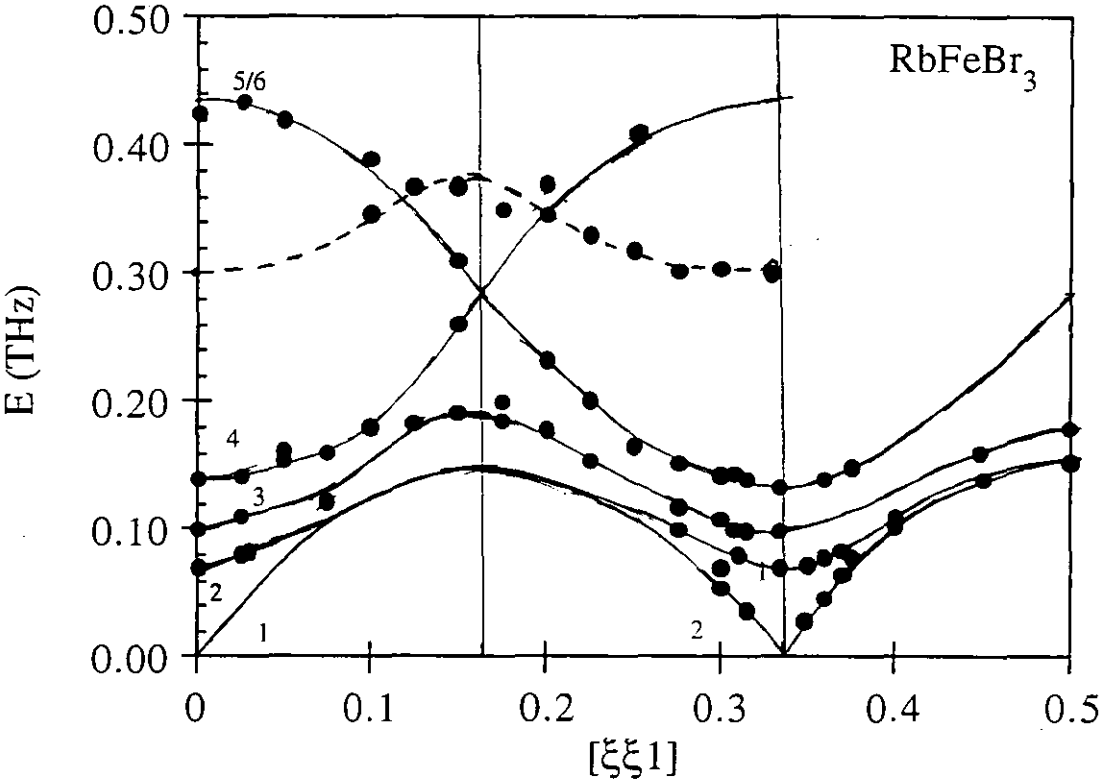


Figure 1. Magnetic excitations of RbFeBr₃ along the [ξξ1] direction at T = 1.35 K. The different modes are indicated 1-6 (see text). The dashed curve resembles a singlet groundstate-like mode.

Results and Discussion

The inelastic neutron scattering measurements along the $[h\ h\ l]$ direction, figure 1, show the typical dispersion of the magnetic excitations of a singlet ground state ABX_3 system with triangular symmetry in the basal plane.³ In principle, one would observe six excitation branches due to the six sublattices of the antiferromagnetic 120° type triangular structure. However, this picture is more complicated for the $AFexX_3$ compounds, due to their induced moment character. In the pure singlet ground state case one would observe only one excitation from the singlet ground state to the excited doublet state. In the case of a magnetically ordered induced moment system with the magnetic moments in the basal plane the internal exchange field splits the doublet state. The magnetic excitations can then be understood on the basis of the pure exciton picture. Thus one would observe three single-ion excitations $0 \rightarrow 1$; ω_1 , $0 \rightarrow -1$; ω_2 and the inner doublet excitation $1 \rightarrow -1$; ω_3 . In principle, this will give rise to eighteen branches for a six sublattice system. Using the anisotropy and exchange parameters D , J_1 , J_2 of $RbFeBr_3$ being 2.55, -0.288 and -0.031 THz, respectively,¹⁰ for the intra doublet splitting ω_3 one calculates an energy of ~ 0.010 THz. Therefore, these excitations will not be resolved by this experiment. The other six branches were observed around 0.8 - 1.0 THz and are not considered here. In figure 1 we have also indicated the excitation branches due to the different sublattices following the notation given by Suzuki.³

Comparing the calculated dispersion curves of the excitations for the 120° type structure¹² with those given in figure 1 one observes that the degeneracy of the $\omega_1^0(2)$ and $\omega_1^+(3)$ modes at the zone boundaries, $Q = (001)$ and $Q = (1/3\ 1/3\ 1)$ is lifted. This is a direct consequence of the introduction of the inequality in the interchain interactions J_2 and J_2' as predicted by Suzuki and Shirai.⁹

The temperature dependence of the magnetic excitations at the magnetic Bragg position $Q = (1/3\ 1/3\ 1)$ has been measured as a function of temperature, fig. 2. The temperature dependence of the excitation energies is displayed in figure 3.

Four different temperature ranges can be indicated in the temperature dependence of the magnetic excitations as given in figure 3:

- A) Below $T = 2.0K$, the $\omega_1^0(1)$ mode shows a soft mode behaviour and still has not reached its final energy at 1.6K. The $\omega_1^+(3)$ and $\omega_2^-(5/6)$ modes at 0.10 THz and 0.145 THz respectively are constant but the $\omega_1^+(3)$ mode gradually loses its intensity. the $\omega_1^-(1)$ functions as the softmode of the 'ordered' part of the system.

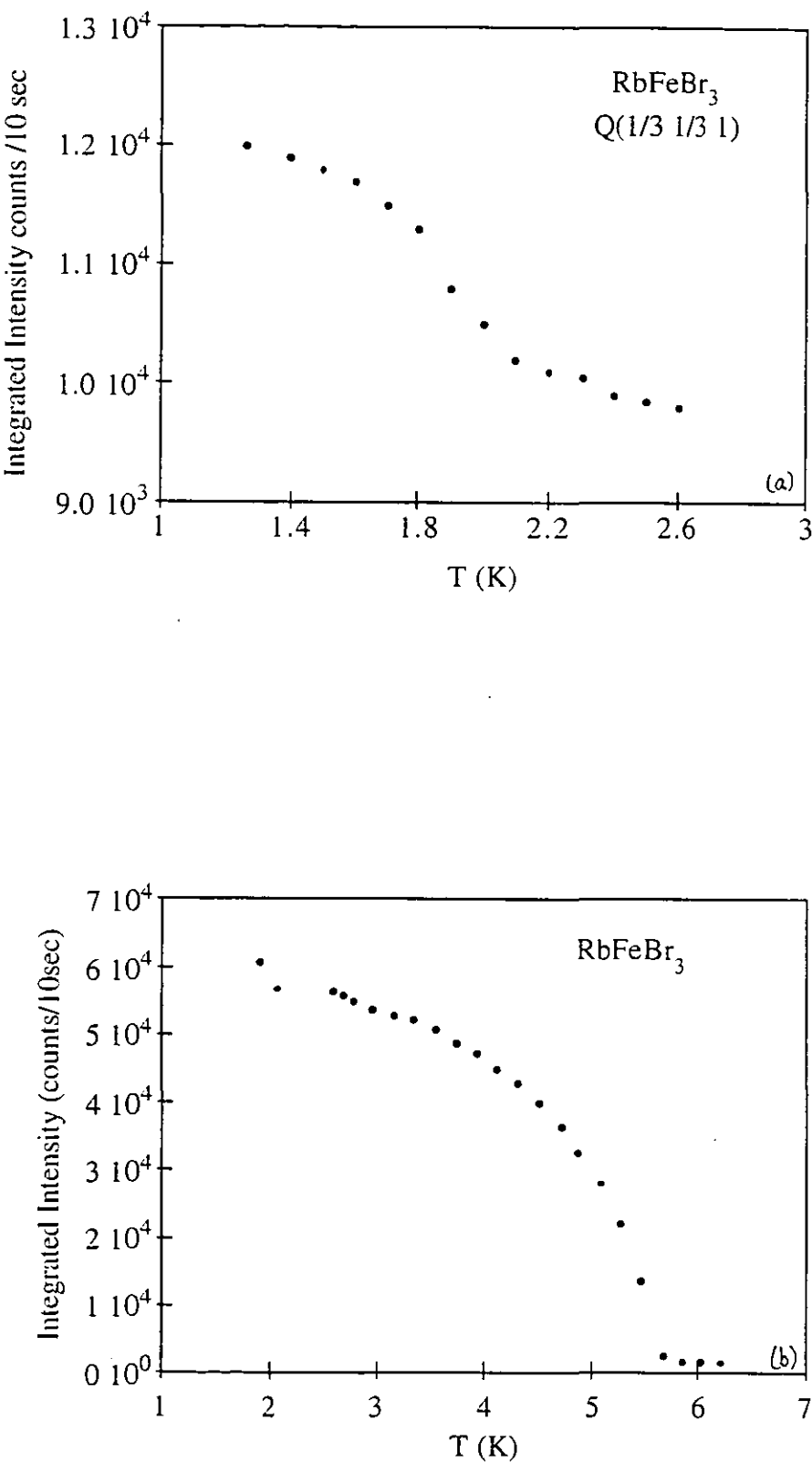


Figure 2. Magnetic sublattice magnetisation measured at $Q(1/3, 1/3, 1)$ (a) on IN12 and (b) on D16. Magnetic transitions are observed at $T \approx 2.0(1)$ K and $T = 5.6(2)$ K.

- B) Between $2\text{K} < T < 3.25\text{K}$, the ω_1^0 mode is not present while the other modes are clearly observable.
- C) At $3.5\text{K} < T < 5.6\text{K}$, the excitations broaden quickly upon increasing the temperature and it is more and more difficult to determine the energies of the individual excitations. It seems that the energy of the excitations changes: ω_1^+ decreases while ω_2^- increases at $T \sim 3.5\text{K}$ and they renormalise towards a single excitation at $T = 5.6\text{K}$.
- D) Above $T > 5.6\text{K}$, only one broad excitation can be observed which renormalises to higher energy as the temperature increases. This behaviour is similar to that observed for RbFeCl_3 in the paramagnetic phase.¹³

Our present measurements confirm the presence of a second magnetic phase transition at $T = 2.00(5)\text{K}$. The disappearance of the ω_1^0 mode at 2.0K supports the assumption that the intermediate magnetic phase is partially ordered. The total of the six sublattices of the fully ordered phase will then be reduced to four and the disappearance of the 0.10 THz excitation in the second magnetic phase will be due to its small intensity in the low temperature phase. At 2.0K the third chain starts to order but has only gained a small moment at our lowest temperature observation as indicated by the magnetic sublattice magnetisation.⁸

In the specific heat study of Adachi *et al.*⁵ a λ -like anomaly has been observed at $T = 5.61(5)\text{K}$ and a small cusp-like transition at $T = 2.00(5)\text{K}$. This cusp is spread out over a temperature range between $\sim 2.8\text{K} - 1.3\text{K}$ and is attributed to the ordering of the third magnetic chain. This feature can now be correlated to our observations as described under A and B. The maximum of the cusp corresponds to the soft mode temperature of the ω_1^0 mode and the temperature range around the transition from a partial to the full ordering of the moments on the chains.

The magnetic excitations as given in figure 1 are all accounted for except for the 0.29 THz excitation at $Q = (1/3\ 1/3\ 1)$. This excitation may arise from the disordered chain of the partially ordered phase, which will be of singlet ground state character. The local exchange fields in the partially ordered and fully ordered magnetic phases should be distinctly different and result in a difference between the magnetic excitations of the two phases. However, the experimental data (see figure 1) show the opposite. The excitation energies are more or less the same although the intensities of the excitations differ. A similar effect has been observed in the Ising-like antiferromagnet CsMnI_3 , which also has a partially disordered intermediate phase.¹⁴

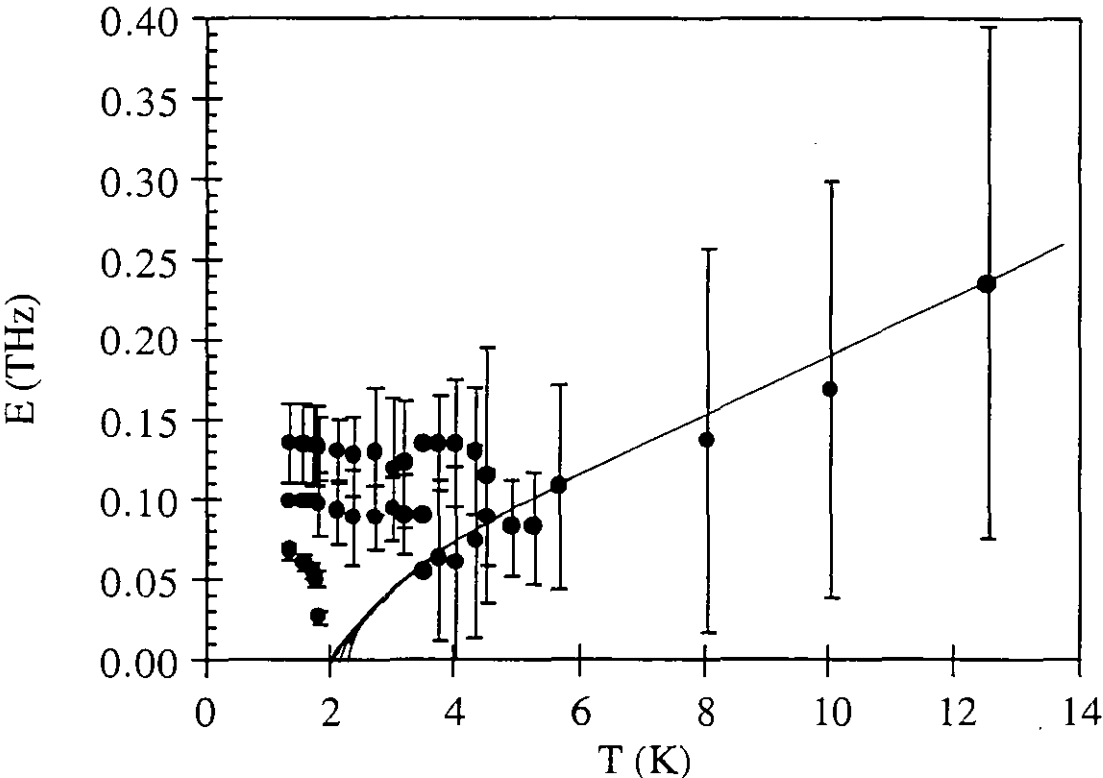


Figure 3. Temperature dependence of the magnetic excitations at $Q (1/3 \ 1/3 \ 1)$. The solid line represents the DCEFA prediction for the softmode behaviour.

In a previous paper¹² we have estimated the transition temperature T_N of RbFeBr_3 within the molecular field approach and the dynamical correlated effective field model based on the 120° type magnetic exchange. In the first case we calculate $T_N = 6.7\text{K}$ and for the second approach $T_N = 2.1\text{K}$. The latter temperature is in good agreement with the transition temperature to the fully ordered magnetic phase of RbFeBr_3 below $T_N = 2.0\text{K}$. Therefore, in this case the exchange field is properly accounted for, the renormalisation of the magnetic excitations calculated using the anisotropic values of J_1 , J_2 and D derived from fits to the dispersion of the magnetic excitations at $T = 4.5\text{K}$ ¹² account well for the renormalisation behaviour above $T_{N1} = 5.6\text{K}$ (see figure 3).

A detailed description of the magnetic dispersion curves of the modified triangular magnetic phase of RbFeBr_3 at 1.6K will be reported in a forthcoming paper while further work on the partially ordered phase and the identification of the character of the magnetic modes with polarised neutrons is in progress.

References

1. D. Visser and A. Harrison, *J. de Phys.* **C8**, 1467 (1988).
2. M. Steiner, *J. App. Phys.* **67**, 5593 (1990). W.J.L. Buyers, R.M. Morra, R.L. Armstrong, M.J. Hogan, P. Gerlach and K. Hirakawa, *Phys. Rev. Lett.* **56**, 371 (1986).
3. N. Suzuki, *J. Phys. Soc. Japan* **52**, 3907 (1983).
4. D. Visser and U. Steigenberger, Annex to the ILL report 1984, p. 78. B. Dorner, D. Visser, U. Steigenberger, K. Kakurai and M. Steiner, *Z. Phys. B* **72**, 487 (1988).
5. K. Adachi, K. Takeda, F. Matsubara, M. Mekata and T. Haseda, *J. Phys. Soc. Japan* **52**, 2202 (1983).
6. M. Eibschutz, G.R. Davidson and D.E. Cox, *A.I.P. Conf. Proc.* **18** (1973). D. Visser, unpublished results 1987.
7. D. Visser, G.C. Verschoor and D.J.W. IJdo, *Acta Cryst.* **B36**, 28 (1980).
8. D. Visser and G.J. McIntyre, to be published.
9. N. Suzuki and M. Shirai, *Physica B* **136**, 346 (1986).
10. A. Harrison and D. Visser, *Phys. Lett. A* **137**, 79 (1989).
11. D. Visser, B. Dorner and A. Harrison, to be published.
12. A. Harrison and D. Visser, *J. Phys. Cond. Matt.* **4**, 6977 (1992).
13. H. Yoshizawa, J.D. Axe and G. Shirane, *Solid State Commun.* **38**, 241 (1981).
14. A. Harrison, M.F. Collins, J. Abu Dayyeh and C.V. Stager, *Phys. Rev.* **B43**, 1708 (1991).

Chapter 4.

Magneto-structural correlations and high pressure induced changes to the magnetic ordering phenomena in AFeX₃

MAGNETO-STRUCTURAL CORRELATIONS IN THE QUASI ONE-DIMENSIONAL INDUCED MOMENT MAGNETS AFeX_3

D. Visser and A. Harrison

Inorganic Chemistry Laboratory, University of Oxford, South Parks Road, OX1 3QR Oxford, G.B.

Abstract. - A correlation between the structural parameters of the AFeX_3 ($A = \text{Cs, Rb}$ and $X = \text{Cl, Br}$) linear chain compounds crystallizing with the hexagonal perovskite structure and the magnetic parameters, superexchange and anisotropy obtained from inelastic neutron scattering data is presented. Special attention is paid to the induced-moment character of the Fe^{2+} ion in these compounds.

The isomorphous compounds AFeX_3 ($A = \text{Cs, Rb}$ and $X = \text{Cl, Br}$) show a variety of magnetic properties that depend on chemical composition and small changes in the crystal structure [1-7]. The structure is that of hexagonal perovskite (spacegroup $P6_3/mmc$) in which chains of trigonally-distorted face-sharing FeX_6^{4-} octahedra lie along the crystal c -axis. The effect of the cubic component of the ligand field and spin-orbit coupling, λ , on the D term of the Fe^{2+} is to give a $J = 1$ ground state. This is split further by the trigonal component, Δ , of the ligand field to produce a singlet ground state and a low-lying excited doublet. At low temperatures only the ground state singlet and the excited doublet are populated significantly and it is convenient to adopt an effective-spin Hamiltonian with $S = 1$:

$$H_i = \sum_{ij} \{ J_{ij}^{\perp} (S_i^x S_j^x + S_i^y S_j^y) + J_{ij}^{\parallel} S_i^z S_j^z \} + \sum_i D (S_i^z)^2 \quad (1)$$

where the superscripts \perp and \parallel denote the perpendicular and parallel components of the superexchange interactions. Within this representation the value of D and the ratio $J_{ij}^{\perp}/J_{ij}^{\parallel}$ depends on the ratio Δ/λ .

The size of the magnetic moment in these materials depends on the ratio J_Q/D , where J_Q is the maximum exchange field. The rubidium salts show long-range magnetic ordering transitions at low temperatures, but the caesium salts which have smaller values of J_Q behave as true singlet ground state materials.

The chain structure leads to anisotropy in the magnetic exchange constants: the interchain exchange J_2 , is an order of magnitude smaller than the intrachain exchange constant, J_1 . Although J_2 is antiferromagnetic in every case, J_1 is ferromagnetic for the chlorides but antiferromagnetic for the bromides.

In the present paper we present an experimental qualitative approach to elucidate the trends between the parameters of (1) and the changes in crystal structure on chemical composition of these materials. We give a description of the magnetic properties of the AFeX_3 compounds using structural parameters obtained at similar temperatures as the magnetic data

using the same experimental methods. Sticking to one class of compounds where only the structural parameters change and the superexchange parameters are obtained from a single suitable theoretical model, one may obtain a true one to one magneto-structural correlation, which is lacking in many such a study to date [9].

The structural data were obtained from neutron powder diffraction data collected on the Curran powder diffractometer at AERE-Harwell at $\lambda = 1.37 \text{ \AA}$. The magnetic data took the form of inelastic neutron scattering measurements performed on single crystals of each material at low temperatures and is reported in the literature elsewhere [3-5, 8]. D is large relative to the exchange parameters in (1) so spin-wave models are inapplicable to the dispersion of the magnetic excitations. Instead, an excitonic model must be used with a suitable method of decoupling the products of spin operators that appear in (1). We choose the Dynamical Correlated Effective Field Approximation [6] (DCEFA) in preference to Molecular Field or Random Phase Approximation [6] decouplings because it makes some attempt to treat the short-range magnetic correlations that are important in low-dimensional induced-moment magnets. Explicitly, this involves the substitution:

$$S_i^x S_j^x = S_i^x [\langle S_j^x \rangle + \alpha (S_j^x - \langle S_j^x \rangle)] + S_j^x [\langle S_i^x \rangle + \alpha (S_i^x - \langle S_i^x \rangle)] \quad (2)$$

where $\langle S_i^x \rangle$ is the mean magnetisation in the direction x and α is a parameter that describes the correlation of nearest-neighbour moments. Both $\langle S_i^x \rangle$ and α have to be determined self-consistently.

In the magnetically ordered phases one dispersion branch is expected for each single-ion excitation on each magnetic sublattice. Using an estimate of the exchange parameters and D the dispersion and scattering cross-section of each branch was calculated and the data were then least-squares fitted to the strongest branches.

The results of the structure refinements are summarised in table I. The results of the least-squares fitting of the DCEFA model to the dispersion of the mag-

netic excitations are presented in table II. In a previous application of the DCEFA model to RbFeCl₃ the ratio of $J_1^\perp / J_1^\parallel$ was taken to be equal to $J_2^\perp / J_2^\parallel$ and governed by the ratio Δ / λ [6]. This assertion is valid if the superexchange pathways along and between the chains make the same use of the σ -bonding 3d orbitals on the iron atoms. It is *not* valid if there is an appreciable direct component of intrachain exchange arising from direct overlap of the t_{2g} orbitals, or any other reason for differing contributions being made by the t_{2g} and e_g orbitals to J_1 and J_2 . We do not consider this to be a reasonable assumption and take the quantities J_1^\parallel , J_1^\perp , J_2^\parallel , J_2^\perp to be independent variables. Indeed, we found that there was a significant improvement in the fit to the data when this approach was taken.

The following conclusions about the magneto-structural correlations in the AFeX₃ compounds may be drawn from table I and II:

(A) the difference between the rubidium and caesium salts appear to arise mainly from a reduction in J_1 and J_2 as the cell parameters increase from rubidium to caesium. It is also obvious from the tables that one has to make the comparison for each type of anion separately. Then J_1 increases with a decreasing superexchange angle θ (Fe-X-Fe). This conclusion is supported by the fact that one expects a larger J for the AFeBr₃ compounds because of the larger contribution of the covalency of the Br-ion. The exchange constants of CsFeBr₃ and RbFeBr₃ are less different than in the chlorides. This means that CsFeBr₃ is much closer to a magnetically ordered groundstate than CsFeCl₃ [3, 4, 8];

(B) the value of D shows little change with crystal structure despite the change in θ ; in an undisturbed octahedron $\theta = 70.53^\circ$. One expects D to increase with decreasing θ . Table II shows actually the opposite trend. One expects D also to be smaller in the bromides than in the chlorides due to a larger orbital reduction effect for the bromides [3], which reduces the effective spin-orbit coupling and hence the values of D in (1). A possible explanation may be found in the rather large correlation between D and J in the fits;

(C) the sign of J_1 on angle is compatible with the idea that there is a competition between "potential" and "kinetic" exchange terms in the Fe-X-Fe superexchange bridge. For such a bridge composed of the e_g orbitals on the Fe²⁺ overlapping p-orbitals on the halogen and a bridging angle θ of 90° , the superex-

Table I. - The structural parameters of the AFeX₃ halides.

A, X	a [Å]	c [Å]	θ°	x_x	T [K]
Cs, Cl	7.121	5.971	74.90	0.1580	4.2
Rb, Cl	6.993	5.954	74.09	0.1628	1.3
Cs, Br	7.507	6.291	73.43	0.1608	1.3
Rb, Br	7.332	6.263	72.45	0.1683	4.2

Table II - The DCEFA magnetic parameters for the AFeX₃ halides

J , D [meV]	CsFeCl ₃	RbFeCl ₃ [6]	CsFeBr ₃	RbFeBr ₃
J_1^\perp	0.309(28)	0.405	-0.381(20)	-0.398(10)
J_2^\perp	-0.019(3)	-0.0344	-0.037(5)	-0.044(3)
J_1^\parallel	0.459(124)	0.527	-0.424(84)	-0.431(44)
J_2^\parallel	-0.029(7)	-0.045	-0.041(6)	1.94(2)
D	1.700(7)	1.92	1.846(78)	1.94(2)
α	0.676	0.779	-0.458	-0.414

change is expected to be "potential" in origin and ferromagnetic. As θ is reduced the linkage acquires non-orthogonal character and antiferromagnetic "kinetic" exchange occurs. The crossover from ferro- to antiferromagnetic J_1 is expected in the region of $\theta = 70 - 80^\circ$. However, recent studies of the magnetic structure of RbFeCl₃ under hydrostatic pressure revealed that J_1 remains ferromagnetic even when θ is forced below the value found in RbFeBr₃ at ambient pressure [10]. This is in further support of the observations under (A).

A further evaluation of the magneto-structural correlations in the AFeX₃ compounds and the dependence of J_1 on θ has to be of a theoretical nature taking the exact geometry of the superexchange unit as well as the electronic character of the anion into account.

Acknowledgments

D. V. and A. H. would like to thank the UK SERC for financial support. A. H. is grateful to St. John's College Oxford for further financial help.

- [1] Lines, M. E. and Eibschutz, M., *Phys. Rev. B* **11** (1975) 4583.
- [2] Eibschutz, M., Lines, M. E. and Sherwood, R. C., *Phys. Rev. B* **11** (1975) 4595.
- [3] Yoshizawa, H., Kozukue, W. and Hirakawa, K., *J. Phys. Soc. Jpn* **49** (1980) 144.
- [4] Steiner, M., Katurai, K., Knop, W., Dorner, B., Pynn, R., Happek, U., Day, P. and McLeen, G., *Solid State Commun.* **38** (1981) 1179.
- [5] Petitgrand, D., Hennion, B., Radhakrishna, P., Escribe, C. and Legrand, S., Recent developments in Condensed Matter Physics, Eds. J. T. Devreese, V. E. van Doren and J. van Royen (Plenum) **4** (1981) 205.
- [6] Suzuki, N., *J. Phys. Soc. Jpn* **52** (1983) 3907.
- [7] Harrison, A. and Visser, D., *J. Phys. C* (submitted).
- [8] Visser, D. and Steigenberger, U., *J. Phys. C* (submitted).
- [9] Magneto Structural Correlations in Exchange Coupled Systems, NATO ASI C140 (1985), Eds. R. D. Willet, D. Gatteschi and O. Kahn (Riedel).
- [10] Harrison, A., Visser, D. and Vettier, C., Annex to the ILL report (1984) 215.

The Influence of Applied Pressure on the Magnetic Excitations of Magnetic Ordering in the Quasi One-Dimensional Induced Moment Magnets AFeX_3

D. Visser¹, A. Harrison², C. Vettier³, B. Schmid³ and P.A. Lindgård⁴

1 Department of Physics, Loughborough University of Technology, Loughborough LE11 3TU, UK.

2 Inorganic Chemistry Laboratory, University of Oxford, South Parks Road, Oxford OX1 3QR, UK.

3 Institut Laue Langevin, BP 156X, F-38042 Grenoble Cedex, France.

4 Department of Solid State Physics, Risø National Laboratory, DK-4000 Roskilde, Denmark.

(Contribution to the European Workshop on Neutron Scattering at High Pressures, 19-21 March 1992, Cosener's House, Abingdon, Oxfordshire, UK)

Introduction

The AFeX_3 ternary halides, with $\text{A} = \text{Cs}$ and $\text{Rb} = \text{Cl}$ and Br , which crystallize with the hexagonal perovskite structure (SG: $\text{P6}/3\text{mmc}$) exhibit quasi one-dimensional magnetic behaviour at low temperature. The trigonally distorted FeX_6^{4-} octahedra in this crystal structure form infinite chains of face-sharing octahedra. Consequently, the magnetic behaviour of the Fe^{2+} ion can be described at low temperature by an effective spin of $S = 1$ and locally with a singlet ground state (SGS), with $m = 0$, due to the single-ion anisotropy. In the case when the intrachain and interchain superexchange interactions are small compared with the single-ion anisotropy of the system, the compound will show an SGS behaviour for $T \rightarrow 0$. This happens for CsFeCl_3 and CsFeBr_3 . For RbFeCl_3 and RbFeBr_3 the overall superexchange interactions are large enough to induce long range magnetic ordering at low temperature.¹

A characteristic feature of these SGS systems is the softening of a magnetic mode at the magnetic zone centre with decreasing temperature due to the increase of magnetic correlations induced by the magnetic superexchange interactions. Soft mode behaviour has been observed for all hexagonal AFeX_3 compounds. For the Rb compounds the energy of the soft mode goes to zero and static long range magnetic order is induced. In Cs compounds the soft mode approaches a finite value for $T \rightarrow 0$.²

The application of an external magnetic field along the c -axis (chain direction) on these SGS systems induces a magnetic phase transition to an ordered state. In

CsFeCl_3 , which has ferromagnetic intrachain superexchange, three consecutive magnetic transitions have been observed at 0.7K. In CsFeBr_3 , which has an antiferromagnetic intrachain superexchange, the applied magnetic field induces commensurate magnetic ordering at 1.6K at $H/c = 4.1\text{T}$. The magnetic moments form a 120° type triangular magnetic structure. In the case of CsFeCl_3 , the final magnetic structure is also of the 120° triangular type while the two incommensurate phases are helical and sinusoidal, respectively. This sequence of magnetic structures is caused by an interplay between magnetic dipolar interaction and the interchain superexchange forces. This occurs only when the intrachain superexchange force is ferromagnetic.

Applying uniaxial pressure along the ordering direction of an SGS system may also induce long-range magnetic ordering. Theoretically it can be shown that applied pressure acts in a similar fashion on an SGS system as an applied magnetic field. It has been demonstrated for Pr metal that magnetic ordering can be induced in this way. The small structural changes caused by applied pressure may influence the superexchange and single-ion anisotropy in such a way that the balance is tipped over from an SGS behaviour to one with an induced magnetic moment.

Theoretical

The materials discussed above can be described by the following Hamiltonian

$$H = -2 \sum_q J_q S_q S_{-q} + D \sum_q (S_q^z)^2 + P \sum_q (S_q^z)^2 \quad (1)$$

where J is the intrachain superexchange parameter and J' the interchain superexchange parameter. The quasi one-dimensional character of these compounds is due to the fact that $J > J'$. The single-ion anisotropy D is positive for all these compounds, which results in an XY-type anisotropy. D equals the energy gap between the singlet ground state $|1\rangle$ and the low-lying degenerate doublet state, $|2\rangle$ and $|3\rangle$. Thus, without superexchange interactions present, this system would have an SGS for $T \rightarrow 0$. The last part of (1) comprises the additional term due to applied pressure parallel to the c -axis.

In the presence of superexchange, but in the absence of additional factors like magnetic field or pressure, there are two regimes which are separated by a second order phase transition. For $T \rightarrow 0$ and $A < 8|J| + 12|J'|$ (2), the system has a magnetic ground state. The SGS appears when $A > 8|J| + 12|J'|$ (3).

An inelastic neutron scattering experiment probes the transition between the ground state $|1\rangle$, $m = 0$, and the low-lying excited doublet, $|2\rangle$ and $|3\rangle$, $\Delta m = \pm 1$. For $D > 0$ and $P = 0$ one observes a doubly degenerate excitation throughout Q -space, which is folded by superexchange. The Hamiltonian (1) can be treated by RPA theory.³ With the use of standard basis operators $a_{pn} = |p\rangle \langle n|$ for calculating the dynamic response function $\chi^{\alpha\alpha}(q, \omega)$ one can show that $\chi^{xx}(q, \omega)$ and $\chi^{zz}(q, \omega)$ are uncoupled in the absence of external pressure. However, $S_q^x = a_{12}^\dagger + a_{21}$ is coupled to the quadrupolar type operator $L_q^x = (S_y S_z + S_z S_y) = i(a_{12}^\dagger - a_{21})$. Using the RPA theory the dispersion of the magnetic excitations as solution of (1) is given for $P \parallel c$ -axis by:

$$\omega_q^2 = \{(D + P) [(D + P) - J_q Q(R)]\} \quad (4)$$

with

$$Q(R) = 2(\langle S_y^2 \rangle - \langle S_z^2 \rangle) = 3/2 [\langle S^+ S^- \rangle + \langle S^- S^+ \rangle] - 2 S(S+1) \quad (5)$$

being the quadrupole moment. In this case no symmetry breaking occurs and the $|2\rangle$ and $|3\rangle$ levels remain degenerate. The energy of the singlet to doublet transition is now given by $(D + P)$ and increases linearly with pressure due to the renormalisation of the Q factor. $Q(R)$ acts as a renormalization factor which depends on the strength of the pressure and is determined self-consistently. $Q(R)$ has the same function and action as the $R(T, H)$ factor in the case of an applied magnetic field.

For $P \perp c$ (1) alters slightly to:

$$H = -2 \sum_q J_q S_q S_{-q} + D \sum_q (S_q^z)^2 + P \sum_q [(S_q^y)^2 - (S_q^x)^2] \quad (6)$$

The RPA theory gives in this case:

$$\omega_q = (D (D - J_q Q(R))^{1/2} \pm P \quad (7)$$

Due to the external pressure $\perp c$ -axis the symmetry is altered, which results in the lifting of the degeneracy of the modes $|2\rangle$ and $|3\rangle$. Going beyond the RPA calculation it is predicted by correlation theory⁴ that the excitonic mode does not go soft but loses its spectral weight to the central peak occurring at the critical pressure P_c . The halfwidth of this mode is $\sim q^2$ at P_c . This indicates a diffusional behaviour. The width of the central peak vanishes at P_c , which indicates a normal critical showing down resulting in a second order phase transition to a magnetically ordered groundstate. In figure 1 and 2

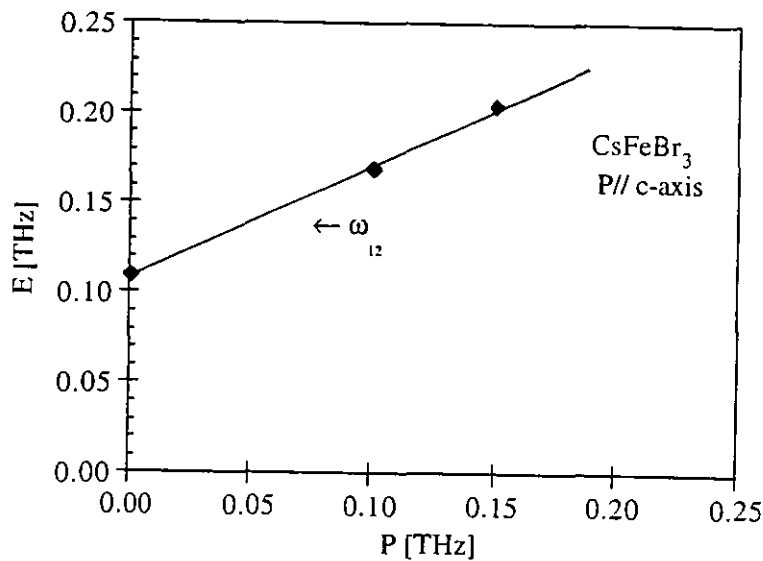


Fig.1 Dependence of the soft-mode frequency ω_{12} at $Q(1/3\ 1/3\ 1(0))$ on the pressure parameter $P // c$ -axis.

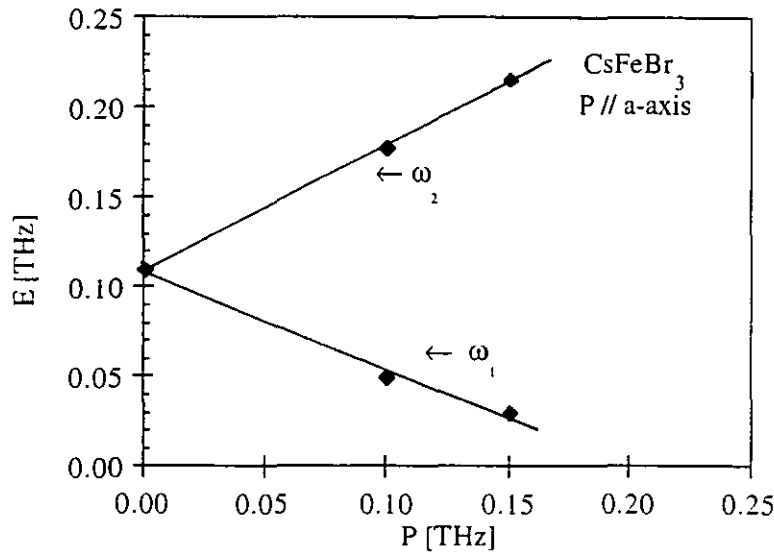


Fig.2 Dependence of the soft-mode parameter ω_1 and ω_2 at $Q(1/3\ 1/3\ 1(0))$ on the pressure parameter $P // a$ -axis.

we show the theoretical predictions of the effect of pressure on the magnetic excitation(s) at the soft mode point Q ($1/3\ 1/3\ 1$) in CsFeBr₃. The variable P has been expressed in the same units as D.

In the case of the induced moment ground state, like RbFeCl₃ one has to take correlation effects explicitly into account. This can be achieved using Suzuki's correlated effective field approach.⁵

The hexagonal ABX₃ structure under pressure

The crystal structure of CsFeCl₃, CsFeBr₃ and RbFeCl₃⁶ were studied under applied *hydrostatic* pressures up to 4.9 kbar. Single crystals of these materials were mounted in a He pressure cell inserted in to an ILL Orange cryostat. The crystals were aligned with the hexagonal ab-plane horizontal. The two-axis diffractometer D15 at the Institut Laue Langevin, Grenoble, France, was used for the elastic neutron scattering experiments. Using D15 in this way allowed us to probe the $l = 0$ as well as the $l = 1$ layer and the reciprocal space perpendicular to these planes. The AFeCl₃ compounds have a ferromagnetic intrachain interaction but an antiferromagnetic interchain interaction. Therefore, one observes the magnetic Bragg reflections for the 120° type triangular magnetic structure at the positions $h + k = 3n, l = 0$ and for the AFeBr₃ compounds where the intrachain interaction is antiferromagnetic the reflections are positioned at $h + k = 3n, l = 1$. The quasi elastic scattering due to the 1-D magnetic correlations may be observed along the [00 l] direction.

For the SGS compounds CsFeCl₃ and CsFeBr₃ we did not observe any magnetic scattering at the K, M respectively A, H points of the Brillouin zone. This indicates that the caesium compounds retain their SGS character up to 4.9 kbar at T = 2.0K. Scans along the [00 l] direction did not give a clear idea of increased 1-D magnetic correlations. This may, however, be due to the fact that the resolution of D15 is very poor for scans perpendicular to the scattering plane.

For RbFeCl₃ we observed an increase in T_N from 2.5K to 4.4K - 6.2K at 4.9 kbar.⁷ A similar magnetic ordering sequence has been observed under pressure as observed at ambient pressure. The same incommensurate magnetic phases are detected with similar displacement vectors with respect to Q ($1/3\ 1/3\ 1$).

The single crystal structure determinations show for all these compounds that the unit cell is anisotropically compressed with the largest change taking place in the c-direction between 0 and 2 kbar. Figure 3 and 4 show the change in length of the a-

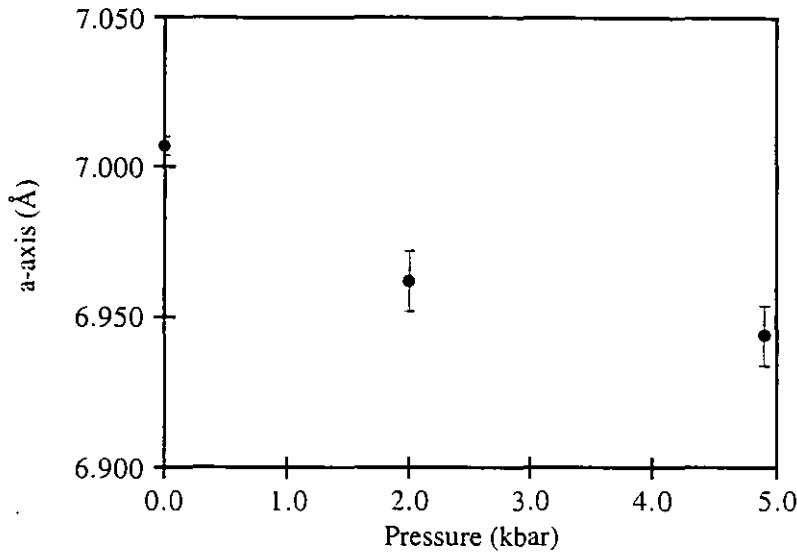


Fig.3 The compression of the a-axis of RbFeCl₃ as function of hydrostatic pressure at T = 10 K.

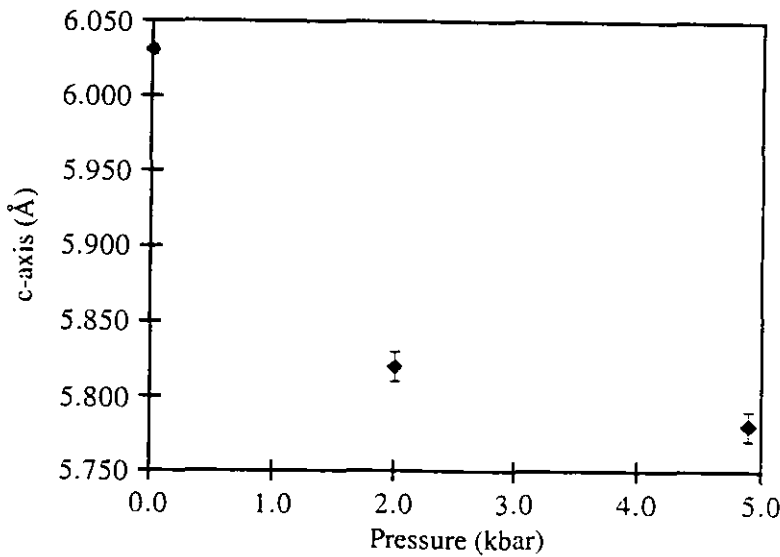


Fig.4 The compression of the c-axis of RbFeCl₃ as function of hydrostatic pressure at T = 10 K.

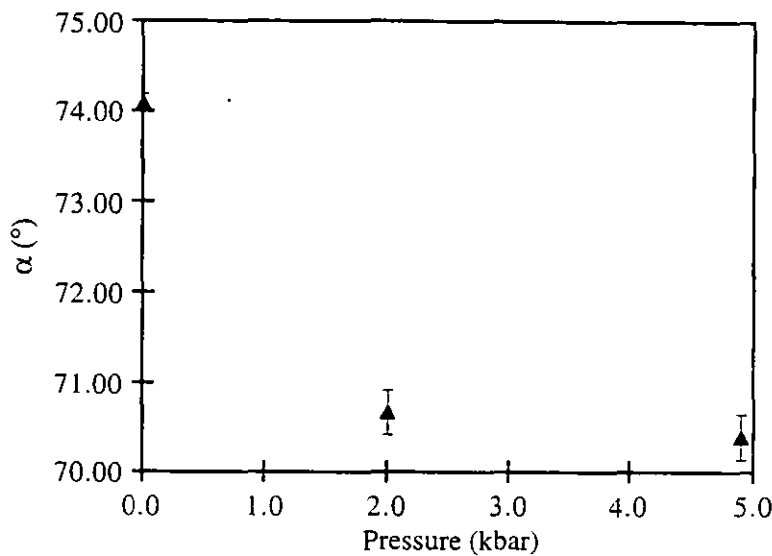


Fig.5 The compression of the Fe - Cl - Fe superexchange angle α of RbFeCl_3 as function of hydrostatic pressure at $T = 10$ K.

axis, c-axis while figure 5 shows the effect on the intrachain superexchange angle α under hydrostatic pressure.

Discussion

Simple arguments following (2) and (3) indicate that one might influence the SGS character of the hexagonal AFeX_3 by applying an external pressure. The single-ion anisotropy D as well as J , J' are directly related to the distortion of the FeX_6^{4-} octahedra. So one might tune the parameters D , J and J' by applying, in an ideal world, a uniaxial pressure and find a way to influence one of these parameters individually. However, in the case of the AFeX_3 compounds one has very brittle materials, which does not allow one to apply uniaxial pressure easily. Furthermore, all variables are simultaneously changed by a hydrostatic as well as a uniaxial pressure.

The equations (4) and (7) show that a uniaxial pressure along the a-axis will eventually induce magnetic ordering, assuming that the value of J does not change under pressure. As indicated by the structure determinations of the AFeX_3 compounds under hydrostatic pressure, a considerable change in the structural parameters is observed. Consequently A , J and J' will change. How much these parameters do actually change can only be ascertained unambiguously from an inelastic neutron scattering experiment. A further difficulty arises from the fact that the ratio of the parameter P in (1) and (5) and the actual pressure in kbar is not known. Therefore, one does not know how much pressure to apply. In the case of AFeX_3 under hydrostatic pressure one observes a combined effect of (4) and (7) as well as a change in D , J and J' . This may explain why both Cs compounds are still SGS up to 4.9 kbar. From the experiment on RbFeCl_3 one may conclude that at least J' is increasing with applied pressure. The dependence of the superexchange J as a function of the superexchange angle α and the structure of the bridging unit ($\text{Fe} - \text{X} - \text{Fe}$)₃ can be evaluated by the procedures as outlined by Ritter *et al.*⁸ However, difficulties may arise when comparing the results of such a magnetostructural correlation and the values of J obtained from the effective Hamiltonian (1).

The observed anisotropic compressibility in the AFeX_3 compounds may actually be of great help to answer many of the problems outlined above. By measuring the magnetic excitations under hydrostatic pressure at different pressures, one may be able to deduce the influence of the \parallel and \perp components due to (4) and (7) and determine P . Thereafter, one may consider if it is useful and feasible to construct a uniaxial pressure cell for this type of material.

References

1. D. Visser and A. Harrison, J. Phys. (Paris), **C8**, 49, 1467 (1988) and references therein.
2. B. Schmid, B. Dorner, D. Visser and M. Steiner, Z. Phys. B **86**, 257 (1992).
3. P.A. Lindgard, J. Phys. **C8**, L178; Physica 120B, 190 (1983).
4. P.A. Lindgard, Spinwaves and Magnetic Excitations I, Chapter 5 in *Theory of Spin Excitations in Rare Earth Systems*, ed. A.S. Borovik, R. Omanov and S.K. Shina, Elsevier North Holland (1988).
5. N. Suzuki, J. Phys. Soc. Japan **52**, 1002, 1009, 3907 (1983).
6. D. Visser, A. Harrison and C. Vettier, Z. Phys. B (submitted).
7. D. Visser, A. Harrison and C. Vettier, Solid State Comm. (submitted).
8. R. Ritter, L. Jansen and E. Lombardi, Phys. Rev. **B8**, 2139 (1973).

High Pressure Research, 1995, Vol. 14, pp. 29–34
Reprints available directly from the publisher
Photocopying permitted by license only

© 1995 OPA (Overseas Publishers Association)
Amsterdam B.V. Published under license by
Gordon and Breach Science Publishers SA
Printed in Malaysia

MAGNETIC EXCITATIONS AND MAGNETIC ORDERING IN THE HEXAGONAL PEROVSKITES AFeX_3 UNDER HYDROSTATIC PRESSURE

D. VISSER*, A. R. MONTEITH*, A. HARRISON** and D. PETITGRAND***

* Department of Physics, Loughborough University of Technology,
Loughborough LE11 3TU, Leicestershire, UK

** Department of Chemistry, University of Edinburgh EH9 3JJ, UK

*** Laboratoire Leon Brillouin, CE Saclay, 91191 Gif sur Yvette Cedex, France

ABSTRACT

Uniform high pressure experiments up to 5 kbar on quasi one-dimensional singlet ground state and the induced magnetic moment systems AFeX_3 are reported. The pressure-induced changes in the magnetic ordering vector are related to induced structural phase transitions. The anisotropic compression of the lattice may give rise to induced moment formation in the CsFeX_3 compounds. Inelastic neutron scattering experiments show that the anisotropic compression effect on the magnetic excitations is not visible. However, structural changes show a marked effect on the magnetic excitation spectrum. Predictions are made for the magnetic excitation spectra of the induced moment systems RbFeCl_3 and TlFeCl_3 .

INTRODUCTION

The AFeX_3 halides with $A = \text{Cs, Rb, Tl}$ and $X = \text{Cl, Br}$, which crystallise with the hexagonal perovskite structure, exhibit quasi one-dimensional behaviour at low temperature. The magnetic behaviour of the Fe^{2+} ion can be described by an effective spin of $S = 1$ and locally with a singlet ground state. In this series of compounds the CsFeX_3 compounds are pure single ground state systems while the Rb and Tl compounds have an induced moment behaviour [1]. Slight structural changes upset the balance of the intra and interchain superexchange as well as the single-ion anisotropy. Their combined action can tip the balance of the singlet ground state to induced moment behaviour. Applied pressure may be, in this case, the appropriate tool to investigate this type of phase transition.

The crystal structure CsFeBr_3 , CsFeCl_3 and RbFeCl_3 were studied in the presence of a hydrostatic pressure [2]. The compression of the hexagonal perovskite turns out to be anisotropic. The magnetic excitations in the singlet ground state systems have also been measured under hydrostatic pressures up to 5 kbar. Again the magnetic excitations change anisotropically with applied pressure.

In general we observe a trend in the AFeCl_3 compounds that T_N increases, and in the case of CsFeCl_3 that the system is driven towards an induced magnetic ordering. In the case of CsFeBr_3 the system is still behaving as a singlet ground state system at 5kbar. An opposite trend to the AFeCl_3 may be present in the AFeBr_3 compounds, in the sense that the AFeBr_3 systems move away from pressure induced magnetic ordering towards a singlet ground state which is less strongly coupled by magnetic superexchange.

D.VISSER *et al.*

The magnetic ordering process in the AFeX₃ compounds is strongly dependent on the details of the crystal structure. Therefore structurally induced changes by means of applying pressure can change the magnetic structure dramatically. Indications of such a behaviour have been found for TlFeCl₃. The effect on the magnetic excitations should also be noticeable and will be discussed in this paper.

Theoretical

The materials discussed above can be described by the following Hamiltonian

$$H = -\frac{1}{2} \sum_q J_q S_q S_{-q} + D \sum_q (S_q^z)^2 + P \sum_q (S_q^z)^2 \quad (1)$$

where J is the intrachain superexchange parameter and J' the interchain superexchange parameter. The quasi one-dimensional character of these compounds arises from the fact that $J > J'$.

Using RPA theory[17], the dispersion of the magnetic excitations as solution of (1) is given for $P \parallel c$ by:

$$\omega_q^2 = \{(D + P)[(D + P) - J_q Q]\}$$

with Q being the quadrupole moment and the perturbation, due to pressure P , being expressed in terms of magnetic anisotropy. For $P \perp c$, (1) alters slightly to:

$$H = -\frac{1}{2} \sum_q J_q S_q S_{-q} + D \sum_q (S_q^z)^2 + P \sum_q [(S_q^y)^2 - (S_q^x)^2] \quad (3)$$

The RPA theory gives in this case:

$$\omega_q = \sqrt{D(D - J_q Q)} \pm P \quad (4)$$

The single ion anisotropy is, for all these compounds, positive which results in an XY-type anisotropy. A is the energy gap between the singlet ground state $|1\rangle$ and the low-lying degenerate doublet state, $|2\rangle$ and $|3\rangle$. Thus in the absence of superexchange interaction, this system would have a SGS for $T \rightarrow 0$. The last part of (1) comprises the additional term due to applied pressure parallel to the c -axis.

In the presence of superexchange, but in the absence of additional factors like magnetic field or pressure, there are two regimes which are separated by a second order phase transition. For $T \rightarrow 0$ and $D < 8|J| + 12|J'|$, the system has a magnetic ground state. The SGS appears when $D > 8|J| + 12|J'|$.

MAGNETIC PROPERTIES OF PEROVSKITES

The Hexagonal ABX₃ Structure Under Pressure

The crystal structure of CsFeCl₃, CsFeBr₃ and RbFeCl₃ were studied under applied hydrostatic pressures up to 4.9 kbar. Single crystals of these materials were mounted in a He pressure cell inserted into an ILL Orange cryostat. The crystals were aligned with the hexagonal ab-plane horizontal. The two-axis diffractometer D15 at the Institut Laue Langevin, Grenoble, France was used for the elastic neutron scattering experiments. Because the AFeCl₃ compounds have a ferromagnetic intrachain interaction but with an antiferromagnetic interchain interaction one observes the magnetic Bragg reflections for the 120° type triangular magnetic structure at the positions $h+k = 3n, l = 0$; for the AFeBr₃ compounds where the intrachain interaction is antiferromagnetic the reflections are positioned at $h + k = 3n, l = 1$. For the SGS compounds CsFeCl₃ and CsFeBr₃ we did not observe any magnetic scattering for $T \rightarrow 0$ at the K, M and A, H points of the Brillouin zone respectively. This indicates that the caesium compounds retain their SGS character up to 4.9 kbar at $T = 2.0$ K.

For RbFeCl₃ we observe the increase of T_N from 2.5 K at ambient pressure, to 4.4 K ($T \uparrow$) - 6.2 K ($T \downarrow$) at 4.9 kbar. The difference in T_N at 4.9 kbar is due to the large hysteresis present. A similar magnetic ordering sequence has been observed under pressure as that observed at ambient pressure. The same incommensurate magnetic phases are detected with similar displacement vectors with respect to Q (1/3 1/3 1). The single crystal structure determination shows for all these compounds, that the unit cell is anisotropically compressed with the largest change taking place in the c direction between 0 to 2 kbar (Table 1).

TABLE 1 Changes in unit cell parameters under hydrostatic pressure at liquid helium pressures.

axis(Å)	0 kbar	1.0 kbar	2.2 kbar	5.0 kbar
CsFeCl ₃ (a)	7.1764	7.1681	7.1538	7.1213
(c)	5.9706	5.9575	5.9440	5.9198
TlFeCl ₃ (a)	6.880			6.856
(c)	5.952			5.933
CsFeBr ₃ (a)	7.4762		7.4527	7.4167
(c)	6.3045		6.2380	6.2237
RbFeCl ₃ (a)	6.993		6.961	6.934
(c)	5.954		5.810	5.744

TlFeCl₃ orders magnetically with an incommensurate magnetic structure, which structure is identical with the IC₁ phase of RbFeCl₃. The magnetic k-vector is nearly commensurate with $k = (0.330, 0.330, 0)$ [8]. The difference in behaviour, in comparison with RbFeCl₃ is due to the structural phase transition in TlFeCl₃ at 179K and 79K [6]. The crystal structure changes from simple hexagonal perovskite to the KNiCl₃ RT-structure [9], which changes further into an incommensurate crystal structure varying only slightly from the structure above. The hexagonal basal plane in the two low temperature phases is similar to that of RbFeBr₃ [10]. There are two different interchain exchange constants in this structure which releases the frustration of the 120° type magnetic structure. It introduces also a partially ordered magnetic phase before a modified 120° type magnetic structure is formed.

D.VISSER *et al.*

When a hydrostatic pressure of 5kbar is applied to TiFeCl_3 we see that the incommensurate magnetic structure disappears and becomes commensurate, $T_{N1} = 5.8(1)\text{K}$ comparable to RbFeCl_3 under pressure. However, we observe a second magnetic phase transition at $T_{N2} = 4.2(1)\text{K}$, fig 1.

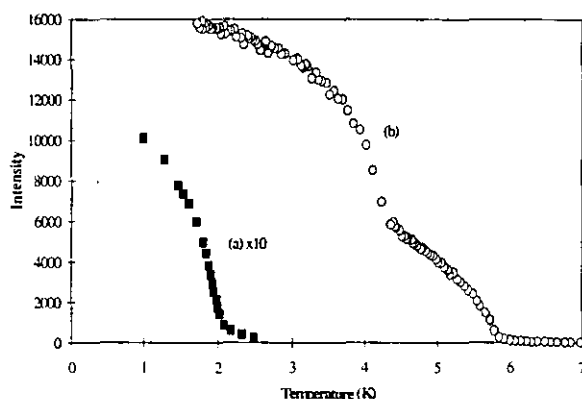


FIGURE 1 Sublattice magnetisation of TiFeCl_3 at (a) 0 kbar and (b) 5.0 kbar.

The observed behaviour is similar to that in RbFeBr_3 where $T_{N1} = 5.5\text{K}$ and $T_{N2} = 2.0\text{K}$ at ambient pressure[11]. The application of pressure is identical to raising the temperature of a crystal, therefore we can conclude that the structure of TiFeCl_3 at 5 kbar has most probably adopted the structure of KNiCl_3 at RT. The magnetic ordering process passes through two stages. It will involve a partially ordered structure between T_{N1} and T_{N2} as well as a modified 120° type structure[12].

Inelastic Neutron Scattering Experiments

The magnetic excitations in the singlet ground state systems CsFeBr_3 and CsFeCl_3 have been studied under hydrostatic pressure conditions at the Institut Leon Brillouin at CEN Saclay on the triple axis spectrometer 4F1. The experimental conditions, the pressure and cryogenic equipment used were identical to that used for the elastic neutron scattering experiments. The results are shown in figs. 2 and 3.

Although the lattice is contracting anisotropically it was not possible to observe any splitting in the magnon modes. Therefore one should consider the conditions applied to the crystal as isotropic. The magnetic excitation can then be treated as a system at ambient pressure but with different anisotropy and superexchange constants. The magnetic excitations should in this case be described by equation 2.

For CsFeBr_3 we observe that the gap energy at $Q(1/3 \ 1/3 \ 1)$ increases, fig 2. The system retains its singlet ground state behaviour at 5kbar as predicted by theory.

For CsFeCl_3 we observe the gap energy at $Q(1/3 \ 1/3 \ 0)$ decreases fig 3. At 5.0kbar the system is close to magnetic ordering. We estimate that a further increase of 1-2 kbar will induce magnetic ordering.

MAGNETIC PROPERTIES OF PEROVSKITES

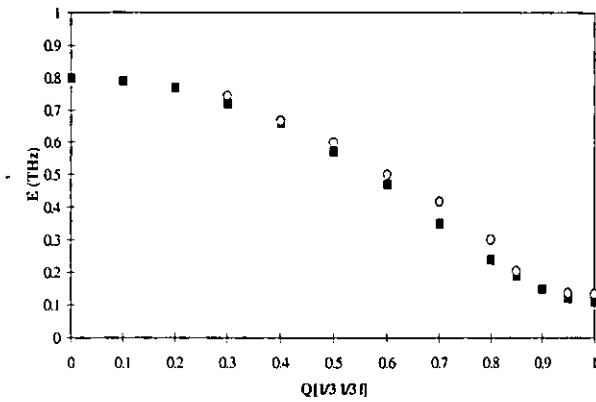


FIGURE 2 Magnetic excitation in CsFeBr_3 along the $[1/3\ 1/3\ 1]$ direction of the reciprocal lattice at $T=2\text{K}$ for ambient pressure and 5kbar hydrostatic uniform pressure. $Q(1/3\ 1/3\ 1)$ represents the soft mode point. (o) 5kbar, (■) 0 kbar.

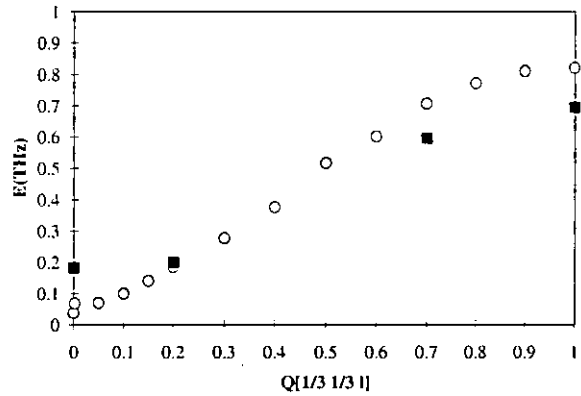


FIGURE 3 Magnetic excitation in CsFeCl_3 along the $[1/3\ 1/3\ 1]$ direction of the reciprocal lattice at $T=2\text{K}$ for ambient pressure and 5kbar hydrostatic uniform pressure. $Q(1/3\ 1/3\ 0)$ represents the soft mode point. (o) 5kbar, (■) 0 kbar.

D.VISSER *et al.*

Discussion

The magnetic ordering behaviour in the undistorted induced moment systems under hydrostatic pressure show the same behaviour as observed for the systems at ambient pressure. The magnetic dipolar force is the driving mechanism to form the incommensurate magnetic phases; the helical IC_1 and the sinusoidal IC_2 phase. In TlFeCl_3 the dipolar magnetic forces must have a reduced influence due to the distortion of the hexagonal ab plane. Incommensurate magnetic ordering may be induced too, by the different inter-plane superexchange interactions J' and J'' . Slight changes in these interactions will modify the magnetic structure as is observed for TlFeCl_3 .

The magnetic excitations in the induced moment systems will change only slightly when the structure is not distorted. Such a system (RbFeCl_3) will be described by modified D , J and J' parameter although changes in these parameters can change the intensities of magnetic excitations dramatically [5]. In the case that one observes a partially ordered magnetic phase followed by a transition to a fully ordered phase, the partially ordered phase will display for one of the chains a singlet ground state behaviour, while the other two chains are magnetically ordered. The number of sublattices will be reduced to two. A similar behaviour is expected as that observed in RbFeCl_3 [13]

The singlet ground state systems under hydrostatic pressure can also be described by modified D , J and J' parameters [14]. For CsFeCl_3 , the deformation of the FeCl_3 - octahedron has either been reduced towards an ideal octahedron, or the gap energy is strongly reduced and a similar behaviour, strong damping of the magnetic excitations, is present around the soft mode point [15,16]. Measurements under increased pressure $>5\text{kbar}$ will provide the information to verify the suggestions made.

References

- [1] D.Visser and A.Harrison. *J. de Phys. Coll.* 8, 49, 1255 (1989).
- [2] D.Visser, A.Harrison and C. Vettier. *Solid State Comm.* submitted.
- [3] P-A: Lindgard. *J.Phys.C8,L178* (1975); *Physica* 120B, 190 (1983).
- [4] P-A. Lindgard *Spinwaves and Magnetic Excitations I. Chapter 5 in Theory of Spin Excitations in Rare Earth systems.* Ed. A.S. Borovik, S. Romanov and S.K. Sinha. Elsevier North Holland (1989).
- [5] N. Suzuki. *J. Phys. Soc. Japan* 52, 1002, 1009, 3907(1983).
- [6] D. Visser and G.J McIntyre. *Acta. Cryst. B* submitted.
- [7] H. Shiba and N. Suzuki. *J. Phys. Soc. Japan* 51, 3488 (1982).
- [8] D. Visser, W.Knop and M.Steiner. *J. Phys. Cond. Matt.* submitted.
- [9] D. Visser, G.C. Verschoor and D.J.W. IJdo. *Acta Cryst. B* 36,28 (1980).
- [10] A. Harrison and D. Visser. *Phys. Lett. A* 137, 79 (1989); *J. Phys. Cond. Matt* 1, 733 (1989).
- [11] D. Visser and A. Harrison. *Phys. Lett.* submitted.
- [12] N. Suzuki and M. Shirai. *Physica* 136B, 346 (1986).
- [13] D. Visser, B. Dorner and A. Harrison. *J. Appl. Phys.* 69, 6232 (1991).
- [14] D. Visser, A.R.Monteith and D. Petitgrand. *J. Magn. Magn. Mat.* submitted; *Physica B* submitted.
- [15] B. Dorner, D. Visser and M. Steiner. *Z. Phys. B* 81, 75 (1990).
- [16] B Schmid. *Dr. Thesis. Regensburg* (1993).
- [17] D. Visser, A. Harrison, C. Vettier, B. Schmid and P-A. Lindgard. *J. Magn. Magn. Mat.* submitted.

Chapter 5.

Chiral ordering in the hexagonal XY-like triangular antiferromagnet

JOURNAL DE PHYSIQUE

Colloque C8, Supplément au n° 12, Tome 49, décembre 1988

THE EFFECT OF MAGNETIC AND NON-MAGNETIC DILUTION ON THE MAGNETIC ORDERING IN THE HEXAGONAL ANTIFERROMAGNET CsMnBr_3 D. Visser, A. Harrison and G. J. McIntyre¹*Inorganic Chemistry Laboratory, University of Oxford, South Parks Road, OX1 3QR Oxford, G.B.*

Abstract. – Elastic neutron scattering measurements on the hexagonal antiferromagnet CsMnBr_3 showed that T_N falls steeply with concentration x of the diamagnetic impurities (Mg^{2+}), becoming zero at $x = 0.14$; the critical exponent of the magnetisation, β , increased from 0.19(1) ($x = 0$) to 0.34(1) ($x = 0.09$). The reduction of T_N and increase in β on addition of induced-moment impurities (Fe^{2+}) is less pronounced.

Introduction

Recent theoretical [1-3] and experimental [5-7] work has revealed that antiferromagnetically coupled Heisenberg or XY -type moments on a triangular lattice show a new type of magnetic ordering. In addition to the three-sublattice 120° antiferromagnetic order, a staggered chirality order may be defined. The chirality of an individual triangular plaquette is defined as the sense of rotation of the moments around its edges. This is believed to create new universality classes, in which the critical exponent of the magnetisation, β , for stacks of such planes is 0.25 and 0.22 for the Heisenberg and XY cases respectively [3, 4]. Recent measurements on CsMnBr_3 and CsVX_3 ($X = \text{Cl}, \text{Br}$) [5, 7], which are pseudo one-dimensional XY antiferromagnets with interchain exchange pathways forming a triangular array in the ab plane, revealed a value of 0.22 ± 0.03 for β . In addition, being frustrated magnets these materials are susceptible to the formation of canted local states [8] on dilution with diamagnetic impurities. Near such impurities the balance of forces that produces the frustrated ground state may be upset and some of the frustration released by a rotation of neighbouring moments [9].

In this paper we describe the effect on the magnetic ordering processes of CsMnBr_3 of doping with diamagnetic (Mg^{2+}) and induced-moment impurities (Fe^{2+}) concerning the disruption of the triangular symmetry that leads to staggered chirality ordering, the relative reduction of T_N on doping both types of impurities and the nature of the diffuse magnetic scattering in the region of the magnetic Bragg peaks [10].

Experimental

Single crystals of $\text{CsMn}_{(1-x)}\text{Mg}_{(x)}\text{Br}_3$ ($x = 0.05, 0.09$) and $\text{CsMn}_{(1-x)}\text{Fe}_{(x)}\text{Br}_3$ ($x = 0.05, 0.11$) were

grown by the Bridgman technique using a Crystallox twin-zone furnace. The neutron scattering measurements were conducted at the Institut Laue-Langevin using the triple-axis instrument D10 in diffraction mode with the analyser set to zero-energy transfer, wavelength $\lambda = 2.36 \text{ \AA}$. The crystals were aligned with the [002] and [110] directions in the horizontal scattering plane. The scattering intensity was measured at the magnetic Bragg positions $Q(1/3, 1/3, 1)$ and $Q(2/3, 2/3, 1)$ from $T = 1.3 \text{ K}$ to 10 K , scanning along the [001] direction. The scattering profile was also measured from (001) to (111) above and below T_N to elucidate the nature of the magnetic correlation in the ab -plane.

Results and discussion

The scattering intensity centred at $(1/3, 1/3, 1)$ and $(2/3, 2/3, 1)$ was fitted to a sum of a Gaussian function and a linear background term. β was derived by fitting the area of this Gaussian, $I(T)$, to the expression

$$I(T) = A\epsilon^{2\beta} \quad (1)$$

where ϵ is the reduced temperature, $(T_N - T)/T_N$, and takes values from 0.25 to 0.005. The values of $T_N(x)/T_N(0)$ are plotted against x in figure 1, and compared with the predictions of the Hone model [10] for diamagnetic and magnetic impurities in a collection of Heisenberg chains coupled by a molecular field. The exchange constants for Mn-Mn, Mn-Fe and Fe-Fe, were taken from [11], and the size of the moment on Fe^{2+} assumed to be 1.0. As expected and supported by the Hone model, Fe^{2+} impurities, which retain exchange links within the chain are seen to reduce T_N less than Mg^{2+} impurities which sever the chains completely. The dependence of β on composition is given in table I. On doping with Mg^{2+} there is a change

¹Institut Laue-Langevin, 156X, 38042 Grenoble, France.

Present address: The Studsvik Neutron Research Laboratory, University of Uppsala, 61182 Nyköping, Sweden.

JOURNAL DE PHYSIQUE

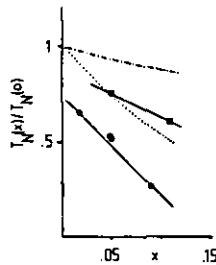


Fig. 1. - The dependence of $T_N(x)/T_N(0)$ on the nature and concentration x of the impurities in CsMnBr_3 . Circles and squares denote Mg^{2+} and Fe^{2+} impurities respectively and the solid lines drawn through these points merely provide a guide to the eye. The prediction of the Hone model for dilution with diamagnetic and reduced moment impurities are given by dotted and dot-dash lines respectively. The values of the solid circles are deduced from [12].

Table I. - The dependence of the reduced ordering temperature, $T_N(x)/T_N(0)$, and β on the type and concentration, x , of the impurity.

A^{2+}	x	$T_N(x)/T_N(0)$	β	reference
Mn		1	0.22	[5]
Mn		1	0.19	[13]
Mg	0.018	0.745		[12]
Mg	0.048	0.531		[12]
Mg	0.050	0.525 (5)	0.31 (1)	
Mg	0.090	0.262 (2)	0.34 (1)	
Fe	0.050	0.740 (5)	0.22 (1)	
Fe	0.110	0.600 (5)	0.24 (1)	

in β from a value close to that predicted for the new universality classes towards that of the 3-D Heisenberg (0.35) or XY (0.33) ones, as might be expected on disruption of the frustrated triangular ground state and the 3-D arrangement of the combined triangular ab -planes. The values of β for Fe^{2+} -doped CsMnBr_3 showed that this type of doping does not disrupt the chirality ordering or its 3-D character.

At temperatures below T_N we observe strong elastic diffuse magnetic scattering centred at the positions of the magnetic Bragg peaks. This scattering was seen in both the pure and the doped compounds and persisted to temperatures well in excess of T_N , being much weaker but still visible at $T = 3T_N$.

The lineshape of this diffuse component was clearly asymmetric along the (110) reciprocal lattice direction, and will be discussed in more detail elsewhere [13].

Acknowledgments

D. V. and A. H. wish to thank the UK SERC for financial support. A. H. is grateful to St. John's College, Oxford for further financial support.

- [1] Miyashita, S., and Shiba, H., *J. Phys. Soc. Jpn* **53** (1984) 1145.
- [2] Lee, D. H., Joannopoulos, J. D., Negele, J. W. and Landau, D. P., *Phys. Rev. B* **33** (1986) 450.
- [3] Kawamura, H. J., *J. Phys. Soc. Jpn* **54** (1985) 3320.
- [4] Kawamura, H. J., *J. Phys. Soc. Jpn* **55** (1986) 2095.
- [5] Mason, T. E., Collins, M. F. and Gaulin, B. D., *J. Phys. C* **20** (1987) L945.
- [6] Kadowaki, H., Ubukoshi, K., Hirakawa, K., Martinez, J. L. and Shirane, G., *J. Phys. Soc. Jpn* **56** (1987) 4027.
- [7] Visser, D. and McIntyre, G. J., *J. Phys. C* submitted.
- [8] Villain, J., *Z. Phys. B* **33** (1979) 31.
- [9] Harrison, A., *J. Phys. C* **20** (1987) 6287.
- [10] Hone, D., Montano, P. A., Tonegawa, T. and Imry, Y., *Phys. Rev. B* **12** (1975) 5141.
- [11] Gaulin, B. D., Collins, M. F. and Sosnowska, I., *Physica B* **136** (1986) 360.
- [12] Paul, O. M., Diplomarbeit ETH-Zurich (1986) unpublished.
- [13] Visser, D. and McIntyre, G. J., *Proc. ICNS '88*.

Ferroelectrics, 1994, Vol. 162, pp. 147–152
Reprints available directly from the publisher
Photocopying permitted by license only

© 1994 OPA (Overseas Publishers Association) Amsterdam B.V.
Published under license by Gordon and Breach Science Publishers SA
Printed in the United States of America

MAGNETIC ORDERING IN THE STACKED TRIANGULAR ANTIFERROMAGNET CsMnBr_3 IN THE PRESENCE OF AN ELECTRIC FIELD

D. VISSER and T. R. COLDWELL

*Loughborough University of Technology, Loughborough LE11 3TU,
United Kingdom*

and

G. J. McINTYRE

Institut Laue-Langevin, BP 156X, 38042 Grenoble Cedex 9, France

and

H. GRAF, L. WEISS and Th. ZEISKE

*BENSC, Hahn Meitner Institut, Glienecker Strasse 100, D1000 Berlin 39,
Germany*

and

M. L. PLUMER

*Département de Physique, Université de Sherbrooke, Sherbrooke, Québec,
Canada J1K 2R1*

(Received September 16, 1993; in final form October 21, 1993)

The magnetic ordering in the stacked triangular antiferromagnet CsMnBr_3 has been studied in an applied electric field. The value of the critical exponent β decreases from 0.245(5) ($E \approx 0$ V/cm) to 0.165(5) ($E = 1.5$ kV/cm). Our observations indicate the possible occurrence of a first order phase transition to a non-chiral, commensurate, linear phase in the presence of an applied electric field in the plane of the ordering vector.

Keywords: *Magneto-electric effect, critical exponent, triangular antiferromagnet.*

I. INTRODUCTION

In recent years a renewed theoretical interest has been shown in the magnetic ordering process of the frustrated triangular lattice. Theoretical predictions made by Kawamura¹ followed by experimental support^{2,3} suggest that the 120° type stacked triangular XY antiferromagnet may belong to a new universality class with critical exponents very different from those of the standard 3D classes. For example, the order parameter exponent β is found from Monte Carlo simulations to be 0.253(10),⁴ in contrast with values 0.33, 0.35 and 0.37 in the cases of Ising, XY

D. VISSER *et al.*

and Heisenberg universality, respectively.⁵ The possibility of novel critical behaviour is due to the presence of an extra degree of degeneracy in these frustrated spin systems, the chirality. In addition to the three sublattice 120° antiferromagnetic structure a staggered chirality order may be defined. The chirality of an individual plaquette is defined as the sense of rotation of the moments around the edges. This helicity degree of freedom gives rise to an Ising-like (Z₂) discrete degeneracy in addition to the XY(S₁) continuous degeneracy. The order parameter is in this case characterised by the symmetry $V = Z_2 \times S_1$. The need to introduce a new universality class has been challenged by Azarai *et al.*^{6,7} who suggest that such systems exhibit either a tricritical ($\beta = \frac{1}{2}$) or first order transition.

CsMnBr₃ crystallizes with the hexagonal perovskite structure. This class of quasi one-dimensional magnetic compounds shows 1D magnetic behaviour at higher temperatures. At low temperatures, the interchain interaction and the XY-anisotropy of the system become important.

The arrangement of the Mn²⁺ ions in the ab-plane forms a triangular array. Tripartite frustration due to the near neighbour antiferromagnetic bonds stabilizes a 120° magnetic structure in CsMnBr₃; $T_N = 8.35$ K and $\beta = 0.245$.^{2,3}

Symmetry arguments⁸ have shown that an electric field applied in the basal plane of a stacked triangular antiferromagnet can break the chirality order of the 120° type spin structure. This is induced by magneto-electric coupling which is the coupling between spin vector **S** and the electric-field (**E**) induced polarisation vector **P**. For the hexagonal lattice, symmetry arguments show that the magnetoelectric coupling term takes a form identical to that of the Dzyaloshinsky-Moriya (DM) exchange interaction and that an electric applied field in the hexagonal basal plane along the [110] direction would stabilize a slightly incommensurate magnetic ordering. It is known and has been demonstrated that the chirality of helically polarised magnetic structures in non-centrosymmetric crystals is determined by the sign of the D-M interaction. Single chiral domains in structures can be obtained by cooling the crystal in the presence of an electric field. An electric field of 2.5 kV/cm was sufficient to produce a single domain sample in ZnCr₂Se₄.⁹

In this paper we report the preliminary results of a study of the magnetic ordering in the triangular 120° type antiferromagnet CsMnBr₃ in the presence of an electric field applied (up to $E = 1.5$ kV/cm) in the basal plane. Changes in domain population were investigated by means of polarization analysis. Changes in the critical behaviour with applied electric field are investigated by determination of the exponent β .

II. EXPERIMENTAL

A large single crystal boule of CsMnBr₃ was grown by means of the Bridgman technique using a Brown-Barrington three zone single crystal furnace. Small diamond-shaped single crystal plates with a thickness of about 2 mm were cut from the boule. The cleavage planes contain the chemical [100] and [001] directions. These plates were mechanically reshaped into blocks with new parallel faces containing the $[-210]$ and $[001]$ directions. Very thin copper wires were attached to these silver-painted faces. In this way the electric field could be applied along [110]

CsMnBr₃ IN THE PRESENCE OF AN ELECTRIC FIELD

direction in reciprocal space. A crystal of dimensions $2.2 \times 2.2 \times 5$ mm prepared in this manner was mounted on a quartz rod inside an ILL Orange-type cryostat (Vacuum Associates). A 3 kV dc power supply was connected to the crystal via high tension cables fed into the cryostat along the sample stick. The sample space contained 4 Torr He exchange gas. This set up allowed an electric field of 1.5 V/cm to be applied to the crystal. Higher electric fields caused electrical discharges over the crystal.

The neutron scattering experiments were conducted at the Berlin Neutron Scattering Centre at the Hahn Meitner Institut, Berlin, using the triple axis instrument E1. This instrument can be operated in a two-axis mode for diffraction experiments or in the conventional three-axis mode for elastic or inelastic experiments. The optional use of Heusler (111) crystals (monochromator, analyser) allows also full polarisation analysis to be carried out.

The scans were made through the Bragg position $(1/3 \ 1/3 \ 1)$ in various applied electric fields from $T = 1.5$ K to 10 K in the two axis-mode. Before the sublattice magnetisation was measured in the presence of an electric field, the temperature was taken up to 30 K, the appropriated electric field was applied and the sample was thereafter slowly cooled (1 h) to 2 K. Some scans with and without an applied field were also made with polarisation analysis.

III. RESULTS

The integrated intensity of the magnetic Bragg peak was obtained by integrating the scattered profile after subtracting a linear background term. β was derived from the integrated intensity, $I(T)$, by fitting to the expression

$$I(T) = A\epsilon^{2\beta} \quad (1)$$

where ϵ is the reduced temperature, $(T_N - T)/T_N$, and takes the values from 0.25 to 0.005 with $T_N = 8.35$ K.

The sublattice magnetization was measured in zero field and an applied electric field along the $[110]$ direction. The log-log plots of $I(T)$ versus ϵ are given in Figure 1. The results for β are given in Table I.

The polarisation analysis of the Bragg scattering at $T = 2.55$ K near $Q = (1/3 \ 1/3 \ 1)$ shows that the spinflip $(+ -)$ and the non-spinflip $(+ +)$ scattering is more or less the same at $E = 0$ kV/cm and $E = 0.6$ kV/cm. Such behaviour is expected for a normal antiferromagnetic ordering.¹⁰ At $E = 1.4$ kV/cm we observe that both spinflip $(+ -)$ and non-spinflip scattering $(+ +)$ has increased slightly; about 5% suggesting some chiral ordering; Figure 2.

IV. DISCUSSION

The critical behaviour of the sublattice magnetisation and the polarisation analysis of the magnetic Bragg scattering shows indeed that a magneto-electric effect occurs in the triangular antiferromagnet CsMnBr₃ when an electric field is applied along the $[110]$ direction. The observed results are summarised in Figure 3. Our exper-

D. VISSER *et al.*

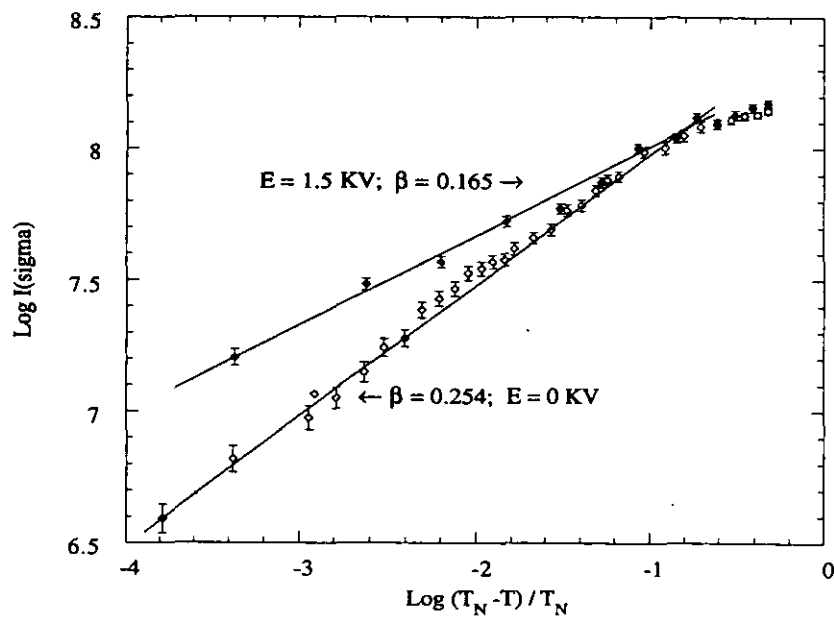


FIGURE 1 Log-Log plot of the sublattice magnetisation for $E = 0 \text{ kV/cm}$ and $E = 1.5 \text{ kV/cm}$.

TABLE I		
The value of the critical exponent β in an applied electric field		
$E \text{ (kV/cm)}$	β	Reference
0	0.19–0.22	2, 3
0	0.254 (5)	This work
1.1	0.193 (5)	This work
1.5	0.165 (5)	This work

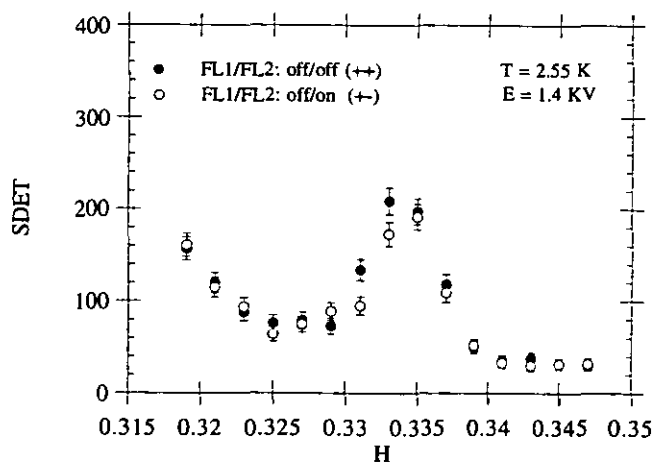


FIGURE 2 Polarization analysis of the magnetic Bragg reflection (1/3 1/3 1).

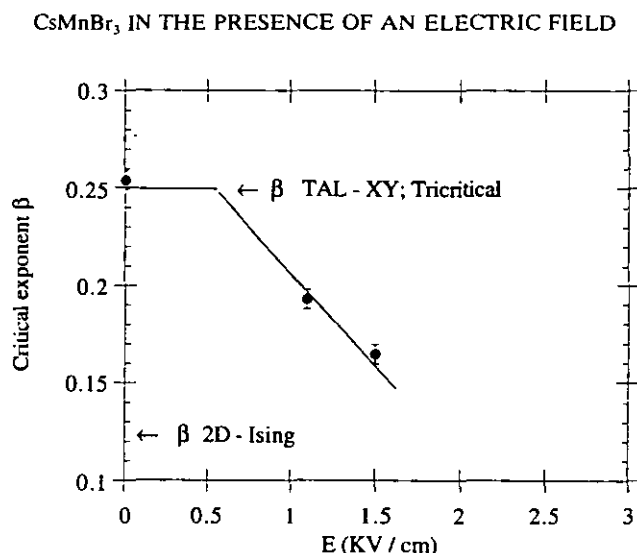


FIGURE 3 Schematic representation of the critical exponent β as function of applied electric field.

iments confirm that the critical exponent of the sublattice magnetisation β in a zero applied field has the value 0.254(5) as predicted for a stacked triangular lattice with chiral degeneracy. The application of the electric field should remove the chiral degeneracy by creating a mono-domain crystal of a single chirality (either right or left handed). This would result in normal XY universality. For such a system one would expect that $\beta = 0.35$. The experimental results show actually an opposite behaviour. It seems that the electric field couples into the crystal at a potential of approximately 0.6 kV/cm. Increasing the E field results in a gradual decrease of β . Unfortunately we were not able to apply electric fields higher than 1.5 kV/cm. So it is not known at which value of E β will level out. The measured values of β : 0.195 and 0.165, are *very unusual*. Only the pure 2-D Ising system has a lower value; $\beta = 0.125$. It is of interest to note that a low value of $\beta = 0.22$ has recently been observed in the stacked triangular Ising antiferromagnet CsCoBr₃¹¹; the magnetic structure of CsMnBr₃ in the presence of an electric field may also be Ising-like.⁸ A transition to such a linearly polarized (Ising-like) phase also occurs in CsMnBr₃ in an applied magnetic field,¹² where an experimental value of $\beta = 0.29$ has been reported.¹³ All of these Ising-like transitions in the frustrated antiferromagnets are expected to be in the XY universality class.¹⁴⁻¹⁶ Low values of β may be indicative of a very weak first order transition since the sublattice magnetization rises more steeply below the transition for decreasing β . Such an interpretation¹⁷ has been made regarding Monte Carlo results for a 2D XY system which exhibited anomalously small values of β in the presence of an applied magnetic field.¹⁸ Mean field theory predicts also the possibility of a first order transition to a non-chiral, commensurate, linear phase (i.e., Ising-like) in the presence of an electric field (see Figure 2b in Reference 8).

It is known that the sense of the chirality in helimagnets can be controlled in the presence of an electric field as has been clearly demonstrated for ZnCr₂Se₄⁹ and also that the chirality of helically polarized magnetic structures in crystals that do not contain a center of inversion symmetry will be determined by the sign of the Dzyaloshinsky-Moriya exchange interaction.^{19,20} The cubic spinel ZnCr₂Se₄

D. VISSER *et al.*

undergoes a structural phase transition, at $T_N \sim 20$ K, to a slightly distorted tetragonal phase.²¹ The loss of the center of symmetry will introduce the a Dzyaloshinsky-Moriya exchange interaction which stabilizes a spiral spin structure.

The symmetry arguments presented by Plumer *et al.*⁸ suggest that a similar behaviour may be seen in CsMnBr₃. However, the structure of CsMnBr₃ does differ essentially from that of ZnCr₂Se₄. The crystal structure of CsMnBr₃ is assumed to be centrosymmetric, SG P6₃/mmc, although recent experiments²² on a 0.5 cm³ crystal showed that the (0 0 *l*) reflections with *l* = odd are present at low-temperature and disappear at $T_{ph} \sim 70$ K indicating that the space group at low temperature is a subgroup of SG P6₃/mmc. The magnetic structure is commensurate with the $\mathbf{k} = (1/3 \ 1/3 \ 1)$. Our present data in the presence of an electric field did not indicate the possible formation of an incommensurate magnetic structure⁸ with $\mathbf{k} = (1/3 + \delta \ 1/3 + \delta \ 1)$. A direct observation of a left handed or right handed screw is in this case not possible. However, the formation of a single chirality domain can be observed by neutron polarisation analysis.²³ These observations are consistent with mean field predictions.⁸ Further studies in higher electric fields and a full polarisation analysis will be carried out in the near future to clarify the nature of the induced phase transition and other experimental tests of the possibility that $E = 0$ is a multicritical point are planned.

ACKNOWLEDGEMENTS

D. V., T. R. C. and G. J. McI. would like to thank the UK SERC and the HMI for financial support. This research has been supported by a grant of the European Community Human Capital and Mobility Programme.

REFERENCES

1. H. Kawamura, *J. Appl. Phys.*, **63**, 3086 (1988).
2. T. E. Mason, M. F. Collins and B. D. Gaulin, *J. Phys.*, **C20**, L945 (1987).
3. D. Visser, A. Harrison and G. J. McIntyre, *J. Phys. (Paris)*, **C8**, 1255 (1988).
4. H. Kawamura, *J. Phys. Soc. Jpn.*, **61**, 1299 (1992).
5. J. C. Le Guillou and J. Zinn Justin, *J. Phys. Lett. (Paris)*, **46**, L137 (1985).
6. P. Azaria, B. Delamotte and T. Jolicoeur, *Phys. Rev. Lett.*, **64**, 3175 (1990).
7. P. Azaria, B. Delamotte, F. Delduc and T. Jolicoeur, *Nucl. Phys. B*, to be published.
8. M. L. Plumer, H. Kawamura and A. Caillé, *Phys. Rev.*, **B43**, 13786 (1991).
9. K. Siratori, J. Akimitsu, E. Kita and M. Nishiki, *J. Phys. Soc. Jpn.*, **48**, 1111 (1980).
10. S. W. Lovesey, "Theory of Thermal Neutron Scattering from Condensed Matter," Oxford: Clarendon Press (1984).
11. A. Farkas, B. D. Gaulin, Z. Tun and B. Briat, *J. Appl. Phys.*, **69**, 6167 (1991).
12. M. L. Plumer and A. Caillé, *Phys. Rev.*, **B41**, 2543 (1990).
13. B. D. Gaulin *et al.*, *Phys. Rev. Lett.*, **62**, 1380 (1989).
14. D. Blankenstein *et al.*, *Phys. Rev.*, **B29**, 5250 (1984).
15. H. Kawamura, M. L. Plumer and A. Caillé, *Phys. Rev.*, **B41**, 4416 (1990).
16. M. L. Plumer *et al.*, *Phys. Rev.*, **B47**, 14312 (1993).
17. P. Azaria, private communication.
18. P. Azaria and H. T. Diep, *Phys. Rev.*, **B39**, 745 (1989).
19. O. Nakanishi *et al.*, *Solid State Comm.*, **35**, 995 (1980).
20. P. Bak and H. M. Jensen, *J. Phys.*, **C13**, L881 (1990).
21. R. Kleinberger and R. de Kouchkovsky, *C. R. Acad. Sc. Paris*, **B262**, 628 (1966).
22. D. Visser and G. J. McIntyre, work in progress.
23. P. J. Brown *et al.*, *J. Phys.: Condens. Matter*, **2**, 9409 (1990).

Chapter 6.

Magnetic ordering phenomena in quasi two-dimensional systems with XY symmetry

J. Phys.: Condens. Matter 5 (1993) 7871–7892. Printed in the UK

Neutron scattering investigation of the static critical properties of Rb_2CrCl_4

J Als-Nielsen^{†¶}, S T Bramwell[‡], M T Hutchings[§], G J McIntyre[‡] and D Visser^{||}

[†] Riso National Laboratory, DK-4000 Roskilde, Denmark

[‡] Institut Max von Laue–Paul Langevin, 156X, 38042 Grenoble Cédex, France

[§] Non-Destructive Testing Department, AEA Industrial Technology, Harwell Laboratory, Didcot OX11 0RA, UK

^{||} Department of Physics, Loughborough University of Technology, Leicestershire LE11 3TU, UK

Received 5 January 1993, in final form 7 July 1993

Abstract. We have investigated the static zero-field critical properties of the ionic ferromagnet Rb_2CrCl_4 , using neutron scattering, under conditions such that the quasi-static approximation is valid. A general consideration of the spin Hamiltonian of Rb_2CrCl_4 , with $S = 2$, shows that it approximates the two-dimensional (2D) XY model, with additional weak perturbations. Rb_2CrCl_4 orders three dimensionally at $T_C = 52.3$ K, and very close to T_C there is a regime of three-dimensional critical behaviour. However, both below and above T_C there is a crossover to regimes of two-dimensional critical fluctuations. In these regimes, there is excellent agreement between experiment and theoretical predictions for a finite-sized 2D XY model, suggesting that Rb_2CrCl_4 is an ideal realization of this system.

1. Introduction

In this paper we report the results of an investigation of the static zero-field critical properties of dirubidium chromous chloride (Rb_2CrCl_4), using neutron scattering techniques. Rb_2CrCl_4 is a rare example of an insulating compound which orders ferromagnetically at $T_C \simeq 52$ K. In terms of its critical properties, the results presented here show that it can be regarded as an experimental realization of the two-dimensional (2D) XY model.

The ferromagnetism of Rb_2CrCl_4 is strongly 2D in character on account of its crystal structure, in space group $Cmca$ [1]. This is a co-operative Jahn–Teller distorted superstructure of that of K_2NiF_4 , itself with the space group $I4/mmm$, in which the magnetic $\text{Cr}^{2+} 3d^4$ ions are arranged in planar square arrays with very weak coupling to adjacent layers (figure 1(a)). The ferromagnetic sign of the dominant superexchange between the nearest-neighbour Cr^{2+} ions arises from the nature of their coupling via the chloride ions. These Cl^- ions are moved slightly off the mid- Cr^{2+} positions, so that the D_{2h} environment of the Cr^{2+} ions approximates to an elongated octahedron of Cl^- ions with the long axis alternating by 90° from one Cr^{2+} ion to its neighbour. With this axis as the z axis, the three t_{2g} orbitals and the $e_g (3z^2 - r^2)$ orbitals of Cr^{2+} are occupied by one electron each, and the $e_g (x^2 - y^2)$ orbital is empty. The orbital moment of the Cr^{2+} ion is quenched, but the D_{2h} crystal field with spin–orbit coupling gives rise to two single-ion anisotropy

[¶] Present address: European Synchrotron Radiation Facility, 156X-38042 Grenoble, France.

J Als-Nielsen et al

terms which, together with the isotropic exchange interaction, act in the spin Hamiltonian on the $S = 2$ spin states. The larger planar anisotropy term confines the spins to lie in the planes [2], while the weaker uniaxial term favours the alignment of alternate spins at 90° . The resultant of the exchange field (favouring parallel alignment) and the in-plane uniaxial anisotropy term is a slight canting of the ordered spins below T_C by approximately $\pm 1^\circ$ from the $\langle 110 \rangle$ direction [1, 3]. We shall, throughout this paper, refer directions to the reciprocal lattice of the related K_2NiF_4 unit cell, which has lattice constants $a_0 = 5.90 \text{ \AA}$ and $c_0 = 15.75 \text{ \AA}$ at 50 K.

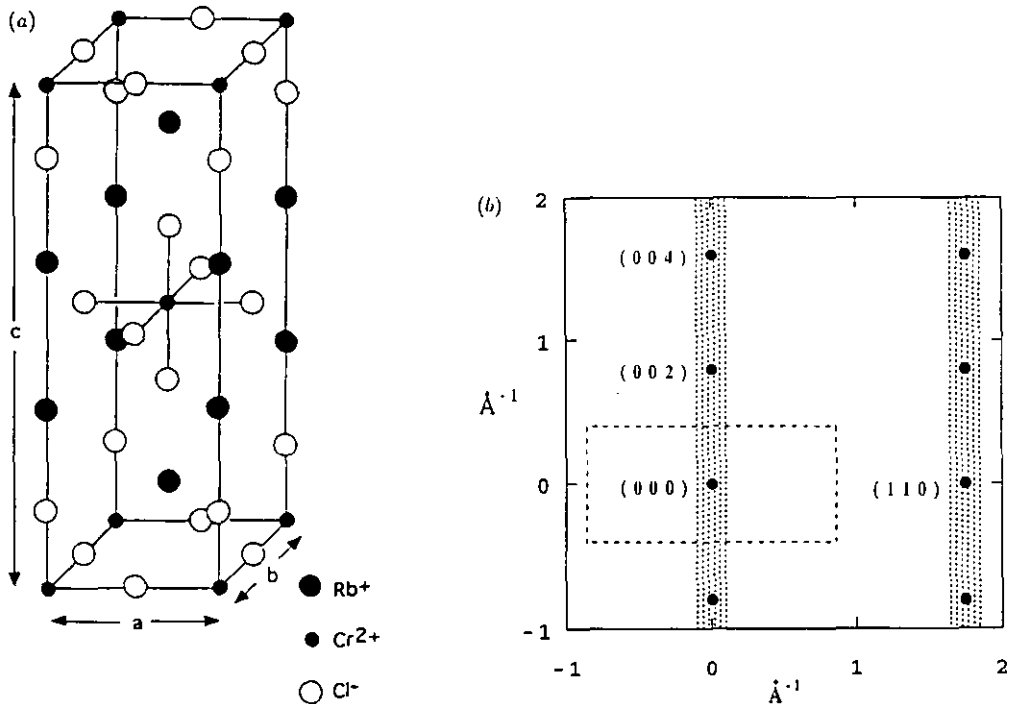


Figure 1. (a) Approximate crystal structure of Rb_2CrCl_4 , represented in the $14/mmm$ space group. The true crystal structure is a Jahn-Teller distorted superstructure of that shown, in which the bridging halogen atoms move slightly off the mid- Cr^{2+} positions. (b) Section in the $(1, -1, 0)$ plane of the reciprocal lattice of Rb_2CrCl_4 ($14/mmm$) corresponding to the scattering plane of the present experiment: ●, reciprocal-lattice points; ----, boundary of the first Brillouin zone; the shaded areas indicate the rods of critical scattering.

The consequence of the presence of several terms in the spin Hamiltonian of differing magnitudes is to give rise to a sequence of crossover behaviour in the critical properties of Rb_2CrCl_4 , between different 'universality classes'. According to the universality hypothesis (see, e.g., [4]), in magnets with short-range interactions, the critical behaviour depends upon only two parameters: the lattice dimensionality D and the spin dimensionality d . In Rb_2CrCl_4 , the major interaction is that of the nearest-neighbour Heisenberg exchange, which cannot alone give long-range order in two dimensions in an infinite system [5], and the next largest is the single-ion anisotropy which confines the spins to the plane. So first Heisenberg ($D = 2$; $d = 3$) and then XY -like ($D = 2$; $d = 2$) behaviour might be expected to dominate as T_C is approached. However, the uniaxial term and small interplanar exchange will become important very close to T_C .

Static critical properties of Rb_2CrCl_4

Of particular interest is the possible 2D XY -like behaviour of Rb_2CrCl_4 . The 2D Heisenberg model is known to be particularly sensitive to planar anisotropy [6], and so in the absence of other perturbations one would expect XY critical behaviour of the 'Kosterlitz-Thouless' (KT) type, with no long-range order, but rather a phase transition involving the unbinding of spin vortices [7,8]. In fact the small in-plane anisotropy and interplanar coupling cause a phase transition to long-range order, but some of the properties of the KT transition appear to survive. Cornelius *et al* [9] analysed the bulk magnetization of Rb_2CrCl_4 according to the predictions of unmodified KT theory and found good agreement. Recently it has been argued [10] that real compounds approximating 2D behaviour with planar anisotropy, of which Rb_2CrCl_4 is probably the best example, may be considered to be equivalent to ideal 2D XY systems of finite size. Well above T_C , these should approximate pure 2D XY behaviour but, below T_C , finite-size effects should become dominant. The finite 2D XY system is predicted [10] to have a spontaneous magnetization below T_C , and a distinct universal critical behaviour characterized by a magnetization exponent $\beta = 0.23$. These theoretical predictions are briefly summarized in section 3. One of the results of the present experimental work will be confirmation of these predictions.

In the next two sections the spin Hamiltonian for Rb_2CrCl_4 will be given in detail, and the expected critical behaviour of the 2D XY model will be discussed. In section 4, details of the neutron scattering experiments and methods of data analysis will be given. The results are presented in section 5 and discussed in section 6. Conclusions are drawn in section 7.

2. Hamiltonian

The spin Hamiltonian for Rb_2CrCl_4 has been discussed by Hutchings *et al* [3] and Harrop [11] (see also Elliott *et al* [12]). In writing the Hamiltonian the true orthorhombic symmetry of the structure may be neglected, since each layer itself has tetragonal symmetry and the coupling between the layers is very weak. We can then write

$$\hat{H} = \hat{H}_{\text{ex}} + \hat{H}_{\text{anis}} + \hat{H}_{\text{dip}} \quad (1)$$

where \hat{H}_{ex} is the exchange term, \hat{H}_{anis} is a single-ion anisotropy term and \hat{H}_{dip} is the dipolar interaction. The dipolar term is relatively small because of the open structure and symmetry of the sites. The exchange term is given by

$$\hat{H}_{\text{ex}} = -J \sum_{ij}^{\text{NN}} \mathbf{S}_{i1} \cdot \mathbf{S}_{j2} - J' \sum_{i'j'}^{\text{3rd NN}} \mathbf{S}_{i'1} \cdot \mathbf{S}_{j'1} \quad (2)$$

where J is the nearest-neighbour (NN) Heisenberg exchange interaction between NN $S = 2$ spins in the (0, 0, 1) plane, and J' is the exchange constant between the third-NN spins, which lie in adjacent planes. The summations are taken over all spins i, j in the two sublattices 1, 2. Hutchings *et al* [3, 13] found $J/k_B = 7.56 \pm 0.19$ K, $J'/k_B = 0.0018 \pm 0.0004$ K, by fitting to the spin-wave energy dispersion at 20 K.

Defining the axes a, b and z , along the [1, 0, 0], [0, 1, 0] and [0, 0, 1] axes of the K_2NiF_4 cell, one has for the single-ion anisotropy

$$\hat{H}_{\text{anis}} = -\tilde{P} \sum_i (S_{i1a}^2 + S_{i2b}^2) + \tilde{D} \sum_i (S_{i1z}^2 + S_{i2z}^2) \quad (3)$$

J Als-Nielsen et al

where \tilde{D} gives the planar anisotropy and \tilde{P} the uniaxial term within the plane. Hutchings *et al* [3] found that $\tilde{D}/k_B = -0.41 \pm 0.17$ K and $\tilde{P}/k_B = 3.14 \pm 0.18$ K. If one neglects the canting of the spins of about 1.5° , one obtains the simpler expression

$$\hat{H}_{\text{anis}} = -P \sum_i S_{ix}^2 + D \sum_i S_{iz}^2 \quad (4)$$

where x now lies along the mean spin direction (110). In this case, $D/k_B = 1.06 \pm 0.15$ K and $P/k_B = 0.123 \pm 0.014$ K [3]. It should be noted that the difference between \tilde{D} and D arises simply from the definition of the uniaxial terms. This may be seen by considering the more conventional form

$$\hat{H}_{\text{anis}} = -P' \sum_i (S_{ix}^2 - S_{iy}^2) + D' \sum_i S_{iz}^2 \quad (5)$$

where both terms now transform in the same way as combinations of spherical harmonics. By adding a constant term $\frac{1}{2}P(S_{ix}^2 + S_{iy}^2 + S_{iz}^2)$ to bring (4) into the form (5) it is seen that $D' = D + \frac{1}{2}P$ and $P' = \frac{1}{2}P$. Referring to (5), the term D' confines the spins to the x - y plane, and P' is a weak anisotropy within the plane. It is found that $D'/k_B = 1.12$ K, and $P'/k_B = 0.062$ K.

The more complete Hamiltonian (3) may be transformed in a similar way, by introducing the terms \tilde{P}' and \tilde{D}' . In this case, it is found that $\tilde{D}'/k_B = 1.15$ K, and $\tilde{P}'/k_B = 1.57$ K. The uniaxial terms \tilde{P}' and P' differ because they are referred to axes at 45° .

The staggered twofold anisotropy of Rb_2CrCl_4 approximates to an effective fourfold in-plane anisotropy field in the ordered phase of approximate magnitude $h_4 = P'S = 0.12$ K [11]. Thus Rb_2CrCl_4 may be regarded as a two-dimensional Heisenberg magnet with dominant planar anisotropy (about $0.15J$) and weaker fourfold anisotropy (about $0.015J$) and interlayer coupling (about $2.4 \times 10^{-4}J$).

3. 2D XY model

The 2D XY model cannot sustain long-range order in the thermodynamic limit, as was rigorously proved by Mermin and Wagner [5]. However, as originally shown by KT [7] and Berezinskii [8], the model does exhibit a phase transition to a low-temperature phase of infinite correlation length but no spontaneous order. This phase is characterized by a spin correlation exponent η defined such that, below the transition temperature T_{KT} ,

$$\langle S_0 \cdot S_r \rangle \sim r^{-\eta} \quad (6)$$

where the angular brackets represent the thermal average of the correlation between spins S separated by a distance r . The exponent η was predicted to increase with increasing temperature, reaching the universal value of 0.25 at T_{KT} [14].

In compounds approximating to 2D XY magnets, one would expect to observe pure model behaviour only in the paramagnetic regime above T_C , when the correlation length is sufficiently short that minor terms in the Hamiltonian are irrelevant. In this regime the 2D XY model has spin correlations which decay exponentially with a characteristic correlation length ξ (which we express in units of the lattice constant). Using renormalization group (RG) theory, Kosterlitz [14] predicted that the correlation length ξ diverges according to

$$\xi \simeq \exp[\pi/\sqrt{c(T - T_{\text{KT}})}] \quad (7)$$

Static critical properties of Rb_2CrCl_4

where $c \simeq 2.1$ is a constant. Note that π/\sqrt{c} has often been incorrectly written as approximately 1.5, following a trivial error in the original work; the correct value is approximately 2.2. The temperature in equation (7) is measured in units of the exchange constant. In terms of our present definition of J , which involves summation over all spins, the temperature is measured in units of $2JS^2$. In these units $T_{\text{KT}} = 1.35$ is the transition temperature of the so-called Villain [16] model, the particular approximation to the 2D XY model studied by Kosterlitz [14] and José *et al* [15]. In this approximation, the original cosine interaction between neighbouring spins is replaced by the quadratic term, but the periodicity of the cosine interaction is maintained in the partition function. Physically, this corresponds to a model containing only harmonic spin waves and vortices. The neglect of anharmonic terms is believed not to affect the critical behaviour, other than to renormalize T_{KT} . The value of $T_{\text{KT}} = 1.35$ for the Villain model, and the original mean-field estimate of KT [7] of about $\frac{1}{2}\pi (= 1.57)$ are both considerably higher than T_{KT} for the 2D XY model, of which the most accurate Monte Carlo estimate obtained by Gupta *et al* [17] is 0.898. In units of the exchange constant of Rb_2CrCl_4 , these three estimates correspond to 82 K, 95 K and 55 K, respectively.

Gupta *et al* [17] determined the correlation length ξ of the 2D XY model from their numerical simulation and found excellent agreement with equation (7) over a wide temperature range above T_{KT} . However, because the transition temperature T_{KT} is in general a non-universal quantity it is more useful to rewrite equation (7) in terms of a dimensionless reduced temperature as follows:

$$\xi \simeq \exp[b/\sqrt{(T - T_{\text{KT}})/T_{\text{KT}}}] \quad (8)$$

where T_{KT} represents the actual KT transition temperature of a particular system. Equation (8) has the advantage that the amplitude b is dimensionless, which is not true of the constant c . The amplitude b , as defined above, is only weakly system dependent [18]. According to the corrected estimate of Kosterlitz, $b = \pi/\sqrt{cT_{\text{KT}}} \simeq 1.9$ and from the parameter b_{ξ} of Gupta *et al* [17] we find that $b \simeq 1.8$. These estimates are probably equal to within the accuracy to which b can be calculated.

In general in layered magnets the interlayer exchange induces both three-dimensional (3D) ordering and 3D critical behaviour. Below T_{C} , the correlation length rapidly decreases to a value ξ_{2D} where the interlayer exchange is irrelevant and 2D behaviour is again obtained. This crossover occurs at a temperature very close to T_{C} , and at lower temperatures the correlation length remains approximately constant. In this region the layered magnet may be considered to be equivalent to a 2D system of effective finite size L_{eff} given by

$$L_{\text{eff}} \simeq \xi_{\text{2D}} \simeq \sqrt{J/J'}. \quad (9)$$

In the case of the XY model, a finite-sized system can sustain a strong spontaneous magnetization, even though the infinite system cannot [19].

We now briefly describe the argument of Bramwell and Holdsworth [10], who considered a finite system of L^2 spins. The magnetization in the 2D regime is calculated through a spin-wave analysis, in which the effective spin-wave stiffness K_{eff} is renormalized by the presence of vortices:

$$M(T)/M(0) \simeq (1/L\sqrt{2})^{1/4\pi K_{\text{eff}}}. \quad (10)$$

The finite size is taken into account by using the system size L as the rescaling parameter in the renormalization group equations of José *et al* [15]. In the infinite system, at T_{KT} , K_{eff}

J Als-Nielsen et al

takes the universal value $2/\pi$ and as the temperature is increased jumps discontinuously to zero [20]. In the finite system the universal jump is rounded out, and K_{eff} decreases smoothly, reaching the value $2/\pi$ at a slightly higher temperature T^* :

$$(T^* - T_{\text{KT}})/T_{\text{KT}} = b^2/4(\ln L)^2. \quad (11)$$

This temperature is equivalent to T_{KT} in the infinite system, with the universal exponents $\eta = 1/2\pi K_{\text{eff}} = 0.25$, $\delta = 15$, and the magnetization (10) given by

$$M(T^*)/M(0) \simeq (1/L\sqrt{2})^{1/8}. \quad (12)$$

In general, T^* occurs quite far from the temperature at which the magnetization becomes close to zero. This temperature, T_C , may be defined as the temperature where the correlation length ξ , given by the Kosterlitz expression (7), becomes equal to the system size L . It is found that

$$(T_C - T_{\text{KT}})/T_{\text{KT}} = b^2/(\ln L)^2. \quad (13)$$

A critical exponent β may be defined with respect to T_C as follows:

$$\beta(L, T) = [\partial \{\ln[M(L, T)]\} / \partial \{\ln[T_C(L) - T]\}]_L \quad (14)$$

which gives a remarkable universal result at T^* :

$$\beta(L, T^*) = 3\pi^2/128 = 0.231 \dots \quad (15)$$

This power-law behaviour of the magnetization directly reflects the absence of the universal jump and the smooth decrease in K_{eff} in the finite system. In the thermodynamic limit, i.e. the limit $L \rightarrow \infty$, the behaviour passes continuously to that of KT theory. The magnetization then disappears as its amplitude becomes zero, through equation (10), but the result (15) remains valid until the limit.

The behaviour of layered XY magnets is obtained by substituting L by L_{eff} in the above equations. A wide variety of layered XY magnets do show $\beta = 0.23$ in the subcritical region, as observed for Rb_2CrCl_4 (e.g. K_2CuF_4 [21] and $\text{Ba}(\text{NiPO}_4)_2$ [22]). In these compounds, β is defined relative to the 3D ordering temperature T_{3D} rather than relative to the temperature T_C as defined above. This is understandable [10], since T_C and T_{3D} are both located in the temperature range where

$$\xi(2D XY) \sim O(\sqrt{J/J'}). \quad (16)$$

The rapid divergence of the 2D XY correlation length $\xi(2D XY)$ ensures that this temperature range is very narrow, and so $T_C \simeq T_{3D}$. However, the fact that T_C and T_{3D} almost exactly coincide is perhaps surprising. We return to a discussion of this point in section 6, and in the meantime use ' T_C ' to denote *both* the effective critical temperature defined in equation (13), and the 3D ordering temperature T_{3D} .

Static critical properties of Rb_2CrCl_4

4. Experimental procedure

We have utilized the quasi-static approximation to magnetic neutron scattering, which is valid for sufficiently high incident neutron energies, or for certain scattering geometries [23,24]. Defining the scattering vector $\mathbf{Q} = \mathbf{k}_i - \mathbf{k}_f$ where \mathbf{k}_i and \mathbf{k}_f are the initial and final neutron wavevectors, the magnetic scattering function $S(\mathbf{Q})$ comprises both the Bragg scattering, which is proportional to the square of the spontaneous magnetization M , and the diffuse scattering, which is proportional to the product of the wavevector-dependent susceptibility $\chi(\mathbf{q})$ and the temperature T . Here \mathbf{q} is defined as $\mathbf{q} = \mathbf{Q} - \boldsymbol{\tau}$, where $\boldsymbol{\tau}$ is the reciprocal-lattice vector of the magnetic structure. In general, scattering arises only from spin components perpendicular to the scattering vector \mathbf{Q} and is weighted by the magnetic form factor. However, the latter varies slowly with \mathbf{Q} and can often be neglected. The observed magnetic scattering as a function of \mathbf{Q} is a convolution of $S(\mathbf{Q})$ with the instrumental resolution function. It has been found experimentally that $\chi(\mathbf{q})$ usually has a Lorentzian profile:

$$\chi(\mathbf{q}) \simeq \chi(0)/[1 + (\mathbf{q}/\kappa)^2] \quad (17)$$

where κ , the Lorentzian half-width at half-maximum, is equal to the inverse correlation length in the Ornstein-Zernike mean-field model [25].

The scattering from Rb_2CrCl_4 exhibits behaviour typical of quasi-2D magnets (see, e.g., Birgeneau *et al* [26]). The evolution of magnetic Bragg peaks reflects 3D ordering below T_C . The diffuse scattering on the other hand reflects the predominant 2D fluctuations, occurring as rods of intensity running parallel to the c direction in reciprocal space, intersecting the reciprocal-lattice points (figure 1(b)). Near to T_C , these rods have a maximum intensity at each Bragg point because of the effect of 3D exchange coupling. The evolution of the critical scattering is shown in figure 2. The intensity profile is approximately given by (17), with \mathbf{q} in this case defined relative to a point on the $[0, 0, \zeta]$ rod (i.e. $\boldsymbol{\tau} = (0, 0, \zeta)$).

We report the results, some of which have already been referred to in previous publications [27], of two experiments on the similar samples, grown by Dr P J Walker at the Clarendon Laboratory, Oxford, using the Czochralski technique [28]. The first was performed in 1977 using the TAS6 spectrometer at Risø, and the second was performed in 1986 on the D10 spectrometer at the Institut Laue-Langevin (ILL), Grenoble. The experiments involved different instruments, personnel and methods of data analysis, and so a comparison of the results provides an unbiased check on systematic errors. The sample examined at Risø was roughly spherical in shape with a diameter of about 8 mm, and that used at the ILL was a roughly ellipsoidal single crystal of approximate dimensions 15 mm \times 8 mm \times 7 mm. In both experiments the sample was oriented with $[1, -1, 0]$ vertical, and so $[1, 1, 0]$ and $[0, 0, 1]$ lay in the scattering plane. The intensity of the $(0, 0, 4)$ Bragg reflection, which has a particularly weak nuclear component, and the $[0, 0, \zeta]$ diffuse rod were measured as a function of temperature and wavevector.

The TAS6 spectrometer at Risø was used in a two-axis mode with 30' horizontal collimation before the pyrolytic graphite $(0, 0, 2)$ plane monochromator; 36' horizontal and 27' vertical collimation before the sample, and 28' horizontal and 22' vertical collimation before the ^3He detector. The neutrons of incident wavelength 2.45 Å passed through a pyrolytic graphite filter placed before the sample, to remove higher orders. The sample was mounted in a helium-filled aluminium can inside a Cryogenics Associates CT14 cryostat, and the temperature was measured using a platinum resistance thermometer. The resolution function for elastic scattering was carefully measured using the $(0, 0, 2)$ and $(0, 0, 4)$ Bragg

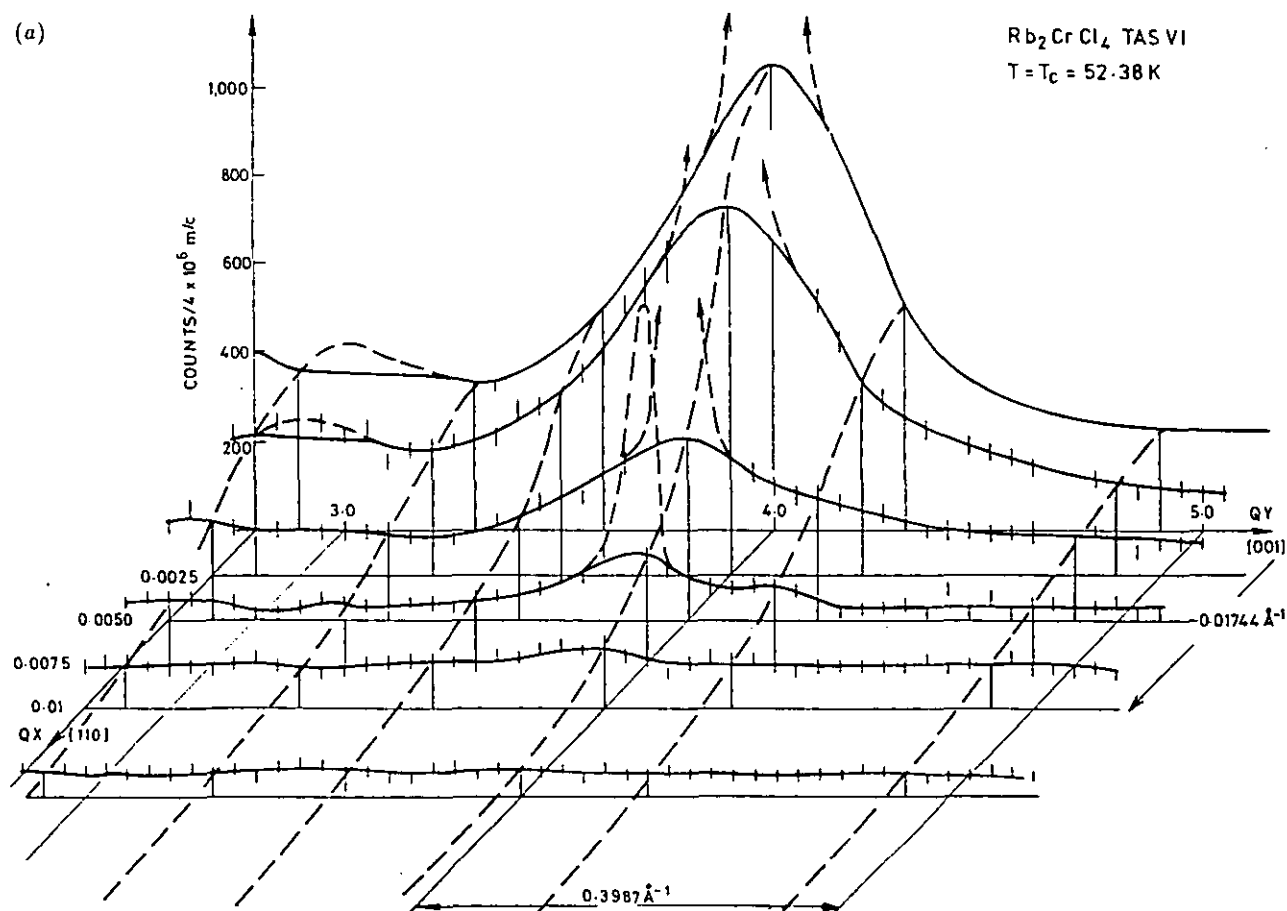
J Als-Nielsen et al

Figure 2. (a) Diffuse scattering of Rb_2CrCl_4 measured using the TAS6 spectrometer, near to the $(0, 0, 4)$ reciprocal-lattice point at $T = 52.28 \text{ K}$: —, guide to the eye; ----, $(0, 0, 4)$ Bragg reflection. The modulation of the critical scattering due to 3D effects is seen to commence below about 55 K .

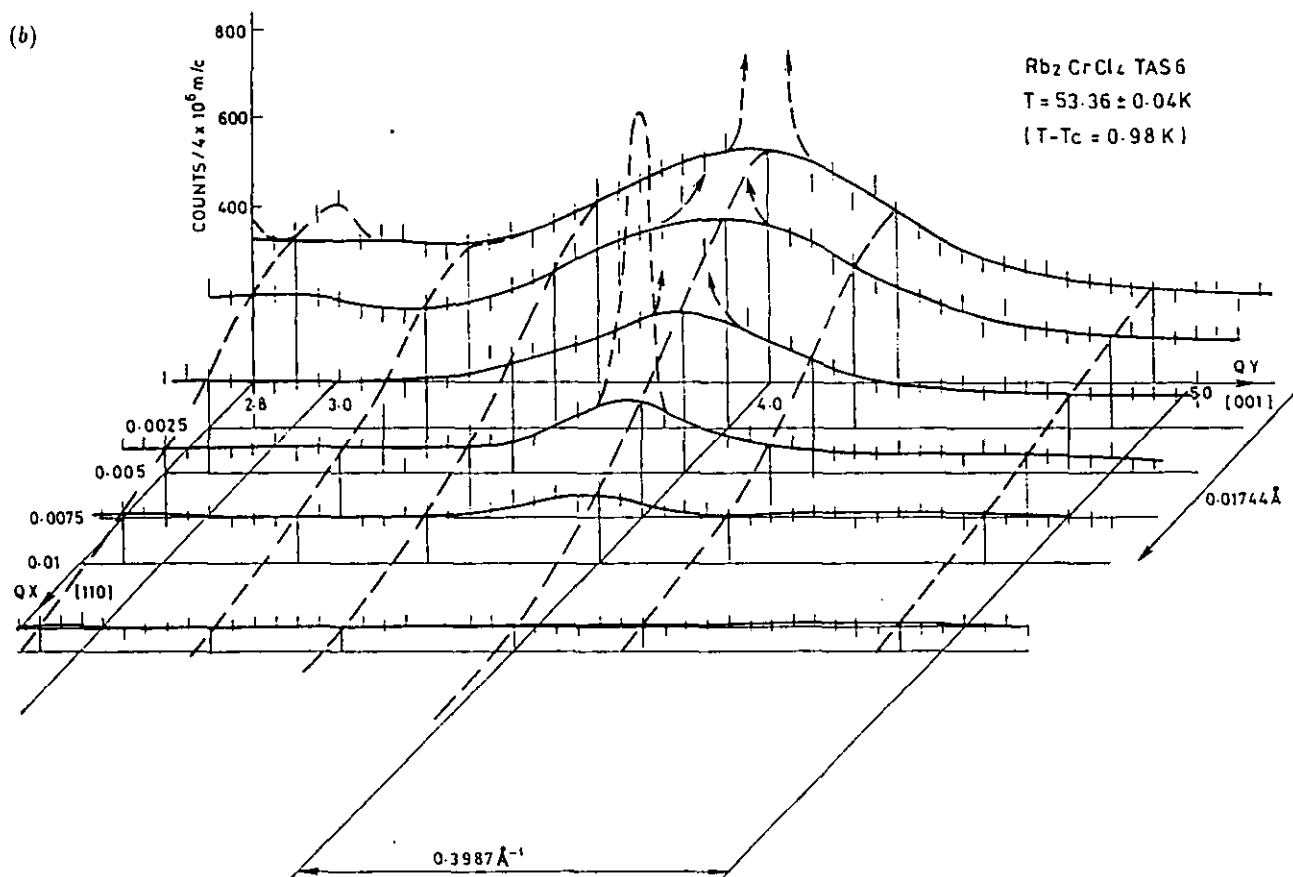
Static critical properties of Rb_2CrCl_4 

Figure 2. (b) Diffuse scattering of Rb_2CrCl_4 measured using the TAS6 spectrometer, near to the $(0, 0, 4)$ reciprocal-lattice point at $T = 53.36 \text{ K}$: —, guide to the eye; ----, $(0, 0, 4)$ Bragg reflection. The modulation of the critical scattering due to 3D effects is seen to commence below about 55 K.

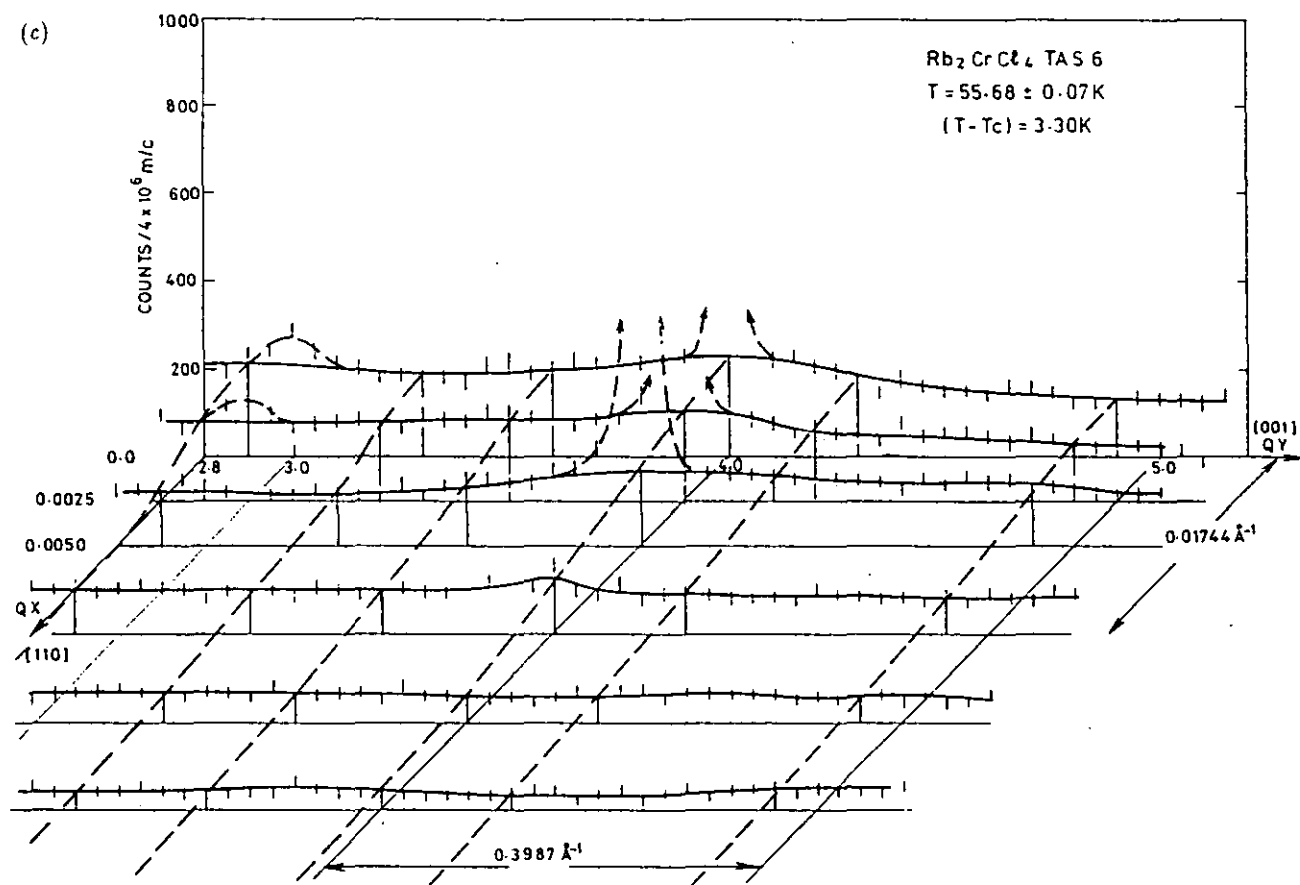
J Als-Nielsen et al

Figure 2. (c) Diffuse scattering of Rb_2CrCl_4 measured using the TAS6 spectrometer, near to the $(0, 0, 4)$ reciprocal-lattice point at $T = 55.68 \text{ K}$: —, guide to the eye; ----, $(0, 0, 4)$ Bragg reflection. The modulation of the critical scattering due to 3D effects is seen to commence below about 55 K.

Static critical properties of Rb_2CrCl_4

reflections. It was used in the Harwell routine FITSQ [29] to analyse the data by convolving it in three dimensions with $S(Q)$, and fitting parameters in $S(Q)$ to the data using the Harwell routine VA02A; a typical fit is illustrated in figure 3(a). The magnetization was measured from the $(0, 0, 4)$ Bragg peak intensity, after carefully subtracting the diffuse critical scattering and nuclear scattering. T_C was estimated to be 52.403 ± 0.016 K. The diffuse scattering was measured at or near $Q = (0, 0, 2.9)$. Figure 2 shows certain scans in this region. By comparing data measured at $(1, 0, 2.9)$ and $(-1, 0, 2.9)$ it was confirmed that the width of the rod measured was independent of the geometry, and so the quasi-static approximation was good.

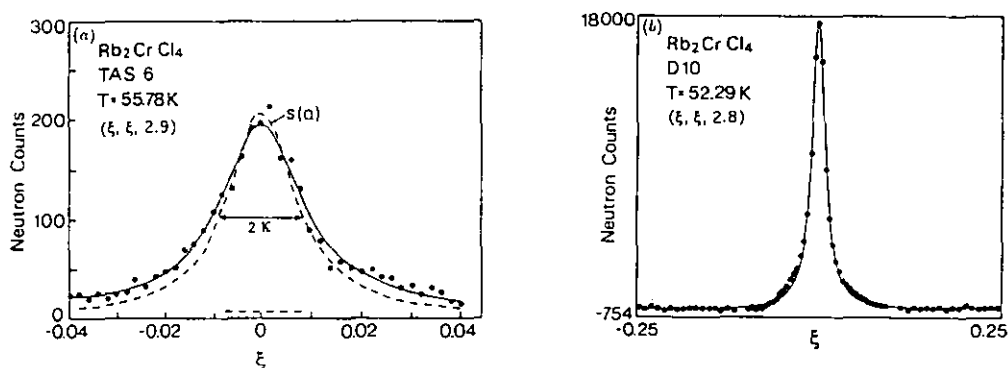


Figure 3. (a) Diffuse scattering of Rb_2CrCl_4 at 55.7 K near to $(0, 0, 2.9)$, measured using the TAS6 spectrometer: —, fit to the data as described in the text; ----, scattering function $S(Q)$ before convolution with the instrumental resolution. (b) Diffuse scattering of Rb_2CrCl_4 at 52.29 K near to $(0, 0, 2.8)$, measured using the D10 spectrometer, with a similar scan at 180 K subtracted: —, fit to the data of a Lorentzian function convolved with a Gaussian function of width (HWHM) $0.0024 \times 2\pi/a_0$, to describe the instrumental resolution.

In the experiment performed using D10, the crystal was contained in a helium-filled can, mounted in an ILL 'Orange' cryostat, with the temperature measured with a platinum resistance thermometer. A neutron wavelength of 1.26 \AA was used. The data were fitted using the one-dimensional fitting routine PKFIT to the Lorentzian function (17), which was convolved with a Gaussian function in order to describe the instrumental resolution. The resolution width (FWHM) was estimated by linear interpolation from the measured widths of the $(0, 0, 2)$ and $(0, 0, 4)$ Bragg reflections and varied between $0.48 \times 10^{-2} \times 2\pi/a_0 \text{ \AA}^{-1}$ and $0.38 \times 10^{-2} \times 2\pi/a_0 \text{ \AA}^{-1}$, respectively. This method of correcting for instrumental resolution was not as rigorous as the method used for the TAS6 data but was expected to be satisfactory so long as the resolution width was an order of magnitude less than the observed width of the diffuse rod. The magnetization was again estimated from scans of the $(0, 0, 4)$ Bragg reflection, and T_C was found to be $52.225(5)$ K. The diffuse scattering was measured in scans of the wavevector perpendicular to $[0, 0, 1]$, centred on $(0, 0, \xi)$, with ξ taking the values 2.2, 2.4, 2.6, 2.8 and 2.9. It was found that fits to the data were greatly facilitated by subtracting an identical scan measured at 180 K as a 'background', thereby removing the effect of any nuclear or other temperature-independent scattering. A typical fit to the data is illustrated in figure 3(b).

J Als-Nielsen et al

5. Results

5.1. Spontaneous magnetization

The relative spontaneous magnetization M was derived as the square root of the magnetic Bragg intensity and is shown in figure 4.

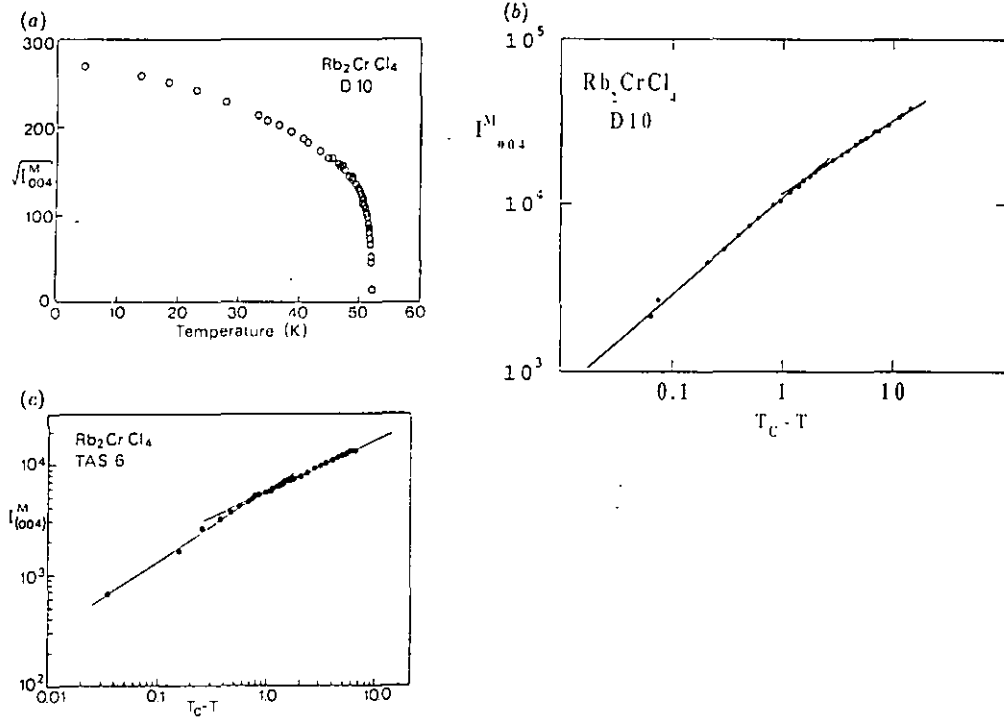


Figure 4. (a) Magnetization versus temperature for Rb_2CrCl_4 , derived as the square root of the magnetic intensity of the (0, 0, 4) Bragg reflection, measured using the D10 spectrometer. (b), (c) The intensity of the (0, 0, 4) magnetic Bragg reflection plotted against the reduced temperature on logarithmic scales. The lines are of slope 2β , where the values of β determined are listed in table 1. The data clearly show two regimes of different β : (b) data measured using the D10 spectrometer; (c) data measured using the TAS6 spectrometer.

The critical behaviour of the magnetization is defined by the equation

$$M = M_0 t^\beta \quad (18)$$

where $t = 1 - T/T_C$ and the magnetization is normalized to unity at $T = 0$ K. The critical exponent β and amplitude M_0 were determined from log-log plots, such as those shown in figure 4(b) and 4(c). The values obtained are listed in table 1. A sharp crossover between two regimes of different exponents β was observed to occur at a reduced temperature of approximately 0.03 (D10 experiment) or 0.015 (TAS6 experiment).

In the asymptotic regime close to T_C , the exponent β was estimated to be 0.33 (TAS6 experiment) or 0.28 (D10 experiment). Both these values are close to the expected 0.31 for the 3D Ising model or 0.33 for the 3D XY model, but significantly different from the value of 0.38 for the 3D Heisenberg model. We discuss the reason for their difference in section 5.4.

Static critical properties of Rb_2CrCl_4 **Table 1.** Summary of results of fits given in figures 4, 5, 7 and 8. The numbers in parentheses are the estimated standard errors.

Figure	Fit to expression	Fitted parameters	Temperature range
4 (TAS6)	$M \sim (52.403 - T)^\beta$	$\beta = 0.230(2)$ $\beta = 0.333(19)$	$T < T_C - 0.8$ $T > T_C - 0.8$
4 (D10)	$M = M_0(1 - T/52.225)^\beta$	$\beta = 0.224(8), M_0 = 0.96$ $\beta = 0.281(8), M_0 = 1.13$	$T < T_C - 1.6$ $T > T_C - 1.6$
5	$\kappa^2 = \kappa_0^2(T - T_C)^{2\nu} + \kappa_z^2$ (see equation (20))	$\kappa_0^2 = 2.2(2) \times 10^{-5}$ $\kappa_z^2 = 5.3(2) \times 10^{-5}$ $T_C = 52.403(16)$ $\nu = 0.825(25)$	$T > T_C$
7	$\kappa = \kappa_0 \exp(-b/\sqrt{t})$ $t = T/T_{KT} - 1$ (see equation (22))	$\kappa_0 = 0.76(39)$ $b = 2.12(57)$ $T_{KT} = 43.4(2.7)$	$T > 55 \text{ K}$
8	$\chi = C \exp(B/\sqrt{t})$ $t = T/43.4 - 1$ (see equation (23))	$C = 0.0071$ $B = 4.36(08)$	$T > 55 \text{ K}$

In the second regime, a well defined exponent $\beta \simeq 0.23$ was observed. As discussed in section 3, this value is characteristic of a finite 2D XY model. The value $\beta = 0.230(2)$ derived from the data measured using TAS6 is in particularly accurate agreement with the theoretical prediction $\beta = 3\pi^2/128 = 0.231 \dots$ [10].

5.2. Wavevector-dependent susceptibility: $T \geq T_C$

The susceptibility and correlation length data were analysed in three different ways:

- (1) via a mean-field formulation of $\chi(q)$;
- (2) according to the Kosterlitz expression (7);
- (3) according to conventional power-law divergences.

5.2.1. Mean-field analysis. This analysis is only of interest as a method of estimating the weak 3D exchange coupling J' .

Above 55 K the intensity and width of the ridge of diffuse scattering did not exhibit significant periodicity along $[0, 0, 1]$, reflecting the absence of 3D correlations. Below 55 K there was a pronounced modulation with wavevector along $[0, 0, 1]$, with maxima in the intensity and minima in the width at the reciprocal-lattice points $(0, 0, 2)$, $(0, 0, 4)$, etc. This behaviour, which is illustrated in part in figure 2, can be described by a mean-field formulation of the wavevector-dependent susceptibility [23, 30]. For Rb_2CrCl_4 , the susceptibility can be written

$$\chi(q) = 4\chi_C/[4(T - T_C)/T_C + a_0^2(q_x^2 + q_y^2) + (J'/J)c_0^2q_z^2] \quad (19)$$

where χ_C is a constant, and q_x, q_y, q_z represent wavevector displacements from a reciprocal-lattice point. If the scattering is fitted to a Lorentzian of half-width κ at half-maximum, then, by analogy with equation (17),

$$\kappa^2 = (\kappa_{\text{MF}})^2 + (\kappa_z)^2 \quad (20)$$

J Als-Nielsen et al

where

$$\begin{aligned}(\kappa_{\text{MF}})^2 &= (\kappa_0)^2 [(T - T_C)/T_C]^{2\nu} \\ (\kappa_z)^2 &= (J'/J)q_c^2\end{aligned}\quad (21)$$

$\nu = 0.5$, $\kappa_0 = 2$ and $q_c = c_0 q_z$ is the displacement from the Brillouin zone centre along the c direction. The parameters κ , κ_{MF} , κ_0 and q_c are all expressed in reciprocal-lattice units, e.g. $q_c = 0.2$ for $Q = (0, 0, 2.2)$. Equation (19) shows that the measured κ consists of a temperature-dependent part κ_{MF} and a temperature-independent part κ_z arising from the 3D correlations.

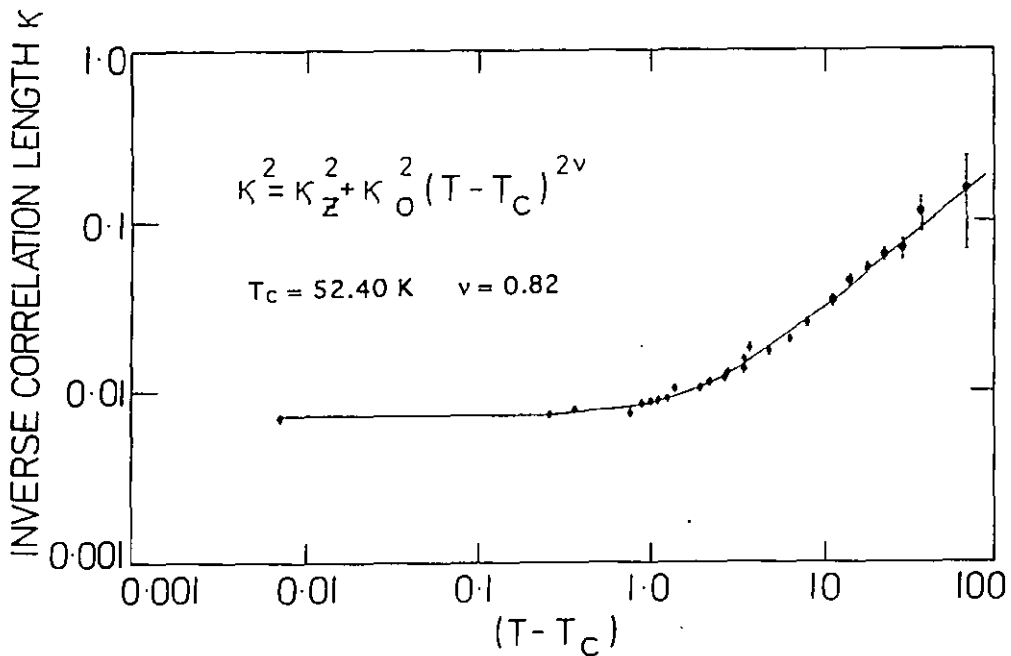


Figure 5. Plot of the fitted Lorentzian width κ measured at $Q = (0, 0, 2.9)$ versus temperature and analysed according to the mean-field approximation equation (20) (see also table 1). The data were measured using the TAS6 spectrometer.

The data were analysed using equations (20) and (21), treating κ_0 , κ_z and ν as adjustable parameters, with the results $\nu = 0.82 \pm 0.01$ (TAS6 data; figure 5 and table 1) and $\nu = 0.61 \pm 0.01$ (D10 data), the difference probably arising from the different methods of correcting for the instrumental resolution (see section 5.4). The deviation of ν from the value $\nu = 0.5$ reflects the inaccuracy of the mean-field approximation. For the data obtained using TAS6 ('TAS6 data'), κ_z^2 was found to be 5.3×10^{-5} at $q_c = 0.9$, corresponding to $J'/J \approx 6.5 \times 10^{-5}$ (see figure 5). Another estimate of J'/J was derived from the data obtained using D10 ('D10 data') at 52.25 K ($\approx T_C$), by plotting κ^2 versus q_c^2 , as shown in figure 6. The result, $J'/J \approx 1.5 \times 10^{-4}$, is in quite good agreement with the direct estimate of Hutchings *et al* [13] of about 2.4×10^{-4} . A comparison of the data of the two experiments showed that the discrepancy between the two estimates of J'/J arose directly from the different fitted widths κ in the critical region, the D10 estimates being a factor of about 1.5 greater than the TAS6 estimates in this region. The discrepancy was not reflected

Static critical properties of Rb_2CrCl_4

in the data at higher temperatures, where the widths were larger, and it was concluded that there was a systematic error in the D10 results near to T_C , arising from the approximate nature of the resolution correction, and possible effects of the more open vertical resolution (see section 4). As argued in section 5.4, the method used—approximating the width of the resolution ellipsoid by the width of a Bragg reflection—would be expected to underestimate the resolution width and to overestimate κ , as observed.

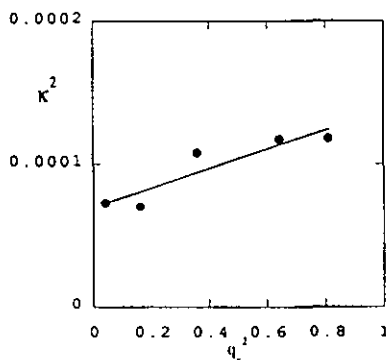


Figure 6. Square of the fitted Lorentzian width κ (measured using the D10 spectrometer) plotted versus the square of q_c (equation (20)). The best-fit line has slope $J'/J = 1.5 \times 10^{-4}$.

5.2.2. Analysis according to the Kosterlitz expression. According to the arguments outlined in section 3, pure 2D XY behaviour is expected to occur at temperatures above the 2D–3D crossover temperature (about 55 K). This corresponds to the paramagnetic regime of the 2D XY model, in which the spin–spin correlations decay exponentially with correlation length ξ (equation (7)). The exact form of $\chi(q)$ is not known with certainty, although the Ornstein–Zernike form (17) is correct for $q < \kappa$ [31], and a good approximation for $q > \kappa$. The susceptibility χ and inverse correlation length κ were therefore obtained from the TAS6 data above 55 K, using equation (17), and then analysed according to the Kosterlitz expression (7).

First, the inverse correlation length was fitted using least-squares minimization to the equation

$$\kappa = \kappa_0 \exp(-bt^{-1/2}) \quad (22)$$

where $t = T/T_{KT} - 1$, by varying the parameters κ_0 , b and T_{KT} . As shown in figure 7, equation (22) is found to fit the data very accurately indeed, with the result $\kappa_0 = 0.76 \pm 0.39$, $b = 2.12 \pm 0.57$ and $T_{KT} = 43.4 \pm 2.7$ K. These values are remarkably close to those expected theoretically; the amplitude κ_0 is of order unity, and the value of $b = 2.1$ is very close to the corrected prediction of Kosterlitz of 1.9 and the best Monte Carlo estimate of Gupta *et al* [17] of 1.8. These results are summarized in table 1 and discussed further in section 6.

The susceptibility χ of the 2D XY model may be derived from the scaling law $\chi \simeq \xi^{2-\eta}$, with the result [14]

$$\chi = C \exp(Bt^{-1/2}) \quad (23)$$

where $B = (2 - \eta)b$ and C is a constant, which in the present context is simply a normalization factor, with no physical meaning. The experimentally derived susceptibility $\chi(0)$ was fitted to (23), using $T_{KT} = 43.4$, derived as described above from the temperature variation in the inverse correlation length. It was found that $B = 4.36 \pm 0.08$. Treating T_{KT}

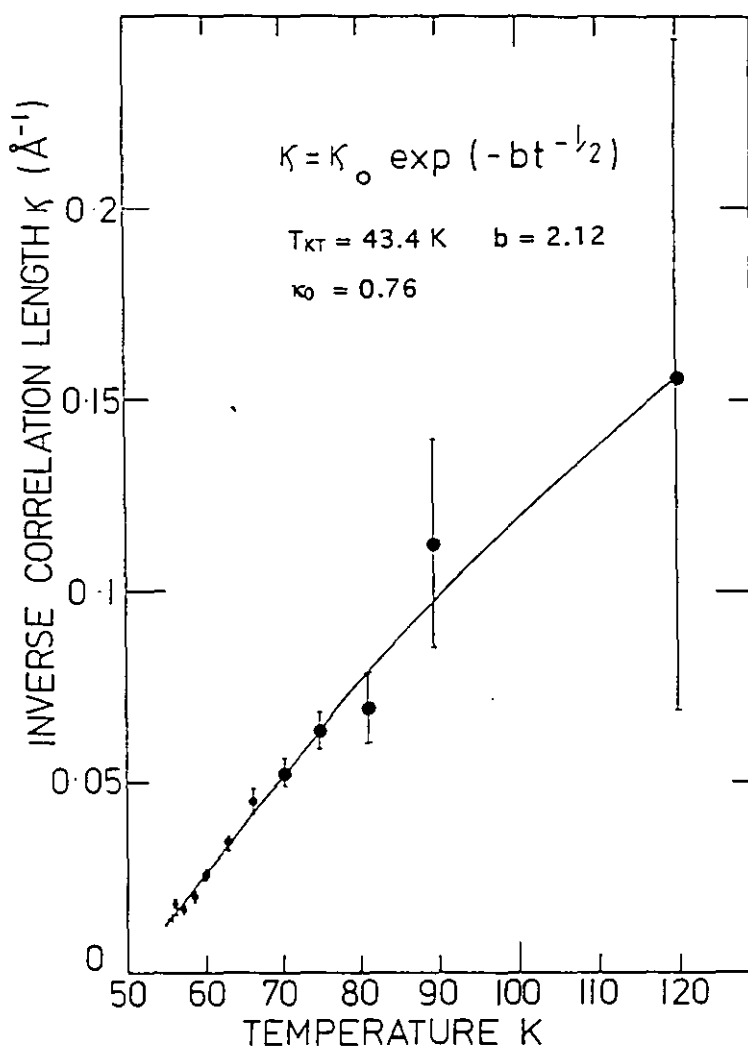
J Als-Nielsen et al

Figure 7. Temperature dependence of κ , the inverse correlation length measured in the 2D regime, measured using the TAS6 spectrometer, fitted to the Kosterlitz expression (22) (see also table 1).

as an adjustable parameter gave $T_{KT} = 43.9 \text{ K}$ and $B = 4.18 \pm 0.66$. These results are in excellent agreement with the results of Cornelius *et al* [9], who found that $B = 4.07 \pm 0.10$ from magnetization measurements on Rb_2CrCl_4 . B is also very close to the value expected from the results of the fits to the correlation length; with $b = 2.12$ and taking $\eta \simeq 0$, we find that $B = 4.24$. An example of a fit to the susceptibility data is illustrated in figure 8, and the results are listed in table 1.

Attempts to estimate the exponent η from the susceptibility data indicated that $\eta \simeq 0$, but the errors were very large (± 0.3). For the 2D XY model, $\eta = 0.25$ at T_{KT} , but the behaviour of η in the paramagnetic regime is not well established [31]. If one assumes that $\eta \neq 0$ in the paramagnetic regime, then η can be estimated by using, rather than the Lorentzian form (11), the expression

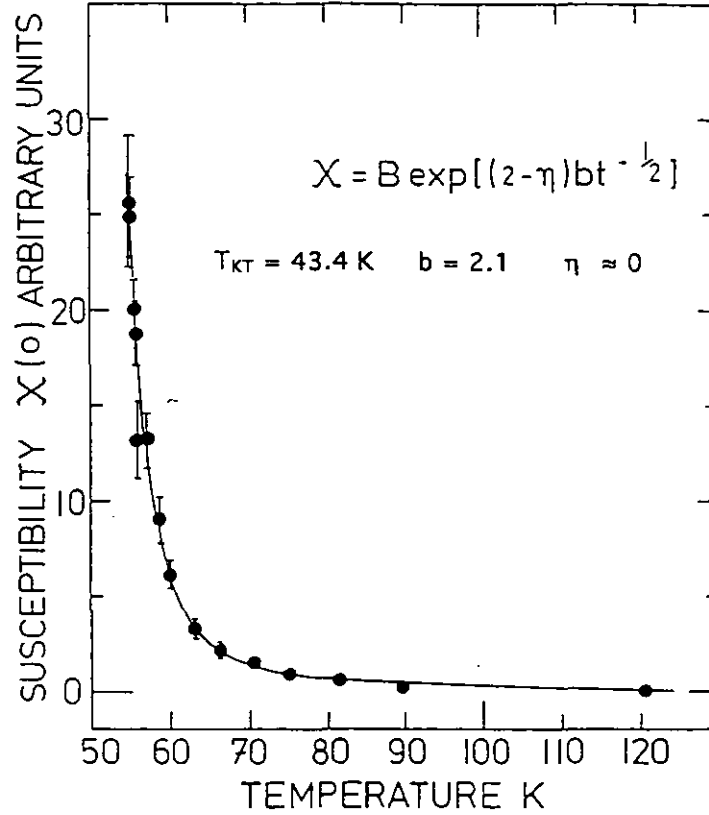
Static critical properties of Rb_2CrCl_4 

Figure 8. Temperature dependence of the susceptibility $\chi(0)$ measured in the 2D regime, using the TAS6 spectrometer, fitted to the Kosterlitz expression (23) (see also table 1). Note that the figure shows the fit for the amplitude B held equal to 4.2 ($= 2b$; see text).

$$\chi(q) \simeq 1/(q^2 + \kappa^2)^{1-\eta/2}. \quad (24)$$

However, we found no significant deviation from a Lorentzian function.

Finally, in another experiment, which we do not report in detail here, we determined the susceptibility by integration over energy transfer of the inelastic neutron scattering spectrum, measured on the IN12 spectrometer at the ILL, Grenoble. The temperature dependence of $T\chi(q=0)$ was found to be in almost exact agreement with the result obtained using TAS6, confirming both the validity of the quasi-static approximation, and the method of analysis of the data.

5.2.3. Analysis according to conventional power laws. For completeness, the correlation length and susceptibility measured using TAS6 were also fitted to the conventional power laws [25]

$$\begin{aligned} \chi T &\propto (1 - T_c/T)^{-\gamma} \\ \kappa &\propto (T/T_c - 1)^\nu. \end{aligned} \quad (25)$$

Fitting the data in the 2D regime above 55 K gave the results $\gamma = 2.5 \pm 0.07$ K and $\nu = 1.06 \pm 0.17$ K (see table 1). These critical exponents are not characteristic of any known universality class.

J Als-Nielsen et al

Since the fits of the data to conventional power laws and to the KT theory are equally accurate, any judgment between the relative merits of the two approaches must rely on the parameters obtained in the fits. We therefore favour the KT theory on the grounds of self-consistency, since all the derived parameters are in excellent agreement with theoretical predictions, and with the conclusions of other experiments. It is probable that the critical exponents γ and ν are simply fitting parameters, with no physical meaning.

5.3. Wavevector-dependent susceptibility: $T \leq T_C$

The wavevector-dependent susceptibility was observed to maintain its approximately Lorentzian form below T_C , with κ initially increasing slightly with decreasing temperature. As shown in figure 9, κ became only weakly temperature dependent below about 51 K, which corresponds to the 2D regime of the magnetization (see section 5.1). The modulation of the width with q_c due to the 3D coupling J' (equation (19)) was also observed to be independent of temperature in this regime (figure 9). The extrapolated value of κ at $q_c = 0$ was estimated from the D10 data to be about $0.0125/a_0$, corresponding to a correlation length of about 80 lattice spacings. However, as explained in section 5.2.1 above, the correlation length estimated from the D10 data was inaccurate by a factor of approximately 1.5 in this region, and so a more accurate estimate is about 120 lattice spacings. The results presented in figure 9 are nevertheless expected to be qualitatively correct.

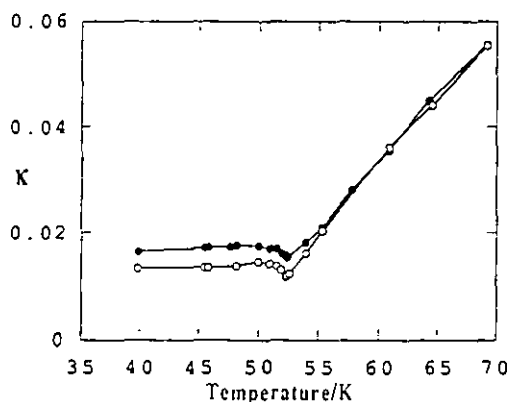


Figure 9. Fitted width κ of the $[0,0,1]$ diffuse rod measured at $Q = (0, 0, 2.4)$ (○) and $Q = (0, 0, 2.8)$ (●), near and below T_C . The data were measured with the D10 spectrometer. Note that the fitted values of κ are a factor of about 1.5 larger than those derived from the data measured with the TAS6 spectrometer, probably as a result of the approximate resolution function used in the fitting procedure (see section 5.2.1).

5.4. Comparison of the results of the two experiments

The two experiments yielded results in qualitative agreement, but with some quantitative differences. Firstly, the value of the three-dimensional ordering temperature T_C was found to be slightly lower in the experiment performed on D10 (52.225 K) than in that performed on TAS6 (52.403 K). This probably reflected the difference between the two samples. That measured on D10 was an older sample at the time of the experiment and so may have been less pure; Rb_2CrCl_4 samples are susceptible to oxidation, even when handled with care.

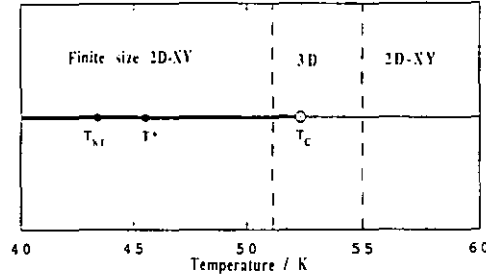
Static critical properties of Rb_2CrCl_4 

Figure 10. Phase diagram of the critical region of Rb_2CrCl_4 in zero magnetic field, indicating regions of universal behaviour: —, region of spontaneous order; ●, ○, experimentally determined temperatures T_{KT} , T^* and T_C , referred to in the text.

Impurities would generally give a lower transition temperature. The lower 3D magnetization exponent measured on D10, $\beta = 0.28$, could also be explained by the presence of impurities. That measured on TAS6, $\beta = 0.33$, is closer to the expected value for 3D ordering.

A more serious discrepancy between the two sets of results was the quantitative differences in the measured correlation length. This certainly resulted from the different methods of correcting for instrumental resolution (see section 5.3). The method used to treat the data collected on D10 involved convolution of the scattering function with a fixed 'resolution width'. The latter was derived from the width of nearby Bragg peaks, a method which underestimates the resolution width, since it measures a diameter of the resolution ellipsoid rather than its projection on the scan direction. The method also neglects the finite vertical resolution of D10, which was used without vertical collimation. An approximate correction for these errors brought the measured correlation length to a value consistent with that obtained on TAS6, where the correction for both horizontal and vertical instrumental resolution was performed rigorously within the theoretical description of Cooper and Nathans [32].

Overall, we expect the results of the experiment performed on TAS6 to be the more accurate. This is confirmed by their very close agreement with the theoretical predictions.

6. Discussion

In general the behaviour of Rb_2CrCl_4 confirms the expected crossover behaviour described in the introduction and in section 3. The asymptotic critical behaviour is 3D, but there are crossovers to 2D XY-like behaviour both above and below T_C .

The experimental T_{KT} (see table 1) of 43.3 K corresponds to a value of about 0.71 in units of $2JS^2$. This may be compared to the prediction of 0.898 for the classical 2D XY model (see section 3). This difference is not surprising, since the out-of-plane fluctuations in Rb_2CrCl_4 would be expected to reduce the absolute value of the transition temperature.

It is now possible to check the detailed predictions for the finite-sized XY behaviour of the ordered phase, described in section 3. We first identify the effective system size L_{eff} . This is a parameter of the order $\sqrt{J/J'}$ but is not necessarily equal to $\sqrt{J/J'}$. Probably the best estimate is the value of the correlation length in the 2D XY regime, which is approximately 120 lattice spacings (see above). This is equal to the mean-field estimate of $\sqrt{J/J'}$ (see figure 5) and is of the order of the more accurate spin-wave estimate of about 60.

J Als-Nielsen et al

The temperature at which $\delta = 15$ and $\eta = 0.25$, which we now understand to be T^* , was previously identified by Cornelius *et al* [9] to be 45.5 K. At T^* , the observed magnetization $M(T)/M(0)$ is predicted to be approximately $(1/L_{\text{eff}}\sqrt{2})^{1/8} \simeq 0.55 \pm 0.02$ (see equation (10)). The observed value (figure 4) is 0.6 ± 0.02 , in quite good agreement. One should perhaps not expect a better agreement between the XY model and Rb_2CrCl_4 as regards the *magnitude* of the magnetization. However, in accord with universality, the subcritical exponent β at T^* , defined relative to $T_C = 52.403$ K, is found to be $0.230(2)$, in extremely accurate agreement with the theoretical prediction $3\pi^2/128 = 0.231\dots$

In order to make a more detailed test of the predictions of section 3, we use equations (11) and (13), and the estimates derived from the behaviour of the correlation length: $T_{KT} = 43.3$ K, $b = 2.12$ and $L_{\text{eff}} = 120$. This gives $T^* \simeq 45.4$ K and $T_C \simeq 52.8$ K. These are, within the error to which they can be estimated, equal to the observed $T^* = 45.5$ K, and the 3D ordering temperature $T_{3D} = 52.4$ K, respectively. As mentioned in section 3, there is no reason why T_C and T_{3D} should be identical. The fact that they are very close ensures that $\beta = 0.23$ is easily observed experimentally.

The excellent agreement between theory and experiment, confirms that Rb_2CrCl_4 behaves like a finite-sized 2D XY system in the 2D subcritical regime both below and above T_C . This suggests that spin vortices exist in Rb_2CrCl_4 , since the theory of Kosterlitz [14], as modified for a finite system [10], assumes their existence, and they are observed in Monte Carlo simulations. However, unbound vortices probably occur only in large numbers at $T > T^*$ [33].

It is perhaps surprising that the temperature dependence of the 3D magnetization should be determined by 2D fluctuations over a wide temperature range. This may be understood as follows. Below T_C , in the 3D ordered phase, the correlation length decreases until it becomes of order $\sqrt{J/J'}$, at the 2D–3D crossover temperature. At lower temperatures, the temperature dependence of the magnetization of each layer is determined by misaligned regions of all sizes up to this correlation length. These regions are in general too small to be correlated with those in neighbouring layers. Thus, while the magnetization of each layer is strongly correlated in 3D, the fluctuations in the magnetization are only weakly correlated. The system therefore behaves as an assembly of layers connected in a mean-field manner, and one measures a 3D magnetization which varies in the manner of a finite 2D system.

It is interesting to observe that the staggered twofold in-plane anisotropy, which approximates to a fourfold bulk anisotropy, is irrelevant in determining the 2D critical properties. José *et al* [15] predicted that a fourfold field h_4 was only marginally relevant, with non-universal critical exponents. One would therefore expect h_4 to manifest itself only very close to T_C , and it is clear that for Rb_2CrCl_4 this does not occur in the 2D regime. It is, however, likely that h_4 becomes important in the 3D regime, probably resulting in Ising-like behaviour. The experiments are consistent with this.

In figure 10 we summarize the crossover behaviour of Rb_2CrCl_4 on a phase diagram. Omitted from the diagram are the 2D Heisenberg regime (which is observed well above T_C) and the low-temperature spin-wave regime [3] (which is non-universal).

7. Summary and conclusions

The critical behaviour of Rb_2CrCl_4 reflects the presence in the Hamiltonian of several terms of differing orders of magnitude. The dominant behaviour is 2D XY like, with crossover to 3D XY or 3D Ising-like behaviour occurring near to T_C .

In the 2D regime below T_C , the behaviour of the magnetization was found to be in excellent quantitative agreement with theoretical predictions [10] for a finite 2D XY model.

Static critical properties of Rb_2CrCl_4

The in-plane correlation length is found to be only weakly temperature dependent, with the approximate value of $\sqrt{J/J'}$ lattice units.

In the 2D regime above T_C , the behaviour of the correlation length was found to be in excellent quantitative agreement with the prediction of Kosterlitz [14] and Monte Carlo simulations [17] for the 2D XY model. In this regime there is no need to distinguish between the finite and infinite systems, because the behaviours are the same.

The effective fourfold anisotropy of Rb_2CrCl_4 appears to have no effect on the critical properties in either 2D critical regime, consistent with the predictions of José *et al* [15].

In general, we have found excellent agreement between experiment and theory. Our principal conclusion is that the RG equations of José *et al* [15] and Kosterlitz [14], when modified for finite-size effects [10], describe all the essential physics of the magnetism of Rb_2CrCl_4 in the subcritical regime.

Acknowledgments

We would like to thank K R A Ziebeck for experimental assistance, I Osborn for help with the data analysis and P C W Holdsworth, M Thorpe and P Day for very useful discussions. MTH would also like to thank Risø National Laboratory for their hospitality during his visit. This work was supported in part by the Underlying Research Programme of the UKAEA, and by the SERC.

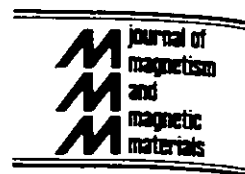
References

- [1] Janke E, Hutchings M T, Day P and Walker P J 1983 *J. Phys. C: Solid State Phys.* **16** 5959
- Day P, Fyne P J, Hellner E, Hutchings M T, Münnhoff G and Tasset F 1986 *Proc. R. Soc. A* **406** 39
- [2] Fair M J, Gregson A K, Day P and Hutchings M T 1977 *Physica B* **86-88** 657
- [3] Hutchings M T, Als-Nielsen J, Lindgard P A and Walker P J 1981 *J. Phys. C: Solid State Phys.* **14** 5327
- [4] Collins M F 1989 *Magnetic Critical Scattering* (Oxford: Oxford University Press)
- [5] Mermin N D and Wagner H 1966 *Phys. Rev. Lett.* **17** 1133
- [6] Kawabata C and Bishop A R 1986 *Solid State Commun.* **60** 167
- [7] Kosterlitz J M and Thouless D J 1973 *J. Phys. C: Solid State Phys.* **6** 1181
- [8] Berezinskii V L 1971 *Sov. Phys.-JETP* **32** 493
- [9] Cornelius C A, Day P, Fyne P J, Hutchings M T and Walker P J 1986 *J. Phys. C: Solid State Phys.* **19** 909
- [10] Bramwell S T and Holdsworth P C W 1993 *J. Phys.: Condens. Matter* **5** L53
- Bramwell S T and Holdsworth P C W 1993 *J. Appl. Phys.* **73** 6096
- [11] Harrop M C 1981 *D.Phil Thesis* University of Oxford
- [12] Elliot R J, Hengeltraub A, Harrop M C and Ziman T A L 1980 *J. Magn. Magn. Mater.* **15-8** 359
- [13] Hutchings M T, Day P and Fyne P J 1984 unpublished results
- Fyne P J 1984 *D.Phil Thesis* University of Oxford
- [14] Kosterlitz J M 1974 *J. Phys. C: Solid State Phys.* **7** 1046
- [15] José J V, Kadanoff L P, Kirkpatrick S and Nelson D R 1977 *Phys. Rev. B* **16** 1217
- [16] Villain J 1975 *J. Physique* **36** 581
- [17] Gupta R, DeLapp J, Batrouni G C, Fox G C, Baillie C F and Apostolakis J 1988 *Phys. Rev. Lett.* **61** 1996
- [18] Bramwell S T and Holdsworth P C W 1993 submitted for publication
- [19] Berezinskii V L and Blank A Ya 1973 *Sov. Phys.-JETP* **37** 369
- [20] Nelson D R and Kosterlitz J M 1977 *Phys. Rev. Lett.* **39** 1201
- [21] Hirakawa K and Ikeda H 1973 *J. Phys. Soc. Japan* **35** 1328
- [22] Regnault L P and Rossat-Mignod J 1990 *Magnetic Properties of Layered Transition Metal Compounds* ed L J de Jongh (Dordrecht: Kluwer)
- [23] Marshall W and Lowde R D 1968 *Rep. Prog. Phys.* **31** 705
- [24] Als-Nielsen J 1976 *Phase Transitions and Critical Phenomena* vol 5a, ed C Domb and M S Green (New York: Academic)

J Als-Nielsen et al

- [25] Stanley H E 1971 *Introduction to Phase Transitions and Critical Phenomena* (reprint 1987) (Oxford: Oxford University Press)
- [26] Birgeneau R J, Guggenheim H J and Shirane G 1970 *Phys. Rev. B* **1** 2211
- [27] Hutchings M T, Day P, Janke E and Pynn R 1896 *J. Magn. Magn. Mater.* **54-7** 673
- [28] Garton G and Walker P J 1976 *J. Cryst. Growth* **36** 351-2
- [29] Hutchings M T, Lowde R D and Tindle G L 1986 *Workshop on Neutron Scattering Data Analysis (Inst. Phys. Conf. Ser. 8)* (Bristol: Institute of Physics) p 151
- [30] Hirakawa K 1982 *J. Appl. Phys.* **53** 1983
- [31] Heinkamp S W and Pelcovits R A 1985 *Phys. Rev. B* **32** 4528
- [32] Cooper M J and Nathans R 1967 *Acta Crystallogr.* **23** 357
- [33] Weber H and Jensen H J 1991 *Phys. Rev. B* **44** 454

Journal of Magnetism and Magnetic Materials 117 (1992) 8–10
North-Holland



The critical line of the 2-dimensional easy plane ferromagnet

S.T. Bramwell^a, P.C.W. Holdsworth^b and D. Visser^c

^a *Institut Laue–Langevin, BP 156X, F-38042 Grenoble Cedex, France*

^b *Laboratoire de Physique, Ecole Normale Supérieure de Lyon, 69364 Lyon, France*

^c *Department of Physics, Loughborough University of Technology, Loughborough LE11 3TU, UK*

The critical properties of the 2-D Heisenberg ferromagnet with planar (XY) anisotropy in a weak symmetry sustaining (z) field have been studied through quasi-elastic neutron scattering and magnetometry experiments on the quasi-2D ferromagnet Rb_2CrCl_4 , and through Monte Carlo (MC) simulations of a comparable purely 2D system. A critical line has been detected in the temperature–field phase diagram. The general trend predicted by the MC calculations is confirmed experimentally.

The application of a uniform field to a ferromagnet in general destroys the critical point, since the field couples directly to the spontaneous ordering mode. An exception may be the 2-dimensional Heisenberg model ferromagnet with planar (XY) anisotropy, which in zero field exhibits a “Kosterlitz–Thouless” phase transition due to the unbinding of metastable planar spin vortex configurations. It may therefore be envisaged that the application of a symmetry-sustaining field perpendicular to the XY plane would at first merely reduce the in-plane spin component, and consequently the transition temperature, without destroying the critical properties. Therefore, at least for weak fields, a critical line should appear in the temperature–field phase diagram [1].

We have recently undertaken a study of the critical properties and magnetic phase diagram of such a system, and in the present paper confine our attention to the (quasi-)static critical properties of the layered insulating ferromagnet Rb_2CrCl_4 [2]. The latter provides a good realisation of an $S = 2$ square lattice 2-dimensional

Heisenberg model ($J \approx 7.6$ K) with planar single-ion anisotropy ($D \approx 1.2$ K). The ideality of the system is weakly perturbed by dipolar interactions, 3-dimensional coupling ($J' \approx 0.002$ K) and 4-fold in-plane anisotropy ($P \approx 0.1$ K); perturbations which are sufficient to induce long range 3D magnetic order below $T_C = 52.2$ K. A previous comparative study of the in-plane and out-of-plane zero-field susceptibility has shown the latter to be strongly suppressed below ~ 75 K [3]. It has been argued that between this temperature and ~ 55 K the critical properties may be 2D- XY like with a crossover to 3D behaviour occurring at lower temperatures [4].

Our investigation has so far comprised three different experiments:

(1) Using a vibrating sample magnetometer (VSM) with magnetic fields of up to 12 T applied parallel to the z axis of a small (≈ 0.1 cm³) crystal of Rb_2CrCl_4 , we have directly measured the out-of-plane magnetisation M_z as a function of field B_z and temperature. Some of the results are illustrated in fig. 1. In very weak fields a small induced out-of-plane magnetisation M_z develops, which peaks at T_C . Below this temperature it decreases, indicating a coupling with the strongly developing in-plane magnetisation. In stronger fields the maximum is less sharp, and above ~ 1.5 T there is no maximum at all, but a distinct

Correspondence to: Dr. S.T. Bramwell, Institut Laue–Langevin, BP 156X, F-38042 Grenoble Cedex, France.

* Paper presented at the International Conference on Magnetism (ICM '91), Edinburgh, Scotland, 2–6 September 1991.

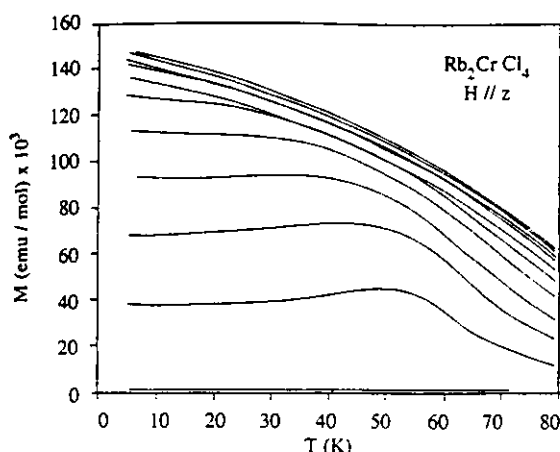


Fig. 1. Magnetisation curves of Rb_2CrCl_4 at constant $H // z$ as function of temperature. These curves have been measured at 0.01, 0.5, 1.0, 1.5, 2.0, 2.25, 2.50, 2.75, 3.0, 3.25 and 3.5 T and are sequentially displayed for the bottom towards the top of the figure.

change in slope may be taken to indicate a transition temperature. T_C as a function of applied field is plotted in fig. 2.

(2) The in-plane spin components of Rb_2CrCl_4 have been probed in a double-axis neutron scattering experiment, using the D10 spectrometer, ILL, Grenoble, with a fixed incident neutron wavelength of 1.26 Å. A horizontal magnetic field of up to 3 T was applied perpendicular to the

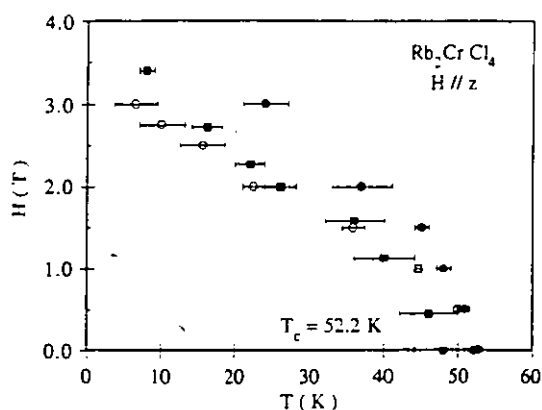


Fig. 2. The temperature-magnetic field diagram of Rb_2CrCl_4 for $H // z$, as obtained from magnetometry and quasi-elastic neutron scattering experiments. The MC predictions are indicated by ■, the magnetometry data by ○, and the neutron data by ●.

easy (x - y) plane of a large ($\sim 1 \text{ cm}^3$) single crystal of Rb_2CrCl_4 . With the scattering vector Q also parallel to z it was possible to derive the in-plane magnetisation M_{\perp} from the Bragg scattering, and the in-plane susceptibility $\chi_{\perp}(q_z)$ and correlation length $\xi_{\perp}(q_z)$ from the diffuse scattering, in the normal way [5]. q_z is a propagation vector measured from the Bragg point, which defines the periodicity of the weak 3D correlations. Measurements were made at $Q = (0, 0, 2.4)$ and $Q = (0, 0, 2.8)$, corresponding to $q_z = 0.4$ and $q_z = 0.8\pi/r_z$ respectively, where r_z is the interplanar spacing ($\approx 7.9 \text{ Å}$). We briefly describe the field and temperature behaviour of the variables M_{\perp} , $\chi_{\perp}(q_z)$ and $\xi_{\perp}(q_z)$ near to T_C . In zero field [6], above $\sim 55 \text{ K}$, $\chi_{\perp}(q_z)$ and $\xi_{\perp}(q_z)$ were observed to have no q_z dependence, indicating 2D correlations. Below this temperature some q_z -dependence was observed, both $\chi_{\perp}(q_z)$ and $\xi_{\perp}(q_z)$ increasing at small q_z . This indicates the presence of 3D correlations resulting from the weak interplanar exchange J' . T_C (52.2 K) was marked by the spontaneous appearance of M_{\perp} , and maxima in $\chi_{\perp}(q_z)$ and $\xi_{\perp}(q_z)$. In applied fields of 0.5, 1.0 and 1.5 T, correlations were again observed to be purely 2D, and not significantly field dependent above $\sim 55 \text{ K}$. Below this temperature $\chi_{\perp}(q_z = 0.8)$, which may be taken to be representative of 2D fluctuations, displayed approximately the same behaviour as in zero field, reaching the same maximum at lower temperatures the larger the applied field (e.g. 45 K for $B_z = 1.5 \text{ T}$). This temperature approximately coincided with appearance of M_{\perp} , and so was taken to indicate ordering of the in-plane spin components. The peak in $\chi_{\perp}(q_z = 0.4)$, which was initially more intense than the $q_z = 0.8$ value, was significantly suppressed by the applied field. For a field of 1.5 T χ_{\perp} again appeared to be approximately q_z -independent. The behaviour of $\xi_{\perp}(q_z)$ was generally more complicated, appearing to reach its maximum below the ordering temperature as defined above. This effect was more distinct at $q_z = 0.4$ than at $q_z = 0.8$. The associated narrowing of the critical scattering line width in reciprocal space made deconvolution of the Bragg and diffuse scattering very difficult, and so limited the accuracy to which T_C could be

estimated. T_C as a function of field is plotted as part of fig. 2, where it can be seen that there is only partial agreement with the magnetometry estimates. However, the important conclusion of the neutron scattering experiment is that the quasi-2D nature of the phase transition is preserved in quite strong fields, with little attenuation of the magnitude of the 2D fluctuations.

(3) In order to test a purely 2D system, we have performed classical Monte Carlo (MC) simulations on a system of 32×32 spins corresponding to the Rb_2CrCl_4 spin Hamiltonian for a single layer [2], with neglect of the dipolar interaction. At each temperature the system was equilibrated for 5000 Monte Carlo steps per particle (MCS), and the data collected over a further 5000 MCS. T_C was identified by in-plane ordering and a maximum in M_z . The phase diagram derived by MC simulations is in quite good agreement with that derived by magnetometry, as shown in fig. 2. The critical field at which in-plane ordering no longer occurs is estimated in both cases to be about 4 T. By minimising the energy of the idealised classical Hamiltonian at $T = 0$, we would expect the critical field to be $\sim 2DS \approx 3.5$ T, which is close to the experimental value.

The present study confirms the prediction of the occurrence of a line of quasi-2D critical behaviour when a magnetic field is applied in the symmetry sustaining direction. A novel feature has been observed in the shape of the field-temperature phase diagram when $H \parallel z$. This feature is reproduced by MC calculations. The MC results show that in finite field M_z displays a sharp maximum at the in-plane ordering transition. The rounding of the M_z curves as observed by magnetometry could therefore be ascribed to 3D or dipolar effects. The decrease of M_z below T_C can be understood by considering that the energy of two neighbouring misaligned spins within the

x - y plane can be reduced by the spins relaxing out of the plane. However, for parallel spins the energy is minimised by alignment within the plane. Therefore below the ordering transition, the system becomes resistant to out-of-plane magnetisation. The transverse (in-plane) response has been probed by quasi-elastic neutron scattering. Transverse correlations which are essentially 2D, are hardly affected by B_z , while those with a 3D component are strongly modified. This reflects the increasing influence of the paramagnetic magnetisation along the z -direction. The critical line as measured by the neutron scattering experiment appears to deviate from that measured by magnetometry at low fields, but probably approaches the same critical field (~ 4 T) as $T \rightarrow 0$.

Acknowledgements

We would like to thank the ILL Grenoble, the ENS, Lyon and the UK SERC for support. D.V. would also like to acknowledge the Department of Physics, University of Southampton for their hospitality during the magnetometry experiments and Dr. T. Young and Dr. P.A.J. de Groot for their support.

References

- [1] K. Hirakawa and U. Ubukoshi, *J. Phys. Soc. Jpn.* 50 (1981) 1909.
- [2] M.T. Hutchings, J. Als-Nielsen, P.A. Lindgård and P.A. Walker, *J. Phys. C* 14 (1981) 5327.
- [3] W.J. Crama, Doctoral Thesis, University of Leiden (1980).
- [4] S.T. Bramwell, M.T. Hutchings, J. Norma, R. Pynn and P. Day, *J. de Phys.* 49 (1988) C8-1435.
- [5] K. Hirakawa, *J. Appl. Phys.* 53 (1982) 1893.
- [6] M.T. Hutchings, J. Als-Nielsen, S.T. Bramwell, D. Visser and G.J. McIntyre, unpublished results.

Magnetic structure of $\text{KMnPO}_4 \cdot \text{H}_2\text{O}$

D. Visser

Department of Physics, Loughborough University of Technology, Loughborough LE11 3TU, United Kingdom

S. G. Carling

Inorganic Chemistry Laboratory, University of Oxford, South Parks Road, Oxford OX1 3QR, United Kingdom

P. Day

Institut Laue Langevin, BP 156X, 38042, Grenoble Cedex, France

J. Deportes

Laboratoire Louis Néel, CNRS, 38042, Grenoble Cedex, France

The compound $\text{KMnPO}_4 \cdot \text{H}_2\text{O}$ adopts the $\text{NH}_4\text{CoPO}_4 \cdot \text{H}_2\text{O}$ structure, in which distorted M^{II} octahedra form corner-sharing sheets, separated by layers of K^+ ions. Within a layer, the divalent metal ions form an approximately square lattice. In the range 75–300 K the magnetic susceptibility of $\text{KMnPO}_4 \cdot \text{H}_2\text{O}$ follows the Curie–Weiss law, with $C = 4.73(6)$ emu K mol $^{-1}$, $\theta = -61(2)$ K. Below 75 K, the susceptibility deviates from this simple model, showing a broad susceptibility maximum with $T(\chi_{\text{max}}) \sim 27(2)$ K, which suggests the presence of two-dimensional magnetic interactions. Below about 18 K, magnetization measurements at 0.068 T indicate a weak ferromagnetic moment, with domain effects apparent below 9 K. High-resolution powder neutron-diffraction profiles have been measured at room temperature and 1.7 K. No change in crystal structure is found between these two temperatures, and all additional magnetic reflections in the low-temperature profile were indexed on the nuclear cell. The space group is $Pmn2_1$, and Bertaut's theorem clearly demonstrates that only two magnetic structures in which ferro- and antiferromagnetic moments coexist are possible. The antiferromagnetic structure has been unambiguously refined, however, the canting was too small to be resolved with the available data.

I. INTRODUCTION

Mineral-like arsenates and phosphates are providing a rich source of new low-dimensional materials as well as a basis for engineering new compounds with designed magnetic properties.¹ The compounds $\text{NH}_4M^{\text{II}}\text{PO}_4 \cdot \text{H}_2\text{O}$, M^{II} being a first-row transition metal, were first reported in 1864.² A powder x-ray-diffraction study on $\text{NH}_4\text{CoPO}_4 \cdot \text{H}_2\text{O}$ (Ref. 3) showed the compound to have a layered structure. The complete crystal structure, including the conformation of the NH_4 and the position of the H_2O molecules, was carried out by means of neutron-diffraction profile refinements.⁴ We found also that the Mn, Fe, Ni, and Co compounds of this series show an interesting range of low-dimensional properties, especially the Mn, Fe compounds which are weak ferromagnets.^{5,6} These materials also form the parent structure for alkyl phosphate and phosphonate materials, in which the interlayer spacing is increased, modifying the anisotropy parameters.^{7–9}

In this paper we report the structural and magnetic characterization of $\text{KMnPO}_4 \cdot \text{H}_2\text{O}$. The magnetic structure is discussed in connection with its static magnetic properties.

II. EXPERIMENT

$\text{KMnPO}_4 \cdot \text{H}_2\text{O}$ was prepared by precipitation from aqueous solution by addition of a solution of MnSO_4 to a large excess of concentrated K_2HPO_4 .

Powder neutron-diffraction data were obtained at 300 K and 1.7 K using the powder diffractometer D2B at the Institut Laue Langevin, Grenoble, France. The wavelength used was 1.594 Å. The crystal and magnetic structures were refined using the Rietveld method.⁴

The magnetization measurements were carried out in magnetic fields up to 6.5 T using an extraction method.

III. CRYSTAL STRUCTURE

The crystal structure was solved using the Rietveld profile method. The initial positional parameters were taken from the isomorphous compound $\text{NH}_4\text{CoPO}_4 \cdot \text{H}_2\text{O}$, K replacing the NH_4 group while the protons of H_2O were accommodated according to the symmetry of space group $Pmn2_1$. The initial unit cell parameters were obtained from x-ray powder-diffraction and further refined using the neutron diffraction profiles. Their values are $a = 5.6767(3)$ Å, $b = 8.3358(4)$ Å, and $c = 4.9057(2)$ Å at 300 K and $a = 5.6646(2)$ Å, $b = 8.2945(3)$ Å, and $c = 4.8891(2)$ Å at 1.7 K, respectively. No structural phase change has been observed between 300 and 1.7 K. The positional parameters of $\text{KMnPO}_4 \cdot \text{H}_2\text{O}$ at both temperatures are given in Table I. The neutron-diffraction profile at 1.7 K, Fig. 1, shows that there is a good agreement between the observed and calculated profile using space group $Pmn2_1$. The intensity (I^2) R factors are 6.28 (nuclear) and 2.89 (expected) for the 300-K data set and 5.96 (nuclear), 9.75 (magnetic) and 2.6 (expected) for the 1.7 K one.

TABLE I. Structural parameters of KMnPO₄·H₂O.

	x	y	z	B _{iso}
K ⁺	0	0.537(1)	0.127(3)	2.4(2)
	0	0.5391(7)	0.134(2)	0.9(1)
Mn	0	−0.017(1)	0.014(5)	0.9(1)
	0	−0.0199(8)	0.0075(9)	0.51(9)
P	0	0.2166(7)	−0.417(2)	1.1(1)
	0	0.2113(6)	−0.4222(1)	1.03(9)
O(1)	0	0.1814(7)	−0.728(2)	1.6(1)
	0	0.1818(6)	−0.7386(2)	0.89(7)
O(2)	0	0.3962(7)	−0.368(2)	1.8(1)
	0	0.3930(9)	−0.3571(1)	0.60(6)
O(3)	0.2191(1)	0.1331(4)	−0.280(2)	1.54(7)
	0.2207(4)	0.1269(4)	−0.2832(1)	0.87(5)
O(4)	0	−0.2245(6)	−0.301(2)	1.7(1)
	0	−0.2161(5)	−0.2930(2)	1.05(7)
H	0.136(1)	−0.207(1)	−0.417(3)	3.9(2)
	0.1396(8)	−0.1986(8)	−0.4065(2)	2.4(1)

*The first line of parameters of each atom corresponds to the 300 K positions and the second line to the 1.7 K ones, respectively.

IV. DESCRIPTION OF THE CRYSTAL STRUCTURE

The structure, (Fig. 2) is formed by sheets of MnO₆ corner-sharing octahedra cross linked by phosphate tetrahedra. These sheets are separated by layers of K⁺ ions. The metal octahedra are highly distorted. The geometry of the metal octahedra is determined by the phosphate group which distorts the O—Mn—O bond angles significantly from 90°. The four Mn—O bonds, $d_{\text{Mn-O}(3)} = 2.22 \text{ \AA}$ (2×) and $d_{\text{Mn-O}(3)} = 2.05 \text{ \AA}$ (2×), responsible for the cross linking in the sheets are coplanar within experimental error. One axial oxygen is provided by a PO₄ group, $d_{\text{Mn-O}(2)} = 2.06 \text{ \AA}$, and is consequently considerably displaced from the normal to the equatorial plane. The remaining axial vertex is provided by the coordinated water,

$d_{\text{Mn-O}(4)} = 2.17 \text{ \AA}$, and lies on the normal through the metal atom to the plane.

V. MAGNETIC CHARACTERIZATION

An initial magnetic characterization of KMnPO₄·H₂O has been performed by means of static magnetization measurements. The static magnetic susceptibility was measured between 2.0–300 K in an applied magnetic field of 1.0 and 0.068 T (Fig. 3).

In the range 75–300, the 1/χ plot (Fig. 3) shows that the magnetic susceptibility of KMnPO₄·H₂O follows the Curie–Weiss law down to 75 K, with $C = 4.73(6) \text{ emu K·mol}^{-1}$ and $\theta = -61(2) \text{ K}$. Below 75 K, the susceptibility deviates from this simple model and shows a broad maximum in the susceptibility at $T(\chi_{\text{max}}) = 27(2) \text{ K}$, which suggests the presence of two-dimensional magnetic interactions. The susceptibility increases again below 20 K. The magnetic susceptibility as well as the sublattice magnetization indicates a T_N of about 18(1) K. The increase of the susceptibility below T_N indicates also the presence of a weak ferromagnetic moment. Down to 8 K this behavior resembles the weak ferromagnetism observed in NH₄FePO₄·H₂O while below 8 K the magnetic susceptibility increases further till it starts to decrease at 2.1 K. The possibility that this might be due to a magnetic impurity was eliminated by repeating the measurement on a separately prepared sample, which showed exactly the same behavior.

The intraplanar superexchange can be estimated from the Curie–Weiss temperature θ through the molecular-field theory which predicts

$$J/k = -3\theta/2zS(S+1). \tag{1}$$

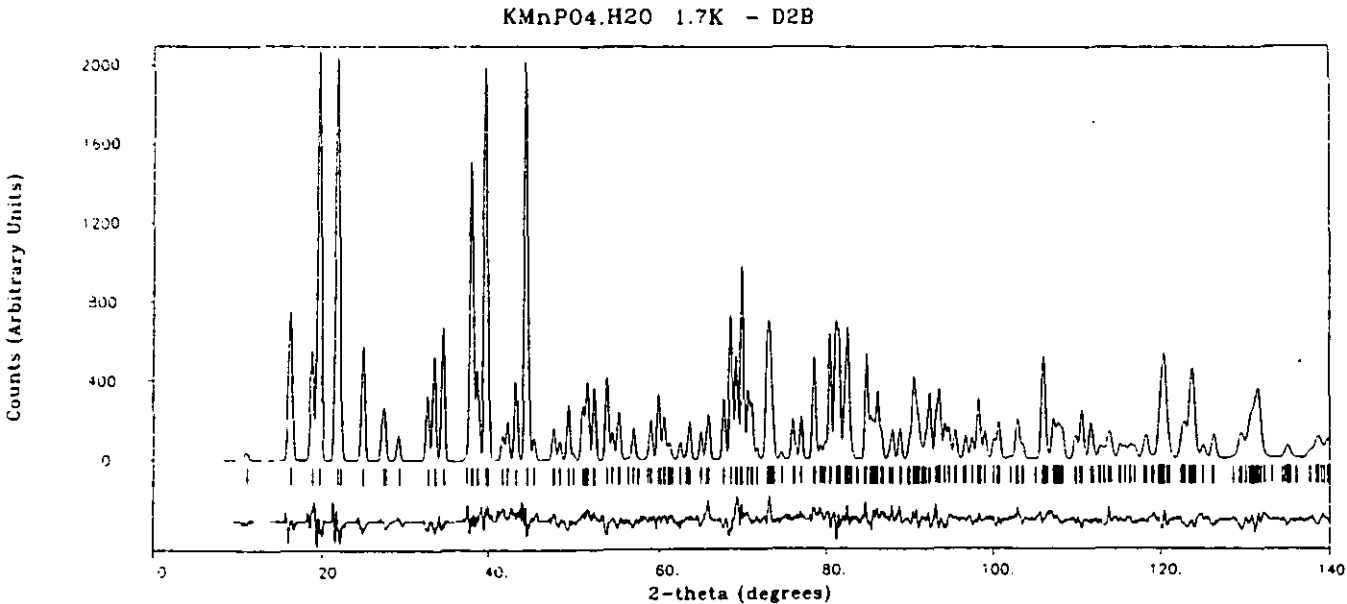


FIG. 1. The neutron-diffraction profile of KMnPO₄·H₂O at 1.7 K. The points are the observed profile. The full line represents the calculated nuclear and magnetic profile. The vertical bars mark the *hkl* reflections. The difference plot is also shown.

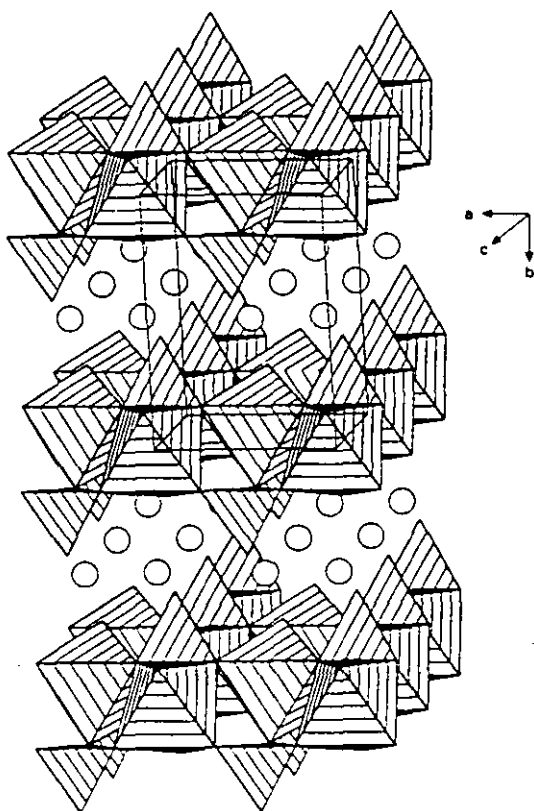


FIG. 2. A STRUPLO '84 representation of the crystal structure of $\text{KMnPO}_4 \cdot \text{H}_2\text{O}$. The circles represent the K^+ ions. The octahedra and tetrahedra represent the Mn^{II}O_6 and PO_4 units.

Taking $z = 4$, $\theta = -61(2)$ K using Eq. (1) gives $J/k = -2.6(1)$ K. A more physical estimate for a square lattice Heisenberg antiferromagnet can be calculated from the temperature at which the maximum in the magnetic susceptibility occurs:¹¹ $J/k = T(\chi_{\text{max}})/2.07S(S+1)$ giving $J/k = -1.5$ K.

VI. MAGNETIC STRUCTURE

The extra intensity in the 1.7-K neutron-diffraction profile is entirely due to magnetic scattering. The extra reflections can be indexed on the nuclear unit cell. Applying Bertaut's method¹⁰ of irreducible representations to the space group $Pmn2_1$ it is found that only two spin arrangements are possible that have a weak ferromagnetic component, namely A_1F_2 and F_1A_2 . Comparison of these models with the experimentally observed reflections shows clearly that the former is correct in this instance, corresponding to the spin structure shown in Fig. 3, with a cooperative canting towards the crystallographic c axis. This mode, corresponding to

$$\begin{pmatrix} 0 & 0 & 0 \\ 0 & -1 & 0 \\ 0 & 0 & 1 \end{pmatrix},$$

was refined to give the moment vector $[0, 4.16(3), 0]$. The canting is too small to be resolved from powder data.

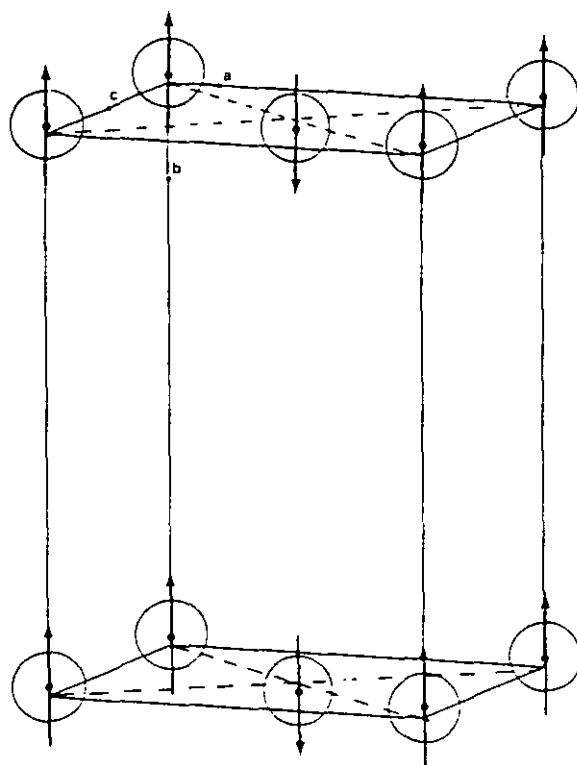


FIG. 3. The antiferromagnetic structure of $\text{KMnPO}_4 \cdot \text{H}_2\text{O}$.

The variation of sublattice magnetization with temperature as shown by the intensity of the magnetic reflections showed no evidence for the existence of the magnetic phase transition found at 8 K in the susceptibility data. It is possible therefore that this phase transition and the weak ferromagnetic behavior are field induced.

ACKNOWLEDGMENTS

The authors wish to thank Dr. J. K. Cockcroft for technical support and assistance during the neutron-scattering experiments. Two of us (D. V. and S. G. C.) would also like to thank the U.K. SERC for financial support.

- ¹S. T. Bramwell, A. M. Buckley, D. Visser, and P. Day, *Phys. Chem. Minerals* **15**, 465 (1988).
- ²M. H. Debray, *C. R. Acad. Sci.* **59**, 40 (1864).
- ³D. Tranqui, A. Durif, J. C. Guitel, and M. T. Averbuch-Pouchet, *Bull. Soc. Min. Cryst.* **91**, 10 (1986).
- ⁴H. M. Rietveld, *J. Appl. Cryst.* **2**, 65 (1969).
- ⁵S. G. Carling, Chemistry Part II thesis, Oxford University, 1987; S. G. Carling, P. Day, and D. Visser, *Acta Cryst. A* **46** (Suppl.), C278 (1990).
- ⁶J. E. Greedan, K. Reubenbauer, T. Birchall, M. Ehler, D. R. Corbin, and M. A. Subramanian, *J. Solid State Chem.* **77**, 376 (1988).
- ⁷G. Cao, H. Lee, V. M. Lynch, and T. E. Mallouk, *Solid State Ionics* **26**, 63 (1988).
- ⁸D. Cunningham, P. J. D. Hennelly, and T. Deeney, *Inorg. Chim. Acta* **37**, 95 (1979).
- ⁹D. Visser, S. G. Carling, and R. K. Kremer, (unpublished).
- ¹⁰R. L. Carlin, *Magneto-Chemistry* (Springer, Berlin, 1986), p. 187.
- ¹¹E. F. Bertaut, *Acta Cryst. A* **24**, 217 (1968).

Solid State Communications, Vol. 88, No. 2, pp. 135–138, 1993.
Printed in Great Britain.

0038–1098/93 \$6.00 + .00
Pergamon Press Ltd

DIMENSIONALITY CROSSOVERS IN THE MAGNETIZATION OF THE CANTED ANTIFERROMAGNETS $\text{NH}_4\text{MnPO}_4\cdot\text{H}_2\text{O}$ AND $\text{ND}_4\text{MnPO}_4\cdot\text{D}_2\text{O}$

S.G. Carling and P. Day

The Royal Institution of Great Britain, 21, Albemarle Street, London W1X 4BS
and

D. Visser

Physics Department, Loughborough University of Technology, Loughborough LE11 3TU, UK

(Received 27 April 1993 by P. Burlet)

Dedicated to Erwin Bertaut on his 80th Birthday

Critical exponents of the magnetization below T_N measured by SQUID magnetometry and neutron diffraction are reported for the two-dimensional canted antiferromagnets $\text{NH}_4\text{MnPO}_4\cdot\text{H}_2\text{O}$ and $\text{ND}_4\text{MnPO}_4\cdot\text{D}_2\text{O}$. Both compounds exhibit a crossover in the power law dependence of magnetization on temperature. In the former we find β_1 0.21(3), β_2 0.40(7), T_N 17.5(1) K; in the latter β_1 0.20(1), β_2 0.39(4), T_N 17.5(3) K. The crossover between the two exponents occurs at a reduced temperature of 0.07(1) in the hydrogenated compound and 0.030(5) in the deuterated one. The values of β_1 are compared with those predicted by two dimensional (2D) models of exchange and the change from β_1 to β_2 is attributed to a crossover in lattice dimensionality from $2d$ – $3d$.

1. INTRODUCTION

Low dimensional magnets have provided valuable examples for testing models of magnetic critical behaviour. The series of compounds $\text{M}^{\text{I}}\text{M}^{\text{II}}\text{PO}_4\cdot\text{H}_2\text{O}$ ($\text{M}^{\text{I}} = \text{NH}_4, \text{K}$; $\text{M}^{\text{II}} = \text{Mn, Fe, Co, Ni}$) is of interest because it has strongly defined layer crystal structure in which the divalent metal ions form approximately square planar sheets perpendicular to the crystallographic b -axis [1]. This leads to 2D antiferromagnetic interactions between these ions. In particular, the magnetic structures of the manganese and iron compounds of the series are not simple collinear antiferromagnets, but show pronounced canting, leading to weak ferromagnetism at low temperature [2, 3]. In these materials, the underlying antiferromagnetic structure consists of spins aligned parallel to the b -axis. Analysis by Bertaut's method of irreducible representations [4] shows that the ferromagnetic components of the moments must lie parallel to the c -axis.

The critical behaviour of such weak ferromagnets has not, to our knowledge, been reported before, so the present note presents data on the magnetization of $\text{NH}_4\text{MnPO}_4\cdot\text{H}_2\text{O}$ and its deuterated analogue in the temperature range below T_N . In the former,

nominally zero field magnetization was measured by SQUID magnetometry while in the latter powder neutron diffraction gave similar information. The transition from predominantly 2D to 3D interaction has been observed in several cases by a change in the critical exponent β of magnetization vs reduced temperature ε , defined by $\varepsilon = (T_N - T)/T_N$, but no examples of such crossovers in low dimensional canted phases appear to have been reported. In the present instance we have observed a crossover in β close to the 3D ordering temperature T_N .

2. EXPERIMENTAL

2.1. Synthesis and characterization

Starting materials were of analytical grade and were used without further purification. Deuterated starting materials were obtained from MSD Isotopes. $\text{NH}_4\text{MnPO}_4\cdot\text{H}_2\text{O}$ was prepared by precipitation from aqueous solution using a method derived from that of Bassett and Bedwell [5]. A 0.5 M solution of the metal chloride was added to a 10 M excess of saturated $(\text{NH}_4)_2\text{HPO}_4$ solution. The resulting precipitate was digested at $85 \pm 5^\circ\text{C}$ for 24–48 h, after which the microcrystalline product was filtered off,

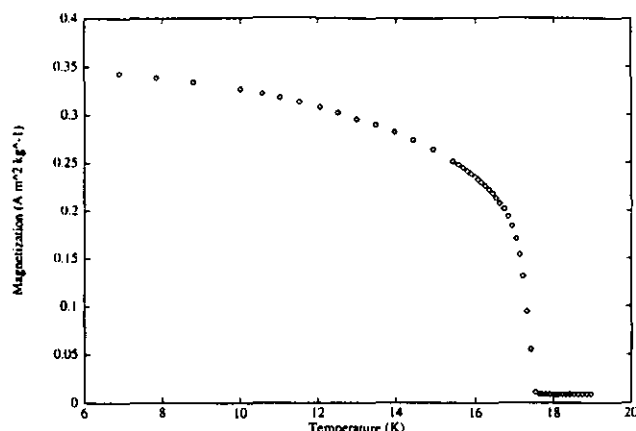
CANTED ANTIFERROMAGNETS $\text{NH}_4\text{MnPO}_4\cdot\text{H}_2\text{O}$ AND $\text{ND}_4\text{MnPO}_4\cdot\text{D}_2\text{O}$ Vol. 88, No. 2

Fig. 1. Temperature dependence of magnetization of $\text{NH}_4\text{MnPO}_4\cdot\text{H}_2\text{O}$, in a field of 50–100 G.

washed with deionized water and dried *in vacuo*. $\text{N}_2\text{H}_4\cdot\text{H}_2\text{SO}_4$ was added to all solutions to prevent aerobic oxidation of the divalent metal ion in the extremely basic conditions. Since the damp product is prone to oxidation, the filtration was carried out under nitrogen. The per-deuterated analogue of $\text{NH}_4\text{MnPO}_4\cdot\text{H}_2\text{O}$ was prepared by a similar method to that described above. All manipulations of solutions or damp products were performed in a glove box purged with dry nitrogen.

Elemental analyses were carried out by the Microanalysis Service of the Inorganic Chemistry Laboratory, Oxford. For $\text{NH}_4\text{MnPO}_4\cdot\text{H}_2\text{O}$, Mn 29.39% (29.54%), N 7.45% (7.53%), H 3.30% (3.25%); for $\text{ND}_4\text{MnPO}_4\cdot\text{D}_2\text{O}$, Mn 28.36% (28.48%), N 7.20% (7.26%). Powder X-ray diffraction profiles were recorded using $\text{Cu-K}\alpha$ radiation by a Phillips PW1710 diffractometer. Samples were mounted on aluminium plates; in the case of the deuterated material, a cell designed for use with air sensitive samples was used, the sample being loaded under nitrogen. Unit cell refinement was carried out with the Dragon and Cellref programs written by J.K. Cockcroft [6]. The observed reflections were indexed on an orthorhombic unit cell of space group $Pmn2_1$. For $\text{NH}_4\text{MnPO}_4\cdot\text{H}_2\text{O}$ the lattice parameters were refined to $a = 5.731(3)$ Å, $b = 8.815(4)$ Å, $c = 4.905(2)$ Å; for $\text{ND}_4\text{MnPO}_4\cdot\text{D}_2\text{O}$, $a = 5.735(3)$ Å, $b = 8.824(5)$ Å, $c = 4.909(2)$ Å.

2.2. Magnetic measurements

Magnetization data was collected on a CCL S600 SQUID magnetometer. Sample temperature was controlled and recorded using a Lakeshore DRC19C temperature controller. Samples were weighed in small quartz buckets, for which a diamagnetic correction was applied to the measured

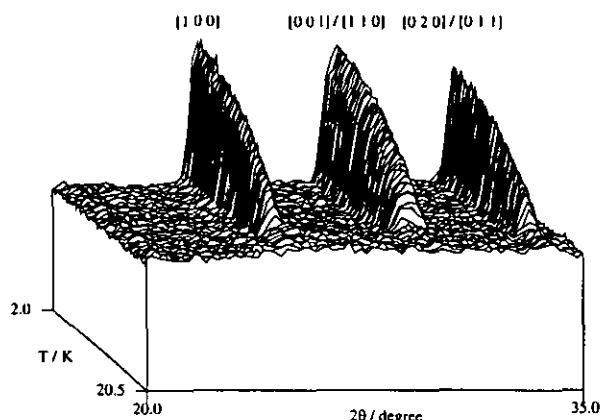


Fig. 2. Low-angle reflections of $\text{ND}_4\text{MnPO}_4\cdot\text{D}_2\text{O}$ as a function of temperature.

magnetization data after collection. The quartz bucket was attached with PTFE tape to a copper wire on the sample rod. The decay of magnetization as $T \rightarrow T_N$ was measured in the following manner: first the sample was cooled in a field of 1.0 kG to ensure a non-zero magnetization; the field was then reduced to zero, and the temperature increased in steps of 0.1 K in the vicinity of T_N . The temperature dependence of the magnetization of $\text{NH}_4\text{MnPO}_4\cdot\text{H}_2\text{O}$ is shown in Fig. 1. T_N is defined at 17.5(1) K.

Neutron powder diffraction profiles of $\text{ND}_4\text{MnPO}_4\cdot\text{D}_2\text{O}$ were measured as a function of temperature on the multidetector diffractometer D1B at the Institut Laue-Langevin, Grenoble. Results are shown in Fig. 2. As the temperature of the sample approached T_N , the background intensity near the magnetic reflections increased, due to inelastic scattering from the long wavelength spin fluctuations which are present in the vicinity of T_N , and also diffuse scattering due to short-range order above T_N .

The [100] and [001] reflections are purely magnetic, as they are systematic absences of space group $Pmn2_1$. Nuclear and magnetic scattering contribute to the intensity of the [110] and [011] reflections although the nuclear component is weak, and the [020] reflection is purely nuclear.

The intensity of the magnetic [100] reflection was fitted at each measurement temperature by a Gaussian peak on a parabolic background using the program ABFit [7]. The temperature dependence of the intensity determined in this way is shown in Fig. 3. As the intensity of the magnetic Bragg scattering falls on approaching T_N , it cannot be distinguished from the Gaussian component in the scattering from the increased background. However, the ordering temperature of $\text{ND}_4\text{MnPO}_4\cdot\text{D}_2\text{O}$ was

Vol. 88, No. 2 CANTED ANTIFERROMAGNETS $\text{NH}_4\text{MnPO}_4\cdot\text{H}_2\text{O}$ AND $\text{ND}_4\text{MnPO}_4\cdot\text{D}_2\text{O}$

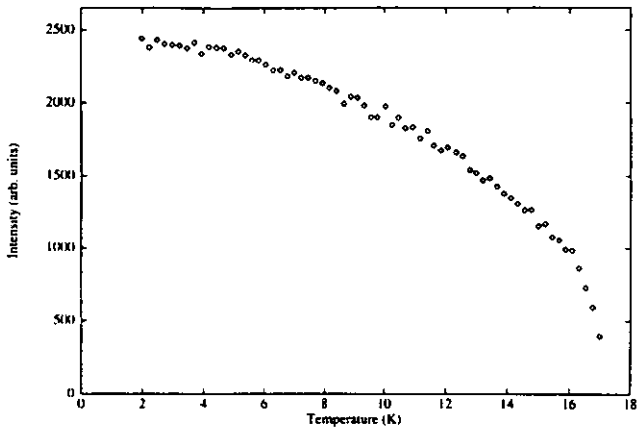


Fig. 3. Intensity of the [100] reflection of $\text{ND}_4\text{MnPO}_4\cdot\text{D}_2\text{O}$ as a function of temperature.

estimated as $T_N = 17.5(3)$ K, in good agreement with that determined for $\text{NH}_4\text{MnPO}_4\cdot\text{H}_2\text{O}$ from the bulk magnetization measurements described above.

3. ESTIMATION OF CRITICAL EXPONENTS

The temperature dependence of both the magnetic reflections measured on D1B and the magnetization measured on the S600 SQUID magnetometer can be used in principle to investigate the critical behaviour of $\text{NH}_4\text{MnPO}_4\cdot\text{H}_2\text{O}$ and its deuterated analogue. The magnetization is expected to follow the form

$$M(\epsilon) = M_0 \epsilon^\beta \tag{1}$$

in the critical region, where ϵ is the reduced temperature

$$\epsilon = \frac{T_N - T}{T_N}.$$

Figure 4 shows the best-fits to the sublattice magnetization of $\text{ND}_4\text{MnPO}_4\cdot\text{D}_2\text{O}$ and the weak ferromagnetic moment of $\text{NH}_4\text{MnPO}_4\cdot\text{H}_2\text{O}$. The magnitude of the [100] intensity has been scaled so that both datasets may be displayed on the same axes. In both cases the values of the critical exponents β change as $\epsilon \rightarrow 0$. Values of the exponents and the reduced temperatures ϵ_{xo} at which the crossover occurs are listed in Table 1.

4. DISCUSSION

Before considering the values of β listed in Table 1, it is important to note potential sources of error in the experimental data. First, in addition to diffraction from the antiferromagnetic sublattices, at temperatures close to T_N the neutron scattering intensity has contributions from critical scattering, indicated in the present case by the broad parabolic feature in the

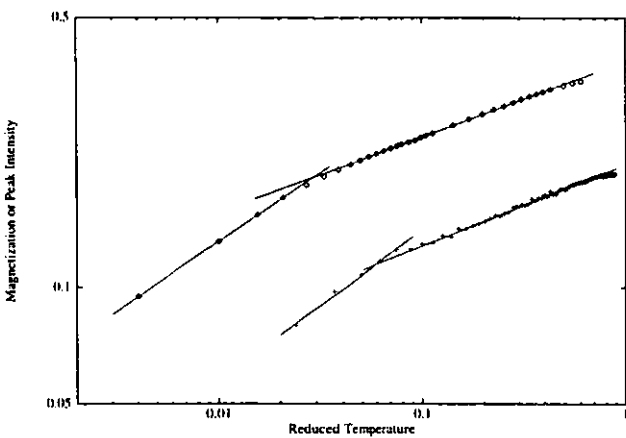


Fig. 4. Sublattice magnetization of $\text{ND}_4\text{MnPO}_4\cdot\text{D}_2\text{O}$ (+) and the weak ferromagnetic moment of $\text{NH}_4\text{MnPO}_4\cdot\text{H}_2\text{O}$ (o) in the critical region. Lines represent fits to the power law.

background. Second, whilst the bulk magnetization measurements were carried out in nominally zero field, the presence of a small non-zero moment above T_N shows clearly that a net field was present as a result of flux trapping in the superconducting magnet. By comparison of the moment in the paramagnetic phase with bulk susceptibility measurements on the same sample, we estimate that the remanent field was 50–100 G.

Further, neither the neutron diffraction nor the bulk susceptibility measurements were made at unambiguously fixed temperatures. In a thermodiffraction experiment, the temperature is continuously ramped from base temperature to $T > T_N$, so that the profiles are measured over a range of temperatures $T = T_i \pm \delta$, where T_i is the nominal temperature of the i th dataset, calculated by averaging the initial and final temperatures of the measurement. In the case of the bulk magnetization experiment, each measurement was performed at a single set temperature T_s , data collection begins when two thermocouples are sufficiently close in temperature both to each other and to T_s . For each data point, four measurements are made and the results averaged. For the present purposes, the temperature of the data point was taken to be the average of the initial and final

Table 1. Critical parameters of $\text{ND}_4\text{MnPO}_4\cdot\text{D}_2\text{O}$ and $\text{NH}_4\text{MnPO}_4\cdot\text{H}_2\text{O}$

Compound	β_1	β_2	ϵ_{xo}
$\text{NH}_4\text{MnPO}_4\cdot\text{H}_2\text{O}$	0.20(1)	0.39(4)	0.030 ± 0.005
$\text{ND}_4\text{MnPO}_4\cdot\text{D}_2\text{O}$	0.21(3)	0.40(7)	0.07 ± 0.01

CANTED ANTIFERROMAGNETS $\text{NH}_4\text{MnPO}_4\cdot\text{H}_2\text{O}$ AND $\text{ND}_4\text{MnPO}_4\cdot\text{D}_2\text{O}$ Vol. 88, No. 2

temperatures measured by the thermocouple closer to the sample.

All these factors contribute to a larger error in the estimates of β_2 than β_1 , as the data from which the former were determined is not only the most sensitive to the errors which were present but also (at least for the thermodiffraction results) prone to errors which were not present at lower temperatures.

Although the value found for β_1 does not correspond to any of those expected for the standard magnetic model systems, values of $\beta \simeq 0.22$ have been found for several 2d Heisenberg systems. Recent work by Bramwell and Holdsworth [8] on 2D Heisenberg systems with varying degrees of XY-type anisotropy shows that $\beta = 0.23$ is a characteristic of such systems. In several cases, crossovers have been observed to regimes with $\beta \geq 0.3$. For example the quadratic Heisenberg antiferromagnet $\text{Cu}(\text{HCOO})_2\cdot 4\text{D}_2\text{O}$ (CFTD) has been studied by ^1H NMR [9] and found to show a crossover from $\beta = 0.22(2) \rightarrow \beta = 0.30(1)$ at a reduced temperature $\varepsilon \simeq 0.06$. Elastic neutron scattering measurements on the perdeuterated analogue of CFTD confirm this result [10]. Measurements on K_2CuF_4 show similar behaviour [11]. The compound $\text{Mn}(\text{HCOO})_2\cdot 2\text{D}_2\text{O}$ is also a quadratic Heisenberg antiferromagnet, though it contains two distinct planes of Mn^{II} ions: the "A" layer in the (100) plane and the "B" layer in the (200) plane. The "A" layer orders antiferromagnetically, whereas the "B" layer remains paramagnetic. A ^1H NMR study [12] showed a crossover from $\beta = 0.22 \pm 0.01 \rightarrow \beta = 0.31 \pm 0.02$ at $\varepsilon \simeq 0.02$.

In the present instance, the values of β_2 are approximately 0.4 for both hydrogenous and deuterated compounds. Theoretical predictions of the value of β for 3D systems are ~ 0.31 for the Ising model, ~ 0.33 for the XY model and ~ 0.35 for the Heisenberg model. The most likely explanation for the observed behaviour is therefore a lattice-dimensionality crossover from $d = 2 \rightarrow d = 3$.

The crossover temperature ε_{xo} in $\text{ND}_4\text{MnPO}_4\cdot\text{D}_2\text{O}$ is less than half that for $\text{NH}_4\text{MnPO}_4\cdot\text{H}_2\text{O}$, whilst their b -parameters differ by only ~ 0.01 Å. A possible explanation for this difference is that the weak remanent field in which the magnetization measurements were performed is influencing the crossover – the thermodiffraction data were of course collected in the absence of an external field.

Acknowledgements — We thank SERC for partial support, the Institut Laue-Langevin for access to neutron beam time, Jeremy K. Cockcroft for technical assistance and Andrew Harrison for useful discussions.

REFERENCES

1. D. Tranqui, A. Durif, J.-C. Guitel & M.T. Averbuch-Pouchot, *Bull. Soc. fr. Minéral. Cristallogr.* **91**, 10 (1968).
2. S.G. Carling, P. Day & D. Visser, *Acta Cryst.* **A46**, (Suppl.) C-278 (1990).
3. D. Visser, S.G. Carling, P. Day & J. Déportes, *J. Appl. Phys.* **69**, 6016 (1991).
4. E.F. Bertaut, *Acta Cryst.* **A24**, 217 (1968).
5. H. Bassett & W.L. Bedwell, *J. Chem. Soc.* **1933**, 137.
6. J.K. Cockcroft, Personal communication.
7. A. Antoniadis, J. Berruyer & A. Filhol, *Affinement de Spectres de Diffraction de Poudre par la Méthode du Maximum de Vraisemblance*, ILL Report 87AN20T (1987).
8. S.T. Bramwell & P.C.W. Holdsworth *J. Phys.: Condens. Matter* **5**, L53 (1993).
9. K. Koyama, H. Nobumasa & M. Matsuura, *J. Phys. Soc. Jpn* **56**, 1553 (1987).
10. S.J. Clarke, A. Harrison, T.E. Mason, G.J. McIntyre & D. Visser, *J. Phys. Cond. Matter* **4** (1992).
11. H. Ikeda & K. Hirakawa, *J. Phys. Soc. Jpn* **33**, 393 (1972).
12. K. Koyama, N. Terata & M. Matsuura, *J. Phys. Soc. Jpn* **56**, 1553 (1987).

J. Phys.: Condens. Matter 7 (1995) L109–L113. Printed in the UK

LETTER TO THE EDITOR

Dimensionality crossovers in the magnetization of the weakly ferromagnetic two-dimensional manganese alkylphosphonate hydrates $\text{MnC}_n\text{H}_{2n+1}\text{PO}_3\cdot\text{H}_2\text{O}$, $n = 2\text{--}4$

S G Carling[†], P Day[†] and D Visser[‡]

[†] The Royal Institution, 21 Albemarle Street, London W1X 4BS, UK

[‡] Physics Department, Loughborough University of Technology, Loughborough LE11 3TU, UK

Received 16 January 1995

Abstract. Critical exponents of magnetization β below T_N in the weakly ferromagnetic layer compounds $\text{MnC}_n\text{H}_{2n+1}\text{PO}_3\cdot\text{H}_2\text{O}$ have been measured by SQUID magnetometry for $n = 2\text{--}4$. In all three compounds crossovers are observed in β as follows (β_1 , β_2): 0.21(2), 0.73(2) ($n = 2$); 0.18(1), 0.42(6) ($n = 3$); 0.18(1), ~ 0.6 ($n = 4$). The crossover occurs at values of the reduced temperature $\epsilon = (T_N - T)/T_N$ that become smaller as the separation between the magnetic layers increases.

Low-dimensional inorganic and metal-organic compounds have proved valuable in testing models of magnetic critical behaviour in lattices containing localized exchange-coupled moments (de Jongh and Miedema 1974). However, very few such compounds show finite spontaneous magnetization because ferromagnetic exchange between localized moments is quite rare. To our knowledge the only examples known belong to the layer perovskite family $(\text{RNH}_3)_2\text{MX}_4$ with $\text{M} = \text{Cr}$ (Bellitto and Day 1992) or Cu (de Jongh 1976). An alternative strategy for creating low-dimensional lattices with finite zero-field magnetization is to synthesize compounds in which the metal ions occupy lattice sites of low symmetry so that, although the near-neighbour exchange interaction may be antiferromagnetic, it competes with strong single-ion anisotropy brought about by second-order spin-orbit coupling. Then the equilibrium distribution of moments is not collinear but canted, leading to a weak ferromagnetic moment along one axis. We have been investigating an extensive series of compounds of this type, $\text{M}^{\text{I}}\text{M}^{\text{II}}\text{PO}_4\cdot\text{H}_2\text{O}$ ($\text{M}^{\text{I}} = \text{NH}_4$, K ; $\text{M}^{\text{II}} = \text{Mn}$, Fe , Co , Ni) (Carling *et al.*, to be published) and the related compounds in which the $\text{M}^{\text{II}}\text{--PO}_4\text{--H}_2\text{O}$ layers are separated, not by M^{I} , but by organic groups (Carling *et al.* 1993). In the latter, varying the chain length of an alkyl group leads to wide variation in the interlayer spacing. For example in $\text{MnCH}_3\text{PO}_3\cdot\text{H}_2\text{O}$ it is 8.82 Å and in $\text{MnC}_4\text{H}_9\text{PO}_3\cdot\text{H}_2\text{O}$ 14.71 Å. Like the ternary metal phosphate hydrates, the alkylphosphonate hydrates are canted antiferromagnets, and hence behave as weak ferromagnets. We studied the critical behaviour of the magnetization of $\text{NH}_4\text{MnPO}_4\cdot\text{H}_2\text{O}$ and its deuterated analogue by a combination of neutron diffraction and bulk magnetometry, finding that the critical exponent β of the magnetization below T_N underwent a crossover from a value of 0.20 when the reduced temperature $\epsilon = (T_N - T)/T_N$ was $>0.03\text{--}0.07$ to a much higher value (0.39–0.40) on approaching T_N (Carling *et al.* 1993). We have therefore examined the alkylphosphonates to see whether there is a corresponding crossover and if so, how it varies with interlayer spacing.

Letter to the Editor

The samples were prepared by the method described by Carling *et al* (1993); all had satisfactory chemical analyses. The variation of magnetization with temperature was measured on polycrystalline samples using a CCL 5600 SQUID magnetometer at the Inorganic Chemistry Laboratory, Oxford. The samples were loaded into quartz buckets suspended on a copper wire. Measurements were made as close as possible to zero field by applying alternately positive and negative fields of successively decreasing magnitude, beginning from a field of 1 kG. In this way the remanent field of the magnet is diminished.

Figures 1(a)–(c) show the magnetization data for the $n = 2$ –4 Mn alkylphosphonate compounds subtracting the appropriate diamagnetism corrections, while figures 2(a)–(c) present the same data in logarithmic form on a reduced scale. In the latter case, data more remote from T_N obey the relationship $M_\epsilon = M_0\epsilon^\beta$ with β in the region of 0.20 for all three compounds. Least squares fitted values of β_1 are listed in table 1. However, as T_N is approached from below the exponential relationship changes and a much higher β exponent becomes evident. The value of β_1 is close to that found in $M^I\text{MnPO}_4\cdot\text{H}_2\text{O}$ ($M^I = \text{NH}_4, \text{ND}_4, \text{K}$ (Carling *et al* 1993)). Our first important conclusion is that a figure of ~ 0.20 for β is far from any of the estimates of [2d] or [3d] magnetic models. Thus in [3d] the Ising, XY and Heisenberg models predict respectively 0.31, 0.33 and 0.35 while the [2d] Ising model predicts 0.125 (de Jongh and Miedema 1974). However, it is important to note that, from an experimental point of view, ^1H NMR measurements on the quadratic layer Heisenberg antiferromagnet $\text{Cu}(\text{HCOO})_2\cdot 4\text{D}_2\text{O}$ give $\beta_1 = 0.22(2)$ (Koyama *et al* 1987), confirmed by neutron scattering (Clarke *et al* 1992). Fluorine NMR gives a similar result for the [2d] ferromagnet K_2CuF_4 (Ikeda and Hirakawa 1972). The related compound $\text{Mn}(\text{HCOO})_2\cdot 2\text{D}_2\text{O}$, also a quadratic layer Heisenberg antiferromagnet, contains two distinct planes of Mn^{II} ions, one which orders antiferromagnetically while the other remains paramagnetic: again ^1H NMR gives $\beta_1 = 0.22(1)$, with a crossover to $\beta_2 = 0.31(2)$ at $\epsilon \sim 0.02$ (Koyama *et al* 1987). Recently, Bramwell and Holdsworth (1993) have shown how β values in the region of 0.23 can arise from a [2d] model.

Table 1. Critical exponents (β_1, β_2) and crossover temperature ϵ_{X0} in Mn phosphate and phosphonate hydrates.

	β_1	β_2	ϵ_{X0}	Interlayer spacing (Å)
$\text{KMnPO}_4\cdot\text{H}_2\text{O}$	0.23(2)	0.4(3)	0.09(1)	8.33
$\text{NH}_4\text{MnPO}_4\cdot\text{H}_2\text{O}$	0.21(3)	0.40(7)	0.07(1)	8.81
$\text{MnC}_2\text{H}_5\text{PO}_3\cdot\text{H}_2\text{O}$	0.21(2)	0.73(2)	0.085(2)	10.24
$\text{MnC}_3\text{H}_7\text{PO}_3\cdot\text{H}_2\text{O}$	0.18(1)	0.42(6)	0.015(2)	11.71
$\text{MnC}_4\text{H}_9\text{PO}_3\cdot\text{H}_2\text{O}$	0.18(1)	0.4(2)	0.010(5)	14.72

The higher temperature β_2 values in the Mn alkylphosphonates are much less well defined than β_1 because they are based on fewer data points. Still, it is clear that β_2 is much bigger than β_1 . The $M^I\text{Mn}^{II}\text{PO}_4\cdot\text{H}_2\text{O}$ compounds ($M^I = \text{NH}_4, \text{ND}_4, \text{K}$) all have $\beta_2 \sim 0.4$ (Carling *et al* 1993), equal to that in $\text{MnC}_3\text{H}_7\text{PO}_3\cdot\text{H}_2\text{O}$. In the C_2H_5 derivative, β_2 is much larger, and though there are only two data points it appears that in the C_4H_9 compound it is comparable in magnitude. Whilst the measured β_2 are larger than predicted for any of the [3d] models it seems safe to say that the crossover is a consequence of an evolution from [2d] to [3d] behaviour.

The reduced temperatures ϵ_{X0} at which the crossovers occur also vary significantly from one compound to another within the Mn phosphate (phosphonate) hydrate series.

Letter to the Editor

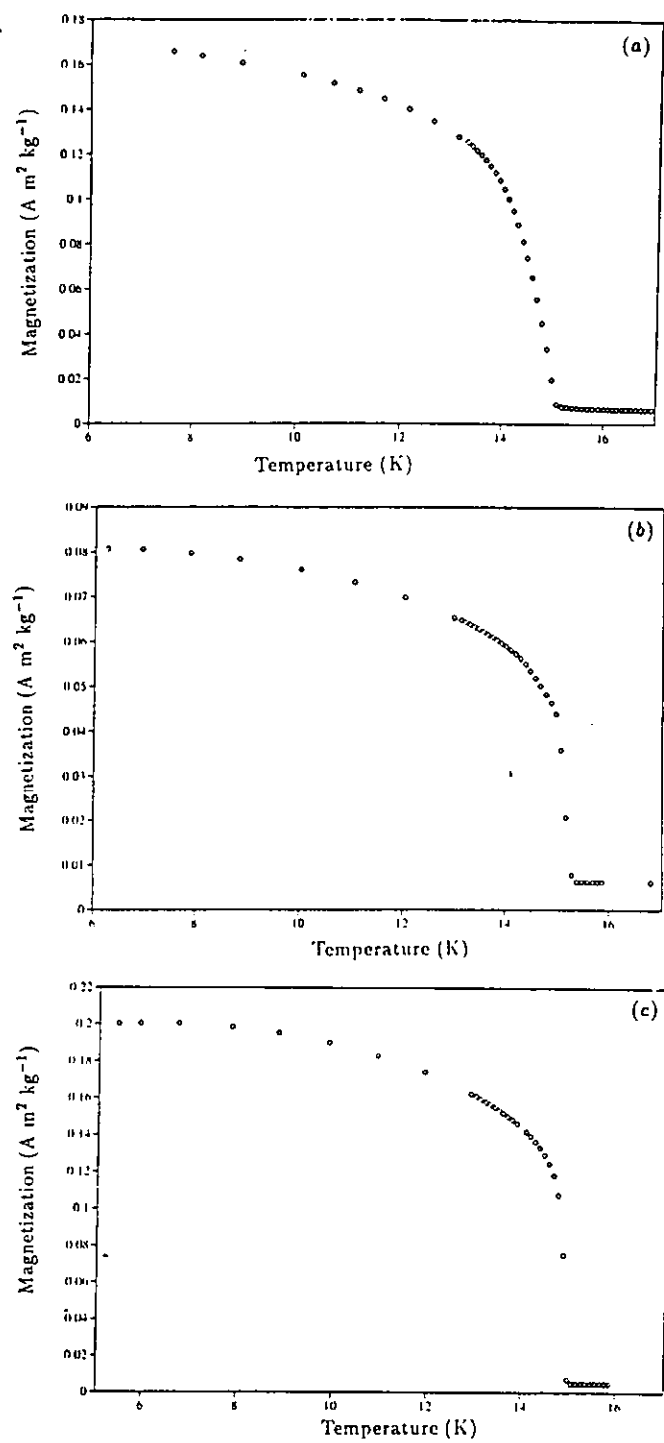


Figure 1. Temperature dependence of magnetization in $\text{MnC}_n\text{H}_{2n-1}\text{PO}_3 \cdot \text{H}_2\text{O}$: $n = 2$ (a); 3(b); 4(c).

Letter to the Editor

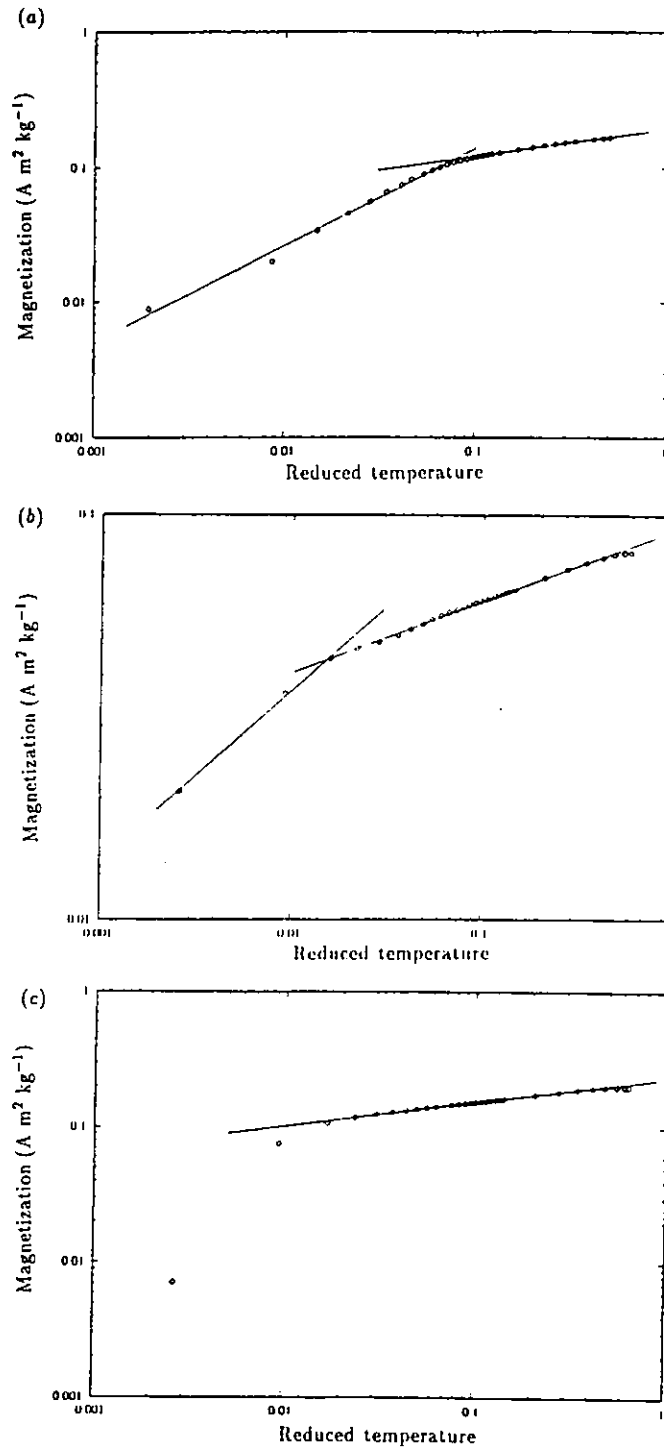


Figure 2. Exponential variation of magnetization with reduced temperature in $\text{MnC}_n\text{H}_{2n+1}\text{PO}_3 \cdot \text{H}_2\text{O}$; $n = 2$ (a); 3(b); 4(c).

Letter to the Editor

Among the M^I compounds ϵ_{X0} is a little larger in $KMnPO_4 \cdot H_2O$ (0.09(1)) than in the NH_4 compound (0.07(1)), no doubt to be correlated with the smaller interlayer separation in the former. In the alkyl phosphonates too, ϵ_{X0} decreases as the interlayer separation increases, corresponding to a decrease in the ratio of in-plane to out-of-plane exchange constants.

We believe we have presented the results of the first systematic study of the critical exponents and crossover temperatures for a series of two-dimensional weak ferromagnets. The correlations of ϵ_{X0} with interlayer separation is clear, while the values of the two exponents β_1 and β_2 do not correspond to the predictions of any of the classical models. On the other hand β_1 is close to the value 0.23 systematically invoked by the calculations of Bramwell and Holdsworth (1993).

We thank SERC for a studentship to SGC (21st Century Materials Initiative).

References

- Bellitto C and Day P 1992 *J. Mater. Chem.* **2** 265
Bramwell S T and Holdsworth P C W 1993 *J. Phys.: Condens. Matter* **5** L53
Carling S G, Day P and Visser D 1993 *J. Solid State Chem.* **106** 111
— 1992 *Solid State Commun.* **88** 135
— *Inorg. Chem.* submitted
Clarke S J, Harrison A, Mason T E, McIntyre G J and Visser D 1992 *J. Phys.: Condens. Matter* **4** L71
de Jongh L J 1976 *Physica B* **82** 247
de Jongh L F and Miedema A R 1974 *Adv. Phys.* **23** 1
Ikeda H and Hirakawa K 1972 *J. Phys. Soc. Japan* **33** 393
Koyama K, Nohumasa H and Matsura M 1987 *J. Phys. Soc. Japan* **56** 1553
Koyama K, Terata N and Matsura M 1987 *J. Phys. Soc. Japan* **56** 1553

Chapter 7.

Summary and Conclusions

This thesis describes the magnetic ordering process in different types of magnetic model systems with XY anisotropy. Changes in crystal structure and as such the dimensionality of the magnetic interactions can introduce either large differences in magnetic ordering or very subtle changes in the critical behaviour. The electronic nature of the magnetic ion determines via the crystal structure the character of the anisotropy of the system. The interplay of these three key features are discussed in detail.

In Chapter 2 the magnetic structure of the AFeX_3 halides crystallising with the hexagonal perovskite structure has been investigated. In principle these systems should show a singlet groundstate behaviour but due to superexchange coupling an induced-moment behaviour may be observed. In the latter case, due to the arrangement of the Fe^{2+} ion in the basal plane in the form of a simple hexagonal lattice, one observes a frustrated 120° type triangular ordering. In the case of the ferromagnetic chain compounds (AFeCl_3), the additional magnetic dipolar force, γ , introduces incommensurate magnetic phases which are directly related to the 120° type triangular ordering, *viz.* a helical structure ($120^\circ + \phi^\circ$) and/or a sinusoidal structure.

Due to the mixing of ferro and antiferromagnetic superexchange, the effects on the magnetic ordering were studied in $\text{RbFeCl}_{3-x}\text{Br}_x$ and $\text{RbFeBr}_{3-x}\text{Cl}_x$ as well as the doping of diamagnetic species in the system $\text{RbFe}_{1-x}\text{Mg}_x\text{Cl}_3$. The experimentally determined compositional phase diagrams were rationalised as function of $D/J(Q)$ and γ/J_2 . In all cases the long-range magnetic order is destroyed upon doping and a semi-spinglass behaviour is introduced.

The decrease of T_N as function of the doping concentration cannot be described by an MF approach for a dilute one-dimensional system. In order to explain the rapid decrease in T_N the explicit nature of the singlet groundstate to induced-moment behaviour has to be taken into account. This assumption has been verified by simulation. From these studies it is obvious that the magnetic ordering behaviour in these systems are very susceptible to small changes in the chemical nature of these compounds. To rationalise the magnetic ordering behaviour quantitative data can only be obtained by inelastic neutron scattering studies.

Chapter 3 describes the magnetic excitations in the singlet groundstate antiferromagnet CsFeBr_3 and the induced-moment antiferromagnet RbFeBr_3 . The magnetic excitations in the singlet groundstate have been described by an excitonic model (Lindgard's RPA approach) and in the case of the induced-moment system by the DCEFA approach of Suzuki. An improved description, especially when this type of system is driven close to the phase transition, from singlet groundstate to induced-moment state, can be obtained by taking spin-correlation effects into account. In this

thesis the effect of a magnetic field ($H \parallel c$) induced ordering in the magnetic excitations has been presented as well as the effect of magnetic ordering on the magnetic excitations in the induced-moment system RbFeBr_3 . The additional features induced by the structural phase transition of RbFeBr_3 at $T_{\text{ph}} = 108\text{K}$ are highlighted by a study of the soft-mode behaviour at $Q(1/3 \ 1/3 \ 1)$. The observed softening of the mode is described well within the DCEFA framework.

Chapter 4 presents the relation between magnetic behaviour and crystal structure, making use of the DCEFA theory, to correlate the behaviour between the singlet groundstate and the phase with the induced moment. In the previous chapter it was demonstrated that an applied field along the ordering direction may induce magnetic ordering. Similarly, applied pressure may also induce magnetic ordering in these AFeX_3 compounds. Small changes in the crystal structure by substitution of Rb instead of Cs in these compounds induce large effects. Similar effects might be obtained by an applied pressure on a particular AFeX_3 compound. Theoretically it has been shown that a symmetry breaking field along the a -axis has the same effect as the applied magnetic field along the c -axis. Preliminary inelastic neutron-scattering data indicate that hydrostatic pressure tends to direct CsFeCl_3 towards magnetic ordering while CsFeBr_3 becomes more singlet groundstate in character.

Chapter 5 presents experimental evidence concerning the chiral ordering in XY-like triangular antiferromagnets. The critical behaviour of the magnetic ordering process in CsMnBr_3 can be described by critical exponents of a new type of universality class as predicted by Kawamura. In this thesis it has been shown that diamagnetic doping of CsMnBr_3 results in an increase of the value of the critical exponent β from 0.19 to 0.34, indicating the loss of chiral ordering upon doping. Plumer predicted on symmetry grounds that the magneto-elastic effect would destroy chiral ordering in triangular antiferromagnets and as such would provide the definite proof for the existence of chiral ordering. Experimentally it has been verified that Plumer's predictions are correct. In the presence of an electric field the exponent β decreases from $\beta = 0.25$ to $\beta = 0.17$.

Finally, the critical behaviour of the magnetic ordering in some two-dimensional XY-like magnetic systems has been investigated. It has been shown that the quasi two-dimensional ferromagnet Rb_2CrCl_4 is an ideal realisation of the finite-sized two-dimensional XY model (characterised by $\beta = 0.23$). This system shows all aspects associated with the ordering behaviour predicted by Kosterlitz-Thouless. As the critical behaviour is driven by the magnetic fluctuations, it proved possible to find other examples of this type of system in largely different chemical compounds. In this thesis a series of quasi two-dimensional weak ferromagnets $\text{AMnPO}_4 \cdot \text{H}_2\text{O}$ have been

investigated. For $\text{KMnPO}_4 \cdot \text{H}_2\text{O}$ it has been established that the critical exponent of the sublattice magnetisation β also equals 0.23. Slight structural distortion in this series of compounds induces a cross-over from XY to Ising-like behaviour. These systems also show a clear dimensionality cross-over behaviour. The similarity between the magnetic ordering behaviour in Rb_2ClCr_4 and $\text{KMnPO}_4 \cdot \text{H}_2\text{O}$ stems from the allowed magnetic ordering of the weak ferromagnetic structure into two possible magnetic structures, which introduce the XY-like anisotropy of this type of compound.

Acknowledgements

I would like to thank:

Andrew Harrison (Oxford and Edinburgh) for many years of stimulating collaboration.

Garry McIntyre (ILL, Grenoble) for your unstinting support of my research program.

Simon Carling and Professor Peter Day for many years of collaboration and support.

Steve Bramwell for collaboration on the 2-D ferromagnets.

Dr Christian Vettier, Dr Bruno Dorner, Dr Daniel Petitgrand, Dr Lothar Weiss, Dr Hans Graf and Dr Thomas Zeiske for their support during the experiments.

Dr Burkhardt Schmid, Dr Per-Anker Lindgard, Dr Peter Holdsworth, Dr Martin Plumer and Professor Michael Steiner for many stimulating discussions.

Many thanks go to the technicians of the Institutes where the described research has been carried out. Without their help the experiments would have been impossible to perform.

